A PHOTOEMISSION STUDY OF SOME LIQUID SIMPLE METALS AND ALLOYS

by

DONALD CHARLES RODWAY

a thesis submitted to the
UNIVERSITY OF LEICESTER

for the degree of
DOCTOR OF PHILOSOPHY

in the Faculty of Science

1978

ProQuest LLC
789 East Eisenhower Parkway
P.O. Box 1346
Ann Arbor, MI 48106-1346

I would like to dedicate this thesis to my mother whose support and encouragement, both financial and moral, made the task far lighter.

CONTENTS

LIST OF DIAGRAMS

ACKNOWLEDGEMENTS

I would like to give my sincere thanks to Dr. C. Norris for his help and guidance throughout the course of this work. I would further like to thank the Science Research Council for the award of a studentship for this work and Professor J.E. Enderby for the provision of laboratory facilities. For their aid in the construction and maintainence of the equipment used I would like to thank Dr. J.P.D. Henessey, Mr. J.S.G. Taylor, Mr. V. Brooksbank, Mr. R. Cox and the staff of the Physics Department Workshop.

For their assistance in the writing of the computer programmes used in this work I would like to thank Mr. G. Tolton, Dr.S. Holloway, Dr. J. Bethel and the staff of the computing department of Leicester University.

For their invaluable contribution towards my education in the field of solid state physics, I would like to thank Professor J.E. Enderby, Dr. G.P.Williams and other members, both past and present, of the Leicester University Solid State Physics Group.

Finally I would like to thank Mr. B. Bygrave and the staff of the drawing office, RSRE(B) for their advice on the preparation of the diagrams for this thesis and last, but by no means least, my wife for her support during the writing of this thesis.

ABSTRACT

Measurements of the work function, quantum yield and low energy (6.0 eV $<$ hV $<$ 21.2 eV) photoelectron spectra are presented for the simple metals In, Al, Pb and Sn in the liquid and frozen solid states, and for Hg and the mercury alloys $Hg_{.50}$- $In_{.50}$, $Hg_{.75}$-$In_{.25}$, $Hg_{.96}$- $Na_{.04}$ in the liquid states only. The results obtained for the solid simple metals are consistent with other published results. The results for the liquid are very similar to those for the solid and are constant over a broad temperature range above the melting point.

A Monte Carlo simulation of the photoemission process, based on the 3-step model of Berglund and Spicer, has been developed and used to examine the effects of variation of the electron-phonon scattering length on the quantum yield and escape depth of the photoelectrons. This programme has been used in conjunction with an analytical programme, based on the work of Krolikowski, to derive optical density of valence states functions and electron-electron scattering lengths for the liquids.

In all cases the optical density of states functions show much stronger structure than expected on the basis of a weak scattering description of the liquid system and agree better with theoretical predictions for the solid, indicating that some aspects of the solid state band structure persist on melting. No evidence for conservation of the momentum vector $\underline{k}$ or for non constant matrix elements is observed.

In the case of mercury and the mercury alloys the results obtained agree well with the pseudogap concept proposed by Mott.

CHAPTER 1:- INTRODUCTION

1.1. Outline

During the past fifteen years there has been increasing interest in the properties of liquid metals and alloys. This has arisen naturally as earlier studies of the crystalline phase have been extended into disordered systems. The liquid system is attractive both to the theoretician and the experimentalist as it is spatially isotropic and, unlike the amorphous solid, offers a degree of disorder that may be easily reproduced.

There are, however, considerable difficulties in this field - for the experimentalist there are the problems of the high temperatures required (resulting in high vapour pressures) and the corrosive nature of liquid metals, whilst for the theoretician there is the problem of treating a disordered system where long range translational order does not exist - precluding the use of Bloch's theorem to simplify matters. This is particularly true with the tight binding systems existing in transition metals.

The work in the field to date has been summarised in three major conferences (Brookhaven 1966, Tokyo 1972 and Bristol 1976) and in several reviews - notably those of Cusack (1972), March (1969), Enderby (1972),and Faber (1972). From these it is apparent that there is relatively little experimental data available on the electronic structure away from the Fermi level, although other aspects (such as the electron transport properties) have been extensively studied and are relatively well understood.

This thesis describes a series of photoemission experiments carried out on five liquid metals - aluminium, indium,

tin, lead and mercury and some mercury alloys. The object of these experiments was to obtain information on the valence band structure of these metals from measurements of their photoemission properties - notably the work function, quantum yield (as a function of photon energy) and photoelectron energy distribution spectra (E.D.C's). A computer model of the photoemission process was developed and used to examine the effects of scattering processes. This model was also used in conjunction with the experimental data to obtain values for the electron mean free paths and an optical density of states which could be compared both with theoretical predictions and the results of other workers.

1.2. Liquid Simple Metals

The metals chosen for this work, with the exception of mercury, are what are normally referred to as 'simple' metals, i.e. metals of high conductivity that do not possess a d or f resonance close to the Fermi level - this excludes transition, noble and rare earth metals and the chalcogenides.

Up to the present it has normally been considered that liquid simple metals could be adequately described in terms of a nearly-free-electron (n.f.e.) model where the disorder has largely reduced the scattering potential. There has been considerable work done in obtaining values for the structure factor S(Q) (defined in the usual way as the expectation value of $Na(Q)a^*(Q)$ where:

$$a(Q) = \sum_i \exp(-i\mathbf{Q}\cdot\mathbf{r}_i) \qquad (1.1)$$

and N = number of scatterers, Q is a wave number and r_i refers to the positions of the nuclei) from X-ray or neutron scattering

experiments and, with the exception of small effects in non-cubic metals such as zinc and cadmium, the results agree well with a simple pairwise interaction between ions. By plotting structure factors against hard sphere diameter, Ashcroft and Leckner (1966) have obtained a universal curve which is in reasonable agreement with the hard sphere solution of the Percus-Yevick equation. However, in the case of the chalcogenides there is some deviation from this model and these must be considered in terms of non-central forces (Enderby and Hawker 1974).

Figure 1.1. shows the structure factor for lead, which is typical of a hard sphere-like metal - a strong first peak followed by oscillations which damp out in a few multiples of Q As may be seen from Table 1.2., the electrons at the Fermi level in a simple metal such as sodium traverse many of the local arrangements between scattering events, which would be expected to cause considerable smearing of the E-k curve as suggested by Edwards (1962). This again contrasts sharply with the chalcogenides, such as tellurium, where the mean free path is only a few times the atomic diameter, with resultant strong local scattering. As will be discussed later, measurements of the optical properties also support this n.f.e. picture, showing little evidence of band structure.

1.3. Electron States in Disordered Systems - Theoretical

There are several different methods that have been used to obtain numerical results for simple liquid metals (a full review of these is given by Cusack 1972), but the majority

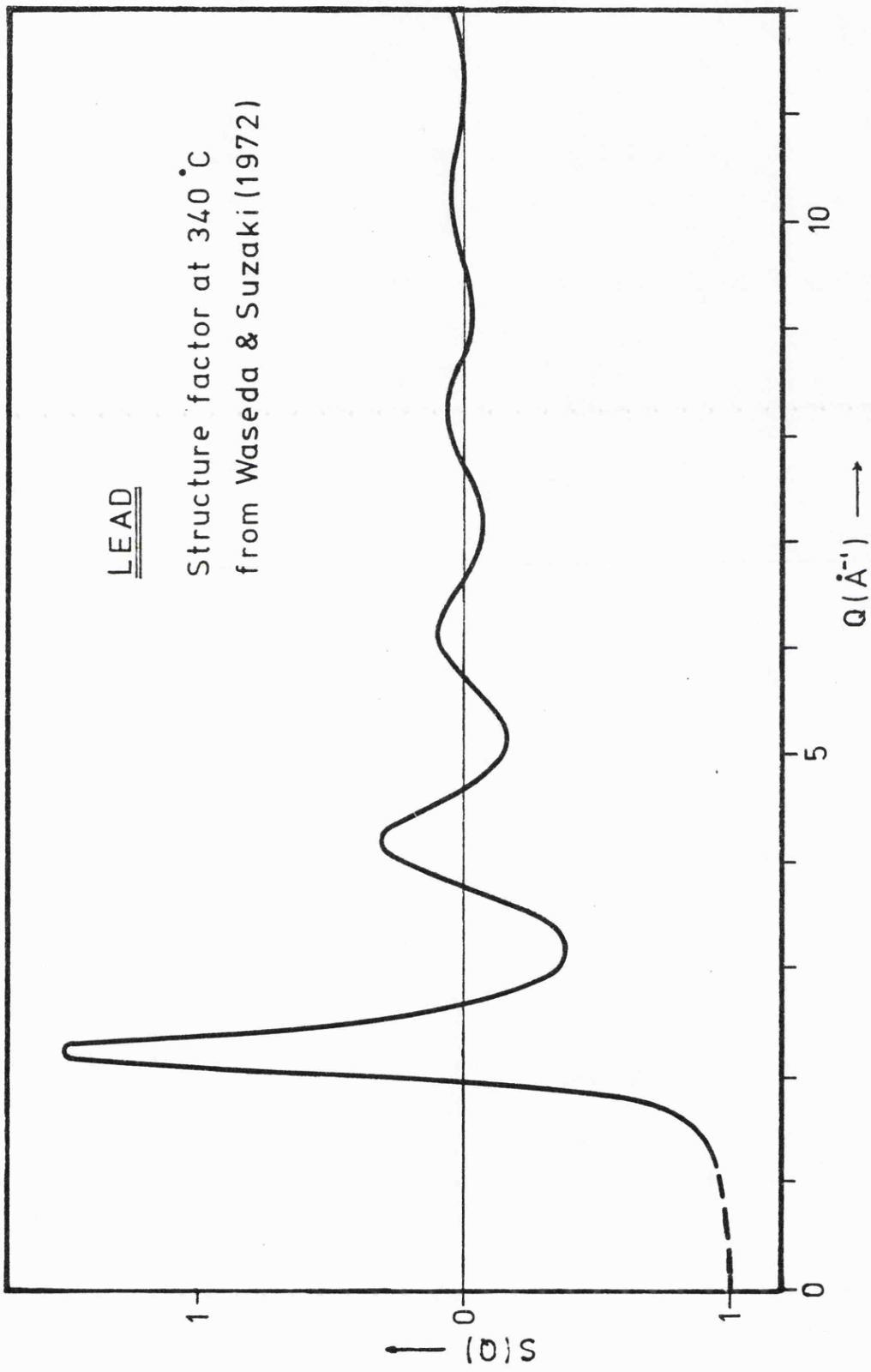

Fig. 1.1 - Structure factor for Lead

Metal	Valence	Melting Point (°C)	Vap. press. at Mpt.(torr)	L (Å)	L/R_a	R/R_o	Purity(%)
Mercury	2	-39	2×10^{-6}	7	4·1	0·98-1·00	99·9
Aluminium	3	660	3×10^{-9}	18	11	1·00	99·999
Indium	4	156	$<1\times10^{-11}$	17	9	0·98-1·04	99·999
Tin	4	232	$<1\times10^{-11}$	10	5·1	0·98-1·00	99·999
Lead	4	327	$1·5\times10^{-8}$	6	2·7	0·51-0·88	99·999

Fig.1.2 - Some basic physical parameters of some simple metals

of results have been obtained using a Greens function method which was introduced by Edwards (1966). This has been used as a basis for two different approaches.

The form of approach used by Chan and Ballentine (1972) and Itami and Shijomi (1972) to obtain results for sodium, aluminium, bismuth, mercury, indium and some alloys defines the resolvant operator in the form:

$$G(E) = (E - H)^{-1} = \sum_n \frac{|\psi\rangle\langle\psi|}{E - E_n} \qquad (1.2.)$$

where $H = p^2/2m + V$ is the Hamiltonian and $|\psi\rangle$ and E_n are its eigenvectors and eigenvalues.

This results in a density of states (per unit energy, per unit vol., for a single spin orientation) of the form:

$$n(E) = L^{-3}\sum_k s(k,E) = (2\pi)^{-3}\int s(k,E)\,d^3k \qquad (1.3.)$$

where the spectral function $s(k,E)$ is defined as:

$$s(k,E) = \frac{-1}{\pi}\,\mathrm{Im}\,G(k,E+i0) \qquad (1.4.)$$

where $G(k,E)$ is the ensemble average Greens function.

Figure 1.3. shows typical results for this method which generally yields a free electron like $n(E)$, lead and bismuth being the metals which show the greatest deviation from this.

Because of the lengthy numerical calculation involved in this method, a simplified version has been used by Shaw and Smith (1969) and Schneider and Stoll (1967) to obtain results for nickel, potassium, lead, bismuth, indium and cadmium. In

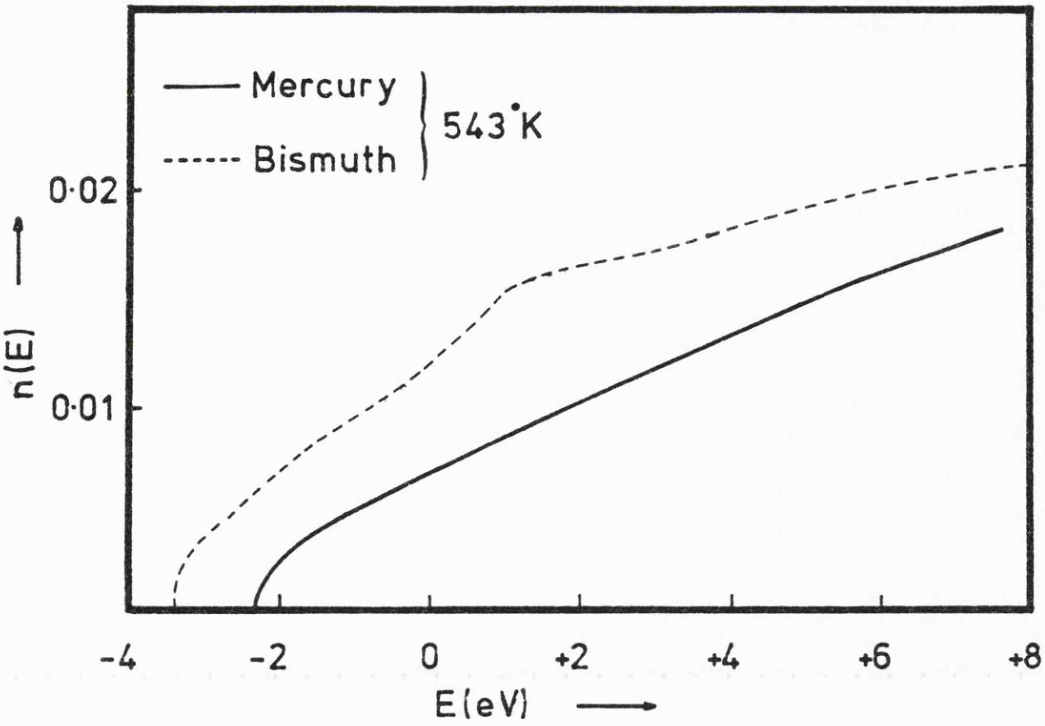

Fig.1.3-Density of states for liquid mercury and liquid bismuth from Itami and Shijomi (1972)

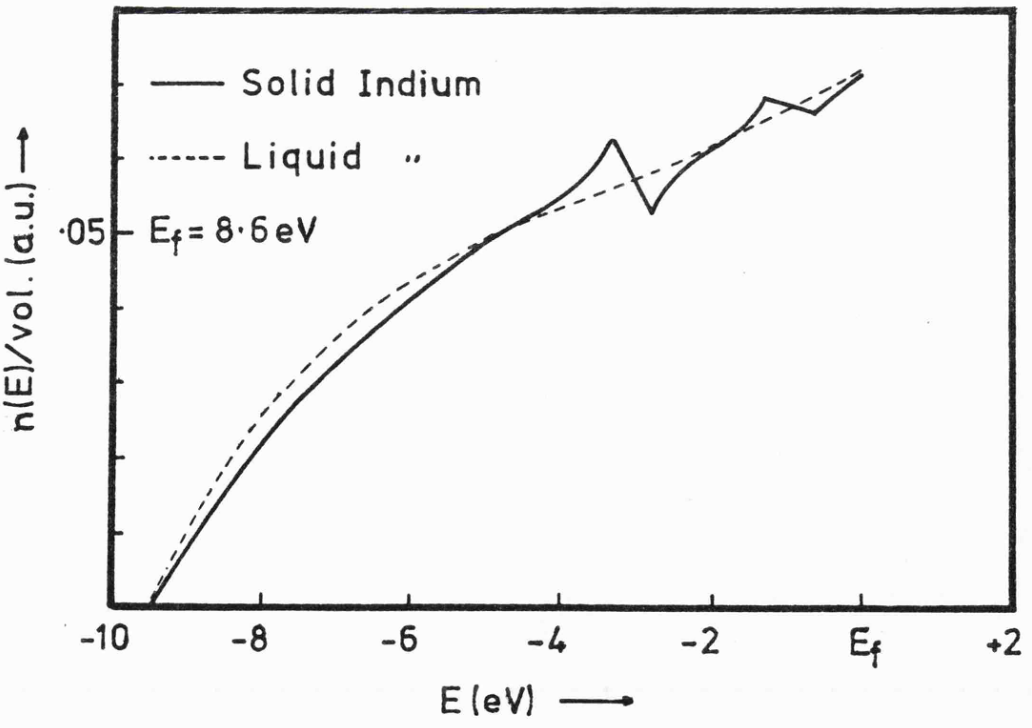

Fig.1.4-Density of states for liquid and solid indium from Shaw and Smith (1969)

this method the formal perturbation expansion for an energy eigenvalue is written as:

$$E = \frac{k^2}{2m} + \langle k|V|k\rangle + \sum_{k' \neq k} \frac{\langle k|V|k'\rangle\langle k'|V|k\rangle}{E - (k')^2/2m} + \ldots\ldots\ldots , \quad (1.5.)$$

By taking the ensemble average and assuming a uniform distribution of states in k space, the following relation for n(E) is obtained:

$$n(E) = \frac{k^2}{2\pi^2}\left[\frac{\partial E(k)}{\partial k}\right]^{-1} \quad (1.6.)$$

Figure 1.4. shows typical results for this method.

This method ignores triplet correlations - the structure that exists from the third term of the expression involving S(q), the 2-body structure factors.

The relationship between these methods has been examined by Ballantine and Chan (1972). They have shown that the second method has given an exaggerated value for the pseudogap (the dip in n(E) at the Fermi level) in mercury, implying that this method is only reliable where the solid state density of states is free electron like.

A third method, that of the Bloch density matrix, has been used by Rousseau et al (1970) to obtain results for beryllium. This method shows appreciable deviation from free electron behaviour, whilst the first two methods show very free electron like behaviour, as may be seen in the diagrams, where the functions associated with crystallinity are washed out and there is only a weak indication of a band gap.

More recently, interest has focussed on the use of a

tight binding method. A discussion of this method and the muffin tin potential which forms the basis of the Ziman-Lloyd formalism is given by Watabe (1977).

1.4. Electron States in Disordered Systems - Experimental

There are several different techniques which have been used to try to gain information on the electronic density of states at or below the Fermi level. Some of these are discussed here.

1.4.1. The Knight Shift (K)

This is a nuclear magnetic resonance (N.M.R.) technique, the shift (K) being the fractional change in the N.M.R. magnetic field when the nuclei form part of a metal, relative to the field for an isolated atom. This gives information on any departure from $N(E_F)$ of the free electron value and on any variation during melting. Results to date show little effect on N(E) on melting except in cadmium (Seymour and Styles 1964), gallium and bismuth (Knight et al 1959). This failure to observe a change in K on melting is not in agreement with the free electron picture. However there are masking effects due to electron-electron interactions, and the observational accuracy is limited.

1.4.2. Positron Annihilation

This technique enables information on the momentum distribution of the electron to be gained by measurements of photon angular correlation from the annihilation of high energy (several MeV) positrons in the material. Unfortunately the interpretation of results is difficult as there is considerable smearing of the angular correlation curve in liquid metals (West et al 1967) which considerably limits the usefulness of the technique.

1.4.3. Electron Transport Properties

A considerable amount of information on liquid metals has been gained from measurements of the electron transport properties, i.e. Conductivity (ρ), Thermopower (Q) and Hall coefficient (R). Using a semiclassical nearly-free-electron approach, where the electrons are described in terms of the plane wave scattering of weak pseudo-potentials, Ziman (1961) has obtained the following expressions for conductivity and thermopower:

$$1/\rho = \frac{3\pi\Omega}{\hbar e^2 v_F^2} \int_0^{2k_F} S(k)|v(k)|^2 k^3 \, dk \qquad (1.7.)$$

$$Q = \frac{\pi k_B T}{3 e k_F} \; 3 - \left\{ \frac{S(2k_F)|v(2k_F)|^2}{\langle |v|^2 S \rangle} - \frac{\langle k_F (\partial |v|/\partial k) S \rangle}{\langle |v|^2 S \rangle} \right\} \qquad (1.8.)$$

where Ω is the atomic volume and k_F is the Fermi wavevector.

This approach has been discussed fully in several articles (see Faber 1972) and although doubts have been cast on its validity, mainly due to its dependance on the Born approximation, it has been quite successful to date. The values of ρ obtained for the alkali metals are in good agreement with experiment, and in the case of divalent metals it has shown clearly why they have lower values. The theory has also been successful in relating the temperature dependance of ρ to the temperature variation of S(q) but was initially unsuccessful in accounting for the experimental values for mercury. More recently the pseudopotential has been modified by Evans (1969) to overcome this problem.

In the case of the Hall effect the n.f.e. theory gives the result:

$$R_H = 1/nec \qquad (1.9.)$$

where

R_H is the Hall coefficient and n is the number of carriers/cm^3.

This expression is in good agreement with the observed results for most materials. It fails in the case of lead, but this could be due to the strong scattering in this material.

However, more recently Edwards (1966) has cast doubt on this n.f.e. explanation and has shown that the simple transport properties are not sensitive to small variations in the density of states.

1.4.4. Optical and Spectroscopic Methods

The results obtained from low energy studies (e.g. Hodgson et al 1962) have provided some of the strongest evidence for the acceptance of the n.f.e. approach.

Almost all the results obtained are consistent with the classical Drude model which yields the expression for the conductivity:

$$\rho(\omega) = ne^2\tau/m(1+\omega^2\tau^2) \qquad (1.10)$$

where τ is the relaxation time.

One of the most notable results is that for aluminium, where the interband transitions are observed to disappear on melting, again in keeping with the predictions of the n.f.e. theory. The agreement is not good in the case of mercury, but there has been some dispute over the properties of this metal.

Schultz (1957) obtained results that were in good

agreement with the Drude model but later workers such as Hodgson (1959) claimed to have measured values for ε_1 and ε_2 significantly greater than those suggested by the theory.

1.4.5. Emission Spectrum Methods

With the development of ultra high vacuum apparatus making it possible to obtain and maintain atomically clean surfaces, the emission spectrum techniques such as ultraviolet photoemission spectroscopy and X-ray photoelectron spectroscopy have come into prominence. These techniques allow the density of states away from the Fermi level to be probed. Early results on liquids (Koyama 1968 and Stevenson 1968) have been quite striking and the whole n.f.e. approach has been cast into doubt by the discovery that structure observed in the density of states persists on melting. Although the interpretation of results is complicated by the effects of electron-electron scattering processes, this technique is one of the most valuable tools for the investigation of electronic structure. Its application to liquid metals is fairly recent, and further work is urgently needed to clarify the initial results. This technique will be fully discussed in later chapters.

1.5. Outline of Thesis

It will be clear from the preceding that there is very little definite information on the density of states in liquid metals. Despite the success of the Ziman model in explaining electron transport data, and the work of Edwards, the failures of the n.f.e. theory show that it cannot be considered to be totally satisfactory. Whilst the technique of photoemission

spectroscopy provides a means of directly probing the density of states away from the Fermi level, the work to date has mostly been on solids and gases, and there is very little data available for liquids. Although there are considerable experimental difficulties, Figure 1.5. shows that the vapour pressures of aluminium, indium, tin and lead are low enough to make these problems soluble, and that even mercury can be handled with the use of a mercury diffusion pump. These metals provide a range of types from the free electron like aluminium to lead with its strong scattering and mercury with its possible pseudogap. Thus a series of experiments on these metals should provide valuable data on the validity of the n.f.e. approach for liquid metals.

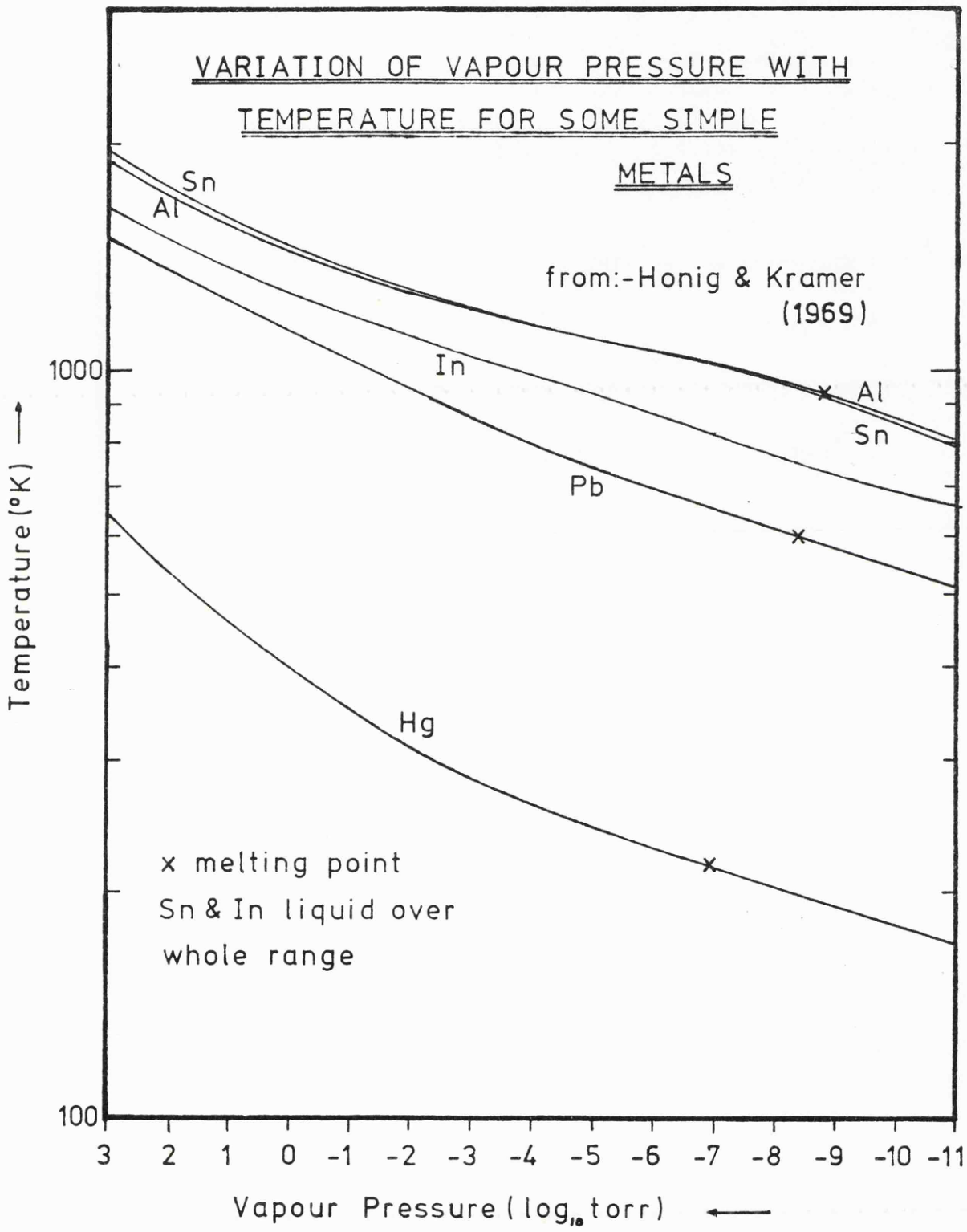

Fig. 1·5 - Vapour pressures

CHAPTER 2:- THE PHOTOEMISSION PROCESS

2.1. Historical Background

The photoelectric effect has been known for some time, the basic equation formulated by Einstein in 1905 being:

$$E = h\nu - \phi \qquad (2.1.)$$

where E = energy of the emitted electron, $h\nu$ = photon energy and ϕ = work function.

Figure 2.1. illustrates the basic process. The electron states in the valence band are filled from the bottom of the band to the Fermi level. Since a metal is being considered there is no forbidden gap above this level, and empty states are continuous to the vacuum level and beyond. If a photon of energy $h\nu$ impinges on the metal and excites an electron of energy E, it will raise the electron energy to $E + h\nu$. If this increase raises the electron above the vacuum level, it may then find its way to the surface and be emitted, its energy outside the metal now being $E' = (E + h\nu) - (E_f + \phi)$. Since the initial energy E may be anywhere in the valence band, E' may be anywhere between $(h\nu - \phi)$ and zero. The probability of an electron being emitted with any particular energy E' is dependant on the number of electrons with energy E - thus, if a large number of photons is considered, the distribution of final energies will be a reflection of the density of states, modified by some function dependant on the internal scattering processes and the escape probability at the surface. This is the basis of the technique of photoelectron spectroscopy.

The first attempt at photoelectron spectroscopy was made by Richardson and Compton (1912). Whilst they provided a useful

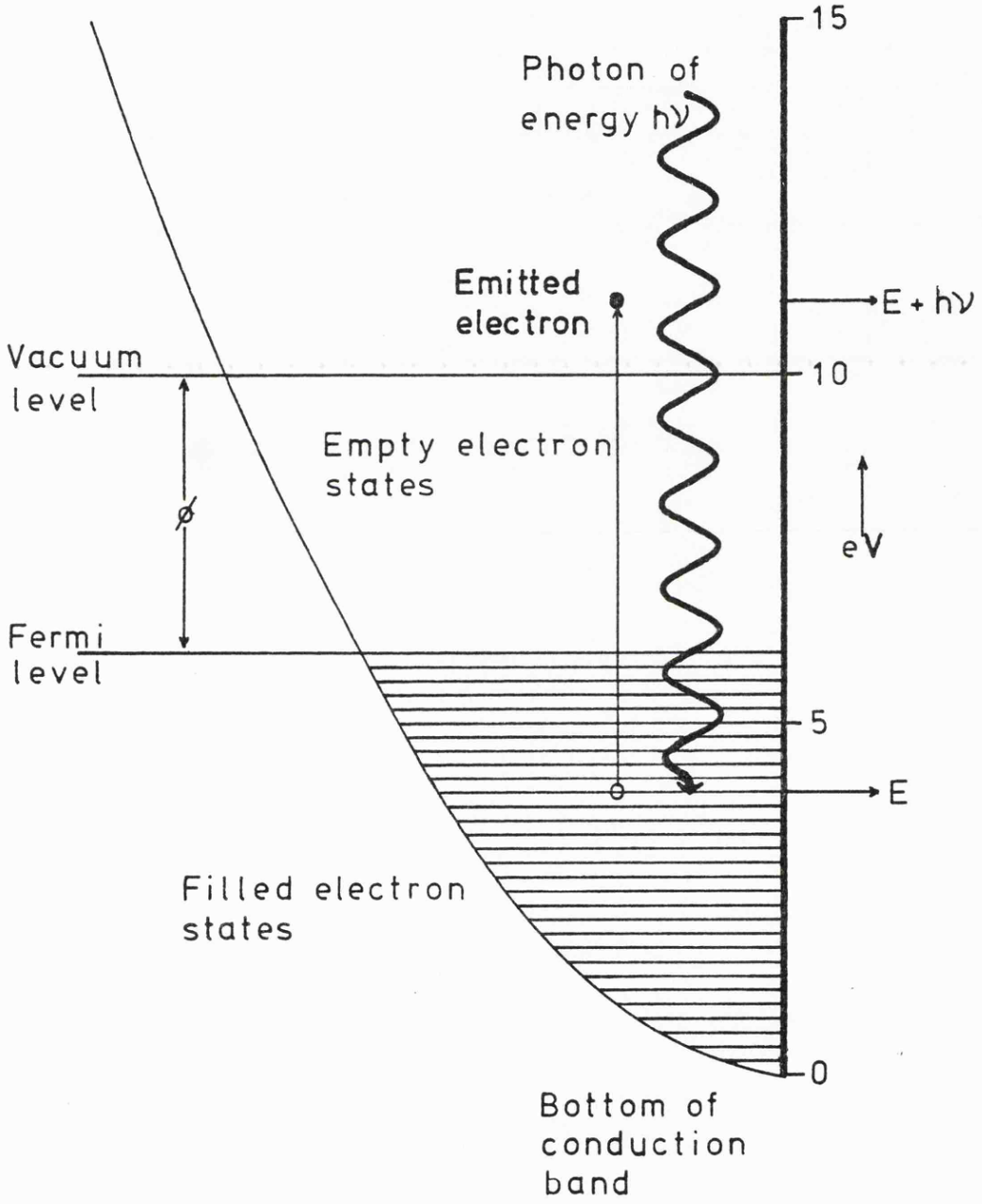

Fig. 2.1 - Basic photoemission process in a metal

illustration of the technique they also revealed its major limitation - which is that, without an atomically clean surface, the electrons are scattered so strongly at the metal-vacuum interface that all information in the spectrum is completely 'washed-out'. Thus it is only in the past two decades, when the advent of ultra high vacuum (U.H.V.) apparatus has made the preparation of atomically clean surfaces possible, that the technique has become viable.

However, theoretical advances were made. Fowler (1931), by the use of Fermi-Dirac statistics, succeeded in explaining theoretically the shape of the i-V curve near threshold (i.e. $(h\nu - \phi)$ is very small). Assuming that (a) only electrons for which $E > (\phi + E_f)$ at right angles to the surface may escape, and (b) that all electrons satisfying (a) have equal probabilities of escape, he obtained the expression:

$$Y \propto (h\nu - \phi)^2 / (E_f + \phi - h\nu)^{\frac{1}{2}} \qquad \text{for a given temperature } T \qquad (2.2.)$$

where Y = quantum yield. Thus, by plotting $Y^{\frac{1}{2}}$ vs $h\nu$, an accurate value of ϕ may be obtained. This is called a Fowler plot and is a very useful technique.

2.2. Present Theories

The current theories of photoemission fall into two main groups, using either a general formalism or a model of the process.

2.2.1. Formalistic Theories

In these theories the generation, travel, scattering and transmission of the photoelectron are treated as a single process

by means of first principle quantum mechanics. This has been done by several workers (e.g. Mahan (1970), Schaich and Ashcroft (1970), Caroli et al (1973)), using a variety of approaches. Mahan has performed calculations using a scattering formalism and Schaich and Ashcroft have considered the quadratic response of the system to an applied electromagnetic field. These theories include the effects of inelastic electron-electron scattering but make no allowance for the effect of electron-ion interaction, which in the case of a liquid metal may well be an important effect. Whilst all these theories are satisfactory from a theoretical point of view, they are highly complicated and, in order to give an effective solution for a real case, it is necessary to make assumptions and simplifications that are not satisfactory.

Norris and Williams (1976) have reported calculations for aluminium based on the theory of Schaich and Ashcroft. Starting from the 'golden rule' expression for the time-averaged photocurrent outside the metal as a summation over a continuum of the form:-

$$\langle J(r)\rangle = \frac{2\pi e}{\hbar}\sum_{m,u} n(E_m)\left|\langle m\right| \frac{i\hbar e}{mc}\,\underline{A}\cdot\nabla\left|u\right\rangle\right|^2 \delta(E_m+\hbar\omega-E_\mu) \quad (2.3.)$$

where $\langle m|$ is an initial one-electron state of the unperturbed system with occupation $n(E_m)$ and $|u\rangle$ is a final state which has an outgoing plane wave component at infinity in the vacuum. It is also a decaying excited state in the presence of a boundary which accounts for transmission and scattering. $\underline{A} = A\hat{\mathcal{E}}$ is the vector potential. By then making suitable assumptions in the preceeding equation, namely that $\hat{\mathcal{E}}$ is parallel to a near perfect surface,

and by factorising out transmission and scattering effects, they obtained the following expression for the energy distribution:-

$$N(E,\hbar\omega) = C\left\{\sum_{i,f} n(E_i)|\langle i|\underline{A}\cdot\nabla|f\rangle|^2 \delta(E_i+\hbar\omega-E_f)\delta(E_f-E)\right\}T(E) \quad (2.4.)$$

i, f being initial and final states of the perturbed system and T(E) being the probability of escape without scattering. This may be simplified further by assuming that, in a disordered system such as a liquid, the matrix elements which impose conservation of the momentum vector may be considered to be constant.

This reduces the above equation to:-

$$N(E,\hbar\omega) = Cp(E-\hbar\omega)p(E)T(E) \quad (2.5.)$$

This does rely on gross simplification but gives a basis for the interpretation of photoemission spectra. Using equation 2.2. and ignoring final state scattering, Norris and Williams obtained EDC's for aluminium of the right general shape but lacking the structure that is observed experimentally.

2.2.2. Model Theories

The earliest effective model theory, and still the most useful, is that of Berglund and Spicer (1964), modelling the photoemission process as a series of 3 semi-classical steps as follows (see Figure 2.2.):-

1. The photon is incident upon a metal surface. It penetrates the surface (assuming the reflectivity is zero), is absorbed and generates a 'hot' or excited electron.

2. The electron travels towards the surface of the material, possibly undergoing some scattering process as it

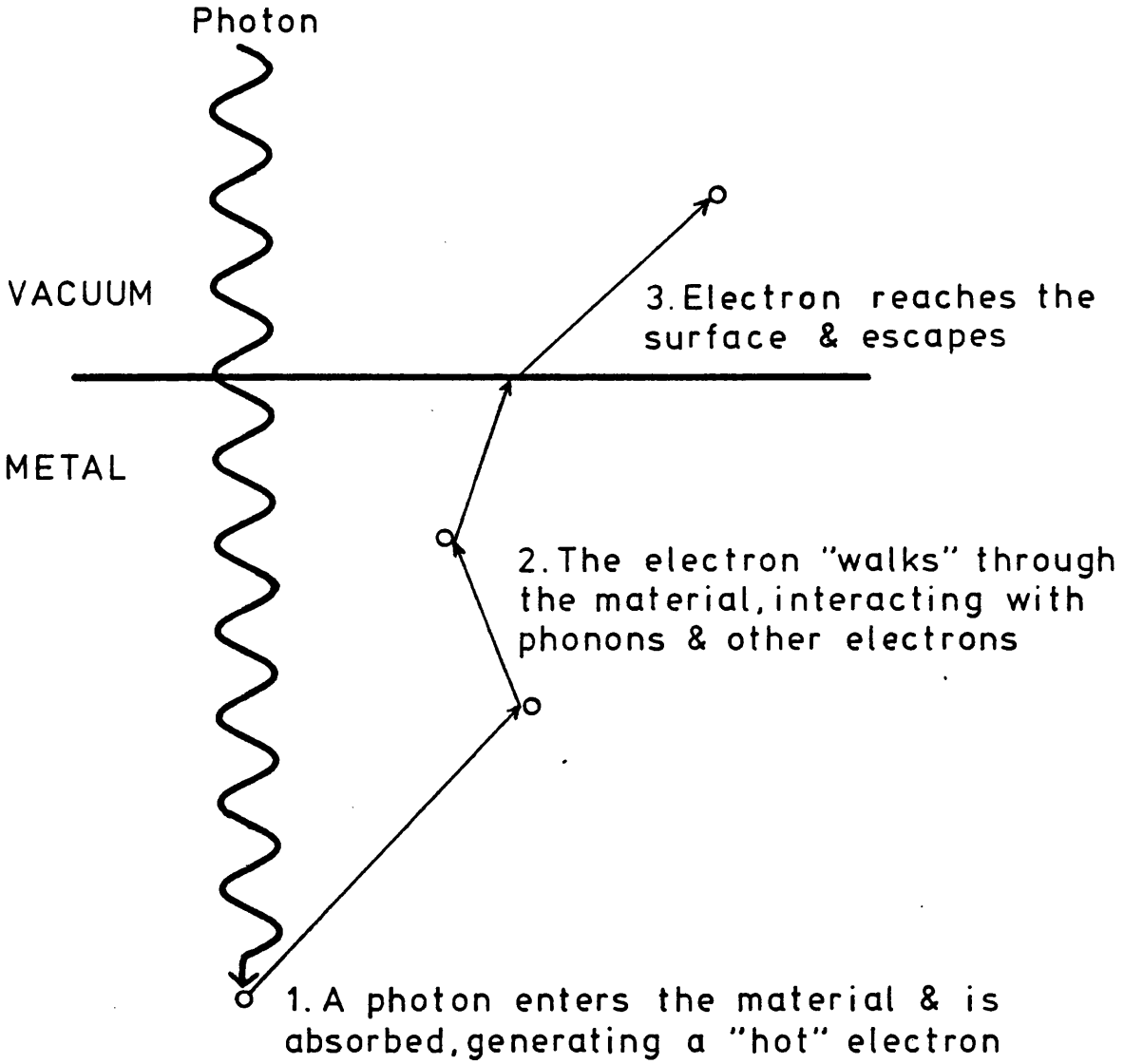

Fig. 2.2 - The 3-step process

does so.

3. The electron reaches the surface and escapes.

Step (1) allows the possibility of two types of optical transitions for the excitation of the electron.

a) Direct transitions: In a crystalline structure, the crystal momentum must be conserved. This means that in a band structure the transitions must be vertical, implying to the photoelectron spectroscopist that the structure he observes in the density of states should vary both in strength and position relative to the Fermi edge as a function of the photon energy, due to the coupling of the initial and final states by matrix elements.

b) Non direct transitions: In this case it is assumed, by presuming some unspecified many body interactions, that crystal momentum need not be conserved. This means that there is little effect from the matrix elements, which are usually assumed to be constant, and hence that the structure observed should be constant both in position and strength relative to the Fermi edge.

Later workers have used both types of transitions in discussing results for different metals (see for example Eastman (1969), Shaw and Smith (1969)) however, as will be seen later, the results obtained in this study are consistent with the non-direct approach and this is considered in more detail in Chapter 3.

The model contains several assumptions which are listed here (see also Eastman (1972)):

1) That the matrix elements are constant.

2) That the emission of electrons is purely a bulk process.

3) That the distribution of the directions of the excited electrons is isotropic.

4) That only inelastic electron-electron scattering is considered.

5) That the probability of an electron-electron event may be defined in terms of a mean free path l_e.

6) That the inelastic scattering is isotropic.

7) That when the electron reaches the surface, its escape probability is assumed to be unity if its momentum normal to the surface is greater than some excited value, and zero if it is less.

These are a fairly drastic set of approximations and it is obvious that some of them are not well justified. However, this model has enjoyed a fair degree of success and, in view of the difficulties inherent in the formalistic theories, it will be adopted as the basis for the interpretation of the results obtained in this work. The model does need to be extended, since in a liquid metal the electron-ion scattering length is very short, which means that it is no longer possible to view the transmission of the electron only in terms of inelastic electron-electron scattering. Other scattering processes must also be taken into account.

2.3. Scattering Processes

There are three major scattering processes which need to be considered for a liquid metal. These are electron-electron, electron-phonon (or electron-ion) and electron-plasmon interaction.

In a metal, electron-electron interaction represents the major source of energy loss for an excited electron. The excited

electron interacts with an electron in the valence band, transferring energy to it. This process (Figure 2.3.) involving the loss of energy E from the excited electron - ignoring $\underline{k}$ conservation - may be shown (Krolikowski 1969) to have a probability of occurence P of the form:-

$$P \propto \int_{E}^{O} N_v(E_b)\, N_c(E_a - E)\, dE_b \qquad (2.6.)$$

N(E) being the density of states at energy E, and E_a, E_b being the energies of primary and secondary electrons.

If this probability P is averaged over many events it can be shown (Stuart and Wooten 1964) that the average energy loss of the excited electron in one electron-electron collision is one-half of its energy in excess of the Fermi energy. It may thus be seen that in the case of say, excitation by 10 eV photons of a metal with a 4 eV work function energy, that the probability of the electron surviving more than two collisions and retaining sufficient energy to excape is small. Therefore the probability of electron-electron interaction is a limiting factor in the quantum yield of the material.

This probability of an electron-electron collision may be expressed in terms of a mean free path or scattering length, which is a function of the energy of the excited electron. A fairly simple treatment of the scattering (Krolikowski 1968) gives an energy dependance of the form $E^{-3/2}$, and if this is compared with more complex predictions (Quinn 1962) or with experimental data, (see Figure 2.4.) it may be seen to be a reasonable fit. Values of the mean free path in liquid metals are of the order of a few tens of angstroms at 10 eV above the

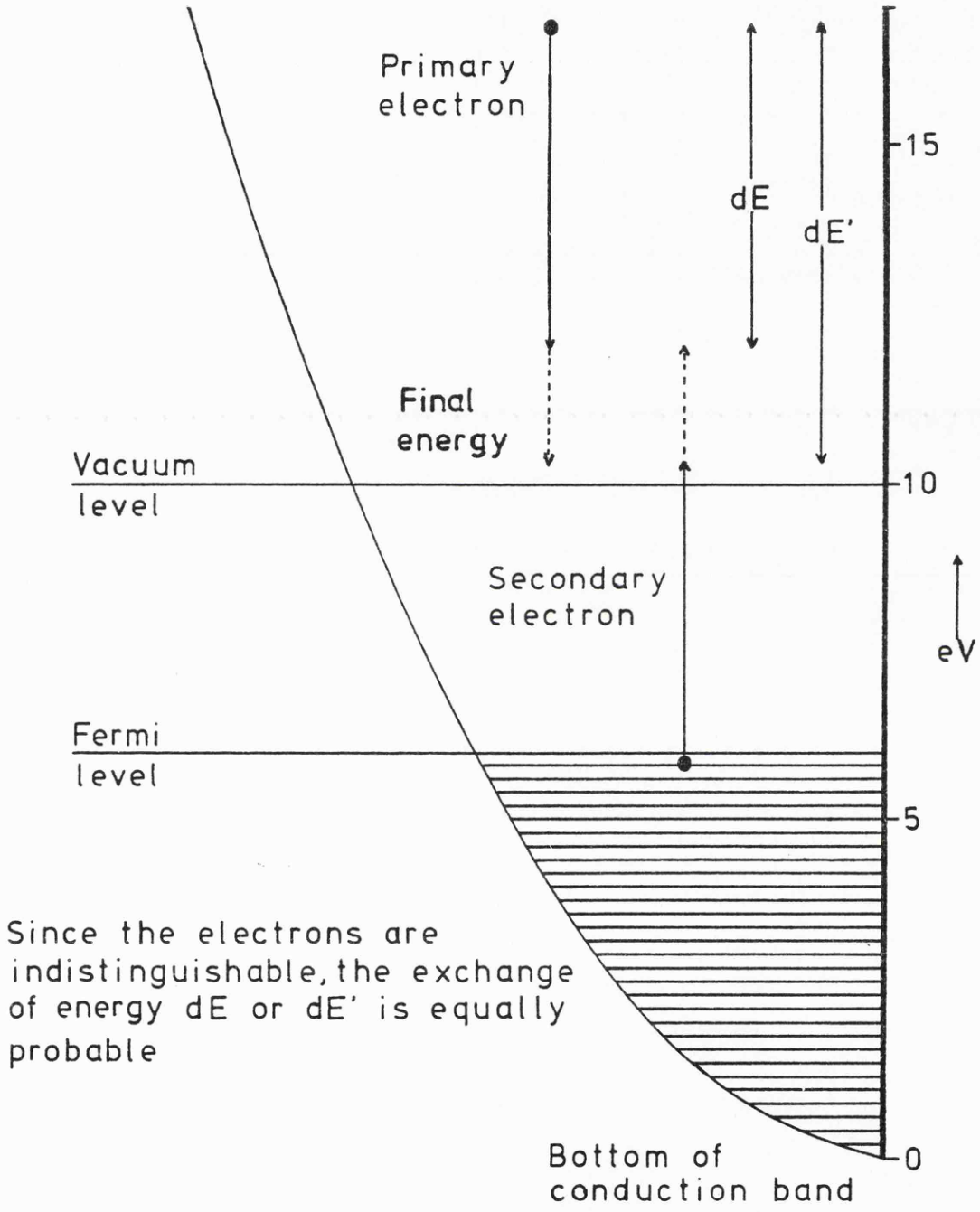

Fig. 2.3 - Electron-electron interaction in a metal

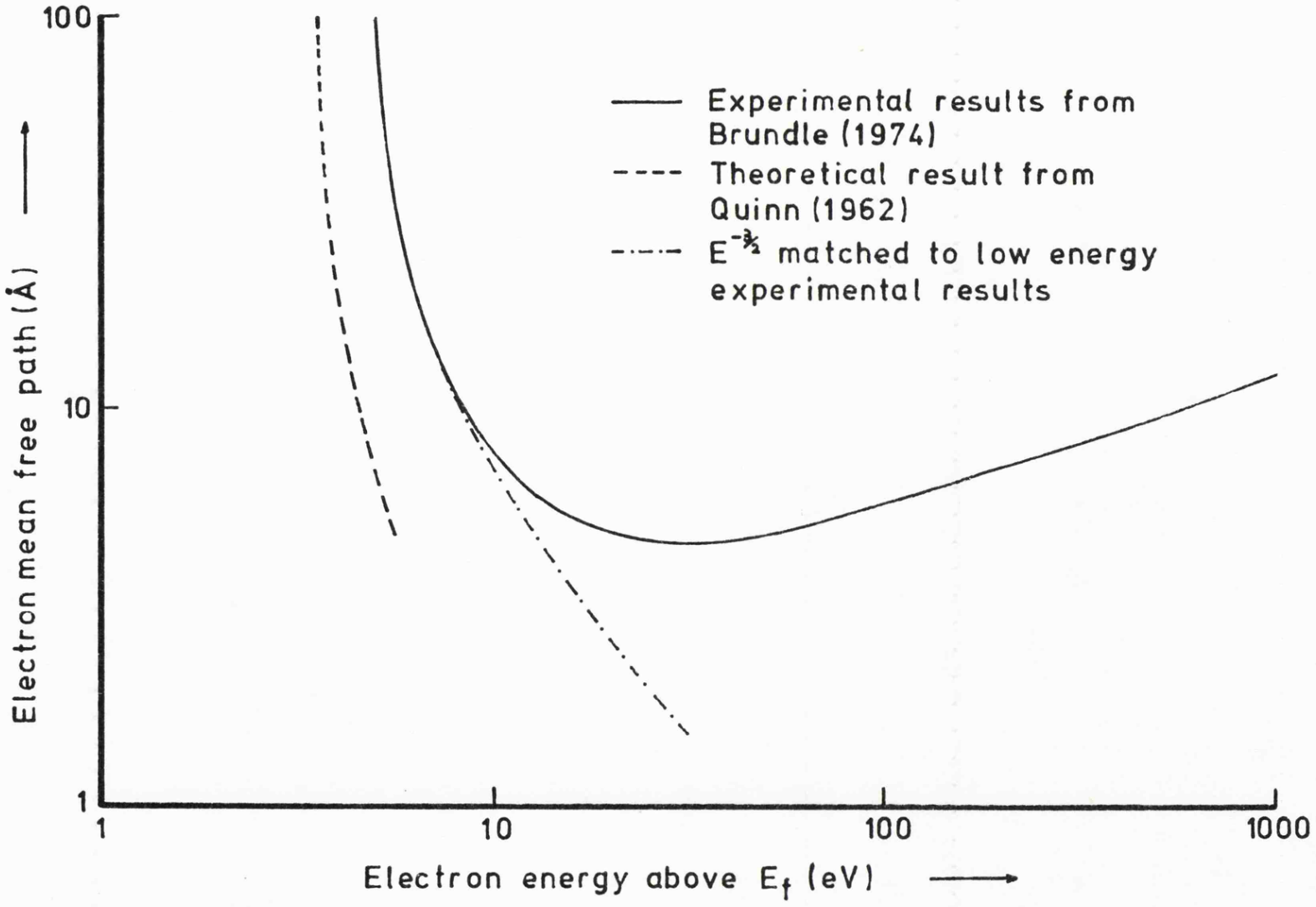

Fig.2.4-Variation of electron mean free path with energy.

Fermi level, rising to several hundreds of angstroms at lower energies so that, in the example above, the mean free path will typically vary in the range 10 - 100 Å. The escape of electrons that have undergone a single collision results in a large peak in the energy distribution spectrum at low energies and in the case of a dirty surface this peak is considerably enhanced, often to the extent of completely blurring out all details in the higher energy part of the spectrum. This possibly arises because the mean free path at the surface is greatly reduced, causing an increased number of collisions, whilst the nearness of the surface still allows a high probability of escape for the electron after collision. It is thus vital to obtain as clean a surface as possible.

The second major scattering process is that of electron-phonon interaction. In this, an excited electron interacts with the lattice in the material and either gains or loses a small amount of energy (of the order of 0.05 eV). As in the previous process, the probability of an event may be expressed in terms of a mean free path (l_p), but this is not significantly energy dependant over the energy range used in this study. In the case of a semiconductor with a tightly organised lattice, this mean free path may be very long - of the order of several hundred angstroms - but in a disordered system such as liquid metal it can be as low as a few angstroms (Cusack 1963).

Since the energy exchange in this interaction is quite small, and may equally well be a loss or a gain, the effect should be not to produce a low energy peak, but rather to blur the structure of the energy distribution spectrum, the amount of blurring increasing as the mean free path decreases. The effect

on the quantum yield is not clear, and this is discussed in more detail in Chapter 3.

The third major process is that of electron-plasmon interaction. In this process the electron causes a plasma oscillation - a longitudinal vibration of the conduction electron gas - losing energy in the process. The plasmon has a definite lifetime and a fixed frequency which may be measured by observing electron energy loss spectra (Powell 1968). There are two types of plasmon - surface and bulk - with different frequencies, the surface effect involving motion of the conduction electrons to a depth of 100 Å. The decay of the plasmon causes a peak in the quantum yield at the characteristic frequency, and this has been observed in photoemission experiments on Al (Endriz and Spicer 1974).

There is one other process which may affect the photoelectron spectrum and the yield. This is the generation of an Auger electron. The excitation of a photoelectron leaves a 'hole', either in a core state or in the valence band, and an electron from a higher state may then combine with this 'hole' releasing energy for the excitation of another electron to above the Fermi energy (see Figure 2.5.). In the case of ultraviolet photoemission, the probability of generation of an electron with sufficient energy to escape is fairly small and, as may be seen from the results in Chapter 3, the contribution to the electron energy spectrum is not significant.

In Chapter 3 it will be shown how these processes may be modelled, and their effects on the final EDC and yield determined.

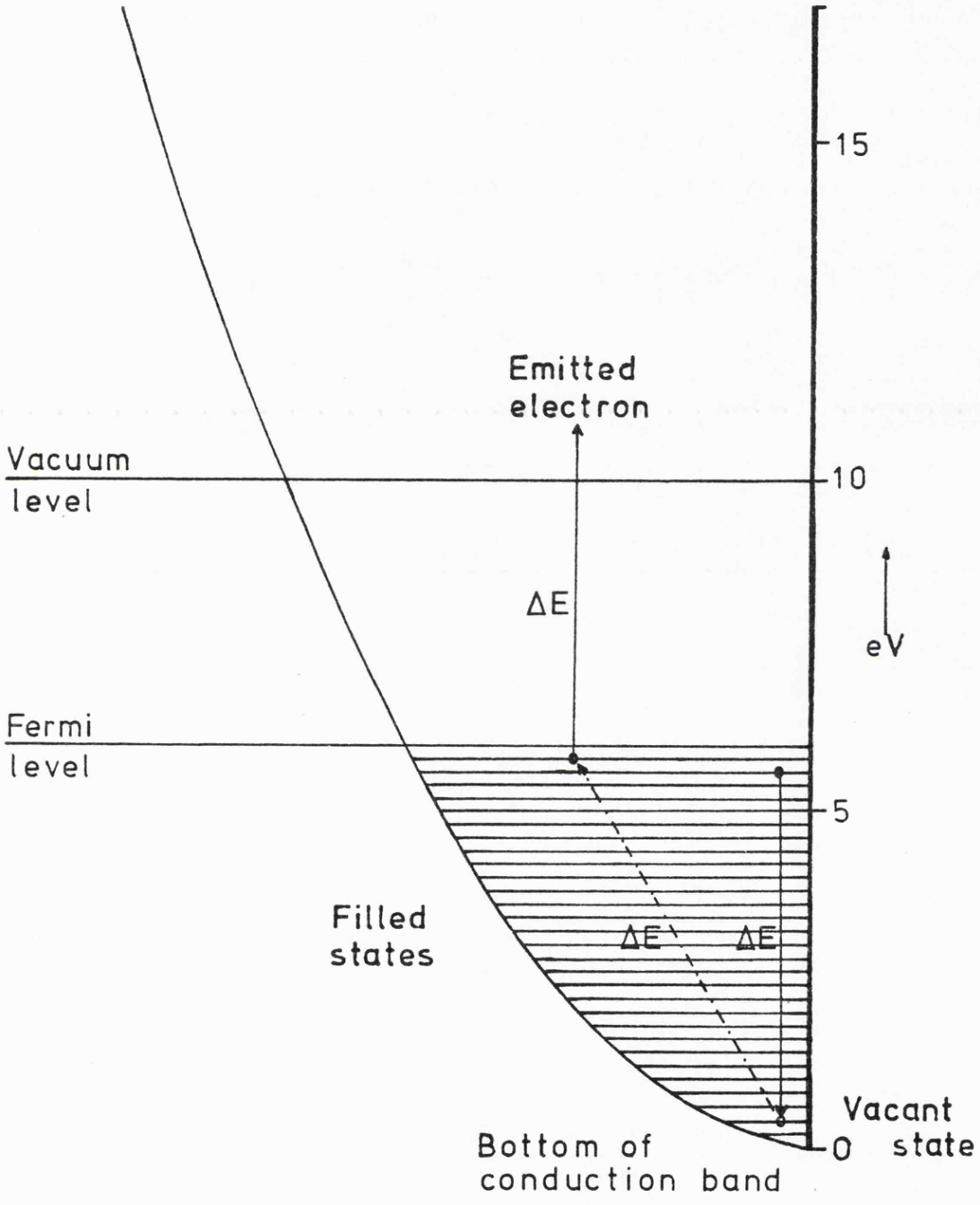

Fig. 2.5 - Generation of an Auger electron

CHAPTER 3:- COMPUTER SIMULATION OF THE PHOTOEMISSION PROCESS

3.1. Introduction

As stated in 2.2., although the complexity of formalistic theories of photoemission tend to preclude their application to real systems, the 3-step model of Berglund and Spicer has enjoyed some success in the interpretation of photoemission results and this has been used as the basis of analytical simulations (notably by Krolikowski 1969) and for Monte Carlo type analyses (notably Stuart and Wooten 1964 and Leckey 1972). However, these analyses have been for solids and,when considering the transport of the excited electrons to the surface, have only taken account of inelastic electron-electron scattering mechanisms. In a solid with a well defined crystal structure this is probably adequate, since the scattering length for an electron-ion interaction is very much larger than that for an electron-electron event, but in the case of a liquid the electron-ion scattering length can be very short (see Cusack 1963), and the effect of this mechanism on the resulting photoelectron spectra and yield is not obvious. There are of course other effects, such as the possibility of electron-plasmon interaction and the Auger generation of photoelectrons which may also influence the final spectra, and whose importance is again not obvious.

In the absence of a satisfactory analytical expression for the electron-ion scattering of electrons in a liquid metal, and the relative importance of the various mechanisms being unknown, it was decided to attempt a Monte Carlo simulation rather than an analytical one.

In this chapter the structure of the Monte Carlo programme is considered in detail. The results obtained for a free electron like metal are compared with those of the Krolikowski analytical approach, and the programme limitations are discussed. The effect of variation of the parameters is also discussed.

3.2. The Monte Carlo Programme

The basis of a Monte Carlo simulation is that the fate of each individual photon and electron is followed - each decision about their fate being made by a random number generator, where the random number distribution has been suitably biased to take account of the relative probabilities of various events. As will be fairly obvious, this technique uses a lot of computer time since a very large number of photons and electrons must be followed to reduce the statistical uncertainty involved to an acceptable level. However, the technique does possess the virtues of great flexibility, since it is only necessary to be able to assign a probability to an event to be able to take account of it.

In order to keep the required computer time down, it was decided to make some simplifying assumptions in addition to those normally made in the 3-step model (see 2.2.).

1. Any electron whose energy fell below that necessary for escape over the surface barrier was considered to have no chance of escape and was ignored from that point.

2. So that it was unnecessary to consider tertiary electrons (i.e. secondaries created by secondaries), the programme was confined to a maximum photon energy of 10.2 eV.

Stuart and Wooten (loc.cit.) have shown that an electron loses, on average, half of its energy in excess of the Fermi edge in each collision. So, as the work functions being considered are between 4 and 4.5 eV, it may be seen that this results in a very small probability of a tertiary electron being generated. After each electron-electron interaction, the electron with the higher final energy was considered to be the primary (the electrons being indistinguishable).

3. Since no evidence of direct transitions was observed in the spectra obtained from the liquid metals being studied, it was assumed that all transitions were non-direct.

4. Since none of the metals being considered are known to have a bulk plasmon in the energy range being considered, the effects of electron-plasmon interaction were neglected.

A full flow chart of the programme is shown in Figure 3.1. Let us now consider the steps in detail:-

3.2.1. The Photon Entry

Only absorbed photons are considered, and the incidence of the photons onto the surface is assumed to be normal. Allowance for reflection at the surface, and for refraction in the case of non-normal incidence, is trivial and it was not felt necessary to include this in the original programme. Non normal incidence will, of course, result in the generation of excited electrons closer to the metal surface - hence it should cause a significant change in the yield.

3.2.2. The Photon Walk

If a photon flux intensity $I_0(\omega)$ and frequency ω

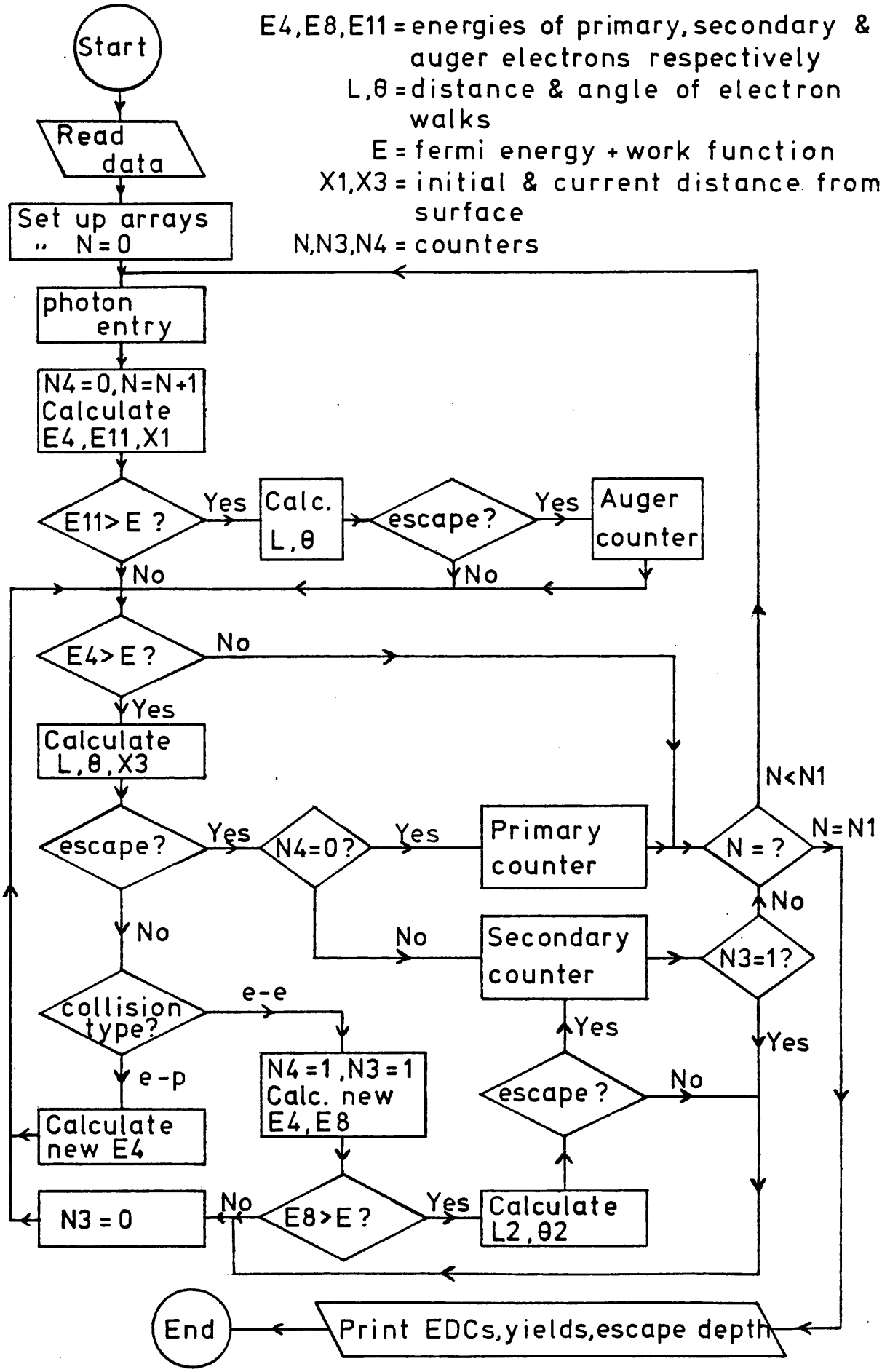

Fig. 3·1 - Flow chart for Monte Carlo programme

penetrates the surface of a metal of an absorption coefficient $\alpha(\omega)$, then the resultant intensity at a point a distance x from the surface may be expressed in the form:-

$$I(x,\omega) = I_o(\omega)\, e^{-\alpha x} \qquad (3.1.)$$

If each photon absorbed then results in an excited electron, the number of excited electrons generated between x and x + dx will be of the form:-

$$G(x) \propto \alpha e^{-\alpha x} \qquad (3.2.)$$

i.e. the probability of a photon creating an electron at a given depth will vary according to the exponential of the depth. Thus if a_1 is a random number from a normalised distribution of random numbers, and x is selected according to the relationship:

$$x = -\alpha \ln(a_1) \qquad (3.3.)$$

then if the values of x selected are considered for a large number of photons, the resulting distribution will be as in (3.2).

A record of x is kept in the programme so that, at the end, the initial value of x for all the photoelectrons which escaped may be averaged to give a value for the effective probe depth at the photon energy under consideration.

3.2.3. Generation of the Photoelectrons

The photon which has penetrated a depth x into the

material is now absorbed by an electron of energy E. Two things are immediately apparent - firstly, E must be such that $E + \hbar\omega > E_f$ (or the exclusion principle will be violated); secondly, that the probability of selecting a given E must vary according to the number of electrons with that energy (i.e. biased to higher values of the density of states $N_v(E)$).

It has been shown by Krolikowski (loc.cit.) that, for constant matrix elements and non-direct transitions, the fractional number of electrons excited from the valence band to a conduction band state of energy E, G(E), may be expressed in the form:-

$$G(E) = N_c(E)\,N_v(E - \hbar\omega) \Big/ \int_{E_f}^{E_f + \hbar\omega} N_c(E)\,N_v(E - \hbar\omega)\,dE \qquad (3.4.)$$

Now, for a fixed ω this may be reduced to:-

$$G(E) \propto N_c(E)\,N_v(E - \hbar\omega) \qquad (3.5.)$$

Therefore, in order to work out the relative probabilities of various transitions we must first work out this expression. Unfortunately, this distribution cannot be described by some simple relation so, instead of considering it analytically, it is necessary to treat the distribution as a histogram of energy interval ΔE. If the histogram is then integrated and normalised, using a Simpsons rule integration, and a normalised random number a_2 is selected, the probability of it falling between

$N_c(E)N_v(E - \hbar\omega)$ and $N_c(E + \Delta E)N_v(E + \Delta E - \hbar\omega)$ will be proportional to the area of that segment of the histogram i.e.

$$N_c(E)N_v(E - \hbar\omega)\Delta E \qquad (3.6.)$$

since ΔE is a constant, this will achieve the desired effect of biasing the energy selection towards higher values of the density of states. However, in practice this results in a problem since the computer must then make a search to determine between which points on the normalised histogram a_2 lies, which is very time consuming. It is thus necessary to take steps to remove the need for this search. This was done by taking a one-dimensional array X of 10,000 'slots'. Each element of this array was assigned a value of E, the number of elements with any particular value of E being proportional to the probability of selection of that E (i.e. $N_c(E)N_v(E - \hbar\omega)$ see Figure 3.2.). Thus in selecting a_2, the value of E assigned to $X[\text{int.}(a_2) \times 10{,}000]$ was chosen as the electron energy, achieving the necessary bias without the need for a search.

In practice, the selection was of course limited to those values of E allowed by the exclusion principle. This technique results in some quantization of the energy selection but, since $\Delta E = 0.1$ eV, this was not significant. A record was kept in the programme of the values of E selected, and this was printed out at the end to check the procedure.

The initial energy E having been selected, the excited energy E4 is thus $E + \hbar\omega$. If $E4 < E_f + \phi$, the electron is considered to be unable to escape and a new photon is then

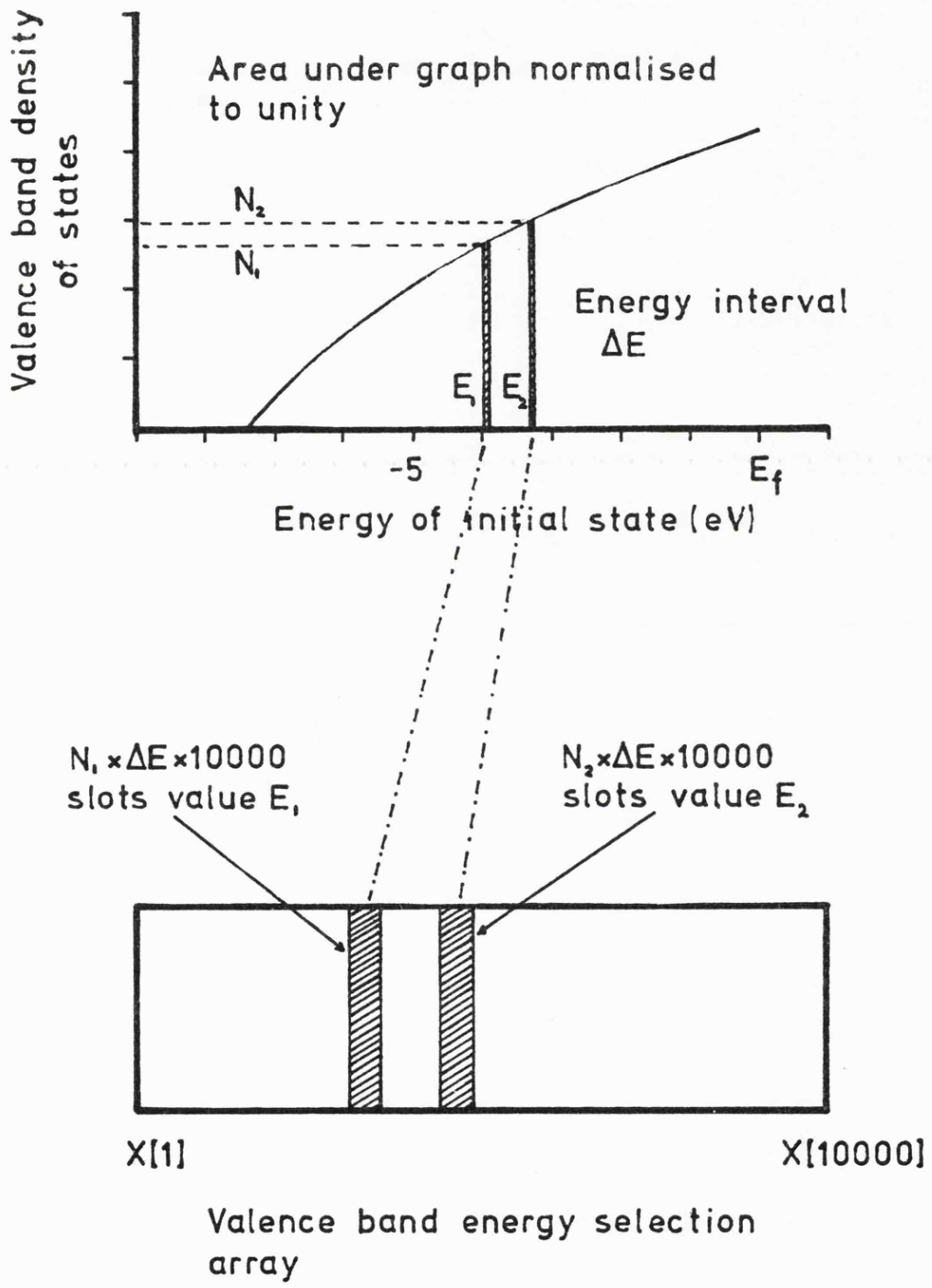

Fig.3.2-Setting up of energy selection array.

considered.

If the initial selection energy E is low enough, there is a possibility of the generation of an Auger electron. This will be considered in 3.2.6.

3.2.4. The Electron Walk

The energy of the excited electron having been decided, it is then necessary to decide how far the electron will travel and in what direction. Since we are dealing with a liquid metal, it is not unreasonable to assume that the material is isotropic and there is an equal probability of the electron travelling in any given direction. In this case the direction of travel may be defined simply in terms of one angle Θ, the angle to the normal to the surface. This assumption is not a limitation of the programme, as it would be simple to programme a bias into the distribution (as for the electron energies) if we were dealing with a crystal. However, if the value of is selected according to the expression:-

$$\cos(\Theta) = 2(a_3 - 1) \qquad (3.7.)$$

where a_3 = normalised random number

as derived by Stuart and Wooten (loc.cit.), it may be seen that this will yield an isotropic distribution.

The determination of the distance 'walked' is rather more difficult. We are concerned with two scattering processes, each with its own mean free path, of which one (l_e) is energy dependant. However, for any given l_e and l_p, it is possible

to define a total mean free path (l_t) in terms of the expression:-

$$\frac{1}{l_t} = \frac{1}{l_e} + \frac{1}{l_p} \qquad (3.8.)$$

As in the case of the photon walk, the probability of the electron travelling a distance l before a collision will vary exponentially, and thus the 'walk' length may be selected according to an expression similar to (2) to give the correct distribution, i.e.

$$l = -l_t \ln(a_4) \qquad (3.9.)$$

where a_4 = normalised random number.

For the purpose of this study it was decided to use the expression for l_e derived by Krolikowski (loc.cit.), i.e.

$$l_e(E) = L_o \frac{\sqrt{E}}{\int_{E_f}^{2E_f - E} d(E_V^o) \int_{(E_f - E_V^o)}^{\frac{1}{2}(E - E_V^o)} d(\Delta E)\, N_V(E - \Delta E)\, N_C(E_V^o + \Delta E)} \qquad (3.10)$$

where L_o is a normalisation constant fixing the value of l_e at a particular final energy E_f^o.

For a free electron material this may be approximated to the form:-

$$l_e(E) = L_o E^{-3/2} \qquad (3.11.)$$

and this was used in the programme. Again, this is not a basic limitation in the simulation - by definition of a suitable one-dimensional array for l_e, any biasing could be achieved. This form for l_e was simply used as a convenient starting point.

The length and direction of the electron walk having been determined by the above means, it now remains to decide whether the walk will bring the electron to the surface. Since the initial depth of generation (x_1) is known, the new distance from the surface will now be:-

$$x = x_1 - l\cos\theta \qquad (3.12.)$$

If this is now negative (i.e. the electron has reached the surface), the energy of the electron normal to the surface is then calculated to see if the electron can escape, i.e.

$$E\cos\theta > \phi \qquad (3.13.)$$

If this is so, then the fact is recorded in the fate counters along with the electron energy outside the material and its angle of escape. If not, then the electron is considered to have been reflected (i.e. x becomes -x).

3.2.5. The Collision Process

If the electron does not reach the surface, or is reflected, the type of scattering event it undergoes must be decided. This may be done simply in terms of the mean free path, since the probability of it undergoing an electron-electron event may be expressed in the form:-

$$P \propto l_t/l_e \qquad (3.14.)$$

see Stuart and Wooten (loc.cit.).

Thus by choosing a normalised random number a_5, correct biasing will be given by the conditions:

if $a_5 > l_t/l_e$ the event is electron-electron

if $a_5 < l_t/l_e$ the event is electron-ion

3.2.5a Electron-ion Events

The process is considered quite simply in terms of the electron either gaining or losing (with equal probability) a quantum of energy E_p. E_p is considered for the purpose of the simulation to be $\simeq 0.04$ eV, but for $E_p < 0.1$ eV the programme was not sensitive to the exact value. The sign of the energy exchange was determined by a normalised random number a_5 by the conditions:

$a_5 > 0.5$ E_p positive

$a_5 < 0.5$ E_p negative

3.2.5b Electron-electron Events

This process is rather more complicated. The probability of an electron of energy E_1 interacting with an electron of energy E_2 with an associated energy exchange of ΔE may be expressed in the form:

$$P \propto \int_{E_1-E_2}^{0} N_c(E_1-\Delta E)\, N_c(E_2+\Delta E)\, d\Delta E \qquad (3.15.)$$

(Since the electrons are indistinguishable, an energy exchange of $\Delta E > (E_1 - E_2)/2$ need not be considered).

To take full account of this in deciding the value of E would be very difficult, since it would be necessary to work out the product $U(E) = N_c(E_1 - \Delta E)\, N_c(E_2 + \Delta E)$

for all possible values of E_1 which would require an impossible amount of storage space in the computer. However if $N_c(E)$ is considered to have a simple form, such as a free electron variation, it may be shown that the form of $U(E)$ does not vary significantly over a large range of E. Thus if $U(E)$ is worked out for the maximum value and put into an array (as for $N_v(E)$ $N_c(E + \hbar\omega)$), ΔE may be selected from this without introducing too much error. E_2 is then selected for the initial probability array, limiting the choices to $E_1 - E_2 > E_f - E$ to take account of the exclusion principle.

Thus E_2 and ΔE have been determined taking account of the necessary factors in the probability expression but in a form that is fairly simple to programme. The final energies will be $E_1 - \Delta E$ and $E_2 + \Delta E$, the higher energy always being considered to be that of the primary.

After the scattering event, the secondary is followed for one further walk to see if it escapes. If it does not, it is then neglected. The primary is followed until its energy is too small to allow it to escape.

3.2.6. The Auger Process

When an electron is excited from below the Fermi level it leaves a hole with which an electron higher in the band may recombine with the release of some energy E°. This energy may then excite another electron to above the Fermi energy (see Figure 2.5.). The energy of the electron which recombines with the hole may be selected using the previously set up probability array - disregarding those energies which are below the energy of the hole, i.e. the random number selection is limited to those

states permitted by energy considerations. This determines the energy available for excitation of the second electron (if this is less than β, the energy is too small to need to be considered). Its energy may be selected from the same probability matrix, having regard for the exclusion principle. The Auger electron is then treated in the same manner as for a secondary electron i.e. is followed for one walk, examined for boundary conditions and then disregarded if it does not escape.

3.2.7. The Fate Counters

There are three sets of counters for the escaped electrons - one for primaries, one for secondaries and one for Auger electrons. For the purposes of these counters a primary is considered as an electron that escapes without undergoing an electron-electron collision. These are basically a series of slots to which the electron is allocated according to its energy and angle of escape.

When all the photons have been considered, these counters may be interrogated to obtain the yield and an EDC (or separate yields and EDC's for the individual angular sections).

3.3. Use of the Programme

As stated earlier, several of the necessary factors for the programme will be known e.g. work function, photon energy, Fermi energy and attenuation depth. The electron-ion interaction energy is not known exactly but experiment shows that it is a non-critical factor. The major unknowns will be l_e, l_p and the form of the density of states. Values for l_e, l_p could be

estimated using a short version of the programme which did not contain the fate counters, but only a totaliser for the yields of primary, secondary and Auger electrons. This allowed several values of l_e, l_p to be tried, since less photons are needed to give a reasonably accurate yield compared with the number required for an EDC (about 25,000 photons was found to be adequate on a basis of reproducibility). Experiment showed that the yield is not critically dependant on the density of states, assuming it is basically free electron like. Thus l_e, l_p may be modified to match the programme yield to the experimental yield, and the density of states may then be modified in the full programme to match the predicted EDC to the experimental one.

3.4. Results

3.4.1. Free Electron Yield

As mentioned earlier, this programme and that of Krolikowski are based on the same 3-step model. It thus follows that, since the major difference in the two programmes is the inclusion of electron-phonon scattering, for $l_p = \infty$ the two should give identical results. Accordingly, both programmes were run for a free electron density of states over a range of photon energies, the results of which are shown in Figure 3.3. It may be seen that the agreement is highly encouraging. The values of α and l_e are fairly typical for a free-electron-like material.

3.4.2. Effects of Electron-phonon Interaction

The programme was run using a free electron density of

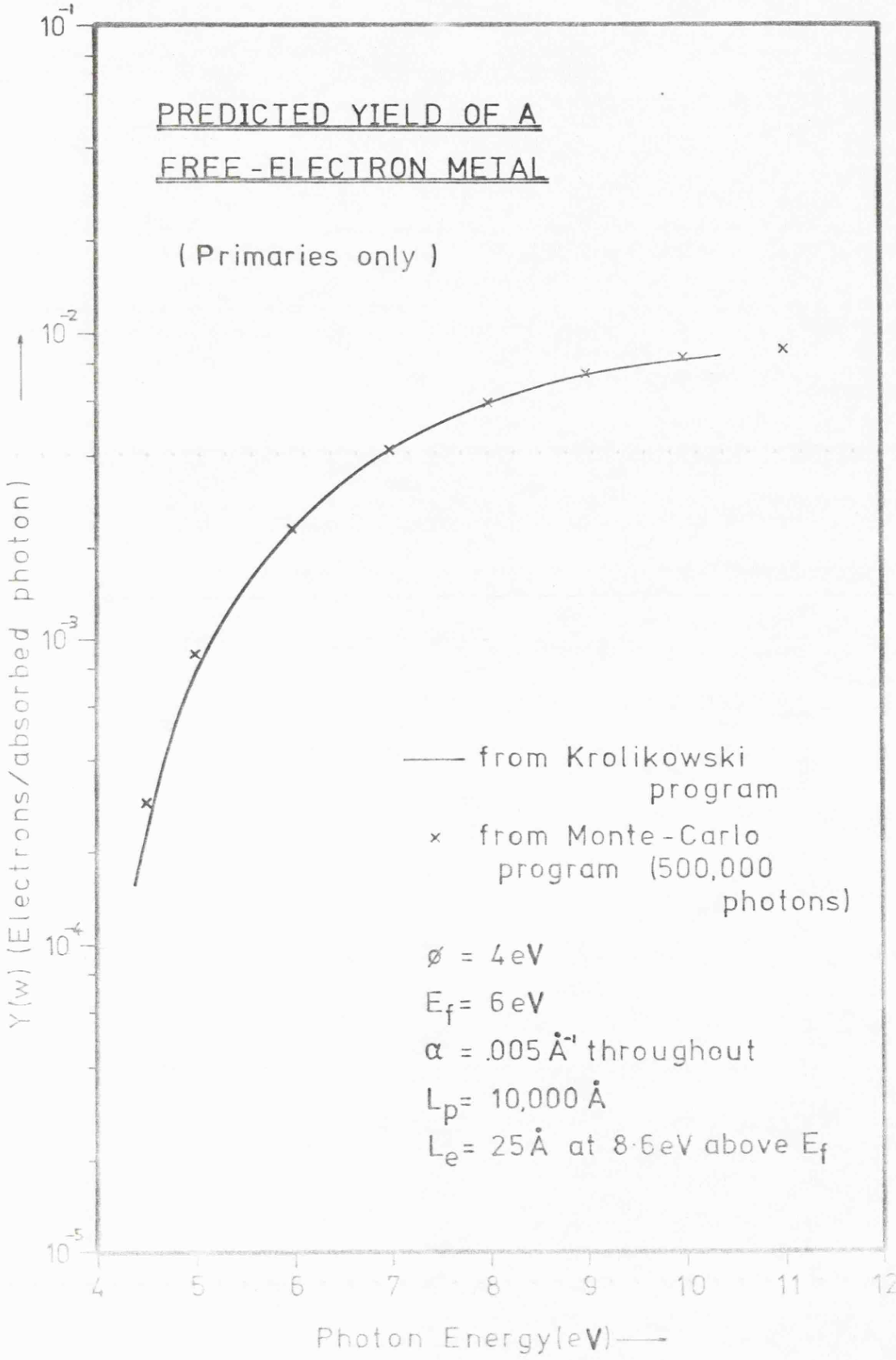

Fig 3.3-Predicted yield of a free-electron metal

states for a range of values of l_e and l_p to determine the effect of electron-ion interaction. Figure 3.4. shows how the escape depth (i.e. the average depth of generation of those photoelectrons that escape) varies with l_p for a variety of values of l_e. It may be seen that it is very strongly dependant upon both parameters, though less dependant on l_p and only becoming seriously affected by this when it is appreciably less than l_e. It does however vary almost linearly with l_e.

Figure 3.5. shows the variation of the primary yield with l_p for a range of values l_e. It is immediately apparent that the yield is not strongly dependant on l_p but varies almost linearly with l_e. A low value of l_p when l_e is large can however cause an increase in the yield. On a simplistic basis this may well be considered to be due to the low l_p causing an increased probability of scattering the electron towards the surface whilst the high l_e reduces the probability of a collision that might result in a significant energy loss.

It is thus apparent that the major effect of a low l_p is on the escape depth rather than the yield, and this indicates that the Krolikowski programme should give adequate results even for a liquid metal.

3.4.3. Prediction of EDC's

As pointed out in 3.1., the major limitation of a Monte Carlo process is that, in order to reduce the statistical uncertainty in a result, a large number of events must be considered, with a consequently long computing time. Figure 3.6. shows a predicted EDC (for a free electron density of states)

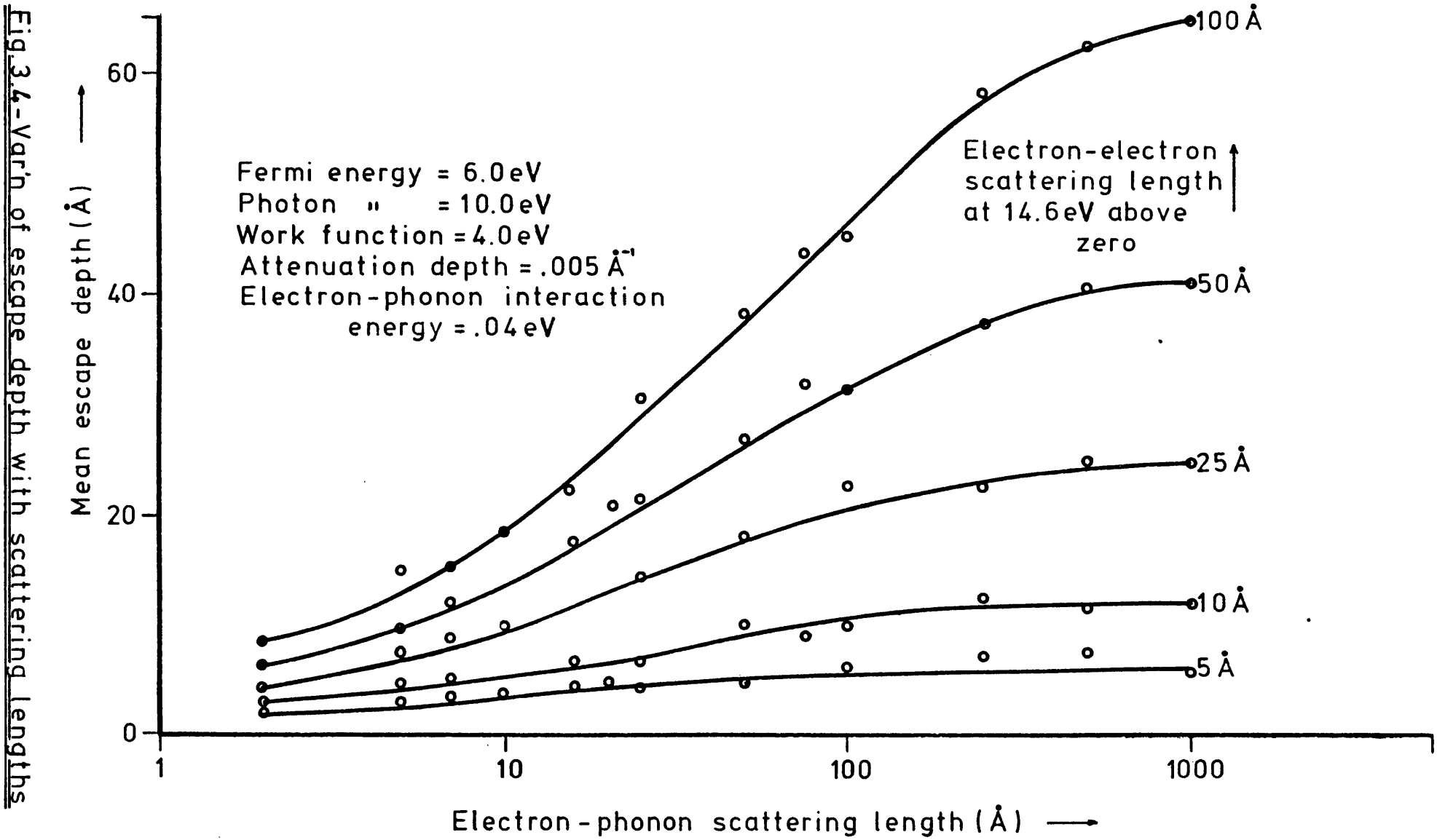

Fig.3.4-Var'n of escape depth with scattering lengths

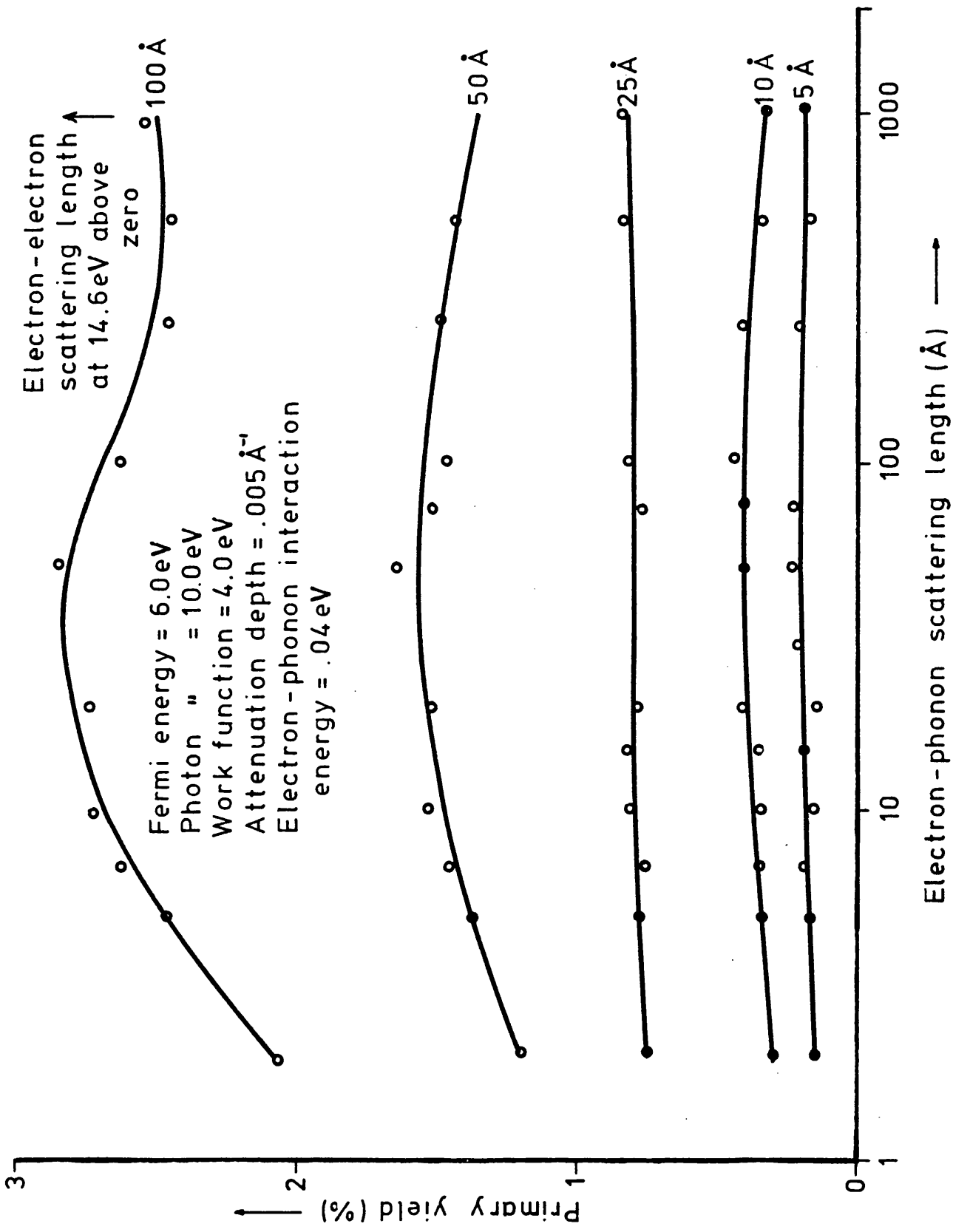

Fig. 3.5 - Variation of primary yield with scattering lengths

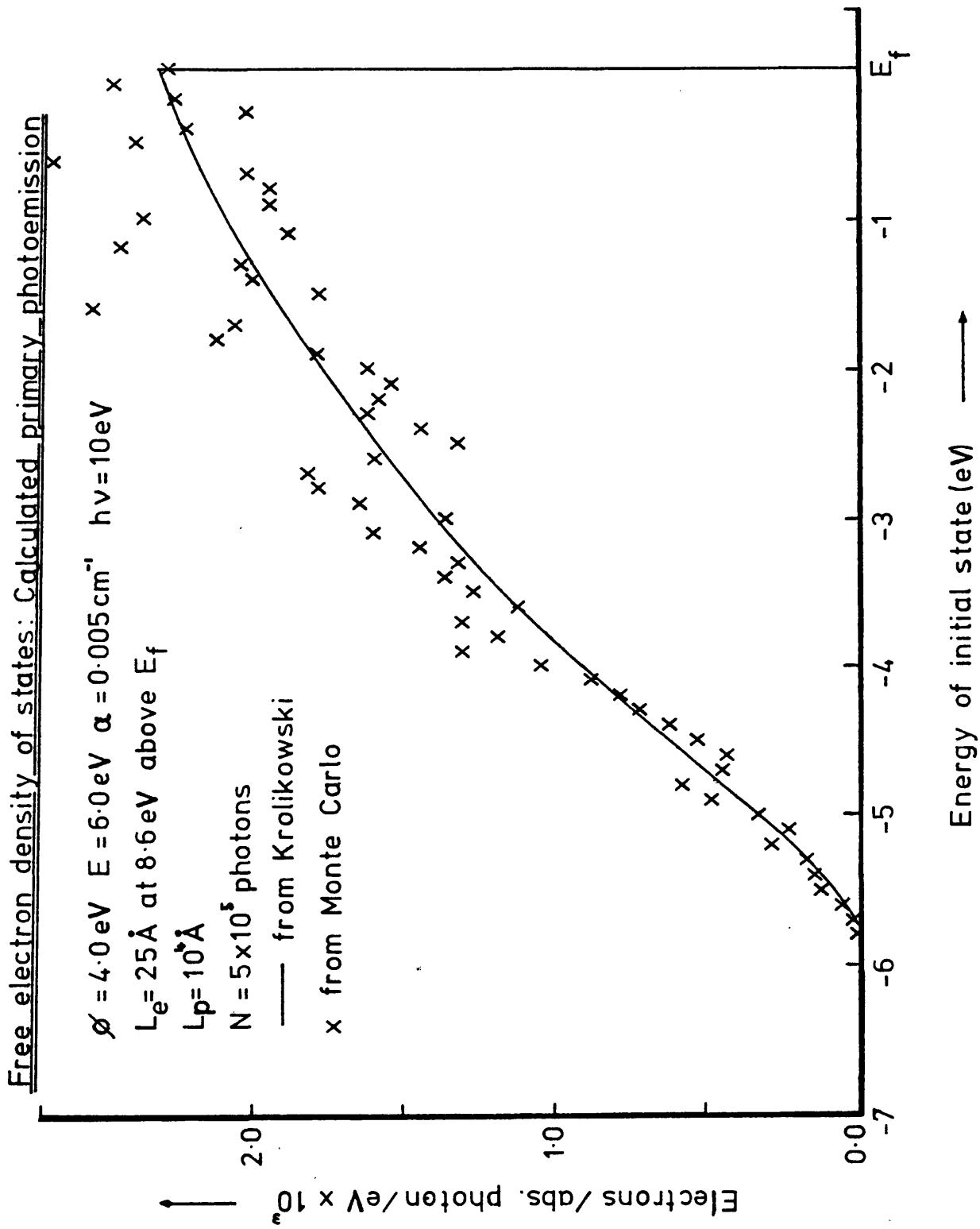

Fig.3.6 - Predicted EDC for a free-electron metal

from the Monte Carlo programme compared with the equivalent Krolikowski EDC. It may be seen that, whilst the general agreement in shape is good, there is a large amount of scatter in the points obtained using the Monte Carlo approach. This could be reduced by increasing the number of photons considered, but it was found that in order to reduce the scatter to an acceptable degree it was necessary to consider of the order of 10,000,000 photons, resulting in the use of an impracticable amount of computer time.

3.5. Interpretation of Results

Whilst this programme was under development, work was also undertaken by Dr. J. Bethel and Dr. S. Holloway of the University of Leicester Physics Dept. to modify the Krolikowski programme to include the effects of both Auger and electron-plasmon processes. These modifications were successful and, in view of the results given in 3.4.2. regarding the effects of variation of l_p and the excessive computer time needed to generate EDC's, it was decided this programme would be adequate for the interpretation of the results obtained in this work.

The programme was used in the following manner to obtain an optical density of states for each material. Using an arbitary density of states as a starting point (usually obtained from the 21.2 eV EDC with the background subtracted), the scattering length l_e was altered on an iterative basis to obtain a match between the predicted yield and the experimental yield at 7.7 eV.

The predicted EDC was then examined and the initial

density of states modified (again on an iterative basis) until there was good agreement between predicted and experimental EDC's at 7.7 and 10.2 eV. Figure 3.7 shows the flow chart for this process. Figure 3.8 shows the resulting EDC's for liquid indium at 10.2 eV. T1 is the initial density of states from the 21.2 eV EDC, T2 is the first modification made, as described above, and T3 is the final optical density of states.

In all cases considered it was found to be unnecessary to take into account the possibility of there being structure in the density of states above the Fermi energy. A free electron density of states was used in all cases and was found to be perfectly adequate (this is not true for other metals - Wotherspoon (1978) found that for bismuth, using the same technique, the existence of structure in this region had to be considered).

So far there has been no consideration of experimental broadening effects. After the final optical density of states had been arrived at, this was deconvoluted assuming the broadening to take the form of a Lorentzian distribution (i.e. a delta function would be reproduced as a curve described by the equation

$$g(x) = \Delta x \Big/ 2\pi\left[(x - x_0)^2 + (\Delta x/2)^2\right] \qquad (3.16.)$$

where x is the half-width and x_0 is the position of the centre of the curve). The deconvolution was done on an iterative basis i.e. a trial density of states was convoluted compared with the final optical density of states and then modified until

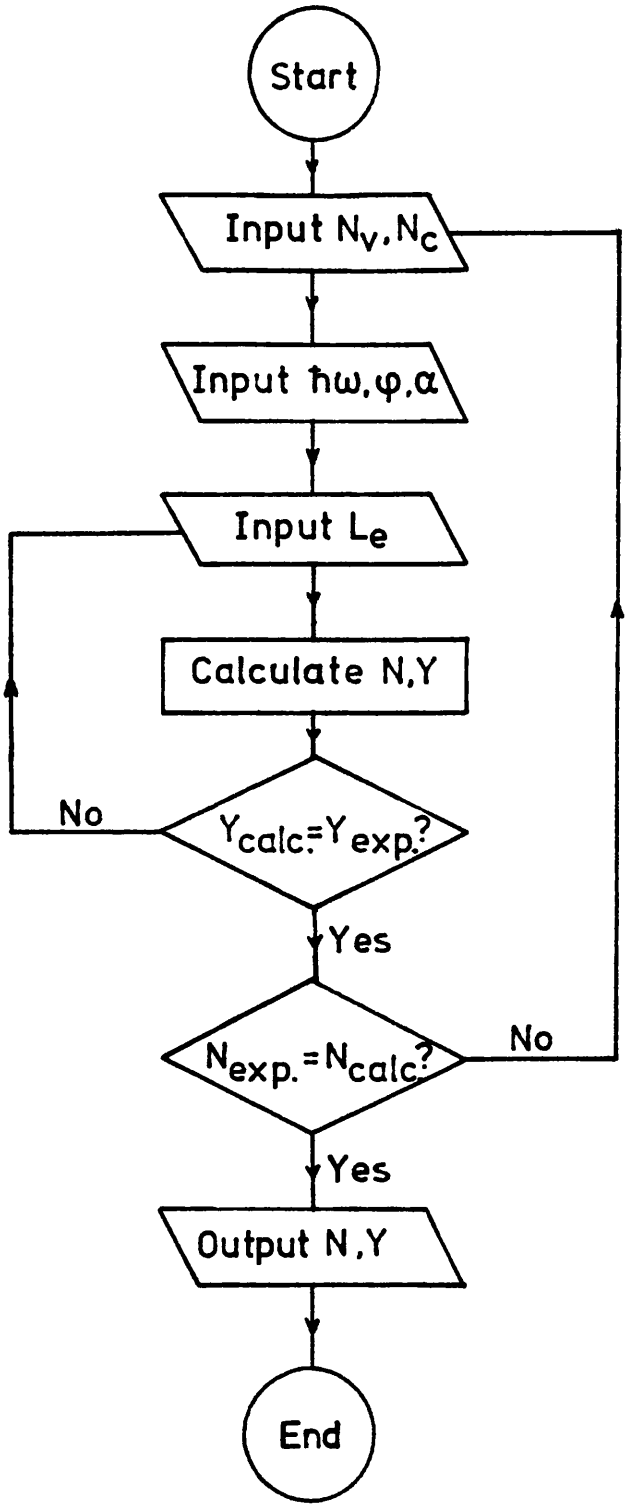

Fig.3.7- Flow chart for the calculation of an optical density of states

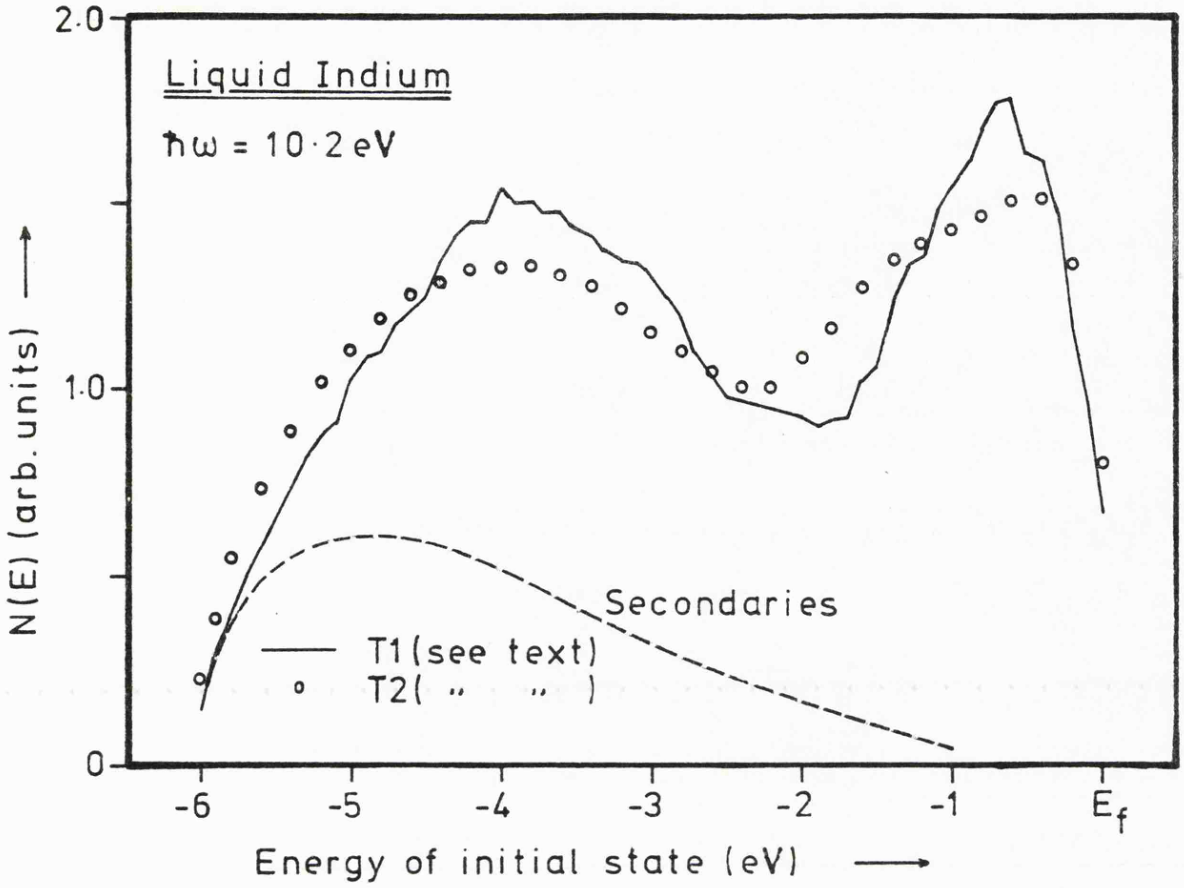

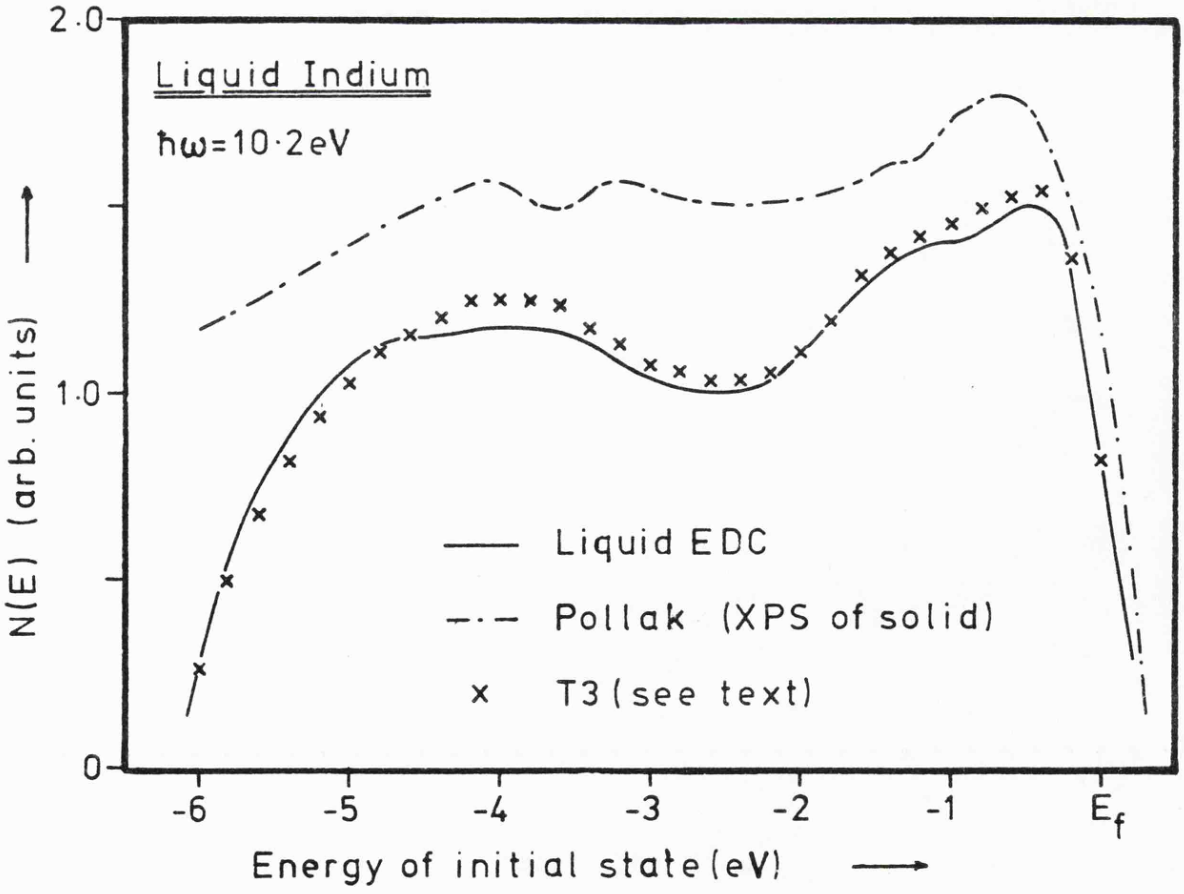

Fig. 3.8 - Trial densities of states for liquid Indium

agreement between the two was reached.

Strictly speaking this deconvolution should have been used on the final EDC to obtain the optical density of states. However it was found that applying the process to the optical density of states already obtained gave an adequate result and, since this was far less time consuming, this technique was adopted.

The optical densities of states obtained are given in the chapters on the different materials. Also shown are the predicted EDC's based on the optical density of states. In these both the total EDC (as a sum of both the primary (Y_p) and background (Y_b) yields) and the contribution due to the background emission (i.e. secondary yield and Auger yield etc.) are indicated.

Typical results for indium give the following yields:-

$h\nu$ = 7.7 eV

Primary yield =	0.0034	electrons/abs. photon
Secondary " =	0.0005	electrons/abs. photon
Auger " =	0.0001	electrons/abs. photon

$h\nu$ = 10.2 eV

Primary yield =	0.0047	electrons/abs. photon
Secondary " =	0.0015	electrons/abs. photon
Auger " =	0.0002	electrons/abs. photon

CHAPTER 4 :- THE EXPERIMENTAL APPARATUS

In this chapter, the apparatus used in this study, the experimental technique, and the possible sources of error are discussed. There are, of course, considerable difficulties involved in the experiment. Extreme surface cleanliness is required, making it necessary both to prepare and keep the surface in ultra high vacuum, and the photocurrents involved are very small, so that highly sensitive electronics are needed for their detection.

The apparatus required for a photoemission experiment may be considered in three main sections. Firstly a source of photons capable of covering the necessary energy range, secondly a vacuum system capable of allowing the preparation and maintenance of an atomically clean surface, and thirdly an electronic system to detect and analyse the photoelectron spectra. Figure 4.1. shows the basic layout of such a system. The apparatus was, of course, under continuous development during the course of the study and it is the final version, with which the major part of the work was done, which is described here. Any modifications required for a particular material are described in the chapter relating to that material.

4.1. The Optical System

Two different photon sources were used for this work, covering the energy range 3 - 21 eV. Since the largest of the valence bands is that of aluminium at 11.1 eV, this means that the whole of the valence bands of all materials used could be studied, and the core states of mercury could also be investigated.

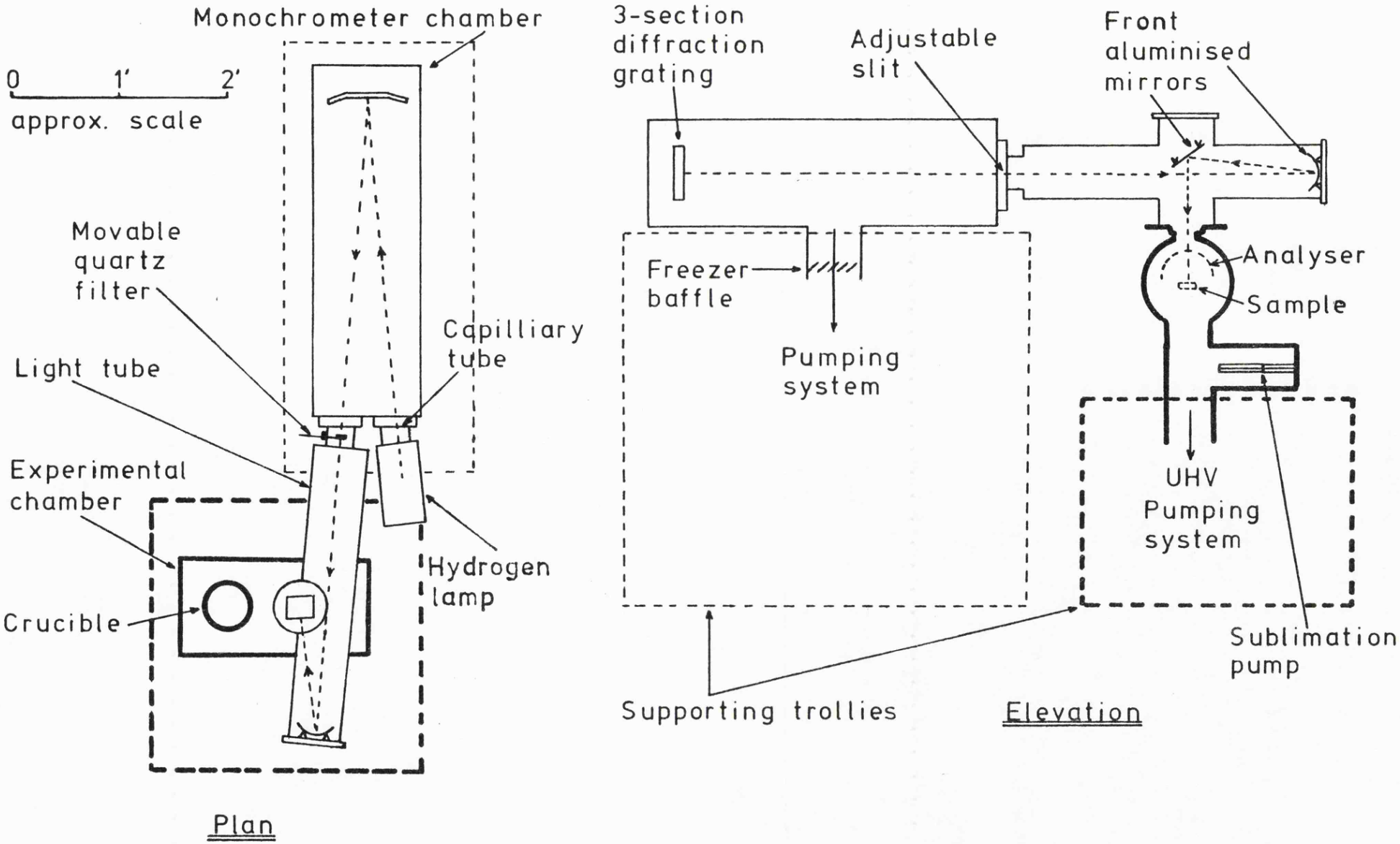

Fig. 4.1 - General system layout

4.1.1. Photon Energies < 12 eV

The range of photon energies from 3 - 12 eV was covered by use of an Hinterregger hydrogen discharge lamp, which gives several strong spectral lines between 11.2 eV and 7.6 eV and a continuous spectra below 6 eV. A typical lamp output spectrum is shown in Figure 4.2. Individual photon energies were selected by coupling the lamp to a 1 metre diffraction grating monochromator (Hilger and Watts type 760). This uses a Bausch and Lomb 3-section 600 line/mm. diffraction grating blazed at 1500 Å with a dispersion of 16.0 Å/mm. at the exit slit. The grating could be rotated either by hand or automatically by means of a variable speed motor. The lamp was modified following an investigation into the possibility of increasing the output by inclusion of a heated filament in the discharge as described by Eastman (1972). Unfortunately this technique was found to be unreliable in operation and damaging to the grating, but it was discovered however that the use of a water-cooled stainless steel cathode (instead of the standard air-cooled aluminium one) resulted in a far more stable lamp output, and the lamp required cleaning much less often.

Typically the lamp output over the range 7 - 10 eV was stable to <5% over a period of several days (including a complete shutdown of the system overnight), and was stable to <2% over a period of 24 hours. The lamp was differentially pumped through a 1 cm. length of 1.5 mm. bore pyrex capilliary connecting it to the monochromator, which replaced the normal entry slits. This enabled the lamp to be run at a pressure of 0.4 torr whilst maintaining the monochromator at 7×10^{-5} torr. Typical

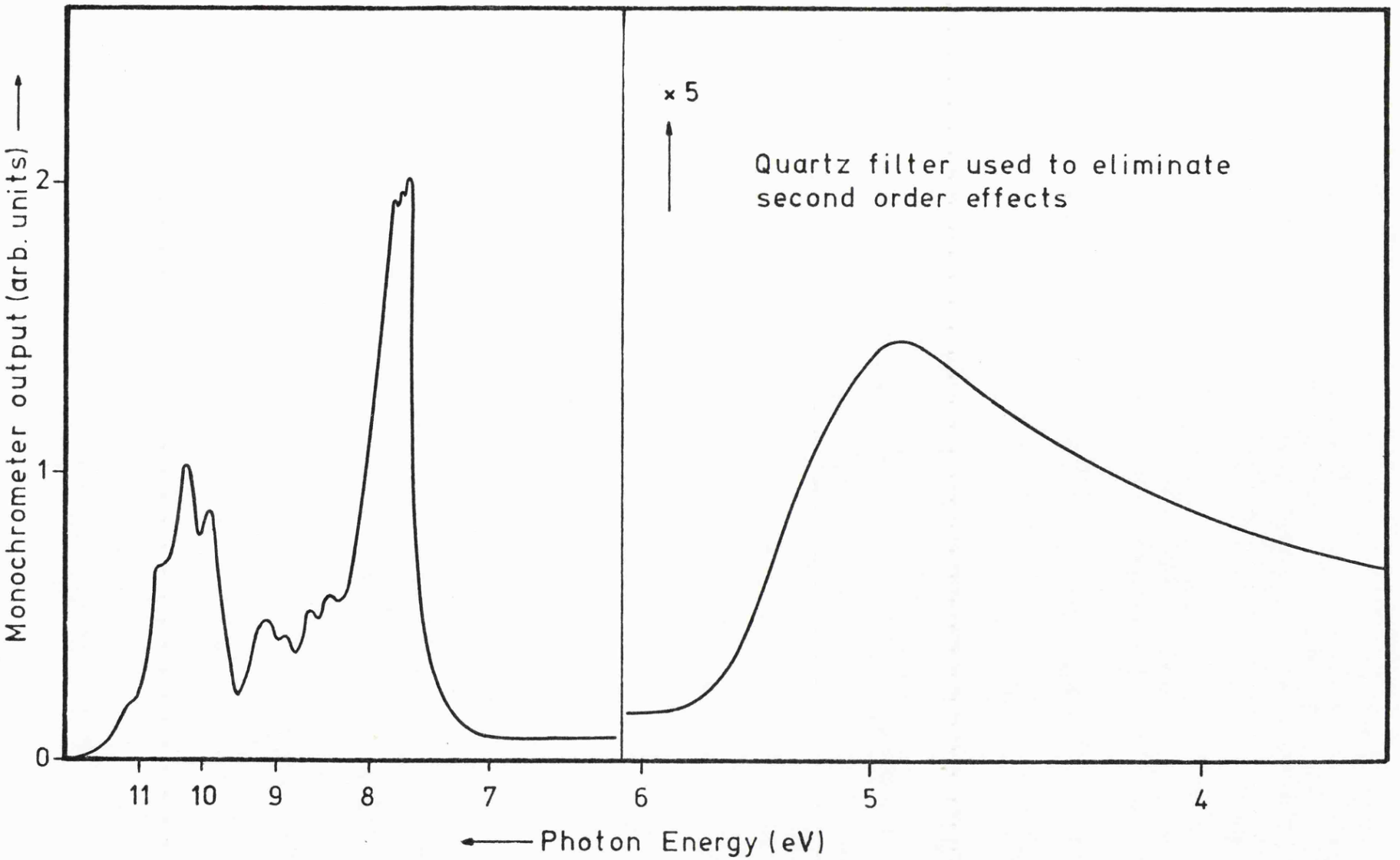

Fig. 4·2 - Output spectrum of the hydrogen lamp

operating current and voltage were 400 mA, 800V DC. An attempt was made to pump the lamp separately using a LiF window between the lamp and the entry slit, so that the lamp could be run at higher pressure, but the static charge caused by the ionizing radiation attracted oil vapour to the window causing a rapid degradation of its transmission.

The monochromator was mounted horizontally and was pumped by a 4" oil diffusion pump using a freezer baffle and Convalex 10 oil to minimise vapour contamination of the grating. Since the system was horizontally mounted, a 2-mirror system was used to bring the photons normally onto the liquid surface. These mirrors were fixed in an evacuated brass tube using adjustable mountings to allow the focussing of the light onto the liquid surface. The tube was coupled to the exit slits of the monochromator and to the window flange on the chamber. The mirrors were front silvered aluminium, coated with MgF_2 and had a reflectivity of >80% at 1216 Å. The tube also contained a quartz filter which could be inserted in the beam path to remove second order effects when working at low photon energies. Instead of coupling the tube to the chamber it could be coupled to a fitting which mounted a sodium salicyclate phosphor in front of a photomultiplier tube (EMI 62568) enabling a relative measure of the lamp output to be obtained. The fitting also allowed the LiF window from the chamber to be placed in the beam path so that its transmission could be measured.

4.1.2. Photon Energies >12 eV

This range of energies was covered by a noble gas

discharge lamp utilising either helium or neon. This gave photons at the resonance energy of the gas - either 16.8 eV (Ne I) for neon or 21.2 eV (He I) for helium. Higher energy discharge lines exist for both gases but due to their low intensity they were not used in this study. The construction of the lamp is essentially the same as that used by Broden, Hagstrom and Norris (1973) with the exception of an 'in-line' Hinterregger-type anode-cathode arrangement. It was connected to the chamber by being directly mounted onto the top flange above the electron analyser, replacing the lithium fluoride window and optical system used for low energy work. The lamp was differentially pumped directly below the discharge by a rotary pump, and between the two narrow-bore light pipes by a diffusion pump. This dual pumping system enabled a pressure of $<10^{-9}$ torr to be maintained in the chamber whilst there was a pressure of 8 torr in the discharge capilliary. Typical operating current and voltage were 100 mA, 800V DC.

The gas used in the lamp was of commercial grade and was purified by passing through filters of activated charcoal cooled by liquid nitrogen. The gas extracted from the lamp, immediately below the discharge, by the rotary pump could be recirculated by passing through an activated alumina trap and then again through the charcoal traps to remove any traces of oil.

An estimate of the contribution of hydrogen contamination to the lamp's spectral output could be gained by insertion of a LiF filter (cut-off at 12.6 eV) between two of the capilliary sections.

4.2. The Vacuum System

Experiments involving the measurement of low energy (< 200 eV) electrons ejected from conductors, whether ultra-violet photoelectron spectroscopy (U.P.S.), low energy electron diffraction (L.E.E.D.) or Auger electron spectroscopy (A.E.S.), tend to be very surface sensitive due to the low electron mean free paths in the contamination layer. Thus it is essential that the surface be prepared and maintained free of contamination. However, a clean surface in air at atmospheric pressure will be covered in a monolayer of oxide in 10^{-6} seconds (if a unity sticking coefficient is assumed), and a practicable experiment of this type takes minutes at the very least. This requires that the experiments be performed in UHV (i.e. pressures < 10^{-9} torr) and, due to the high vapour pressure of liquid metals, a special technique must be devised to prepare a clean surface.

4.2.1. The Experimental Chamber

The preparation and measurement were carried out in a single stainless steel chamber in the form of a cylinder 6" in diameter and 15" long (see Figures 4.3. and 4.4.), at one end of which was fitted a 5" diameter observation window and at the other the main analyser flange. On top of the chamber were mounted two ports, to one of which was fitted the sample preparation flange, the other being fitted with a LiF window and connected to the light tube. On the side of the chamber were mounted an ion gauge, a linear motion drive holding a small stainless steel bucket to catch waste material from the pourer, and a flange supporting a gold evaporation assembly to provide a standard

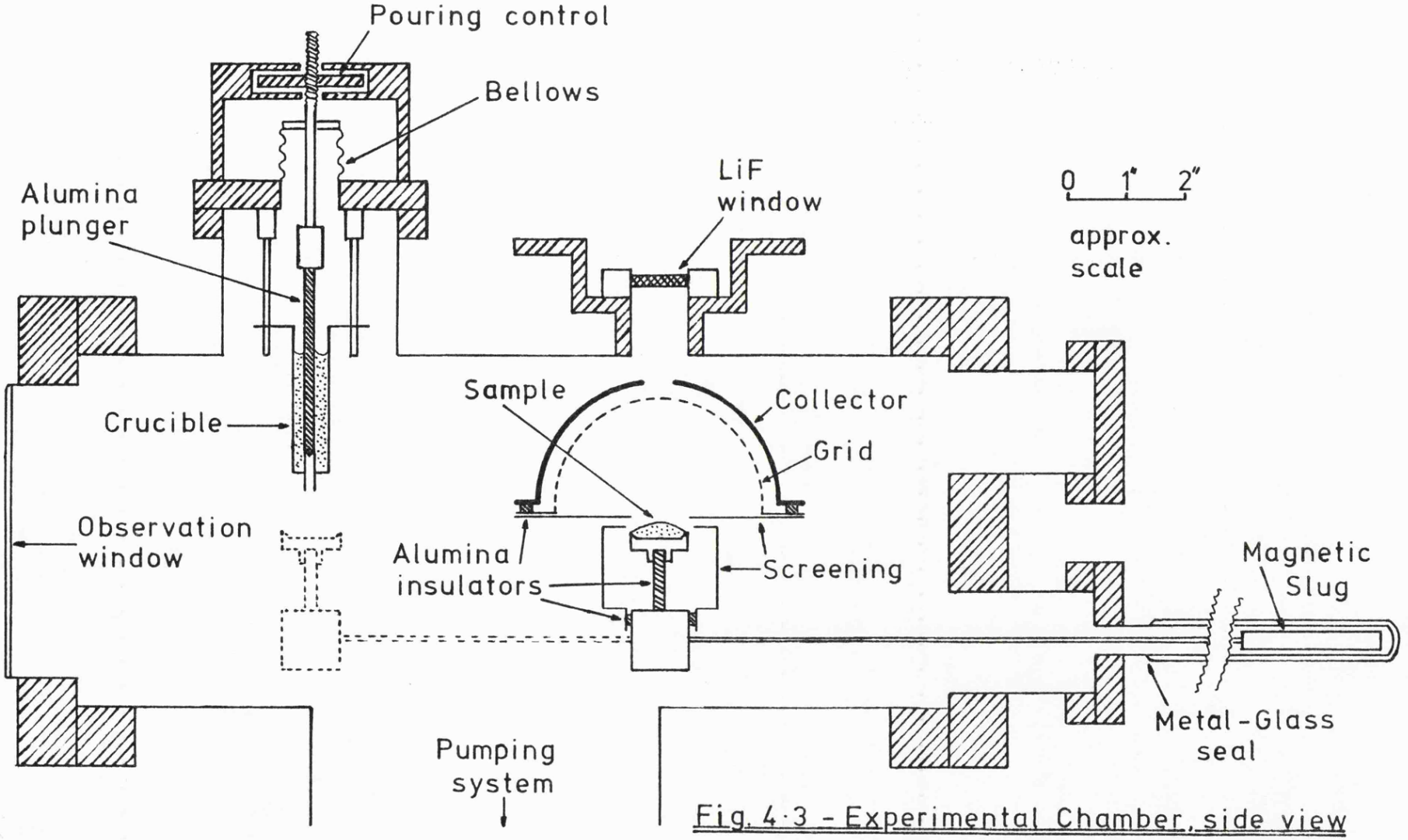

Fig. 4·3 - Experimental Chamber, side view

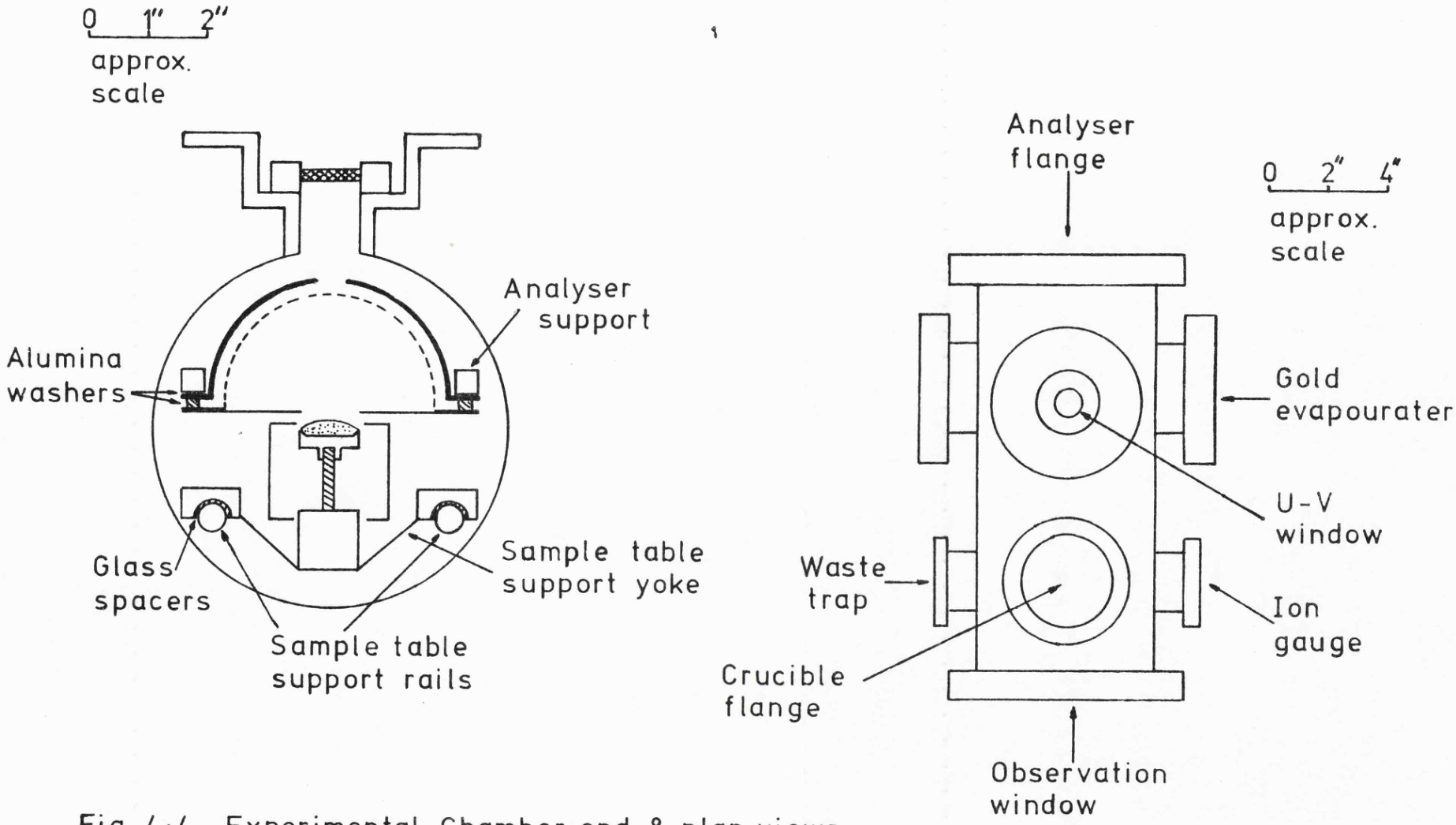

Fig. 4·4 - Experimental Chamber, end & plan views

for yield measurements. The latter consisted of a small stainless steel plate mounted on a magnetic drive which enabled it to be moved from underneath the screened evaporation filament to directly below the aperture in the grid screening where the sample was normally placed. All flanges were sealed with Conflat® knife edge seals and OFHC copper gaskets.

4.2.2. The Pumping System

At the commencement of this study, it was expected that there would be difficulties in pumping the chamber due to the large vapour transport anticipated with liquid metals. For this reason a pumping system consisting of a water cooled Titanium sublimation pump (T.S.P.), and a 3-stage mercury diffusion pump (Edwards UHVM2A) was chosen. This was backed by a 2" mercury diffusion pump and a rotary pump (Edwards ED50). The top of the main pump was fitted with a liquid nitrogen trap and a thermoelectrically cooled chevron baffle. Oil backstreaming was prevented by two molecular sieve filters connected above the rotary pump. A base pressure of $< 3 \times 10^{-10}$ torr could be achieved after a 12 hour bake at 250°C. (The baking temperature being limited by the AgCl seal on the LiF window). The residual partial pressure of mercury after bakeout, as measured by mass spectrometer, was $\simeq 2 \times 10^{-12}$ torr. The principal contaminants remaining in the system were H_2O, N_2 and CO.

In practice, except in the case of mercury, vapour transport was found not to be a problem, and later an ion pump (Ferranti 220l/sec) - TSP combination was successfully used instead.

The pumping system and chamber were mounted on a trolley to enable bakeout to be carried out away from the optical system.

4.2.3. The Crucible Flange

The extreme surface cleanliness required in a photoemission experiment raises several problems. Owing to the ease of evaporation of liquid metals, it is not always possible to use heat cleaning, as this could result in loss of the sample. Simply melting cleaned solid indium has been tried (Koyama 1968), but it has proved virtually impossible to remove oxide from the surface. Argon ion bombardment has also been tried (Stevenson 1968) but this has been unsuccessful - possibly because the surface is mobile and non flat.

The method decided upon was that of pouring from a crucible. This has been used before (Stevenson loc.cit.), but in the present case had two important additions. Firstly the entire crucible was mounted within the vacuum chamber, enabling the material to be outgassed in a good vacuum at a temperature well above the working temperature without evaporation in the working area, and secondly the crucible had a re-entrant tube to allow pouring from the centre of the melt which was free of oxide film or heavy contaminants. The success of this technique may be seen from the results given later, this being the only monitor of surface cleanliness.

The construction of the crucible is shown in Figure 4.5. Crucibles of three materials were used - stainless steel, quartz and alumina. Those of steel and quartz were heated by electron bombardment from a thoriated tungsten filament (the quartz having been covered in an outer sheath of several layers of 0.002" stainless steel). With +2000V applied to the crucible, and an emission current of 40 mA, temperatures in the region of 700^{o}C

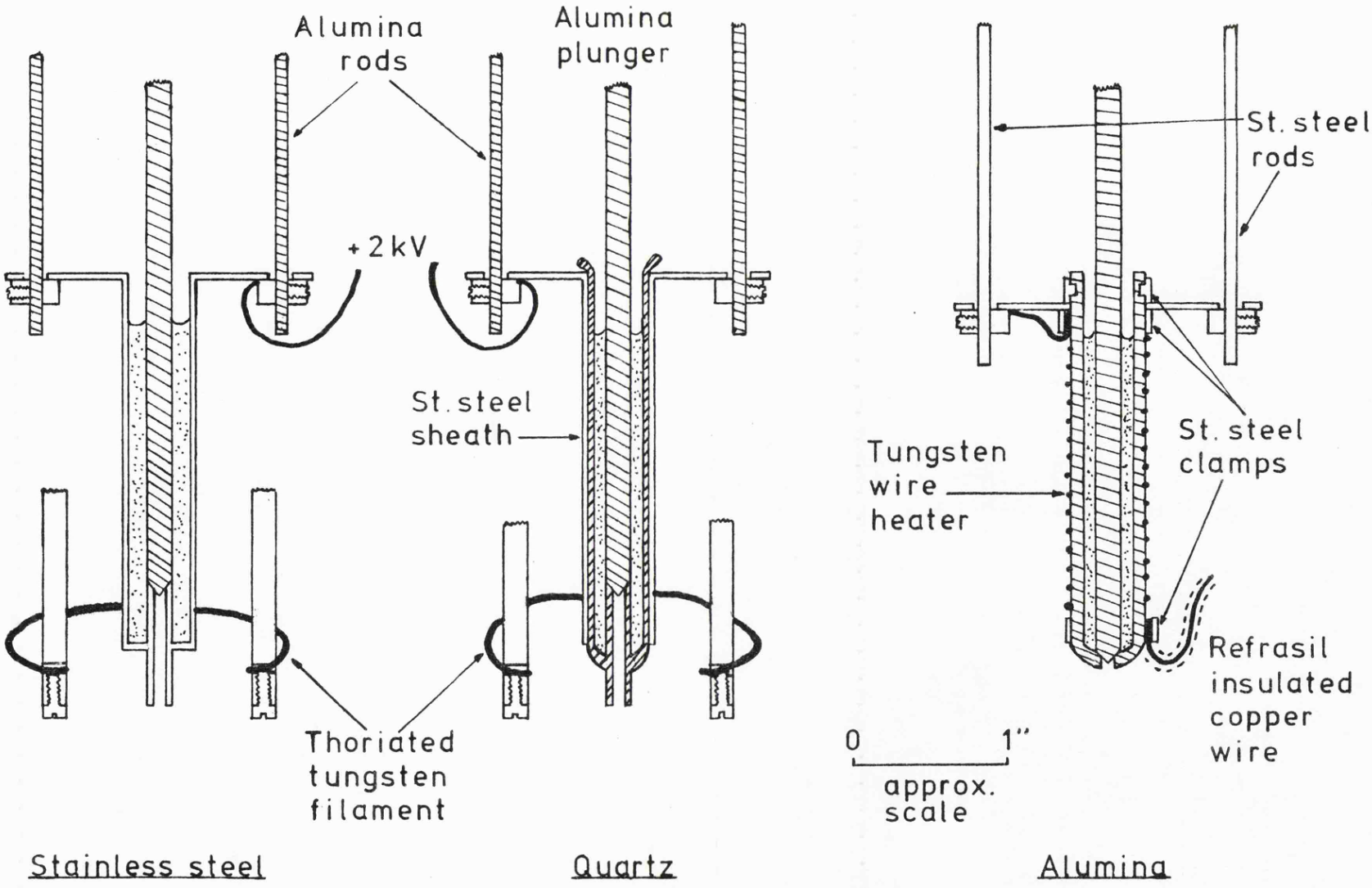

Fig. 4·5 - Types of crucible & heating methods

were achieved. The alumina crucibles were heated (up to 900°C) by a tungsten filament wound round the outside. These alumina crucibles lacked a re-entrant tube, due to manufacturing difficulties, and heavy contaminants were removed by allowing several drops of metal to fall into the waste trap before pouring the sample. All crucibles were sealed by alumina rods which were carefully ground in to achieve a good seal. With alumina and quartz crucibles, care was needed when heating to avoid thermal shock to the materials.

4.2.4. The Photoelectron Analyser.

The electron analyser itself was a retarding field instrument. It had 3 electrodes - the specimen table and an aluminium hemispherical collector 4" in diameter inside which was mounted a hemispherical grid of stainless steel mesh (0.001" diameter wire, >90% transmission), three inches in diameter. A flat plate of 0.005" stainless steel covered the bottom of the hemisphere. Holes 1" in diameter in the centre of the collector and the bottom plate allowed for the passage of photons and photo-electrons. To even out the work function of the inside of the collector, it was coated in a layer of fine carbon. This was achieved by spraying a suspension of graphite in alcohol over the surface with an artists' air-brush, giving a very even greyish appearance to the inside. A retarding field was applied between screen and collector, and a fixed potential between screen and specimen. The whole assembly was mounted upon a stainless steel yoke affixed to a stainless steel plate which was secured to the main flange by four ½" diameter steel rods, this mounting allowing the centralisation of the light aperture under

the LiF window. Whilst other forms of electron analyser are known to give better resolution, a retarding field type was chosen since it could be used even when there was considerable evaporation and condensation from the heated sample.

The specimen table (Figure 4.6.) consisted of a 1" metal or alumina dish. It was recessed on the underside to accept a tungsten wire heating filament which was held in place by a flat stainless steel plate and insulated with alumina washers. The whole was supported on a 3/16" diameter alumina rod in a 1" cube of stainless steel, electrical connections being passed through the cube in alumina sheaths. A screen of 0.005" stainless steel surrounded the specimen assembly and was mounted on the cube with insulating washers. The cube was supported on the rods affixed to the flange by means of a yoke and could be moved by means of a magnetic drive. The screening around the specimen, whilst normally connected to the grid when in use, had a separate connection to a feedthrough on the flange so that shorting of the screen to the specimen did not necessarily terminate the experiment.

4.3. The Detection System

The circuit used, shown in Figure 4.7., was a modified form of that used by Eden (1970). A balancing capacitor in parallel with the photo-diode was not used as this was found to be unnecessary, the grid screen reducing the out-of-phase AC pick-up sufficiently for it to be suppressed by the phase sensitive detector.

As may be seen from Figure 4.7., the specimen potential

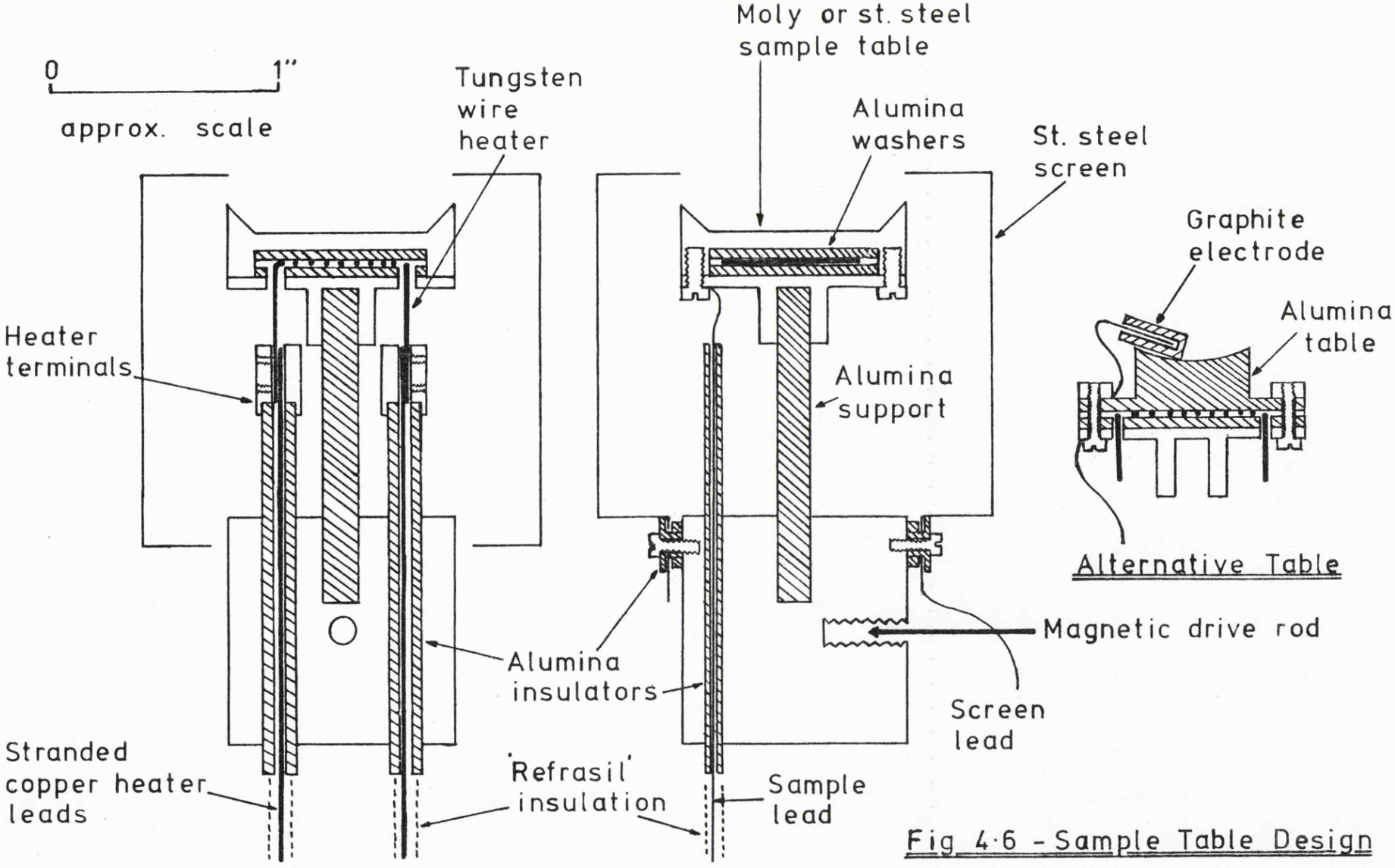

Fig 4·6 - Sample Table Design

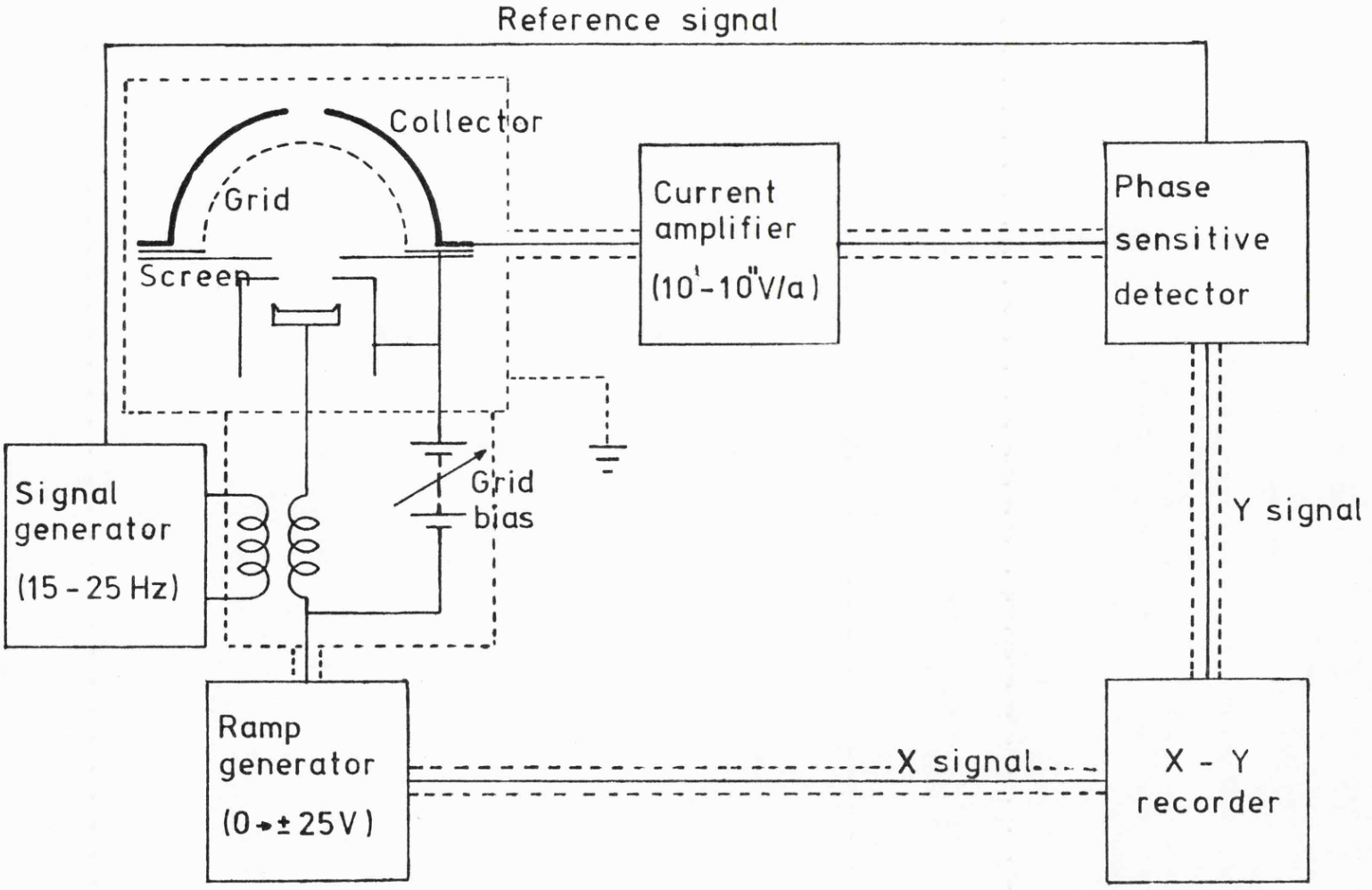

Fig. 4·7 - Detector circuit

was varied by a ramp generator modulated at 15 - 20 Hz, the frequency being chosen to minimise the effects of 'beating' in the electronics. Typical modulation voltage was 0.4V p-p. Photoelectrons travelled first to the screen, which was maintained at a fixed potential with respect to the specimen and then across the retard potential to the collector. The current resulting was then amplified by means of a Keithley 427 current amplifier. High frequency noise and D.C. bias were eliminated by means of the amplifier's variable rise time and D.C. offset facilities (typically 10^{10}V/A amplification, 30 mS rise time).

The signal was then analysed by a phase sensitive detector (PSD) (Brookdeal 401A) and fed directly into the Y amplifier of a chart recorder. Since the X signal for the recorder was taken from the ramp generator, and the photoelectron signal was differentiated in the PSD, a direct plot of the photoelectron energy distribution could be obtained. By using a slow ramp voltage (typically 40 secs/volt) and a long time constant on the PSD (typically 3 secs), a very low noise trace could be obtained. Noise level is indicated in Figure 4.8.

For measurements of the yield, the collector and grid were connected together and biased to +25V. The current amplifier was connected between the specimen and earth and the output fed directly to the XY plotter, giving a measurement of the total photoelectron current from the specimen. The maximum rise time (300 mS) was used to eliminate noise, and extreme care was taken with the earthing and screening. Zero calibration was by interruption of the light source and, with care, currents of $<10^{-13}$ amps could be measured.

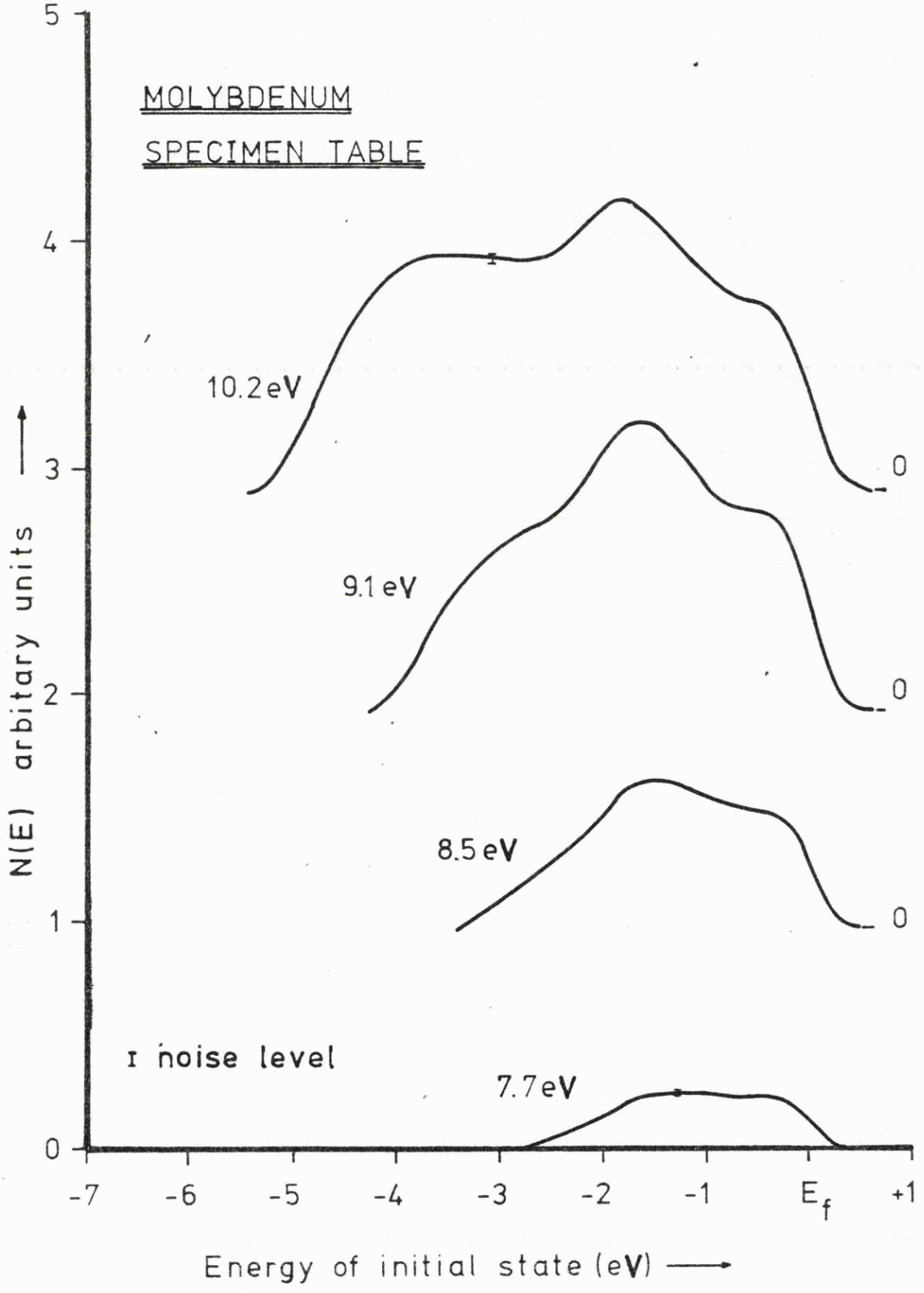

Fig. 4.8 - Unnormalised EDCs from a specimen table

4.4. Experimental Procedure

Setting up. Before assembly the flanges and chamber were thoroughly cleaned with a degreasing agent. Alumina and quartz parts were cleaned by heating in an air oven to 900°C, molybdenum parts by heating in vacuo to 1500°C using a radio frequency induction heater. Small stainless steel parts were cleaned by electropolishing.

The crucible was filled with material that had been scraped clean of oxide and then cut into small pieces. After assembly of the system this material was then melted under vacuum, the crucible flange removed and the process repeated until the crucible was filled.

After leak testing, the chamber was baked at 250°C for periods of up to 24 hours and towards the end of this bake, the specimen table and crucible heaters were switched on for initial outgassing. Final outgassing of both was done at near their maximum attainable temperatures when the chamber was cold. The cleanliness of the specimen table may be judged from Figure 4.8 which shows EDC's taken from a molybdenum specimen table after outgassing. Finally the electronics and optical system were connected to the chamber.

The table was then cooled to below, and the crucible to just above, the melting point of the material. A few drops of material were poured into the trap in the system to clean the pouring tube of the crucible, and the specimen table was then moved into position below the crucible and filled. The material having been allowed to freeze (to minimise the danger of spillage with possible shorting of connections), the table was moved back

into position below the analyser.

A series of EDC's were then taken for both the solid and liquid material for the energy range of the lamp in use. The other factor of interest was, of course, the yield of the material and this was measured for both solid and liquid before the EDC's were taken, as a clean surface was vital for this measurement.

The wavelength setting of the monochromator was scanned automatically across the full energy range of the lamp (the quartz filter being used below 6 eV to remove second order effects) and a plot of photocurrent against wavelength obtained on the chart recorder. Following this, the lamp was calibrated using the gold evaporator. The cleanliness of the gold surface was checked by taking an EDC and comparing it with published data (Nilsson, Norris and Wallden 1971). Since the work function of the materials in this study is less than that of gold (5.6 eV), lamp calibration below 5.6 eV was achieved by measuring the lamp output using the salicyclate phosphor and photomultiplier, correcting this for the LiF window by measuring its transmission at the end of the experiment. By fitting this to the known output above 5.6 eV, the result could be used as a sub-standard below 5.6 eV.

4.5. Analysis and Treatment of Results

4.5.1. The Yield and Work Function

The yield of a material may be specified either as electrons/absorbed photon or electrons/incident photon. Using a gold standard to calibrate the lamp, the yield/incident photon could be calculated from the data already available. The yield/absorbed photon Y_m was obtained using published reflectivity data

to evaluate the expression:

$$Y_m = Y_g \times \frac{(1 - R_g)}{(1 - R_m)} \times \frac{I_m}{I_g} \qquad (4.1.)$$

where:

R = reflectivity, I = photocurrent, m= material, g = gold

The yield having been calculated, the work function was then calculated from a Fowler plot of $Y^{½}$ against photon energy. Y_g and R_g were taken from Krolikowski's work (see Figure 4.9.), R_m from suitable published data where available.

4.5.2. Normalisation of EDC's

The yield of the material having been determined, the EDC's were normalised by digitizing the spectra, then using a Simpson's rule integration to determine the area encompassed by the EDC and hence the total photocurrent represented. The spectra could then be multiplied by the appropriate factor to achieve normalisation.

4.6. System Resolution

The resolution of the system was determined empirically from the width of the Fermi edge on the EDC's (typically 0.4 eV from 10% - 90%), this width appearing to be independant of specimen temperature. There are several factors which may contribute to this broadening.

4.6.1. Optical Broadening

The monochromator does not, of course, provide a truly monoenergetic source of photons, though the value for dispersion quoted by the manufacturers is quite small (16 Å/mm). Since the lamp is being operated in a windowless, slitless mode through a capilliary of ⌀ = 1.5 mm., and the exit slit must be wide open at

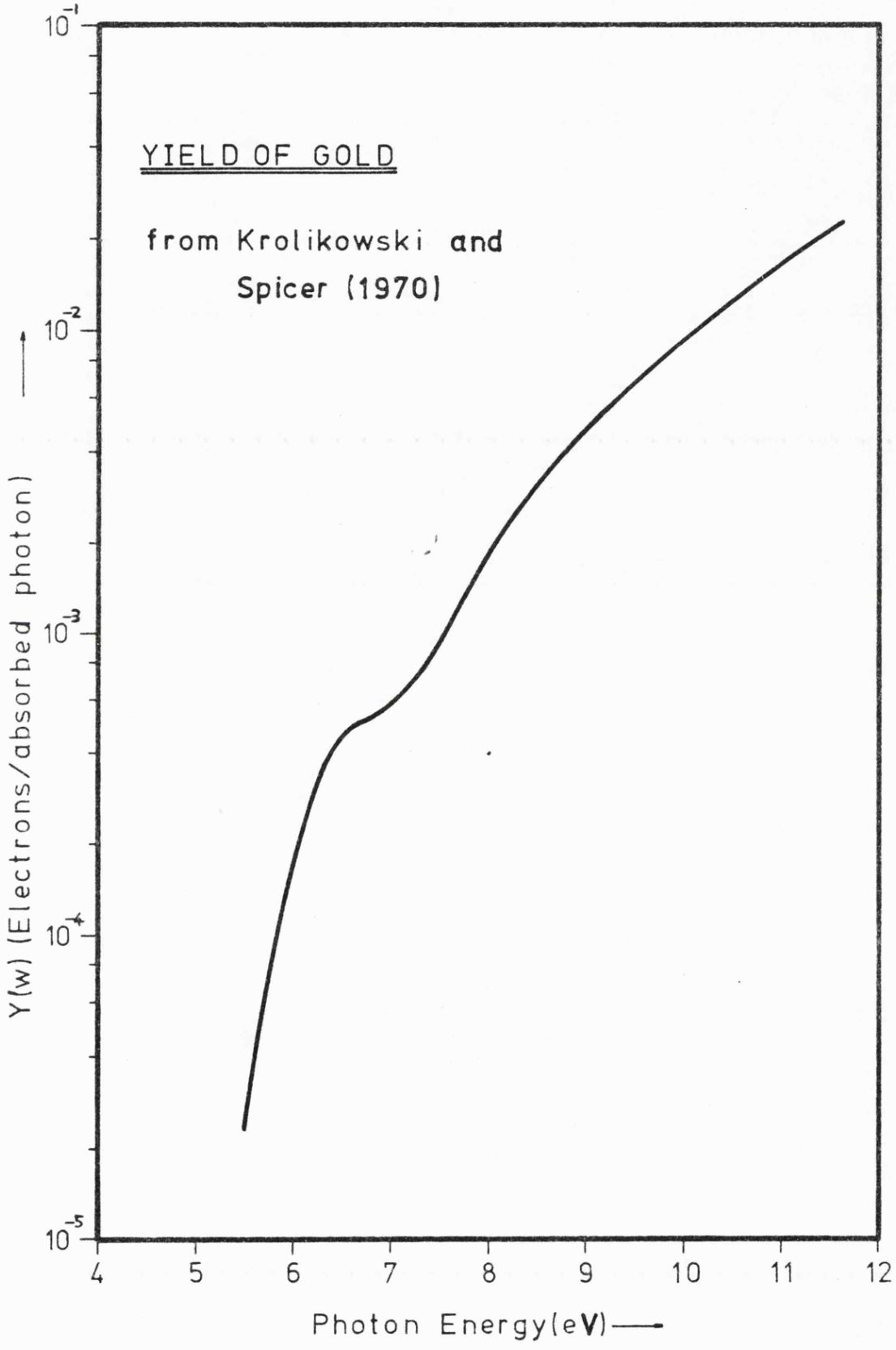

Fig.4.9 - Quantum yield of gold (used as reference)

1.5 mm. to give an adequate signal/noise ratio, the monochromator is operating under the worst possible conditions. However the calculated value for the dispersion is still quite small (= 0.2 eV at 10.2 eV in the worst case) and this is borne out by examination of the variation of Fermi edge width with exit slit width which appears to be negligible.

4.6.2. Modulation Broadening

This arises from the necessity of having a modulated ramp voltage so that phase sensitive detection may be used to obtain a good signal-to-noise ratio. Since the magnitude of the modulation is known, an estimate may be made of the broadening due to this source, and Figure 4.10 shows a computer simulation of the effects of the modulation upon various features such as the Fermi edge. This simulation indicates that the value of the broadening expected for the modulation normally used (0.4V p-p) is approximately 0.4 eV and hence implies that this is the predominant broadening mechanism present in the system. The variation of the edge width observed with modulation voltage appears to bear this out. The problem has been dealt with in some detail by Houston and Park (1972) but since the present work uses only a simple sine wave modulation, a simplified numerical approach appears to give adequate results.

4.6.3. Field Distortion

If the specimen to be dealt with was a point source at the centre of a perfectly spherical collector there would, of course, be no broadening from this source. In practice, however, the specimen is in the form of a flat dish 1" across and the

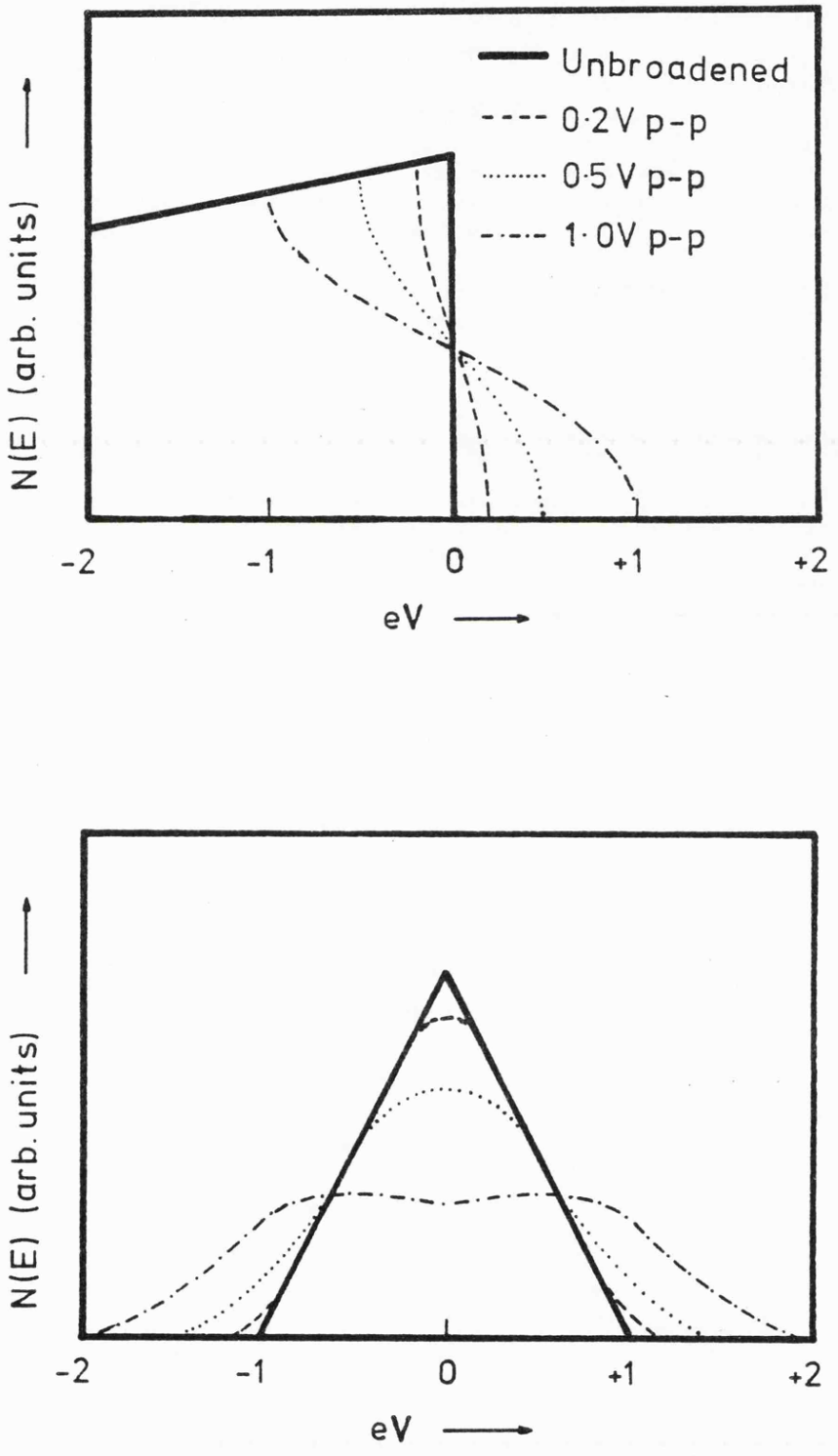

Fig. 4·10 - Effects of modulation broadening on EDCs

light spot is of a finite size (≈ 2mm. x 1mm.). The exact effect of this is rather hard to determine but has been covered in some detail by Di Stefano and Pierce (1970) who showed that the use of a fine screen between the specimen and collector could result in a considerable improvement in the system resolution (of the order of 0.1 eV for electrons with kinetic energies of several volts). There were some variations in system geometry made during the course of the work (notably in the vertical position of the specimen table), and these appeared to have little effect on the final resolution.

4.6.4. Magnetic Distortion

The presence of a magnetic field near the analyser can cause distortion of the electron trajectories between specimen and collector. Some care was taken to avoid this effect, particularly in the case of the ion pumped system, by the use of screening. No magnetic distortion could be observed on bringing a small horseshoe magnet near the system - so this appears to have been eliminated as a significant source of broadening.

4.6.5. Work Function Distortion

Variation of the work function of the collector or the specimen surface may also result in distortion of the EDC's. However Di Stephano and Pierce (loc.cit.) showed that this is only a problem when large crystallites (>10μ) are present, and the technique adopted of coating the collector surface with colloidal graphite appeared to be successful in eliminating errors from this source. In the case of the specimen itself there is the

problem of fringing fields from areas of the emitter with a different work function. However the use of a large specimen should reduce this effect, and an angular analysis of the photoemitted electrons given by the computer programme of Chapter 3 indicates a strong bias towards emission normal to the surface which is the direction of minimum distortion of the field, which would also tend to reduce the effect. The use of an emitter screen (see Figure 4.6.) connected to the specimen acts as a guard ring and further reduces the distortion of the field.

CHAPTER 5:- INDIUM AND ALUMINIUM

5.1. Introduction

Indium and aluminium have long been regarded as highly free electron like in the liquid state and as such were fairly obvious starting points for this work. Both metals are in Group IIIA (Al: $3s^2 3p$; In: $5s^2 5p$). The structure of aluminium is face centered cubic (f.c.c.) in the solid phase and hard sphere like in the liquid. Solid indium is basically f.c.c. with some small tetragonal distortion. In liquid indium the structure factor S(q) is very similar to the result expected on the basis of a hard sphere assembly, except for a small asymmetry in the first peak (Ocken and Wagner 1966) consistent with distortions found in the solid phase.

As mentioned in Chapter 1, transport properties and other measurements for both these materials are consistent with the free electron picture. There is little previous spectroscopic work in the liquid state - liquid aluminium has been examined by soft X-ray spectroscopy by Caterall and Trotter (1963) and Fabian (1972),and although some features were apparent, little difference was observed between solid and liquid. Liquid indium has been examined by UPS by both Koyama (1968) and Stevenson (1968). However both sets of results showed large scattered electron peaks and hence there still exists some doubt as to the UPS spectra of indium. In the solid, evaporated films of both materials have been studied, aluminium by Wooten et al (1966), indium by Koyama (loc.cit.), and both by Pollak (1972) using XPS.

In this chapter, results are presented for indium and

aluminium in both solid and liquid states. They will be analysed in terms of the 3-step approach using both Monte Carlo and analytical approaches as detailed in Chapter 3.

5.2. Indium

5.2.1. Experimental

Indium was chosen as the initial subject for investigation as it presented the fewest problems from an experimental point of view. Indium is a ductile metal of low toxicity with a melting point of 154^{o}C. It is not highly reactive in the liquid state and may be contained with ease in austenitic stainless steel (Liquid Metals Handbook 1955). The only problem arises from its low surface tension which, whilst making it easy to pour, does mean that care must be taken over the seal of the crucible and in moving the specimen table.

The optical properties of indium in the U-V are fairly well documented, having been measured both by Wilson and Rice (1966) and Koyama (loc.cit.). Also of note is a very careful measurement by Van Laar and Scheer (1965) of the photoyield of evaporated indium films near to the threshold. There has also been considerable theoretical work on indium, and densities of states have been published by Koyama and Spicer (1971), Ashcroft and Lawrence (1969), Shaw and Smith (1969), and Chan and Ballentine (1972).

The results given here are from a series of four experiments, and some preliminary results have already been published (Norris et al 1973). An effect noted in the later work on this metal, and also during work on lead, is that the

rate of freezing of the liquid can affect the structure observed in the solid. Contrary to normal expectation, rapid freezing of the melt (i.e. heater suddenly turned off) was found to give much more distinct structure than slow freezing (i.e. heater power slowly reduced). This effect is believed to be due to the presence, observed in some specimens, of a light skin on the surface of the specimen which broke up in the centre on melting (probably due to convection effects). Although tracking of the light spot over the specimen revealed no difference in solid EDC's due directly to its presence it may, by acting as a source of condensation nuclei during slow freezing when it was allowed time to reform, have prevented the formation of large single crystals.

5.2.2. Yield of Indium

Figure 5.1. shows the yield of indium for the liquid and both the rapidly and slowly frozen solid. The overlay is the results of Koyama for liquid, frozen liquid and crystal specimens. The reflection data used was from Wilson and Rice (loc.cit) for the liquid and from Koyama (loc.cit.) for the solid. The two sets of results are in good qualitative agreement, the difference in magnitude probably being due to the difference in surface cleanliness. The similarity between the behaviour of the rapidly frozen solid in this work and the crystal specimen in Koyama's work (relative to the liquid in both cases) gives support to the idea that the rapidly frozen solid consists of large single crystals. The major features of the yield are peaks at 6.9 eV, 8.9 eV and 10.7 eV with corresponding dips at 5.8 eV and 7.9 eV. The lower two peaks correspond with

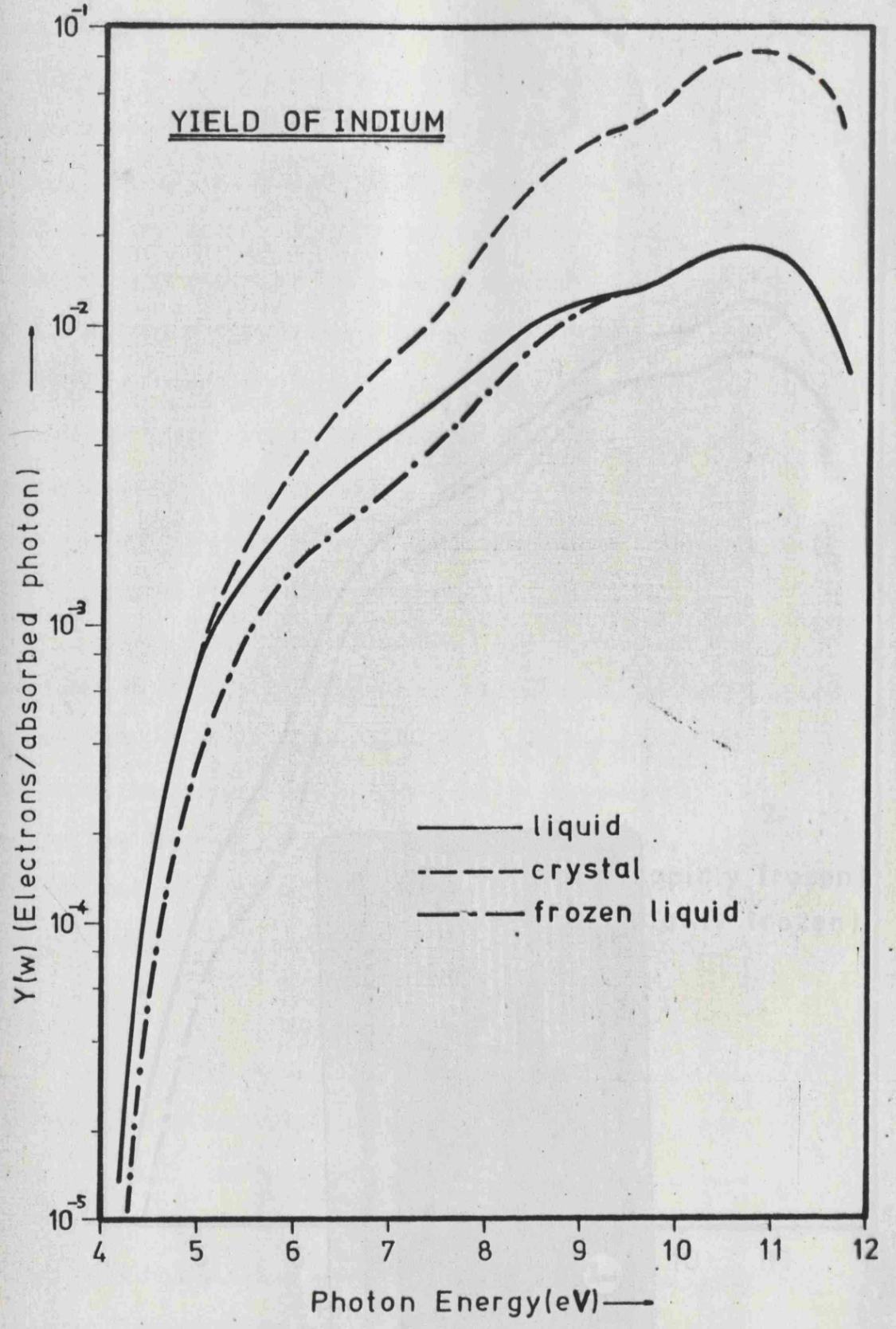

Fig.5.1'-Yield of solid & liquid indium (Koyama)

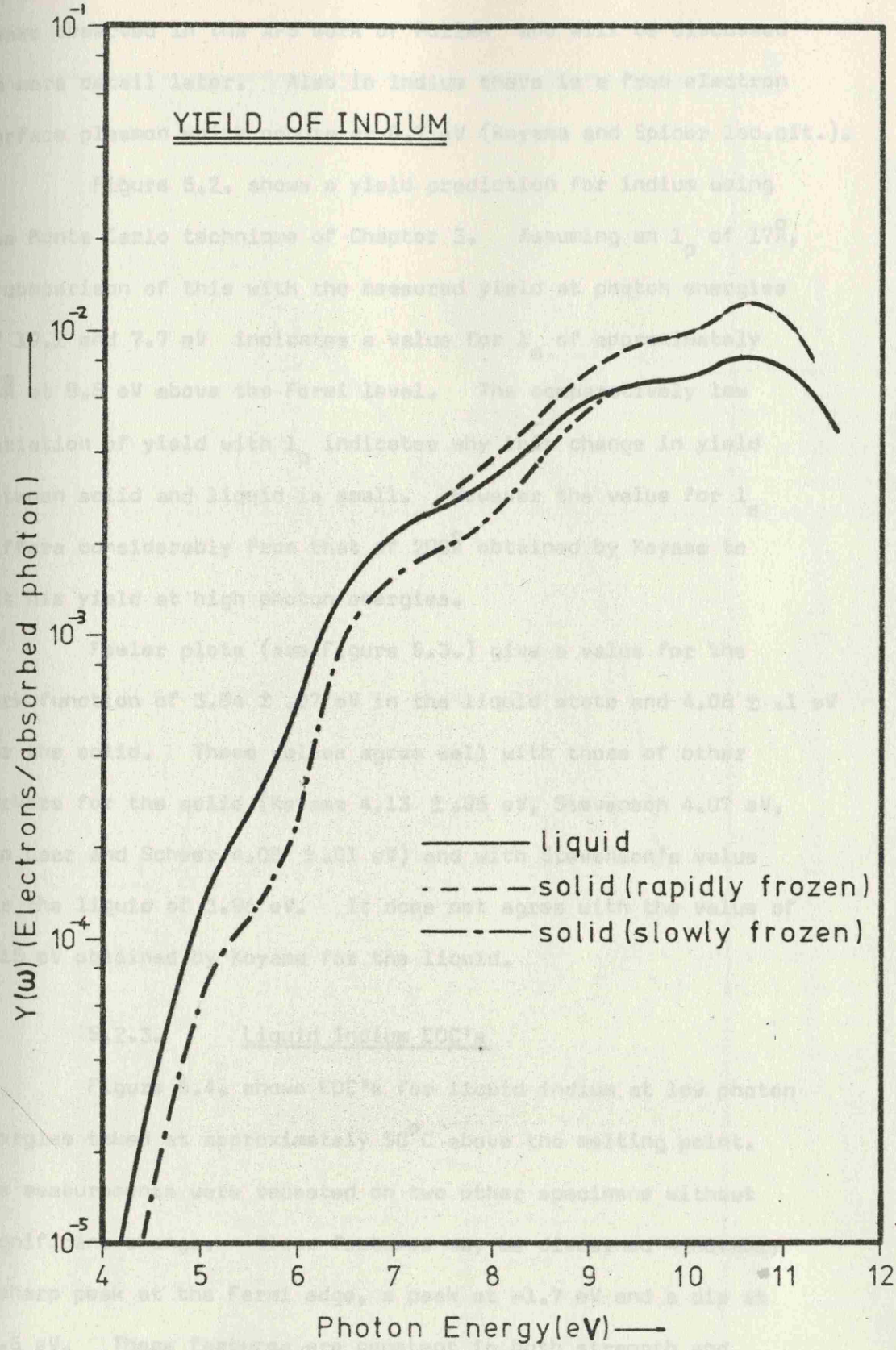

Fig. 5.1 - Yield of solid & liquid indium (present work)

peaks observed in the XPS work of Pollak and will be discussed in more detail later. Also in indium there is a free electron surface plasmon which occurs at 8.7 eV (Koyama and Spicer loc.cit.).

Figure 5.2. shows a yield prediction for indium using the Monte Carlo technique of Chapter 3. Assuming an l_p of 17Å, a comparison of this with the measured yield at photon energies of 10.2 and 7.7 eV indicates a value for l_e of approximately 14Å at 8.5 eV above the Fermi level. The comparatively low variation of yield with l_p indicates why this change in yield between solid and liquid is small. However the value for l_e differs considerably from that of 200Å obtained by Koyama to fit his yield at high photon energies.

Fowler plots (see Figure 5.3.) give a value for the work function of 3.94 ± .07 eV in the liquid state and 4.06 ± .1 eV for the solid. These values agree well with those of other workers for the solid (Koyama 4.13 ± .05 eV, Stevenson 4.07 eV, Van Laar and Scheer 4.08 ± .01 eV) and with Stevenson's value for the liquid of 3.96 eV. It does not agree with the value of 4.15 eV obtained by Koyama for the liquid.

5.2.3. Liquid Indium EDC's

Figure 5.4. shows EDC's for liquid indium at low photon energies taken at approximately 50°C above the melting point. The measurements were repeated on two other specimens without significant change. Clear features may be discerned - notably a sharp peak at the Fermi edge, a peak at -1.7 eV and a dip at -2.6 eV. These features are constant in both strength and position with changing photon energy. In addition a weak feature at -3.6 eV may just be discerned. These results differ

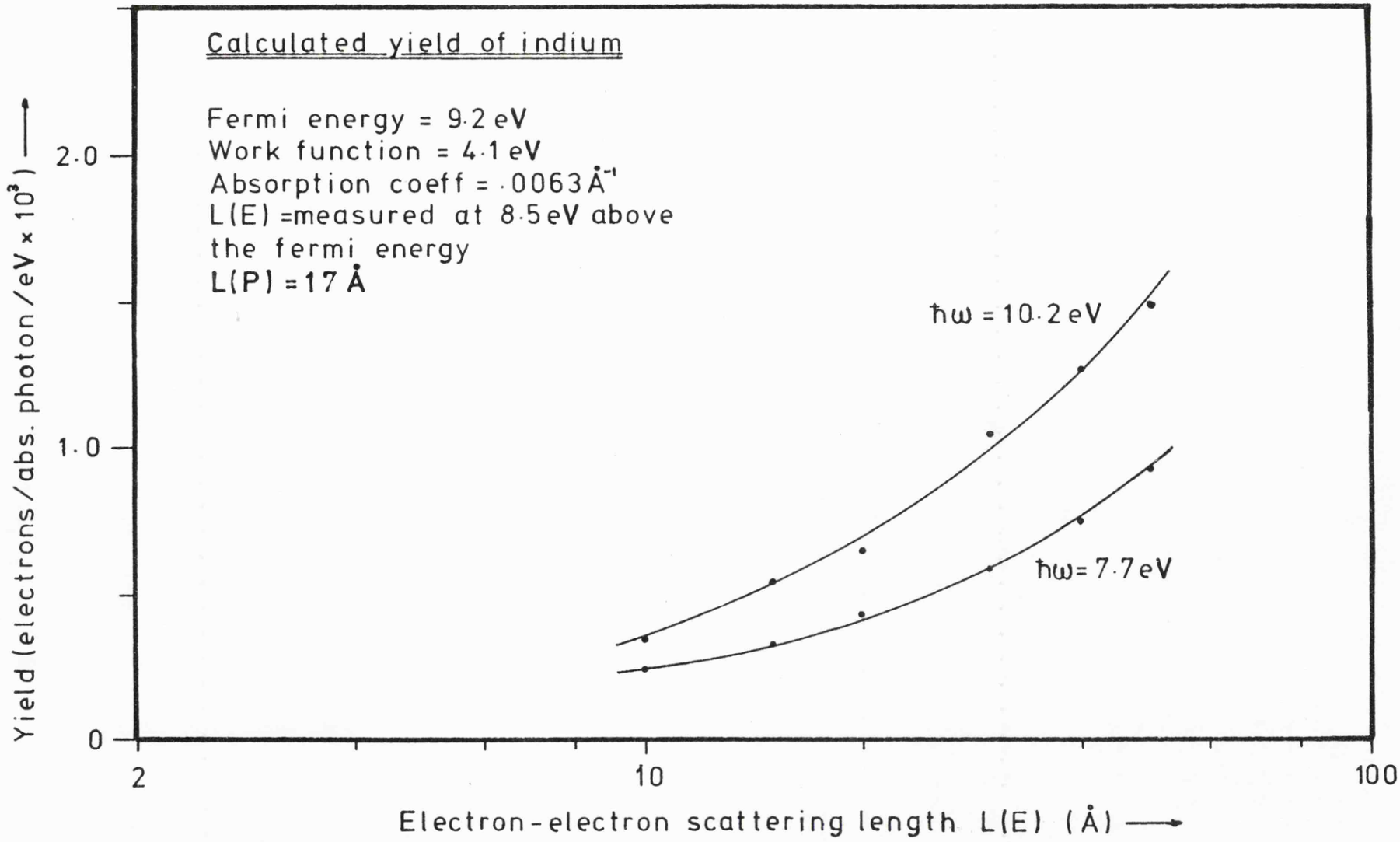

Fig.5.2 - Calculated variation of yield with scattering length for indium

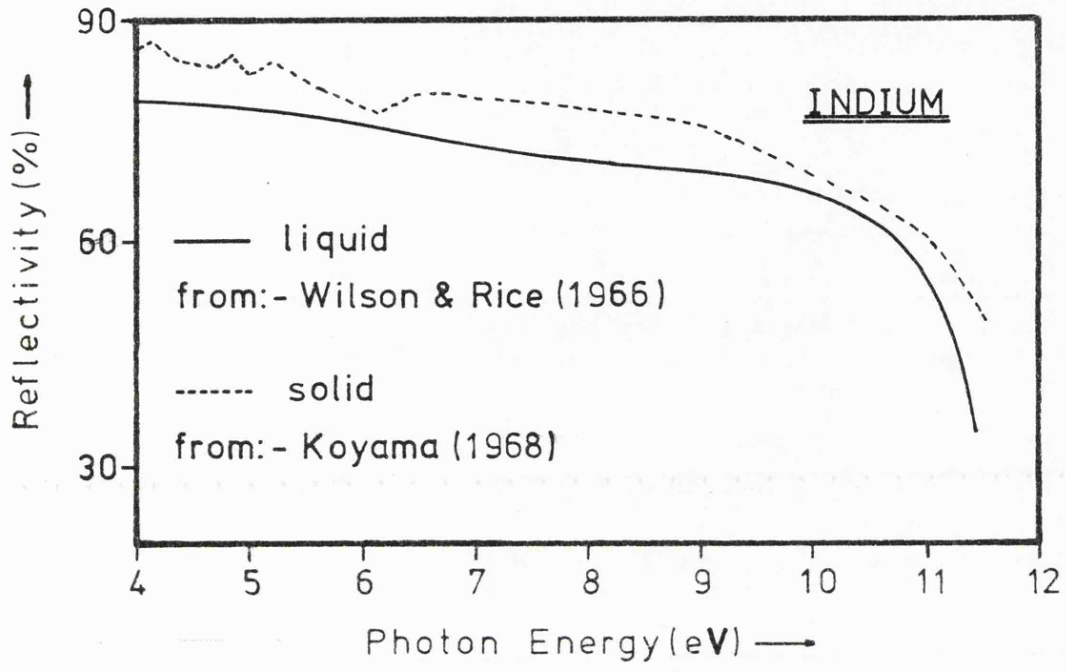

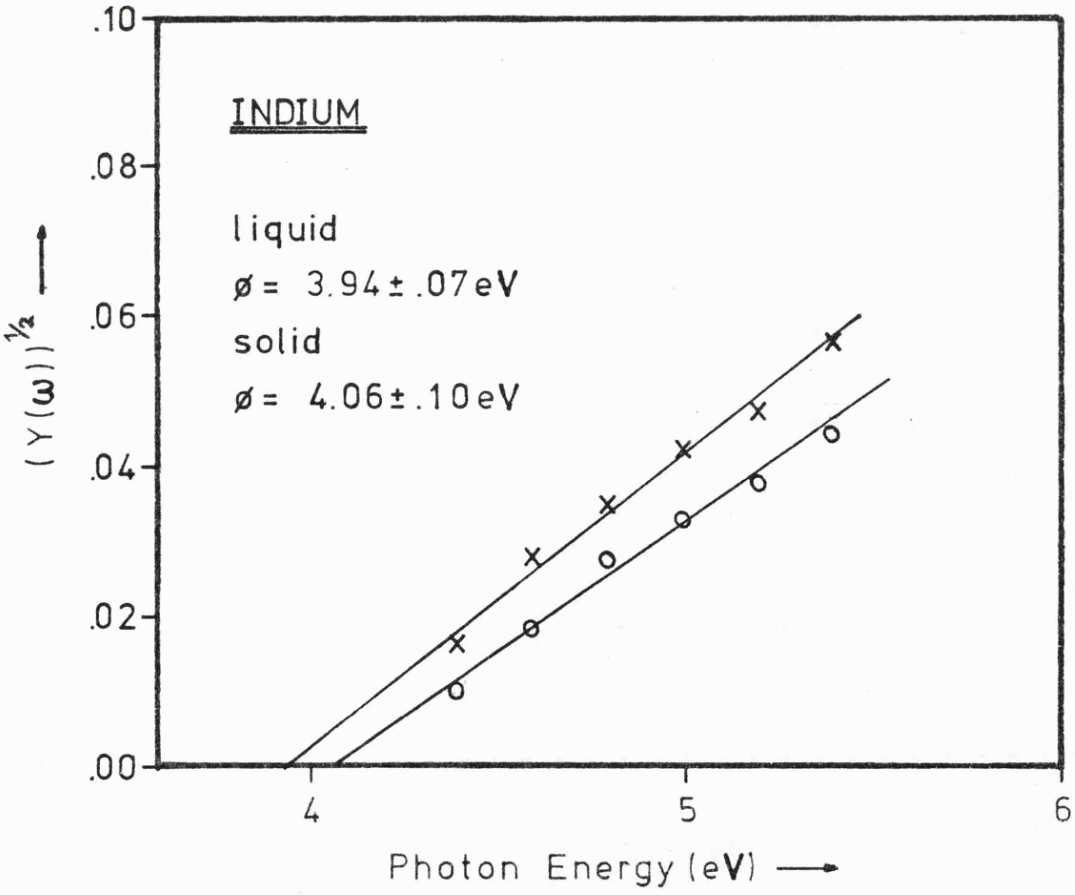

Fig.5.3-Reflectivity & Fowler plot for solid & liquid indium

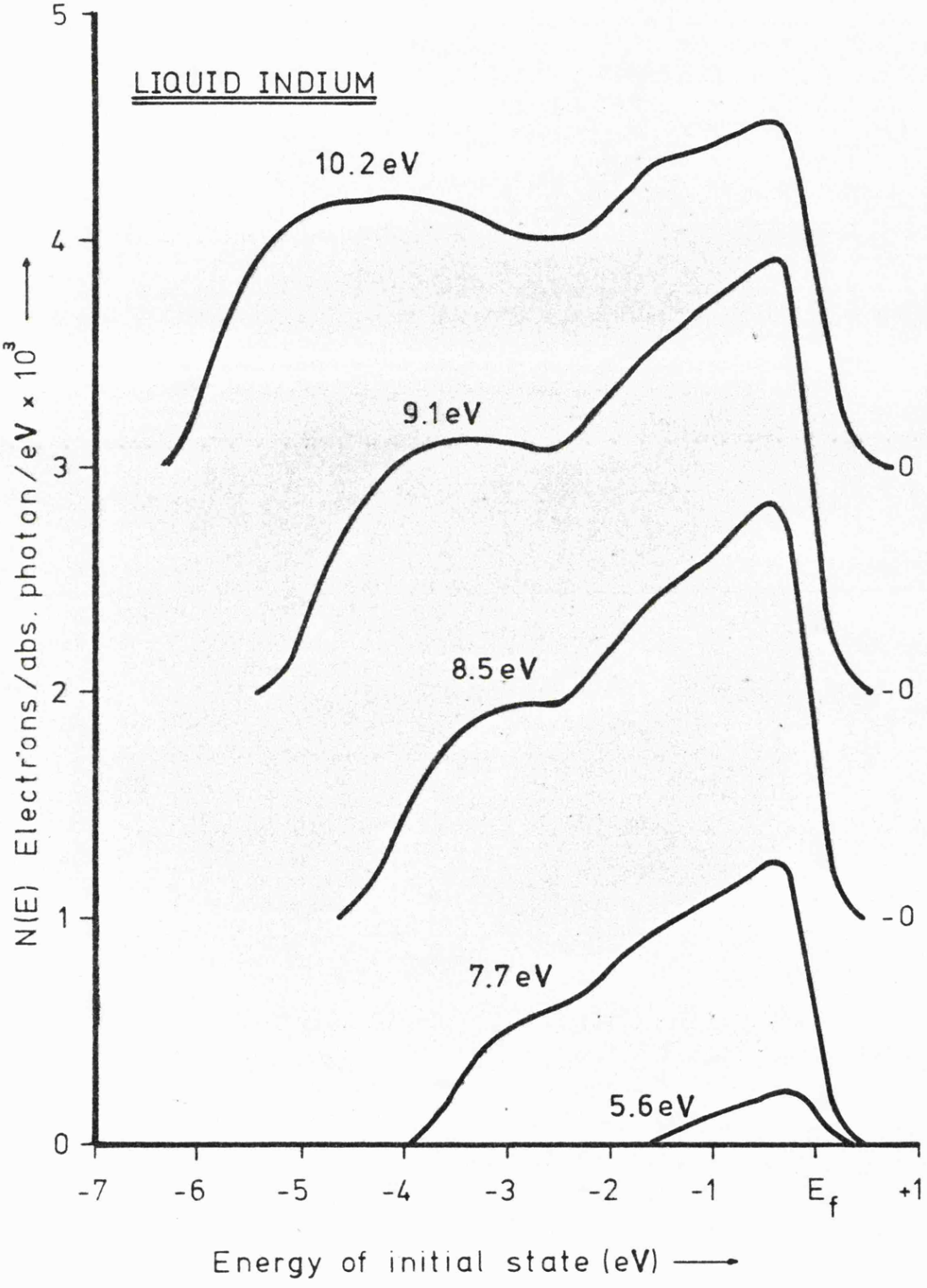

Fig. 5.4 - Low energy EDCs for Liquid Indium

slightly from those reported earlier (Norris et al loc.cit.) in that a weak dip at -1.3 eV is not now seen. This change is believed to be due to the temperature in the initial work being too close to the melting point, resulting in the existence of small regions of solid indium formed around impurities at the surface.

Figure 5.5. shows a comparison between the present work and that of Koyama and Spicer. These agree well in the position of the main minimum at -2.6 e V. In the present work, the comparative absence of a scattered peak at low energies and the appearance of structure is believed to be due to the improved resolution and surface preparation technique used. The admittance of air to the system was seen to cause a general degradation of the EDC's and a sharp increase in the scattered peak - seen in Figure 5.4. at low energy extreme. An attempt was made to see if a temperature variation could be observed in the EDC's,but no variation was apparent up to $\simeq 400^{o}C$,and attempts to raise the temperature above this point resulted in evaporation of indium onto the LiF window.

5.2.4. Solid Indium EDC's

Figures 5.6. and 5.7. show EDC's for solid indium both in the rapidly and slowly frozen states. The two minor features observed in both are identical in position but vary considerably in strength. They are firstly, a peak varying in position from -1.1 to -0.9 eV being notably stronger at the higher photon energies and secondly, a peak varying in position from -1.8 to -1.5 eV with increasing photon energy, being strongest at the intermediate energies. The main minimum is at -2.4 eV at all

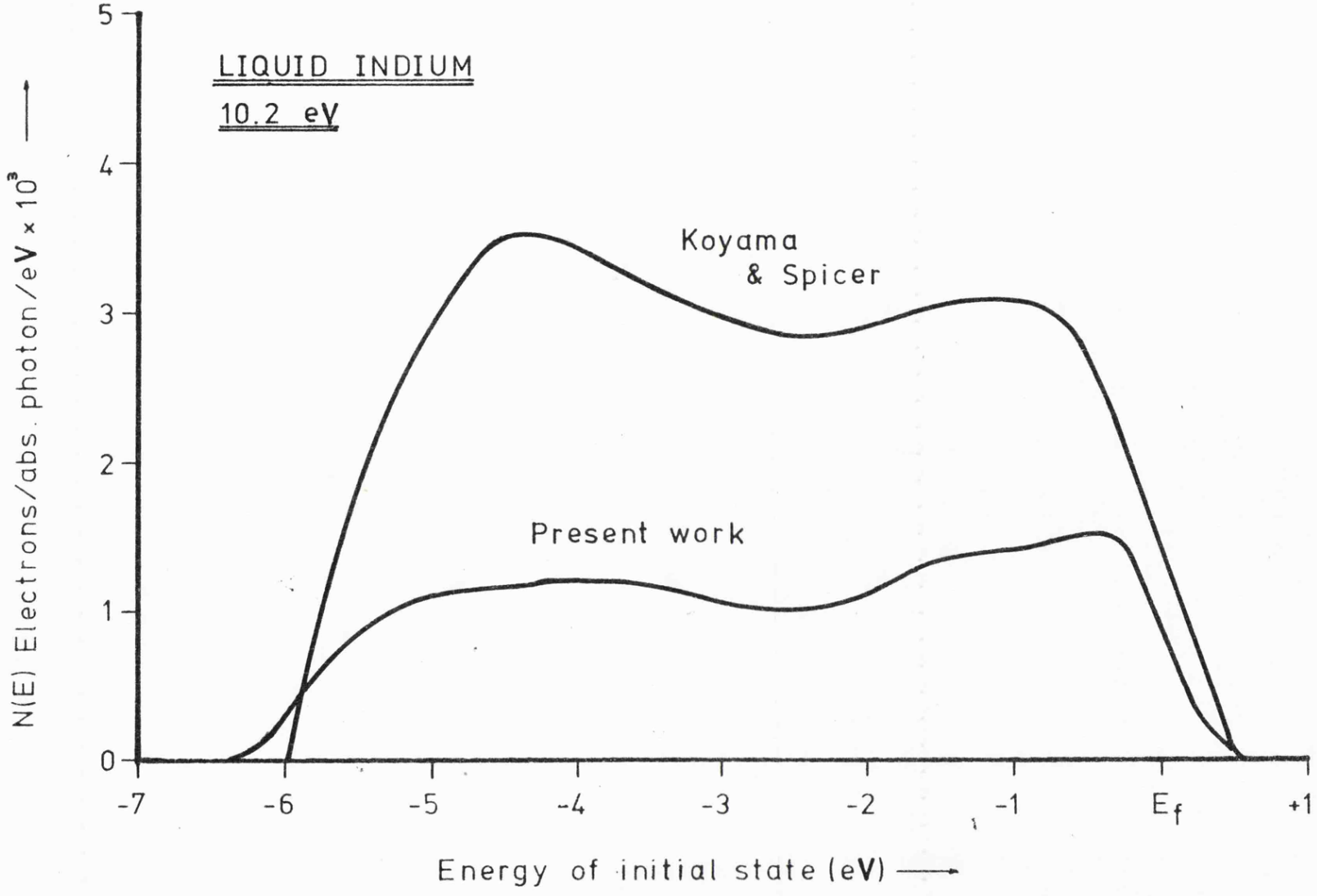

Fig. 5.5 - Comparison of EDCs for liquid indium at $h\nu = 10.2$ eV

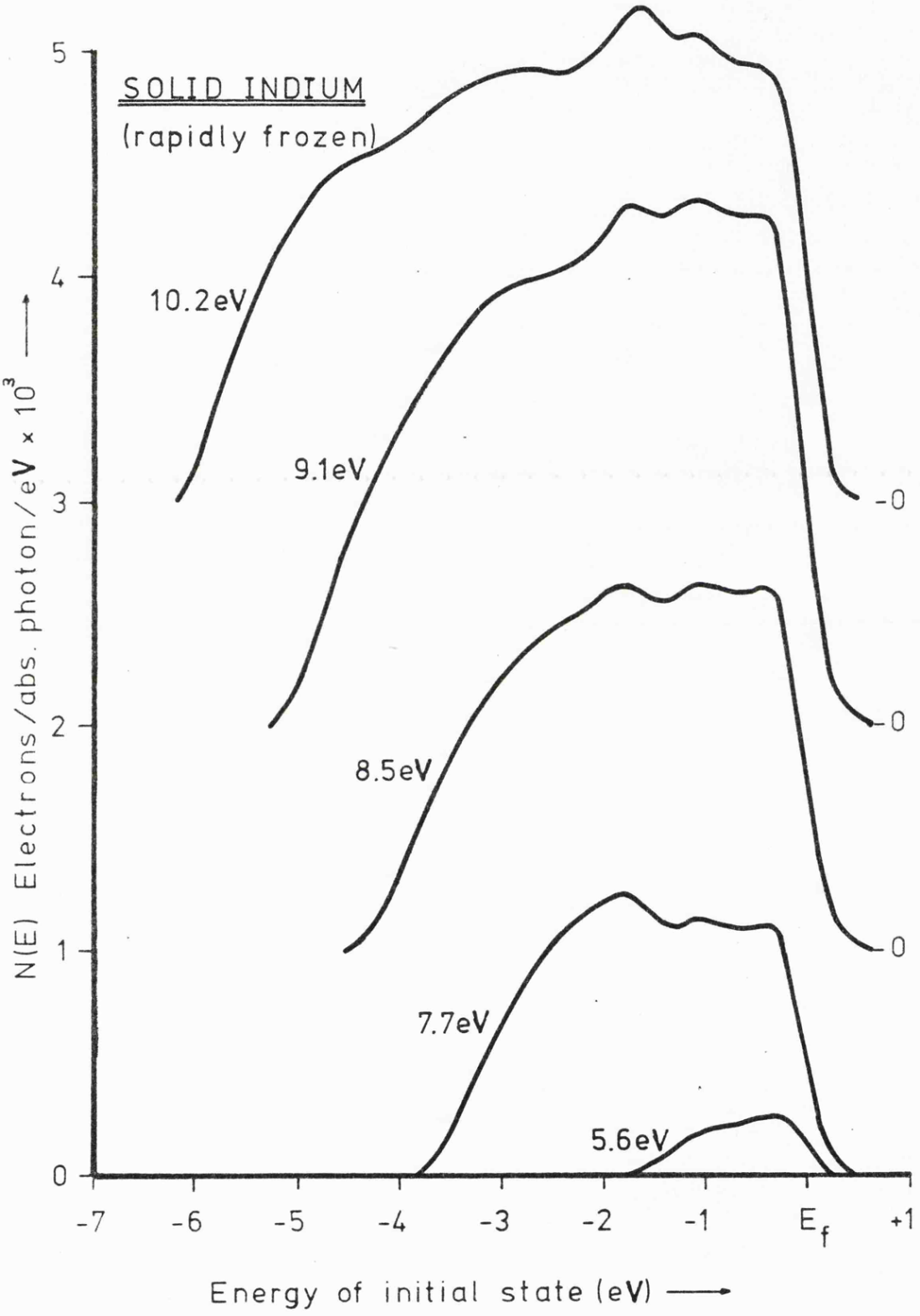

Fig.5.6-Low energy EDCs from rapidly frozen Indium

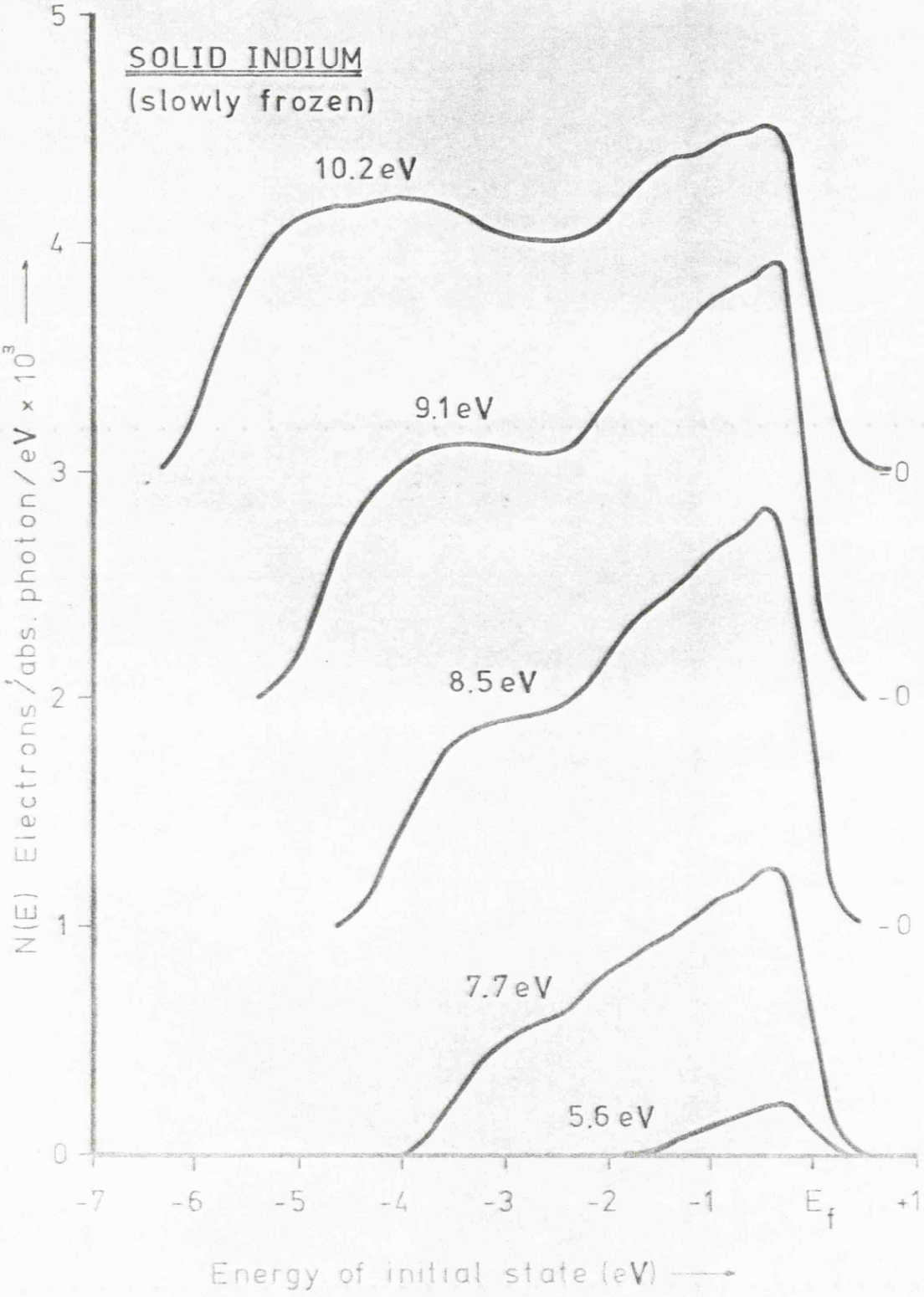

Fig. 5.7 - Low energy EDCs for slowly frozen Indium

photon energies. In the rapidly frozen solid there is also a strong feature at -3.1 eV. This feature is seen in a weaker form at -3.6 eV in the slowly frozen solid, and a weak dip at -4.4 eV is just discernable. Figure 5.8. shows a typical frozen indium surface.

The experimental EDC's were compared with theoretical EDC's from calculations by Koyama and Spicer (1971). These calculations were based on the 3-step model, assuming direct transitions and adopting the method given by Koyama and Smith (1970) for aluminium. Due to the tetragonal distortion of the f.c.c. structure in indium the calculation is rather more complex, involving the division of each 1/16th symmetry segment of the Brillouin zone in unequal parts and solving the appropriate 4-OPW equation for each. The use of unequal segments (done to reduce computing time) results in some mismatch in the energy bands, but this was found not to be significant when the final result was calculated.

In each sector Koyama and Spicer solved an equation of the form:

$$0 = \begin{vmatrix} T_1(\vec{k})-E_i(\vec{k}) & V_{111} & V_{111} & V_{200} \\ V_{111} & T_2(\vec{k})-E_i(\vec{k}) & V_{002} & V_{111} \\ V_{111} & V_{002} & T_3(\vec{k})-E_i(\vec{k}) & V_{111} \\ V_{200} & V_{111} & V_{111} & T_4(\vec{k})-E_i(\vec{k}) \end{vmatrix} \qquad (5.1.)$$

where

$$T_1(\vec{k}) = \vec{k}^2 \qquad T_2(\vec{k}) = (\vec{k} - \vec{K}_{111})^2$$

$$T_3(\vec{k}) = (\vec{k} - \vec{K}_{111})^2 \qquad T(\vec{k}) = (\vec{k} - \vec{K}_{200})^2$$

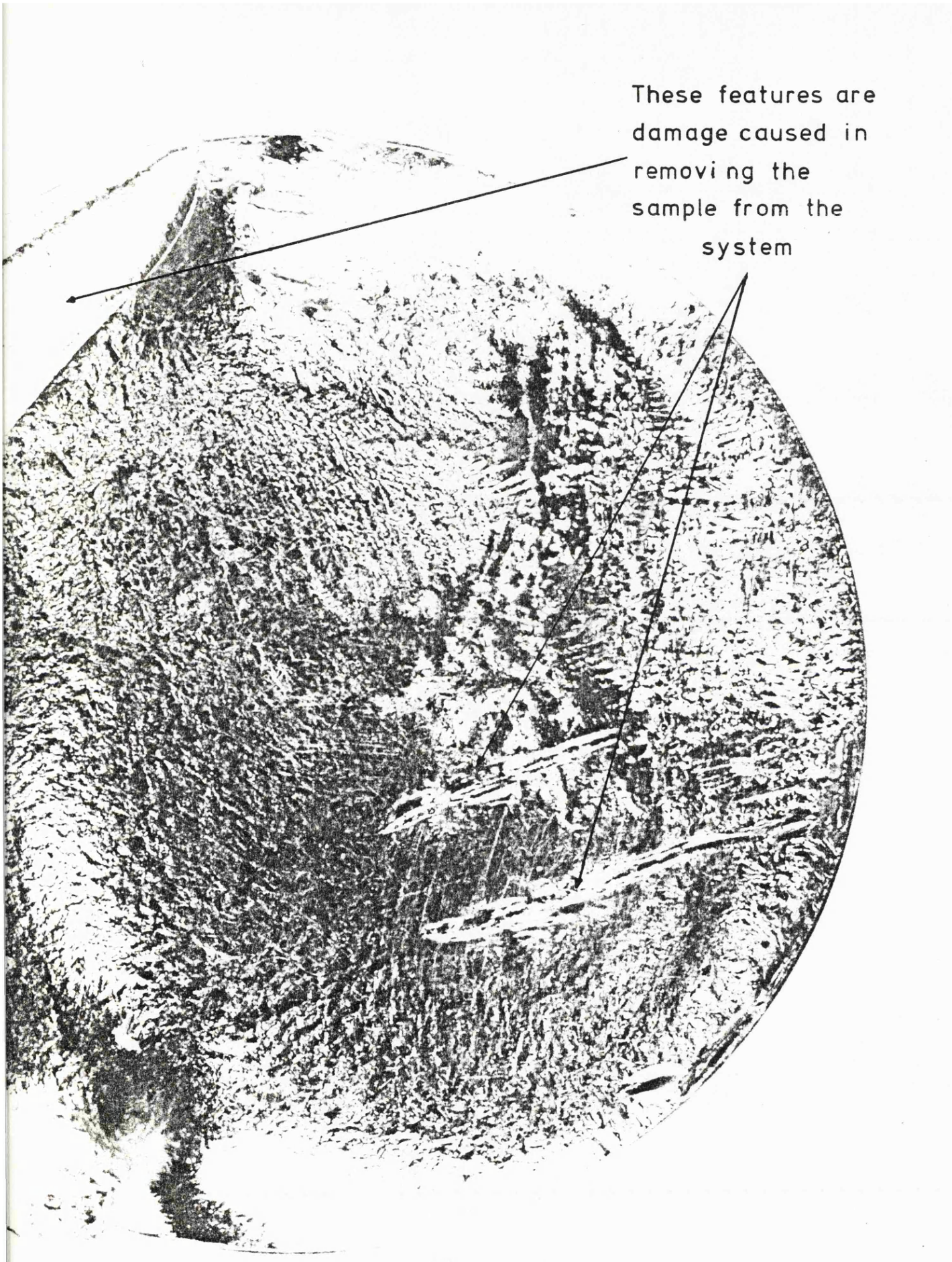

Fig.5.8 - Surface of frozen Indium

$E_i(\vec{k})$ are the eigen values for the energy bands, V_k are the Fourier coefficients of the potential arising from the k th. lattice wave vector.

Figure 5.9. shows the comparison of calculated and experimental EDC's. It may be seen that the agreement in the position of structure close to the Fermi edge, particularly in the peak at -1.8 eV, is good. Whilst the agreement between the strengths of the features is less good, it should be remembered that the analysis takes no account of matrix elements or of the possibility that the escape probability may vary with the different crystal faces.

5.2.5. High Energy EDC's

Figure 5.10. shows high energy EDC's for both solid and liquid indium. There is a large scattered background which makes comparison with the low energy spectrum difficult. However, there appears to be good correspondence in the structure, particularly near the Fermi edge in the feature at -2.6 eV which shows clearly in both solid and liquid. A dip is also observed at -3.6 eV in both solid and liquid, corresponding to the weak feature observed in the low energy EDC's. Closer to the Fermi edge in the liquid EDC it is possible to discern the feature at -1.7 eV observed before, and in the solid the features are observed at -1.0 eV and -1.8 eV corresponding to those seen at low energies. The solid appears to be in the rapidly frozen form. Moving towards the low energy end of the EDC, a break in slope may be observed at -8.6 eV. This value corresponds well with the value calculated by Kittel (1968) for the bottom of the free electron band. The hump lower in energy centered at

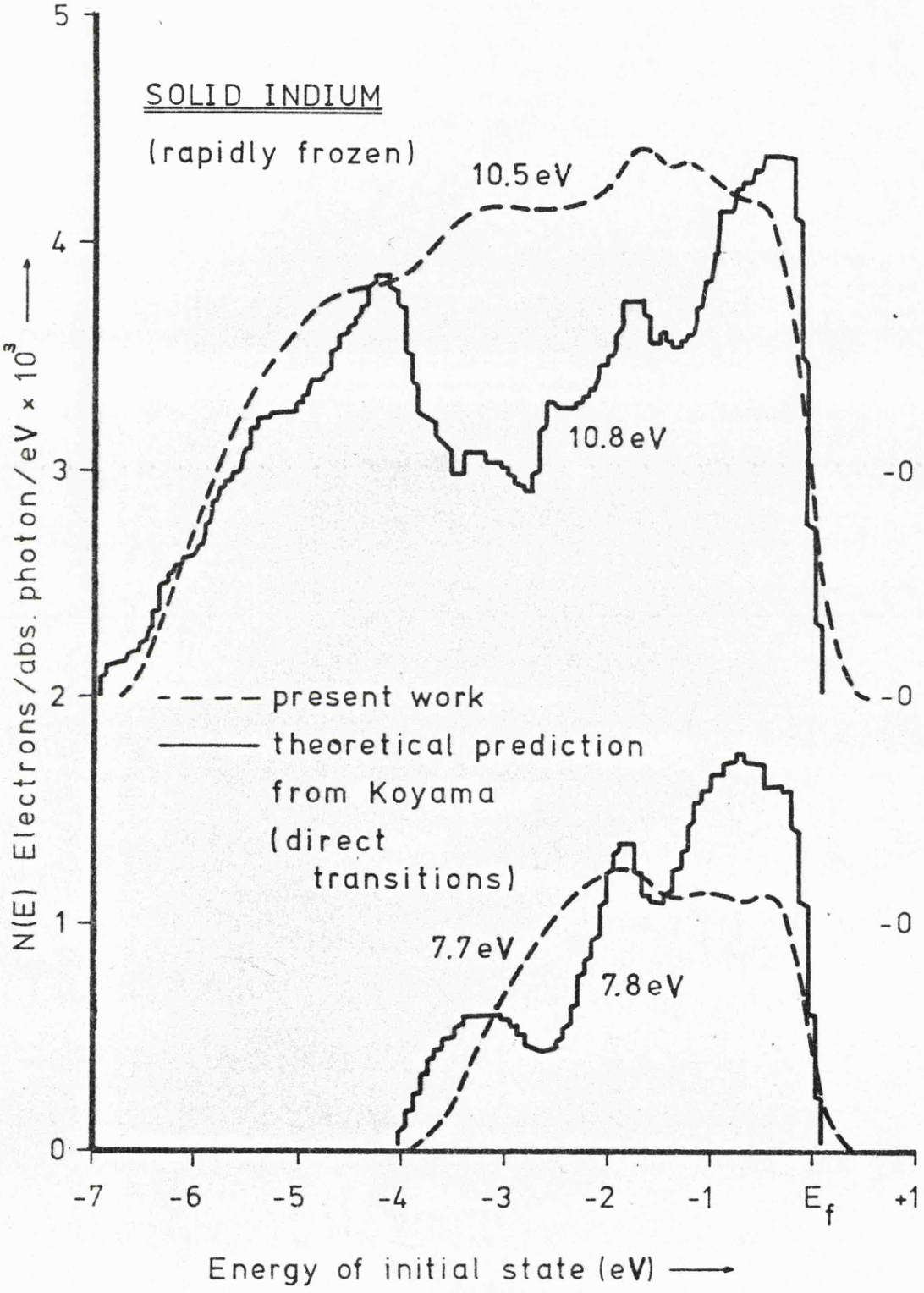

Fig.5.9-Comparison of EDCs for solid indium with theoretical predictions

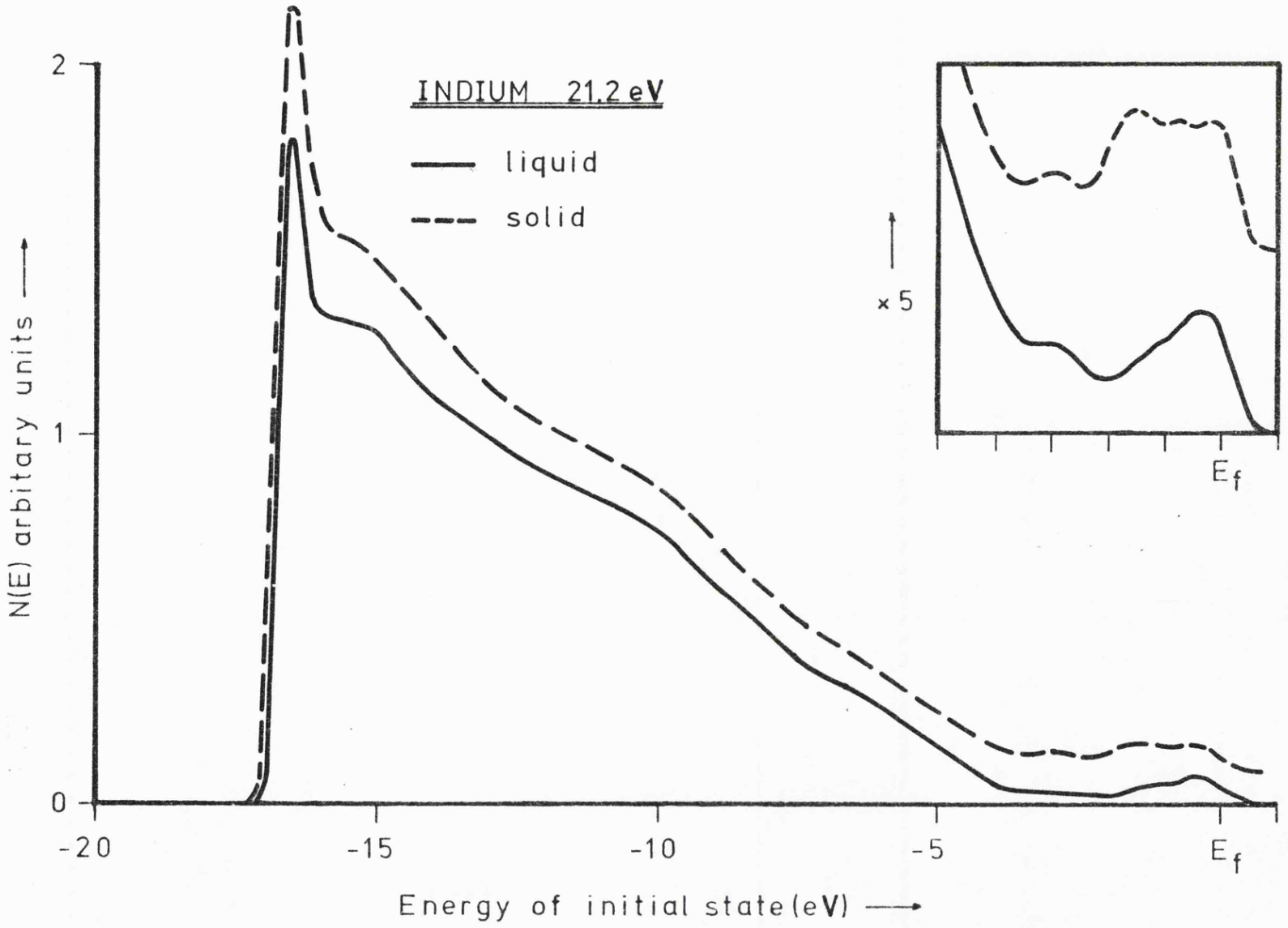

Fig.5.10- High energy EDCs from solid & liquid Indium

approximately -11 eV corresponds in position with a bulk plasmon observed by Pollak (loc.cit) at 11.7 eV and, at the extreme low energy end of the EDC, the strong peak at -17.1 eV is in good agreement with the position of the 4d peak (also observed by Pollak).

5.2.6. Optical Density of States

The high energy end of the liquid EDC, with the background subtracted, was used as a basis for calculating an optical density of states. Figure 5.11 shows the density of states thus obtained compared with the XPS spectrum obtained by Pollak from an evaporated film of indium. It may be seen that there is broad agreement in the presence of a feature at -3.6 eV, although the other feature observed by Pollak at -4.2 eV is not seen. This trial density of states was used in the modified Krolikowski programme (as detailed in Chapter 3) to obtain a final optical density of states. The scattering length used in the programme was selected to give agreement between calculated and experimental yields at 7.7 eV. The final density of states thus obtained is shown in Figure 5.12 compared with a free electron curve. It can be seen that there is considerable disparity between the two. Figure 5.13 shows the comparison of simulated EDC's using these two densities of states with the experimental curves at 10.2 and 7.7 eV. The value for the absorption coefficient was taken from Lemmonier et al (1969). The value of l_e used was 14Å. This is considerably shorter than the value of l_e = 50Å used by Koyama (loc.cit.) to fit the yield at low photon energies. However, the yield obtained in this work is considerably lower, probably due to the increased surface cleanliness, and the present result is in good agreement with the work of Brundle (1974).

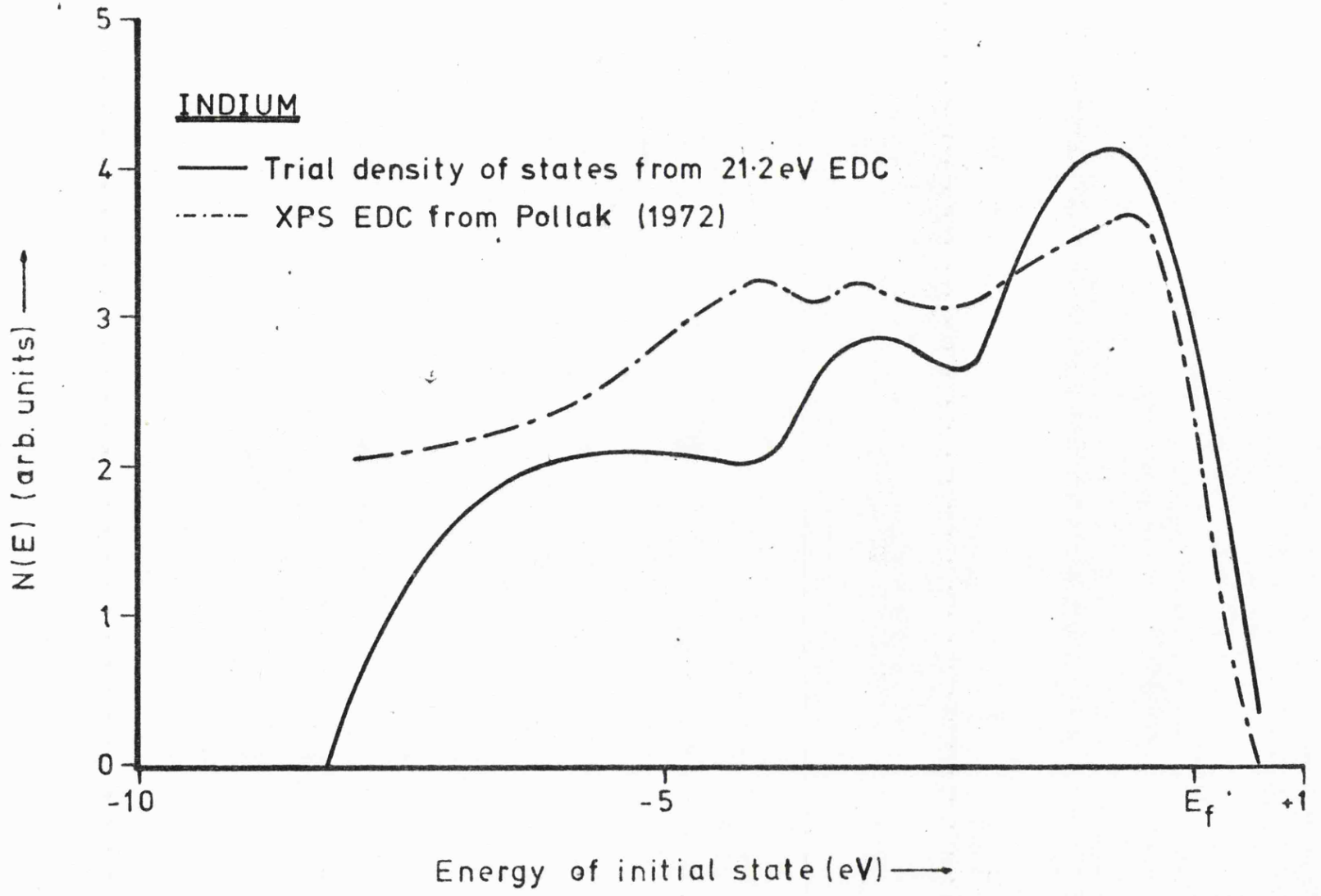

Fig. 5.11 - Trial optical density of states for Indium

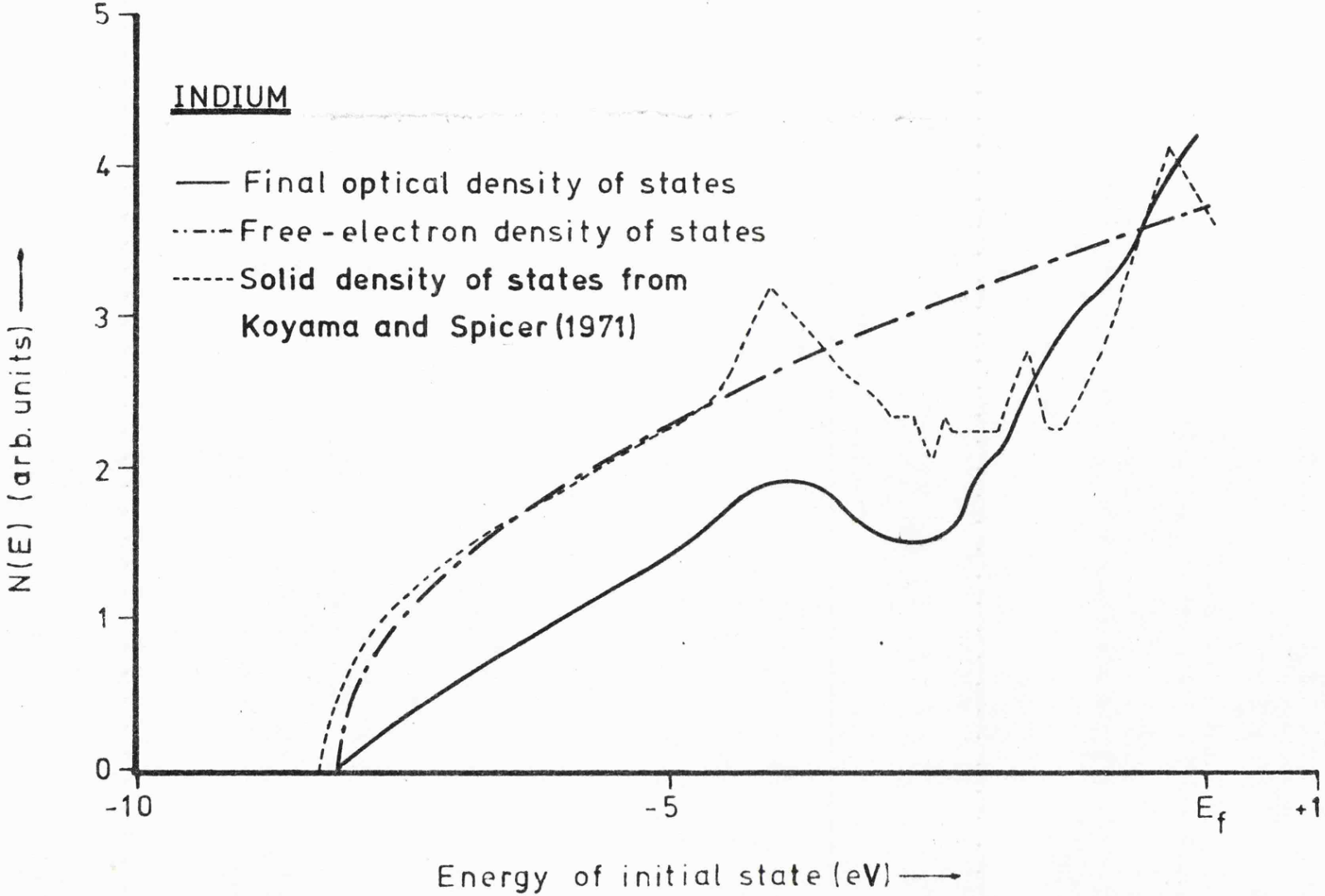

Fig.5.12 - Final optical density of states for Indium

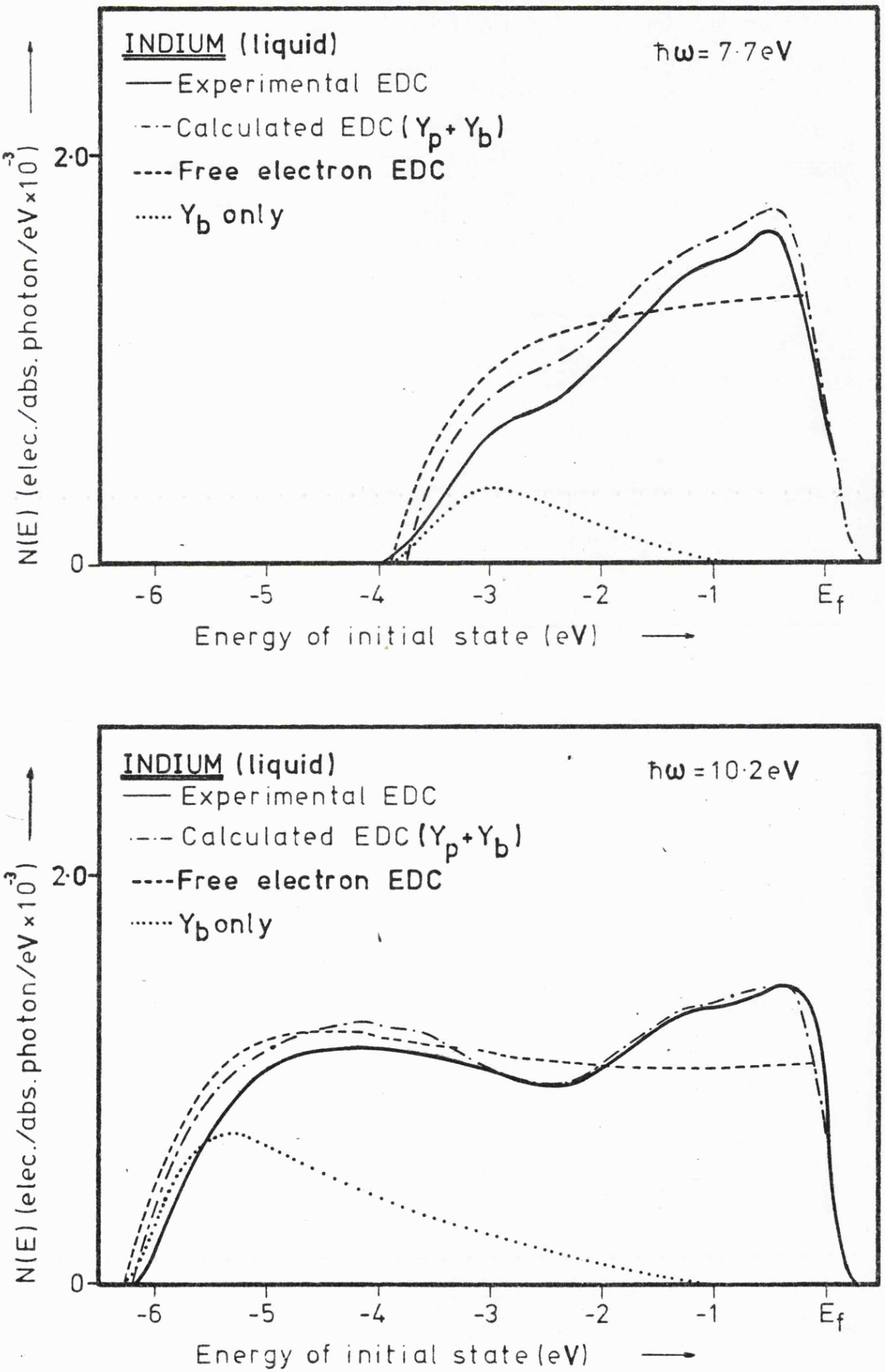

Fig.5.13-Comparison of calculated & experimental EDCs for liquid indium

In Figure 5.12 the final optical density of states is compared with the density of states obtained by Koyama for the solid. This is shown since the densities of states published for the liquid (Shaw and Smith 1969 and Chan and Ballentine 1971) are essentially featureless. It may be seen that there is good agreement in the position of the main maximum at ≈ 4 eV and in the main minimum at ≈ -3 eV. The agreement is less good closer to the Fermi edge. The densities of states for the solid obtained by Shaw and Smith (loc.cit.) and Ashcroft and Lawrence (1968) are in less good agreement - Shaw and Smith placing the main maximum at ≈ -3 eV and Ashcroft and Lawrence placing it at ≈ -5 eV.

5.2.7. Discussion

There are several features of note in these results. Firstly, although the structure observed in the liquid shows behaviour characteristic of non-direct transitions, whilst that in the solid is characteristic of direct transitions (particularly in the rapidly frozen form), the broad density of states features remain unchanged. This implies strongly that aspects of the solid state band structure persist on melting - notably the peak at ≈ -4 eV with an associated dip at -2.6 eV. These may be related to the large band gap at the L face of the Brillouin zone. Secondly, the fact that the broad density of states features remain unchanged over a large range of energies (including the XPS results of Pollak) indicates that the effect of matrix elements is not significant since these would show an energy dependance.

The good agreement between the theoretical EDC's calculated using a 3-step model with non-direct transitions, and the experimental EDC's is highly encouraging.

5.3. Aluminium

5.3.1. Experimental

Aluminium is an archetypal free electron metal and, as such, has naturally attracted a lot of interest both from a theoretical and practical viewpoint. Experimentally it was the most difficult to handle of the materials used. Liquid aluminium is very corrosive (Liquid Metals Handbook 1955), necessitating the use of an alumina crucible and specimen table, and, due to the relatively high expansion coefficient of solid aluminium, considerable problems were encountered with cracking of these crucibles. The high surface tension of the liquid also made it very difficult to pour. Further, the high specimen heater currents needed to maintain the aluminium in a liquid state resulted in a high background noise level. However, since the oxide of aluminium is denser than the metal itself, even a fairly badly contaminated solid surface could be recovered by remelting.

The results given here are from two experiments, and some preliminary results have already been published (Norris et al 1974).

5.3.2. Yield of Aluminium

Figure 5.14 shows the yield of aluminium obtained in the present work. This is given in electrons/incident photon rather than electrons/absorbed photon for the purposes of comparison with the results of other workers. Due to problems

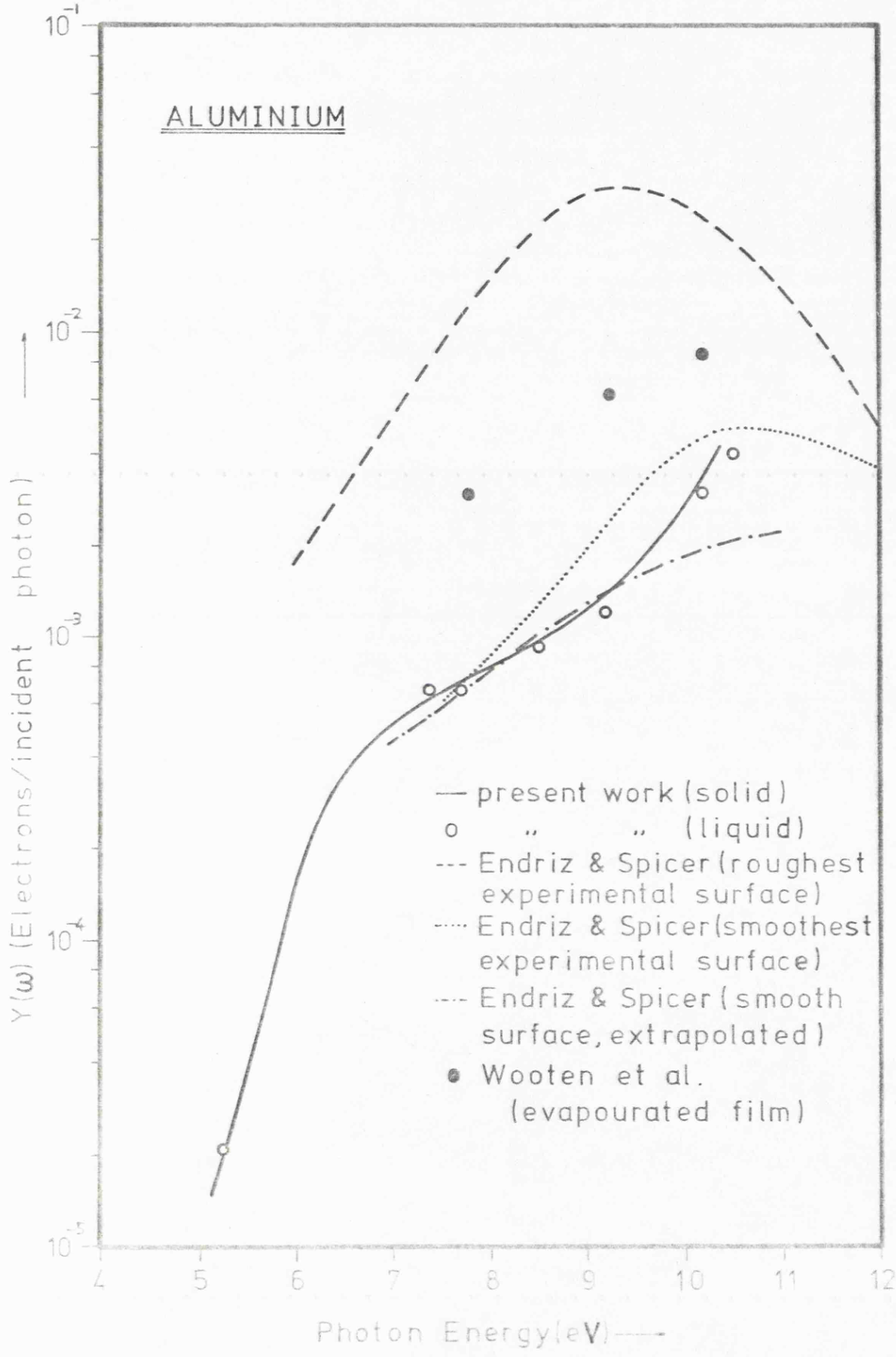

Fig.5.14 - Yield of Aluminium

mentioned earlier with the high specimen heater current required, only isolated values of the yield of the liquid are given as the high background noise level made more detailed measurement impossible. However, the isolated results obtained agree well with the results for the solid. There is a known surface plasmon in aluminium at 10.4 eV, and the variation of the strength of this with surface roughness has been examined in some detail by Endriz and Spicer(1974). They examined a series of evaporated aluminium films of varying surface roughness over the range $\chi = 8 - 28\text{Å}$ where χ = the rms height variation of the surface. On the basis of these results they calculated the yield for a perfectly smooth aluminium surface. Their results for $\chi = 8\text{Å}$ and $\chi = 28\text{Å}$ are shown on diagram 5.13, with the calculated yield. It may be seen that their prediction of the yield for $\chi = 0\text{Å}$ is in good agreement with the observed yield in this work at low photon energies, implying that the liquid surface is very smooth.

Faber (1972 P.91) has derived an expression for the estimation of the roughness of a free liquid surface of the form:- f being the surface tension

$$\chi = \left(\sum \overline{\xi^2}\right)^{1/2} = \frac{k_B T}{4\pi f} \log_e \left(\frac{4\pi f}{d g a}\right) \qquad (5.2.)$$

where ξ = the displacement due to a given ripple mode for a close packed surface, $a = 1.09\ (^m/_d)^{2/3}$, m = atomic mass, d = density. Filling in the appropriate values for aluminium, this gives a value for χ of 2.08Å which is in good agreement with the observed result for photon energies below 9.5 eV. Above

this energy the yield begins to rise sharply. The reason for this is not obvious since the lower energy result indicates that the plasmon effect should be small. However it is possible that, since the high surface tension of aluminium resulted in a sharply curved surface ($d \simeq 0.4$ cm.), that this effect is due to non normal incidence of the light on the specimen. This would result in the generation of photo-electrons closer to the surface than in the case of normal incidence, giving a higher yield, particularly at higher photon energies.

More surprising is the coincidence between the yields for solid and liquid. This suggests strongly that the solid surface retains many of the physical characteristics of the liquid - a suggestion that is borne out by the observation that the frozen surface was very liquid-like in appearance and remained non-oxidised for a considerable period of time after removal from the vacuum system. Figure 5.15 shows a typical frozen aluminium surface. Figure 5.16 shows a Fowler plot for solid aluminium. This gives a value for the yield of 4.02 ± 0.04 eV, which differs somewhat from the results of other workers (Riviere 1969).

5.3.3. Liquid Aluminium EDC's

Figure 5.17 shows EDC's for liquid aluminium taken at low photon energies at approximately 50^{o}C above the melting point. The major feature seen is a peak at -2.5 eV with a corresponding dip at -3.7 eV. However, there is also a very weak feature visible in the form of a peak at -1 eV. These features do not appear to vary with photon energy, although the peak at -1 eV is so weak that it is impossible to be sure

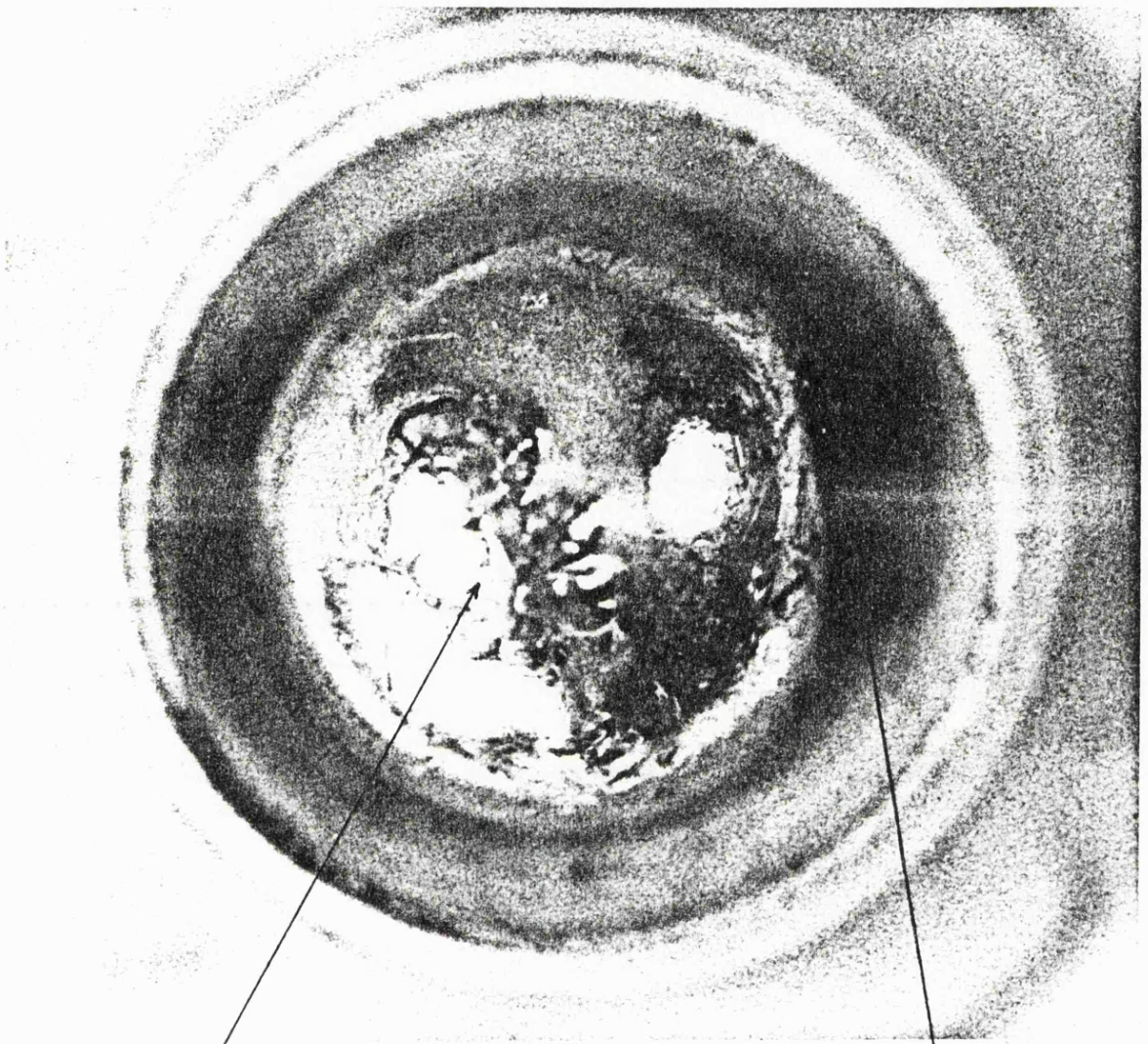

Fig.5.15 Surface of frozen aluminium

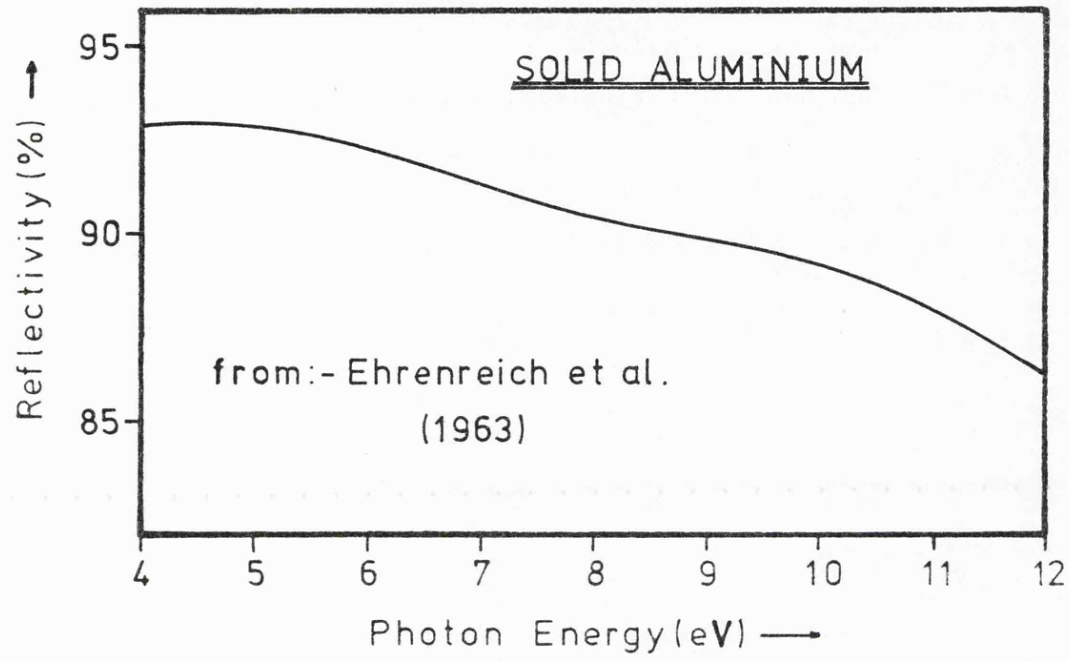

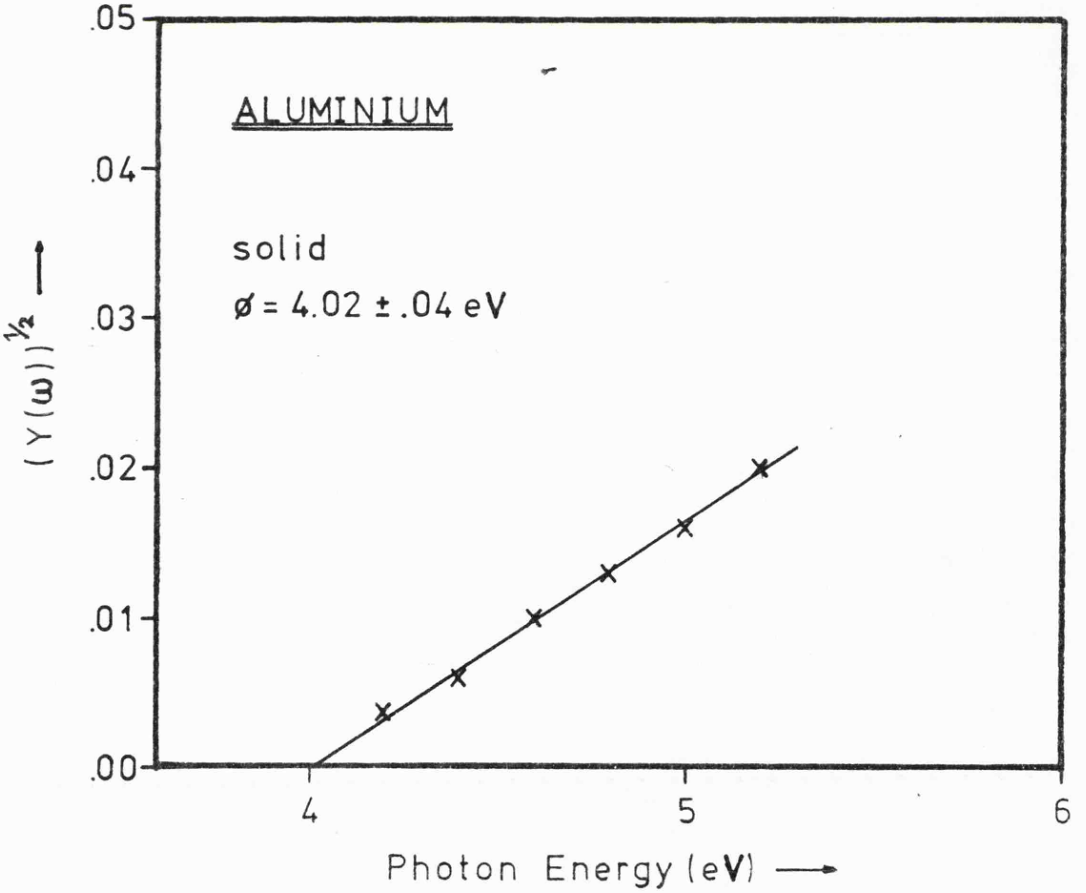

Fig.5.16-Reflectivity & Fowler plot for solid Aluminium

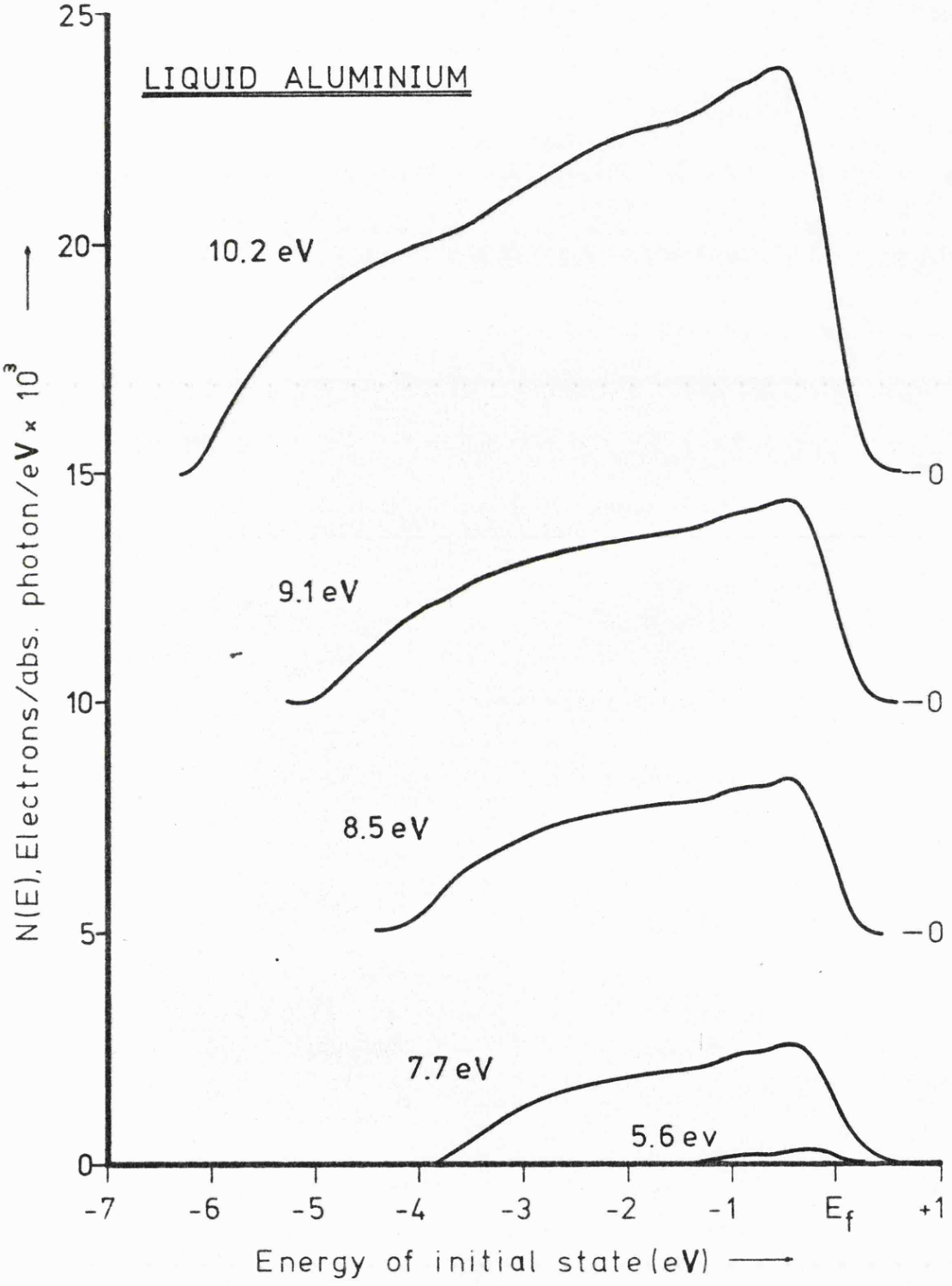

Fig 5.17- Low energy EDCs from liquid Aluminium

of this, so that the peaks may well reflect structure in the density of states. Attempts to work at higher temperatures were unsuccessful due to limitations in the heater design.

5.3.4. Solid Aluminium EDC's

Figure 5.18 shows EDC's for solid aluminium at low photon energies. The major feature still occurs at -2.5 eV with a dip at -3.7 eV, and this is in good agreement with a feature observed both by Wooten et al (loc.cit.) and by Endriz and Spicer (loc.cit.). However there are also two other features in the form of very weak peaks at -1 eV and -1.5 eV which become stronger with increasing photon energy, though they are too weak for any changes in position to be discerned.

5.3.5. High Energy EDC's

Figure 5.19 shows a set of EDC's for liquid aluminium obtained at 21.2 eV. Curve (c) is for freshly poured aluminium and shows features at -2.5 eV, -6.5 eV and -11 eV, the peak at -1.0 eV observed in the low energy EDC's not being resolved. Curves (a) and (b) show the same specimen after a period of time. The peak at -6.5 eV has increased sharply in strength showing clearly that this is due to contamination (aluminium has a very strong affinity for oxygen). The features at -2.5 eV and -11 eV appear unaffected and may well be characteristic of the pure material. The sharp edge at -10.2 eV interpreted by Lindau et al (1971) as being due to a plasmon loss does not appear, suggesting again that the surface is very smooth.

Figure 5.20 shows the high energy parts of the EDC for solid (b) and liquid (a) aluminium. These are very similar

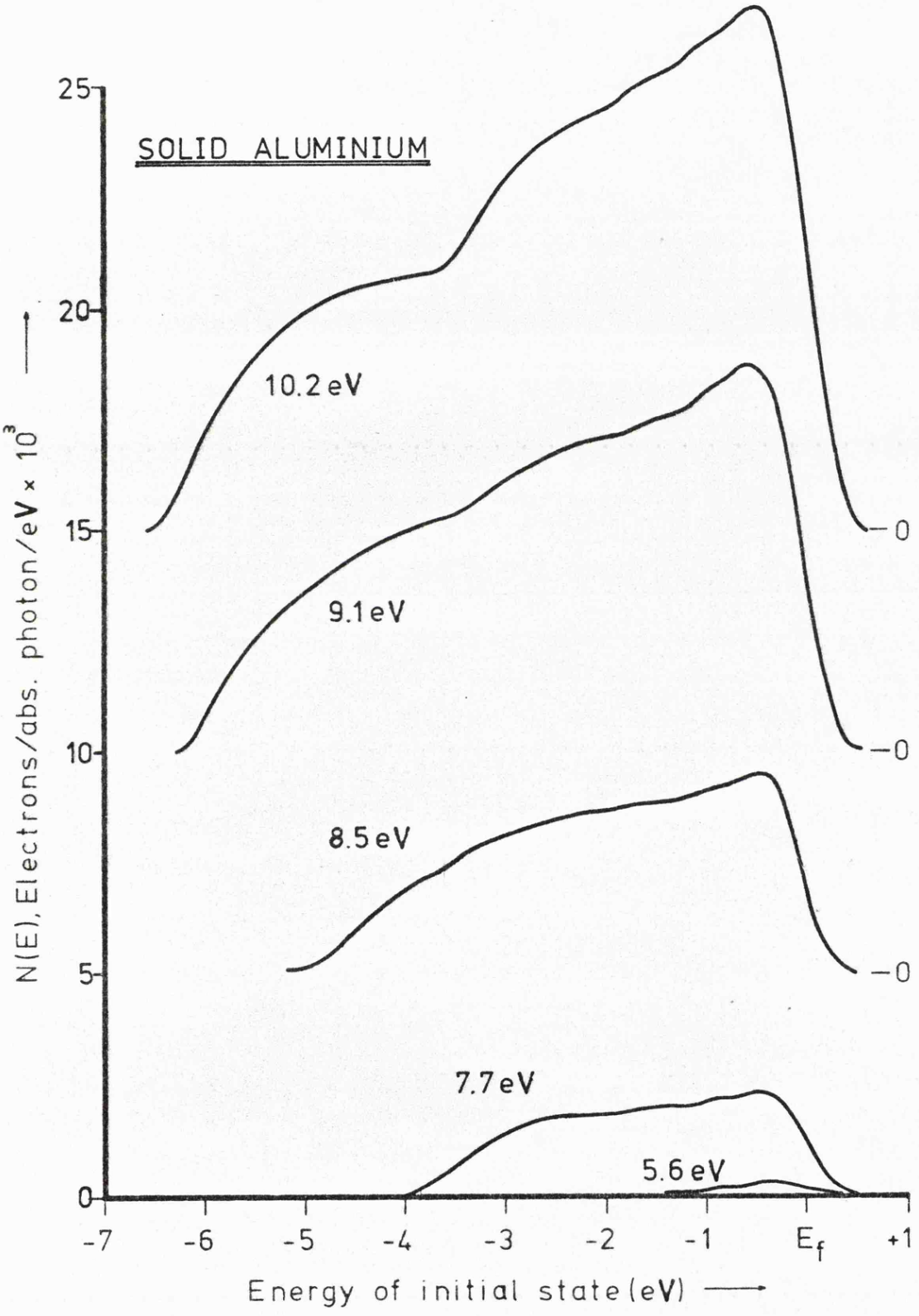

Fig.5.18-Low energy EDCs from solid Aluminium

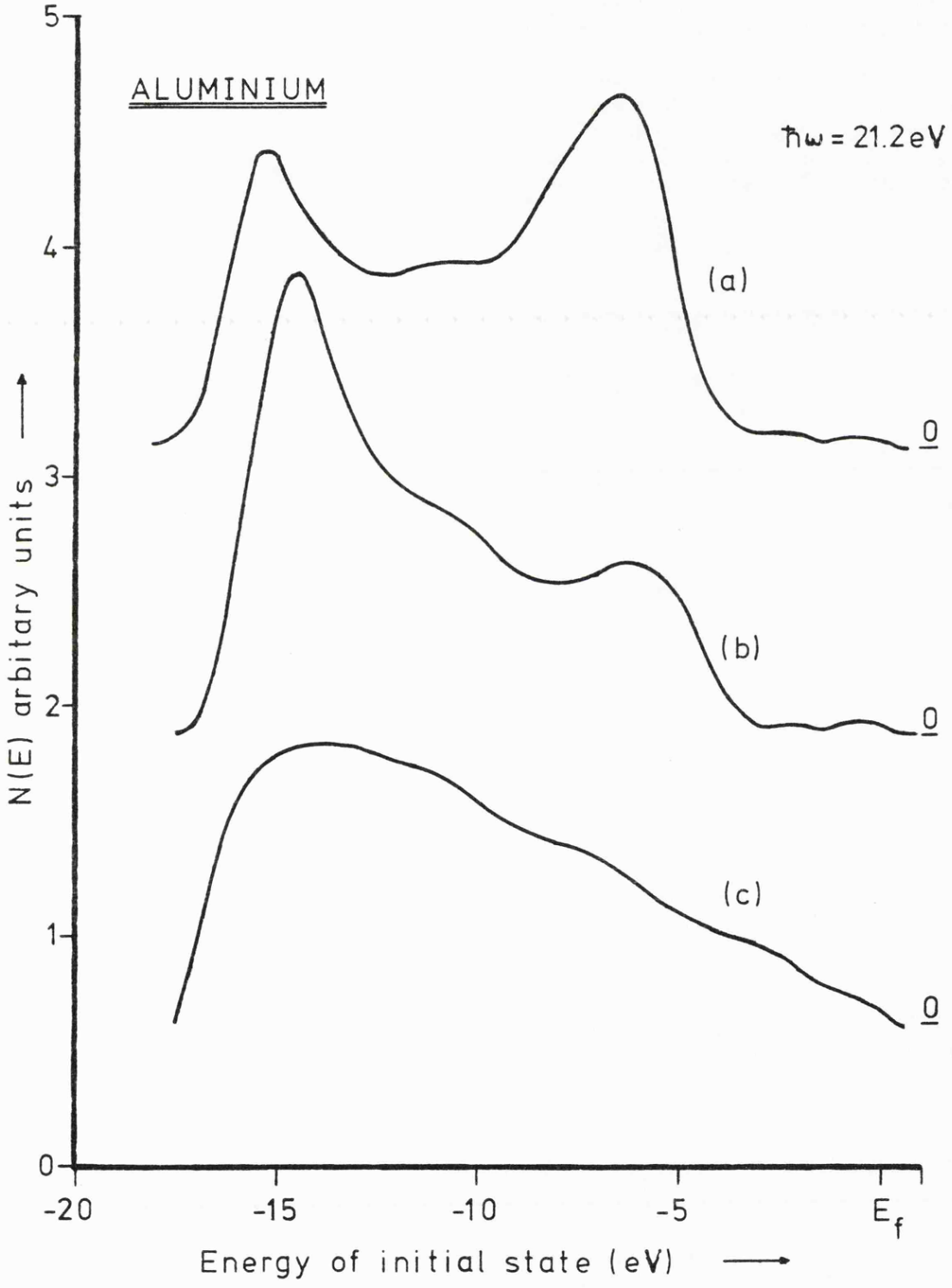

Fig.5.19-High energy EDCs from liquid Aluminium

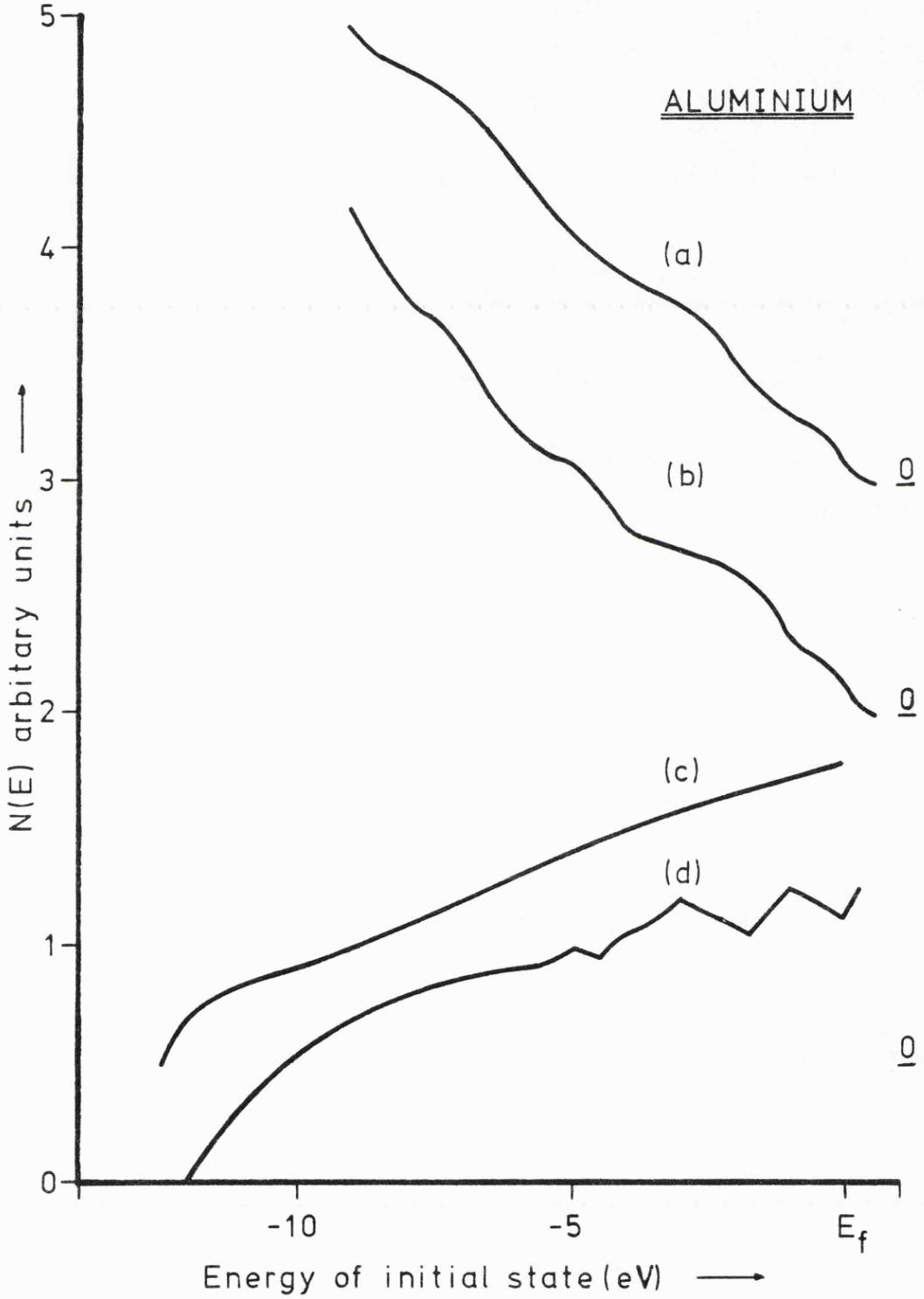

Fig.5.20-Structure near the Fermi edge in high energy EDCs from solid and liquid Aluminium

except for the appearance of a small feature at -4.9 eV in the solid. They are compared with theoretical densities of states for the liquid from Chan and Ballentine (c) and for the solid from Ashcroft (d). Although no structure is apparent in the liquid density of states, it is noteworthy that the feature at -2.5 eV observed in the liquid and solid EDC's corresponds with a strong peak in the solid density of states.

5.3.6. Optical Density of States

A free electron density of states was used as the basis for a repetition of the iterative process used for indium. Figure 5.21 shows the final optical density of states compared with a free electron density of states.

The theoretical curves are compared with the experimental results in Figure 5.22 at 10.2 eV and 7.7 eV. It may be seen that the use of a free electron density of states results in a far greater scattered background than is observed experimentally. The value of the yield obtained theoretically is not in agreement with that measured experimentally although the agreement of the EDC's is structurally good. The theoretical yield does however agree with the extrapolated smooth surface yield of Endriz and Spicer (loc.cit.). The values of absorption coefficient used were from Philipp et al (1964). The value of l_e required to give agreement with the measured yield at 7.7 eV was 18Å. This is much shorter than the value of l_e = 70Å given by Wooten et al (1966) and is in good agreement with the results of Callcott and Arakawa (1975) for the solid. However, the smooth surface in the present work appears to remove most of the plasmon

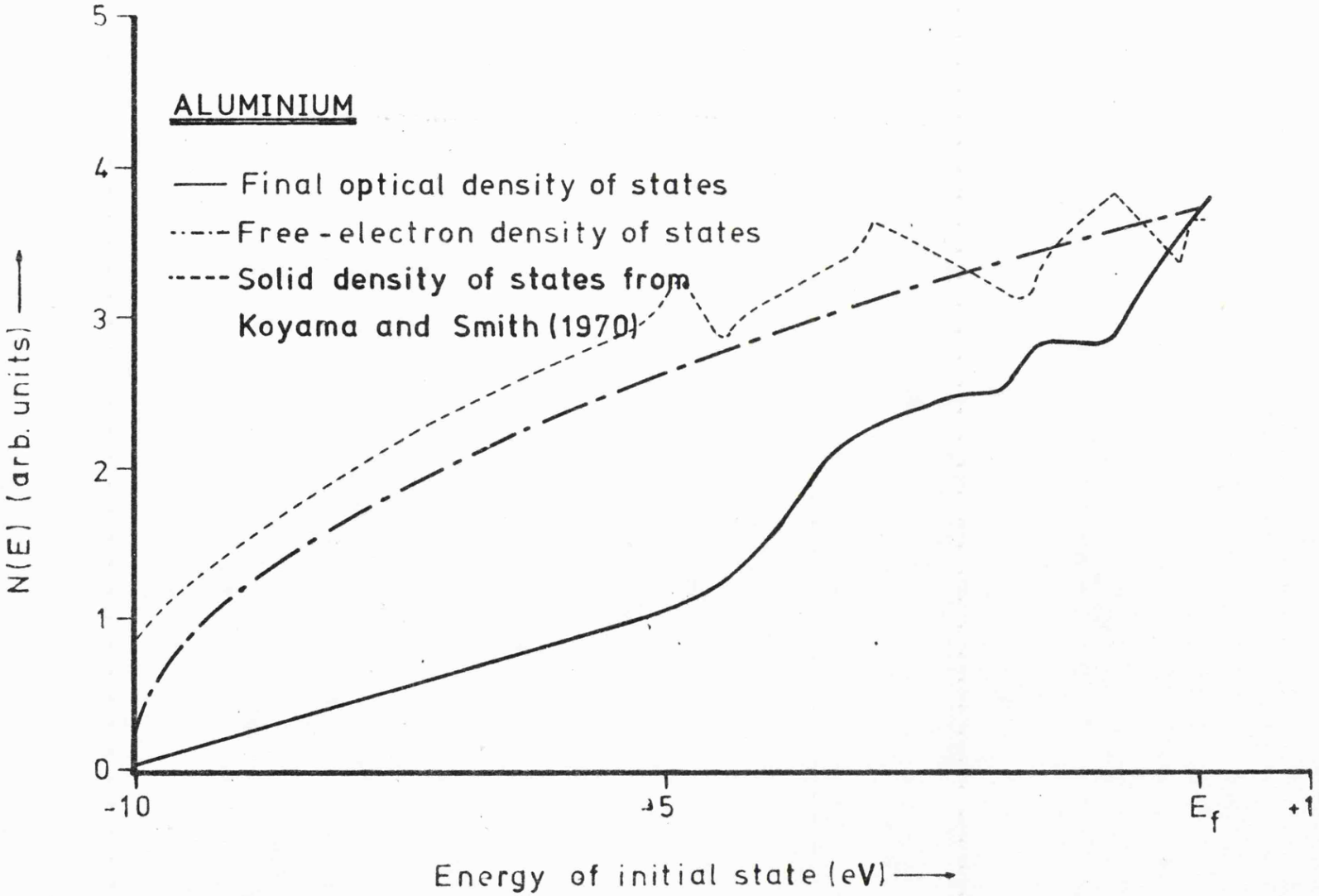

Fig.5.21-Final optical density of states for Aluminium

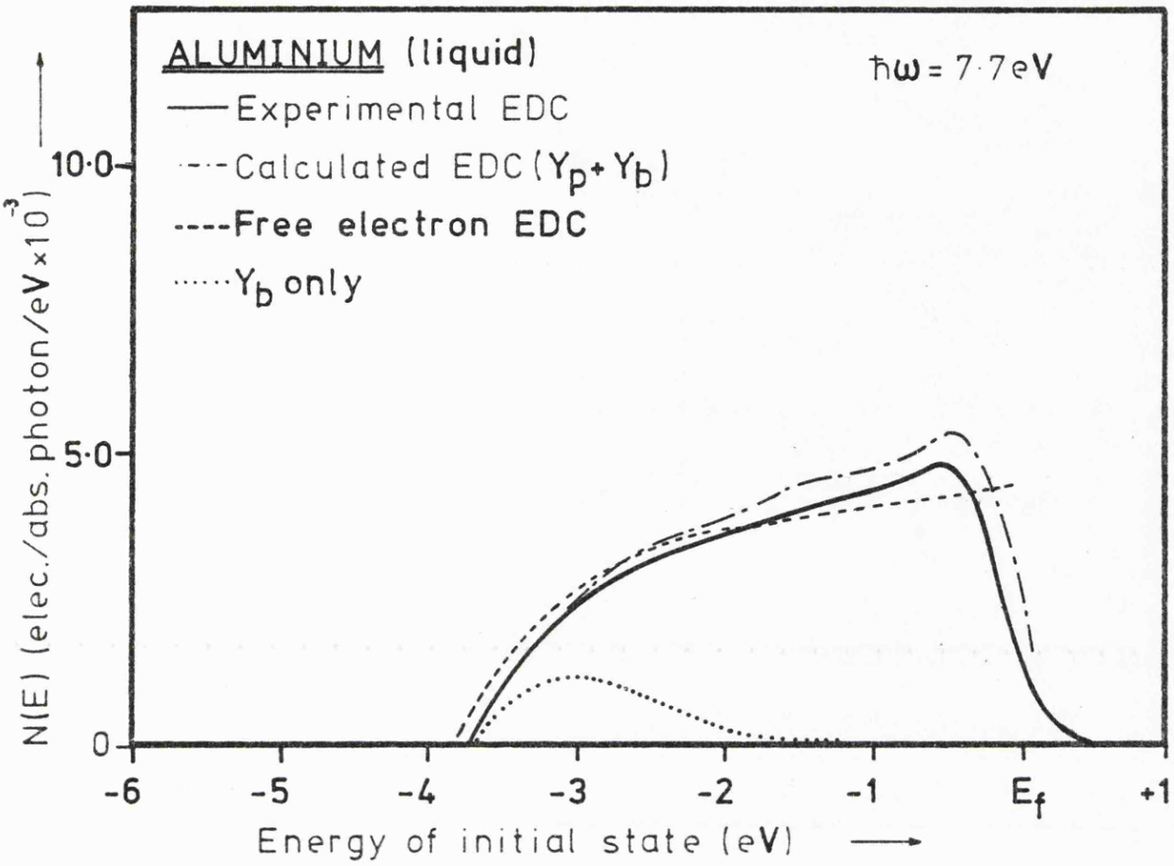

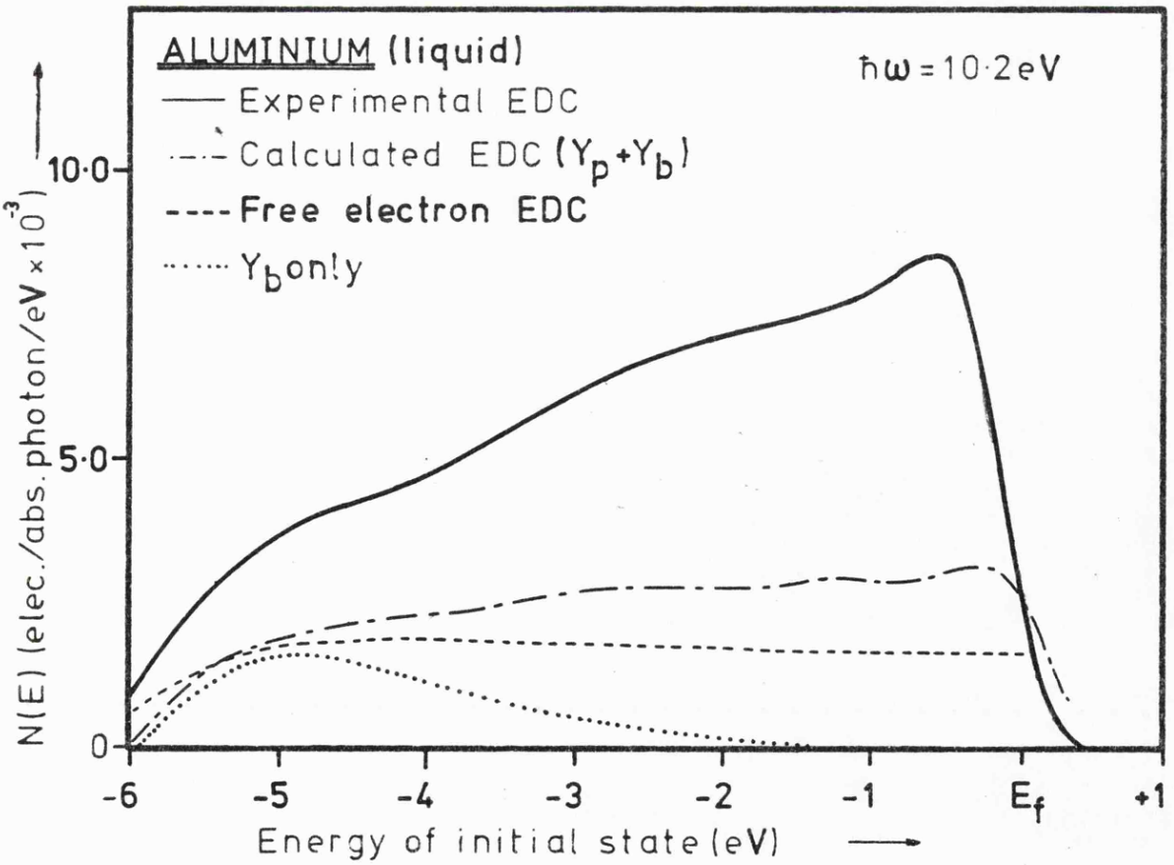

Fig.5.22 - Comparison of calculated & experimental EDCs for liquid aluminium

effects that could cause error in the estimation of l_e, and this may account for the above difference. In Figure 5.21 the final optical density of states is compared with the calculated density of states of Koyama and Smith (loc.cit.) for the solid. This shows good agreement in the position of the main maximum around -3 eV, but not in the structure closer to the Fermi edge. This density of states is used for comparison in preference to one for the liquid since these are essentially featureless (e.g. Chan and Ballentine 1971) as is the XPS result of Pollak (1972).

5.3.7. Discussion

The results obtained for aluminium appear to generally confirm the picture presented for indium. The structure in the liquid again shows behaviour more characteristic of non-direct transitions, whilst that in the solid is characteristic of direct transitions. The broad features are, however, unchanged from solid to liquid and are also seen in the high energy spectra. The XPS result is featureless, but this may well be due to the generally poorer resolution in this technique. The major feature - the dip at -4 eV which corresponds with the onset of the second band - is weaker than the dip in indium. This is consistent with the smaller band gaps in the band diagram of aluminium and its generally more free electron like nature. However, as may be seen in Figure 5.21, the optical density of states still differs considerably from the free electron model.

CHAPTER 6:- LEAD AND TIN

6.1. Introduction

Lead and tin are both quadrivalent materials of group IVA. In the solid phase lead ($6s^2 6p^2$) has a f.c.c. structure; metallic (white) tin ($5s^2 5p^2$) has a body centered tetragonal structure. Both metals have been studied fairly extensively, but lead is of particular interest to liquid metal theoreticians as it has some anomalous properties. As stated in 1.4.3., measurements of the Hall effect for liquid lead give a result considerably different from that predicted by n.f.e. theory. Transport measurements also indicate a very low mean free path ($\simeq 4\text{Å}$). Over the past few years there has been considerable work done on the band structure of lead. Early OPW calculations by Anderson and Gold (1965) were followed by Loucks' (1965) Relatavistic APW calculation. More recently, band structures have been published by Breeze (1974) and McFeely et al. (1975), where particular attention has been paid to the splitting of the 6p band, attributed to crystal field effects by Breeze and to spin orbit splitting by Ley et al. (1972). Previous spectroscopic work on lead is confined to measurements of evaporated films by Norris et al. (1972), but since the conclusion of this work, further experiments have been done on the liquid by Wotherspoon (1978). XPS measurements have been done on evaporated films by Pollak (1972) and Ley et al. (loc.cit.).

Solid tin has also been the subject of considerable study, several band structures having been published, the most recent being those of Ament and de Vroomen (1975) and Craven (1969). However, spectroscopic data is confined to the results

of Pollak (1972), Hochst et al.(1976) and most recently Castelijns et al.(1977), all on evaporated films. Stevenson (1968) examined liquid tin but only at low photon energies.

In this chapter UPS results are presented for tin and lead in both solid and liquid phases. They are analysed as before in terms of the 3-step model, and it will be shown that this yields an optical density of states that differs considerably from the free electron picture.

6.2. Lead

6.2.1. Experimental

Lead was found to be a comparatively easy material for this experiment. It has a low melting point ($366^{o}C$), is ductile and is easy to pour. Lead is not highly reactive in the liquid, enabling the use of molybdenum specimen tables and quartz crucibles. Some trouble was experienced with quartz crucibles breaking due to thermal shock, and in one later experiment an alumina crucible was used. The results presented here are from three separate experiments.

6.2.2. Yield

Figure 6.1. shows the quantum yield for lead in both the solid and liquid states. The liquid yield has three major features - sharp peaks at 5.9 and 7.9 eV, with a broad peak centered at 9.5 eV. On freezing, the peak at 9.5 eV largely disappears and the peak at 5.9 eV splits into two peaks - a sharp one at 6.4 eV and a weaker feature at 5.5 eV. The magnitude of the yield remains largely the same although it is much higher than that observed by Norris et al (1972) and in the

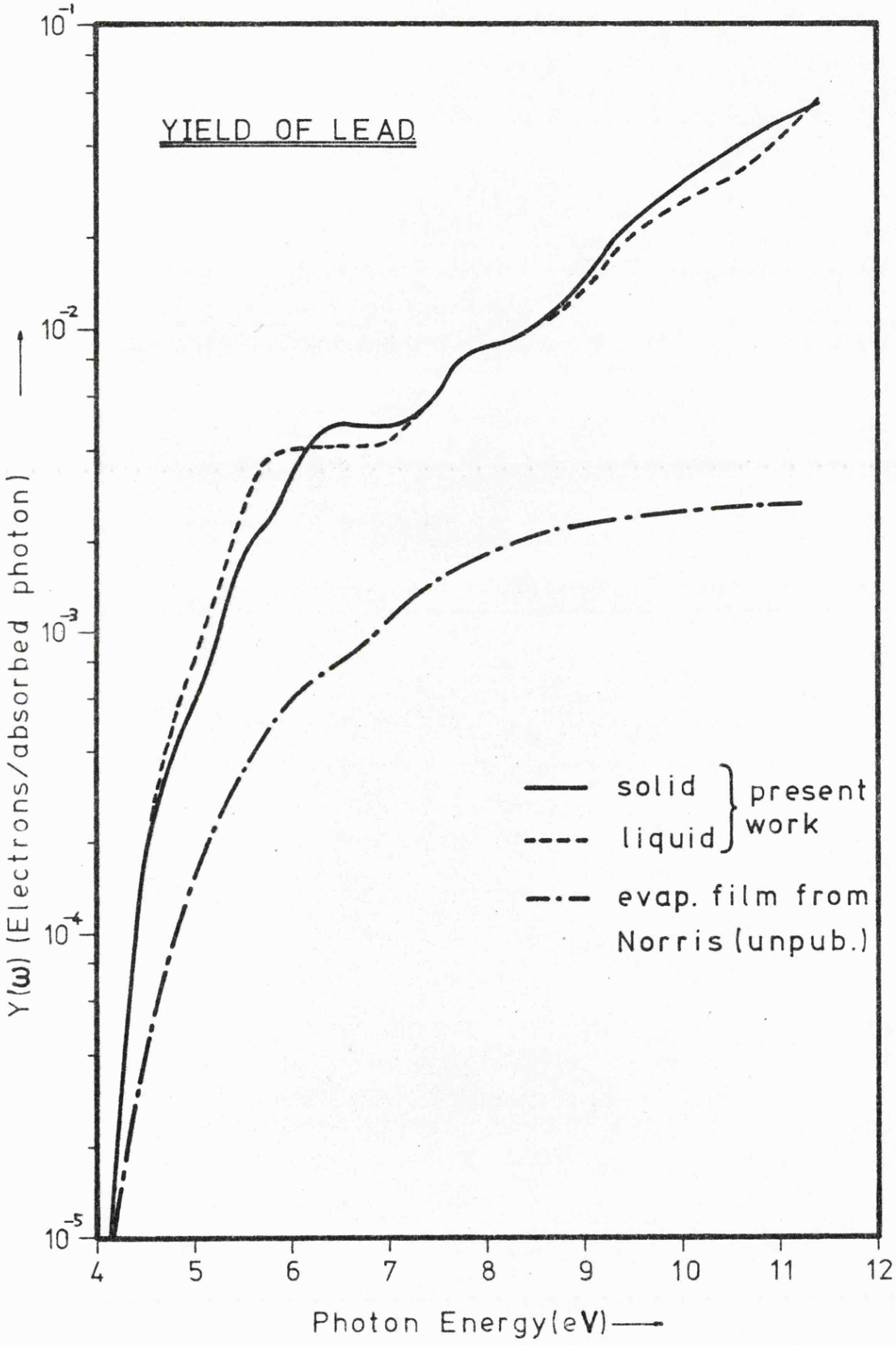

Fig.6.1-Yield of solid & liquid Lead

later work of Wotherspoon (loc.cit.). However, Wotherspoon did observe similar behaviour on freezing.

A Fowler plot (Figure 6.2.) gives a value for the work function of 3.94 ± .03 eV for the solid and 3.99 ± .03 eV for the liquid. This is in excellent agreement with the value of 3.95 eV obtained by Norris et al (1972). In the absence of any suitable reflectivity data for liquid lead, both solid and liquid yields were calculated using the results of Lemmonier et al (1973) for evaporated films (Figure 6.2.).

6.2.3. Liquid Lead

Figure 6.3. shows EDC's obtained for liquid lead for low photon energies. Only one major feature is apparent – the peak at -2.6 eV which is very strong. These EDC's are very similar to those obtained by Norris et al (1972) for an evaporated film except that the peak seen in that work, just below the Fermi edge, does not appear. The structure seen appears to be constant both in position and strength. The position of the major feature differs from that observed by Wotherspoon (loc.cit.) who placed it at -1.9 eV in the liquid.

6.2.4. Solid Lead

There are two sets of EDC's for solid lead. As explained in Chapter 5 the rate of freezing appears to affect the crystallinity of the surface, which is very highly structured (see Figure 6.4.) and, as may be seen from Figures 6.5. and 6.6, the EDC's contain many features.

In the rapidly frozen solid the single major feature of the liquid has split into three peaks. There is a major peak

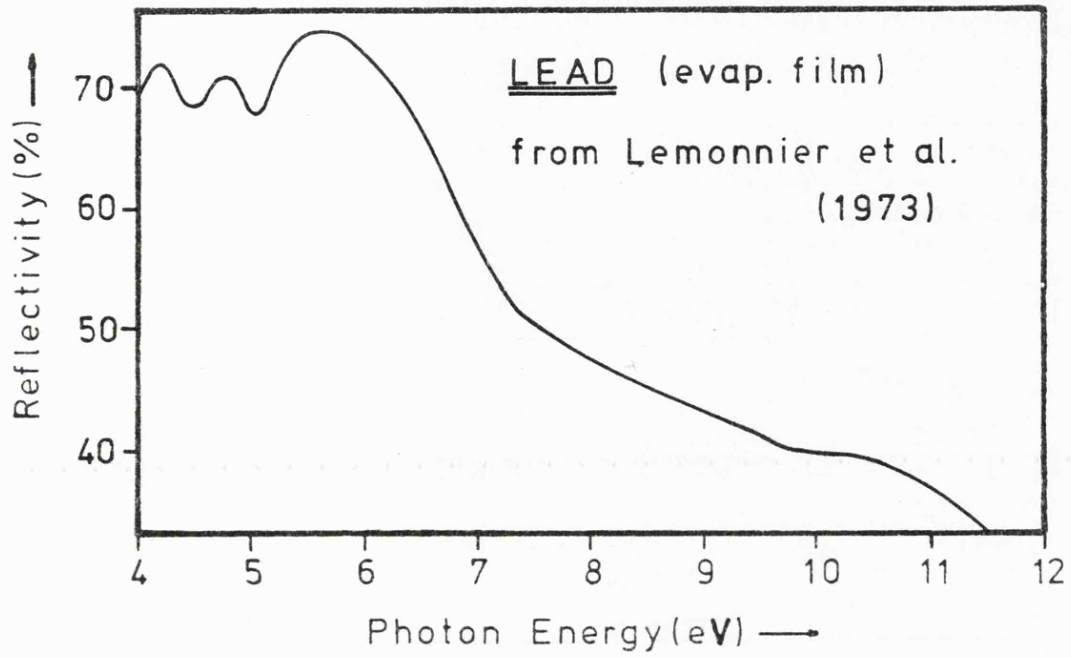

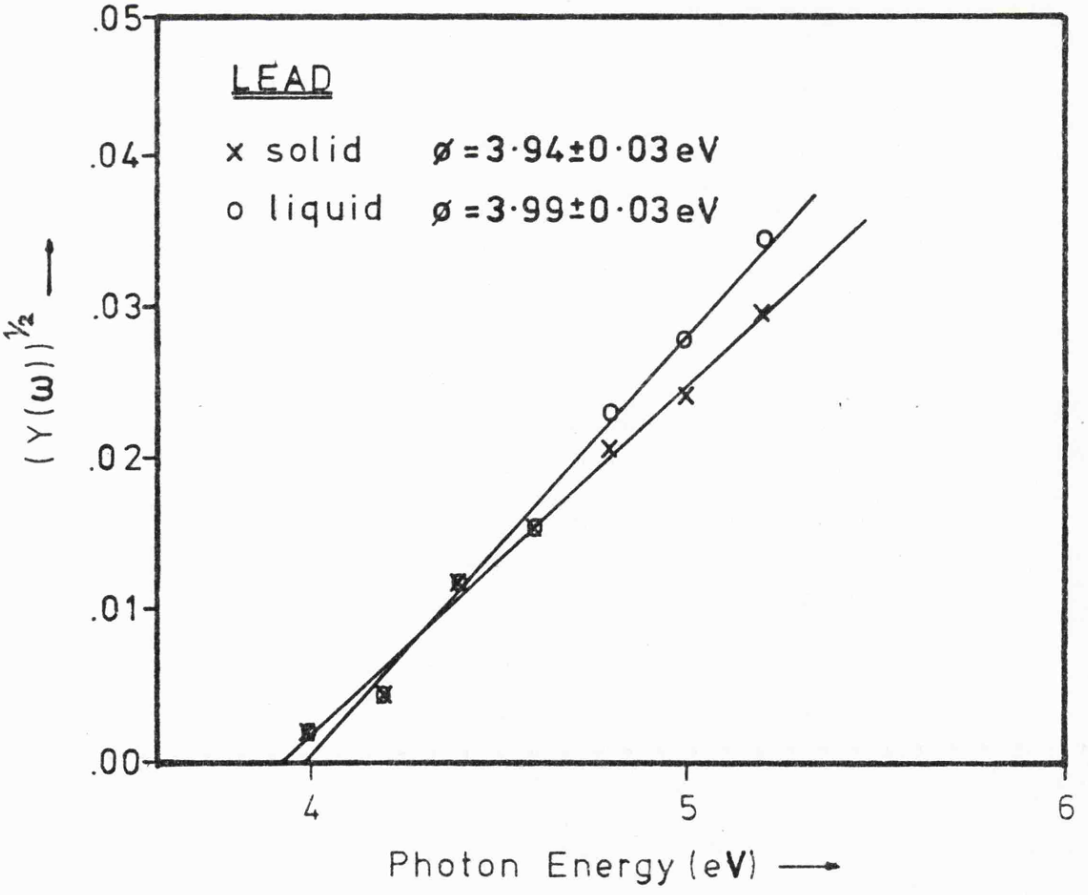

Fig 6.2 - Reflectivity & Fowler plot for solid & liquid Lead

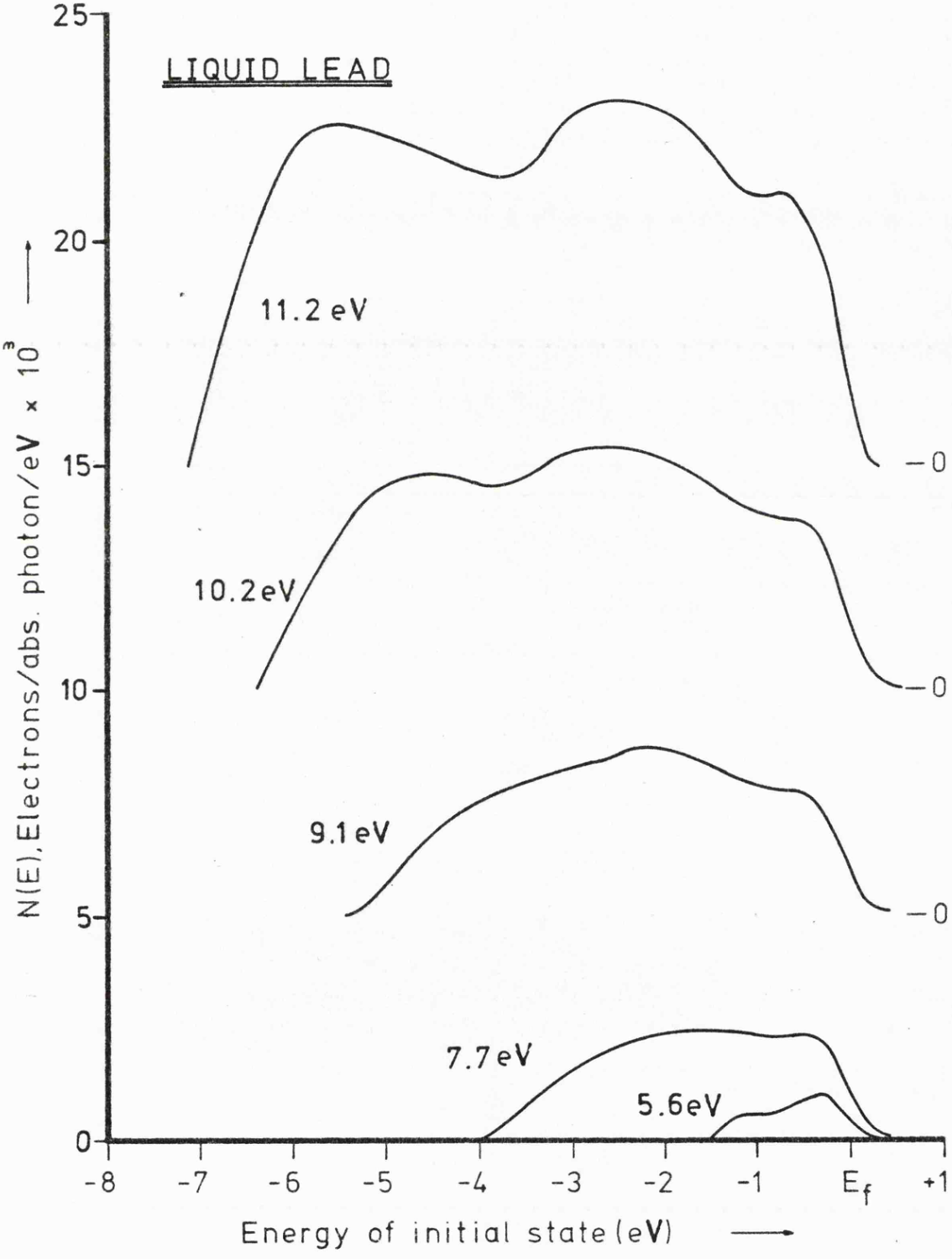

Fig.6.3-Low energy EDCs for liquid Lead

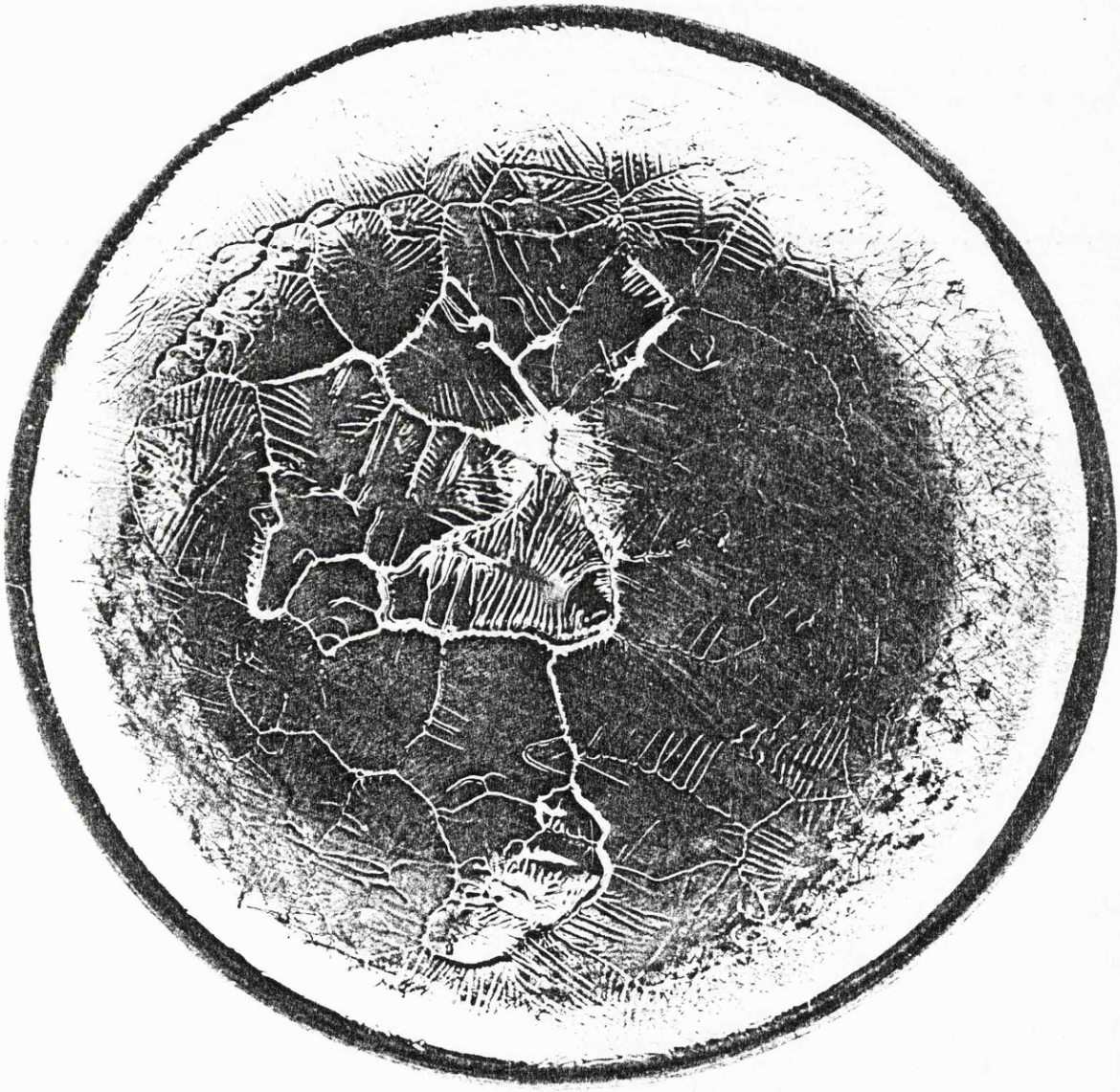

Fig.6.4-Surface of frozen Lead

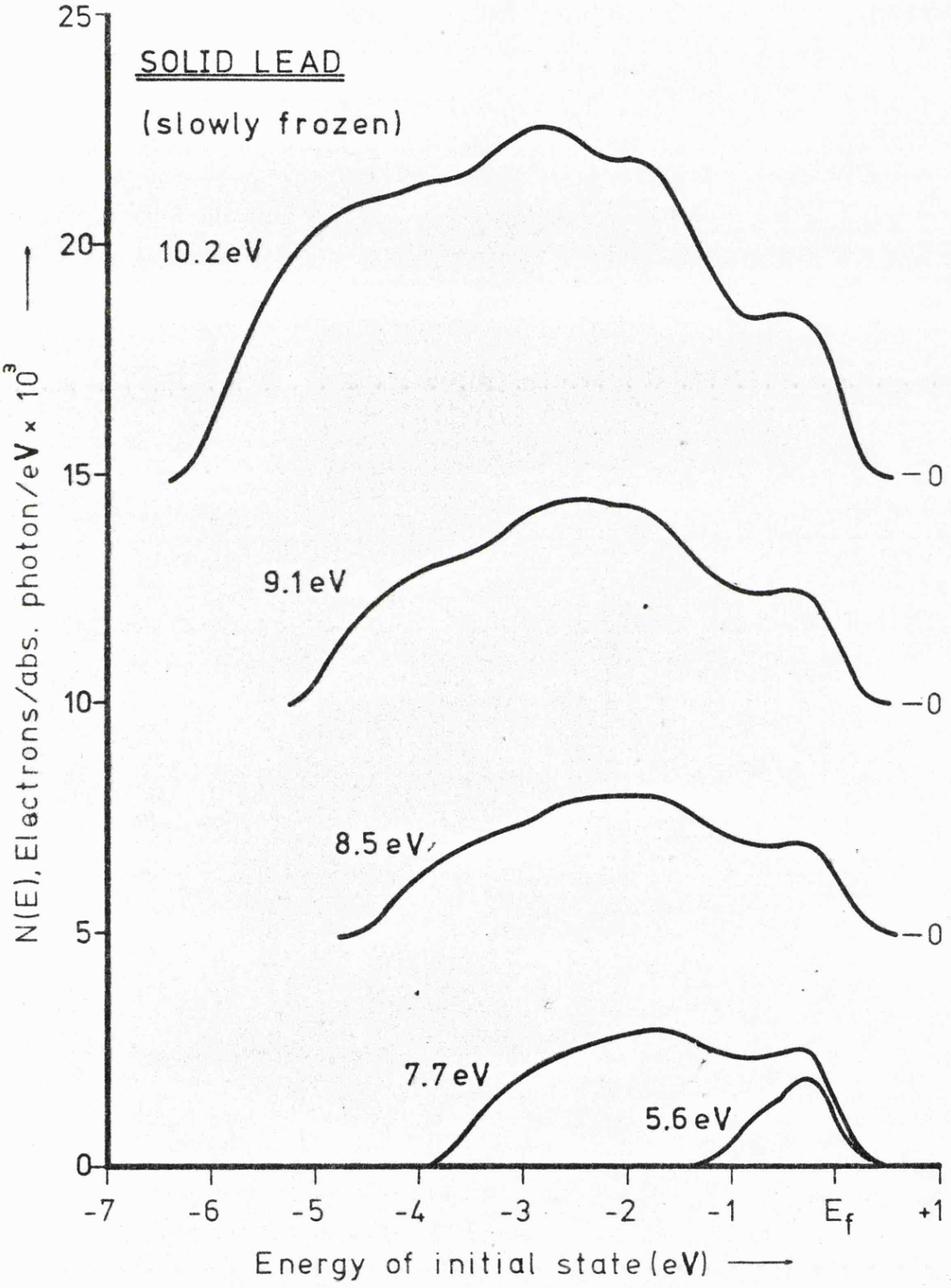

Fig.6.5-Low energy EDCs for slowly frozen Lead

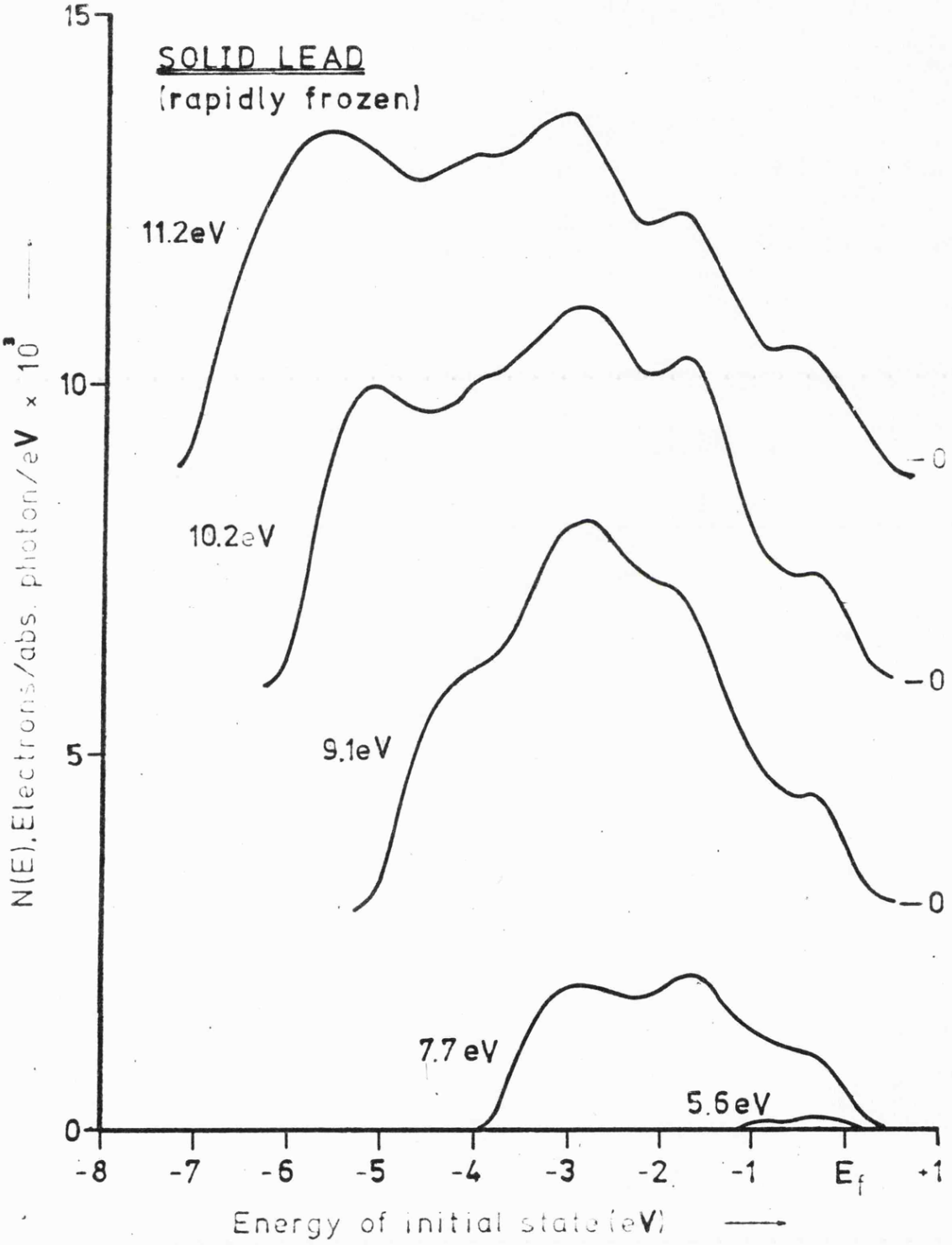

Fig.6.6-Low energy EDCs for rapidly frozen Lead

centered at -3 eV, which appears to be fairly constant in strength. This is flanked by two minor peaks, both of which vary in strength, one varying in position between -1.8 and -2 eV, appearing at maximum strength at 10.2 eV photon energy, and one at -4.1 eV appearing to increase in strength with photon energy. There is a suggestion that the major peak at -3 eV may be a doublet, as it appears to be flat topped at higher photon energies, but this is not resolved fully.

In the slowly frozen solid the same structure is apparent but in a greatly weakened form. The separate peaks are only properly resolved at high photon energies, so that at lower energies the merging of the peaks at -3.0 eV and -1.8 eV give the appearance of a single peak centered at -2.6 eV as in the liquid. The slowly frozen solid thus appears to be an intermediate step in structure between the rapidly frozen solid and the liquid - this is supported by the observation that the evaporated film results of Norris et al (1972) are very liquid like.

6.2.5. High Energy EDC's

Figures 6.7. and 6.8. show EDC's for solid and liquid lead at 16.8 and 21.2 eV compared with those of Wotherspoon (loc.cit.). At these energies the separate peaks seen at low energy in the solid are not resolved, and both liquid and solid have a single feature at -2.6 eV. The solid and liquid differ quite strongly away from the Fermi edge, only one feature being observed in the liquid - a peak at -7.5 eV. In the solid two features were observed - peaks at -5.5 and -11 eV, there being a dip at -7.5 eV. The results of Wotherspoon do not confirm these features in the solid, although this may be due to freezing

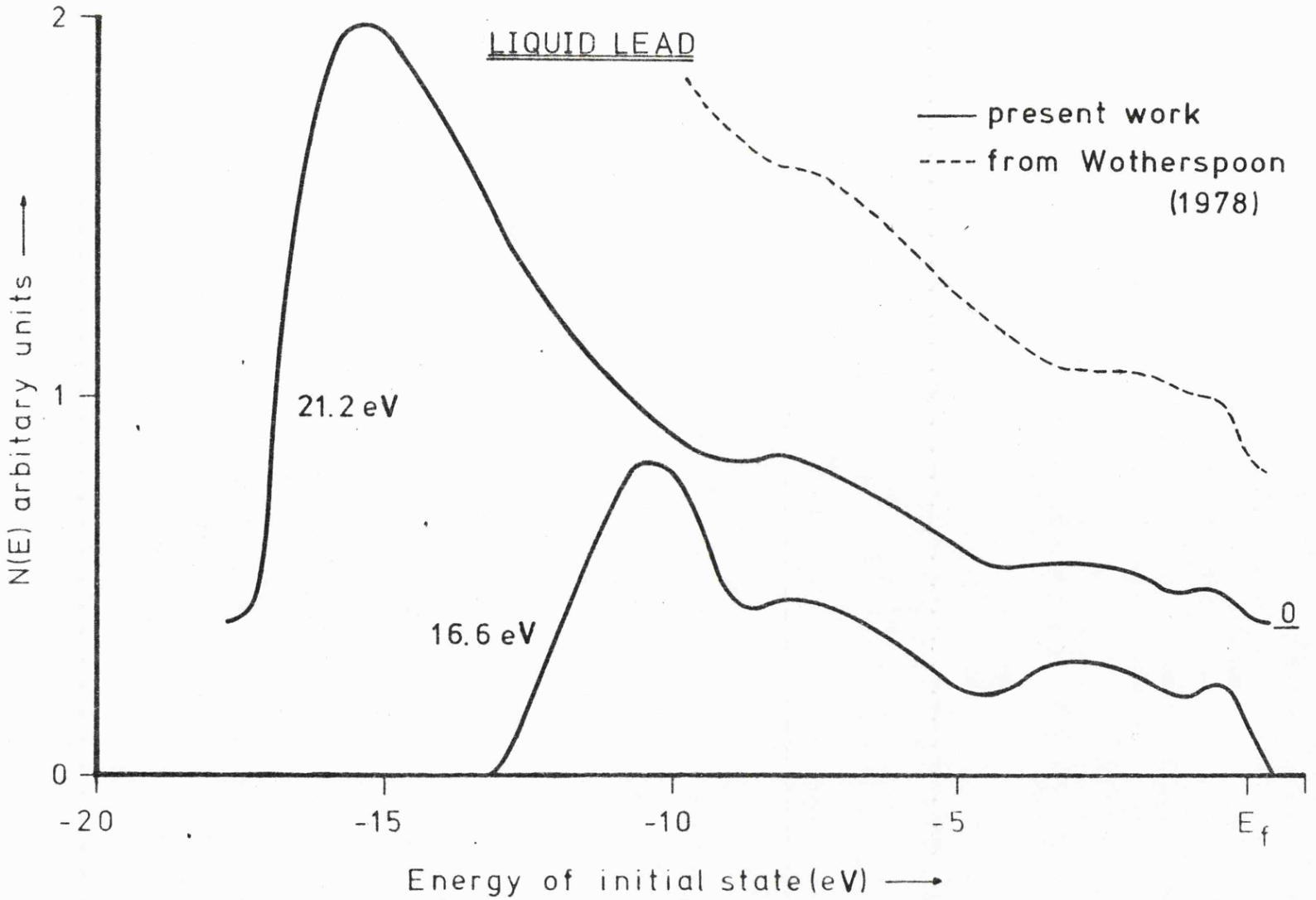

Fig.6.7-High energy EDCs from liquid Lead

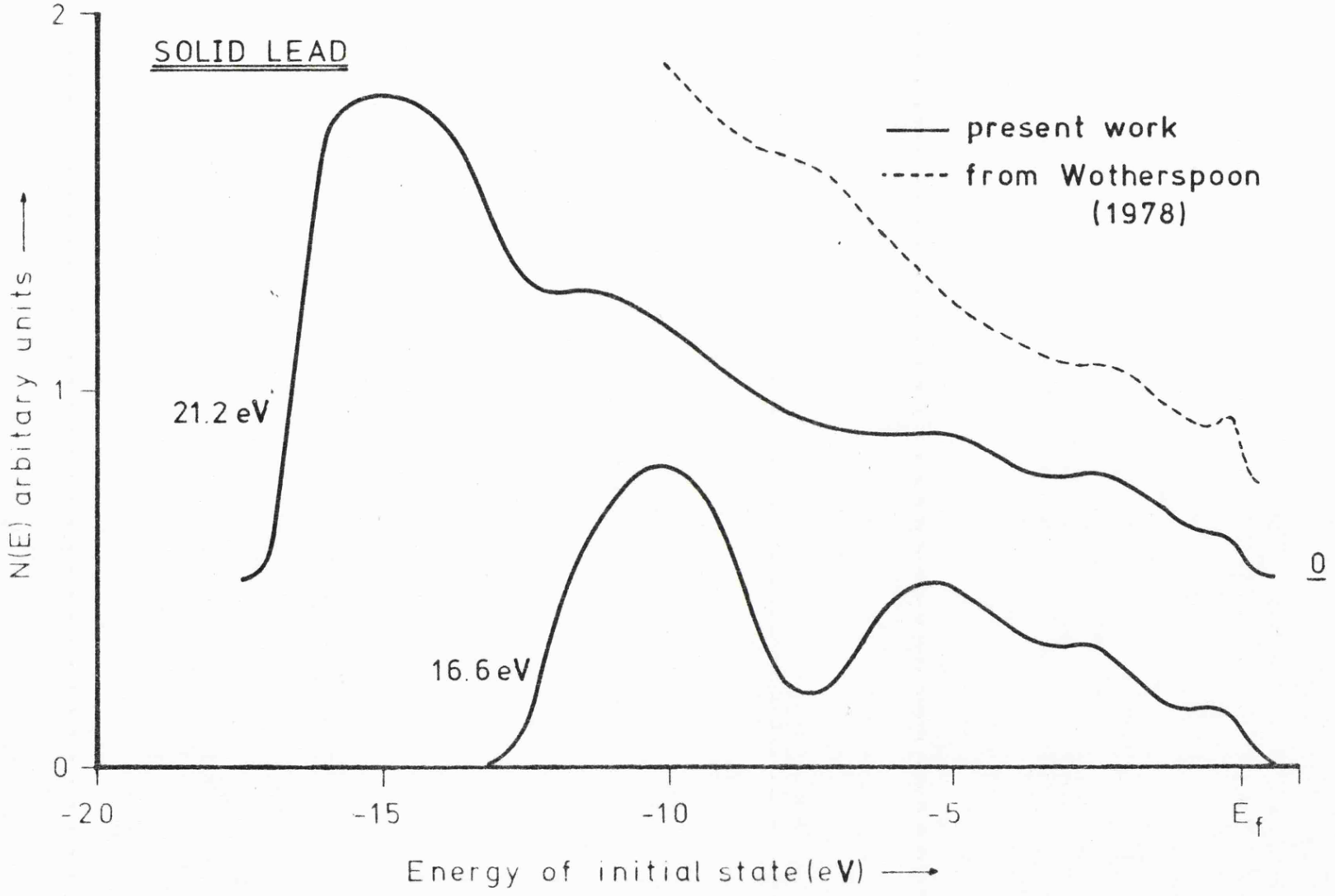

Fig.6.8-High energy EDCs for solid Lead

the liquid in a different form. However, both his results for the liquid and those of Norris et al (1972) for an evaporated film agree on the existence of a peak at -7.5 eV.

6.2.6. Optical Density of States

The 21.2 eV EDC for liquid lead was used, with the background subtracted, as the starting point for an analysis, as detailed previously. In Figure 6.9 it is compared with the XPS result of Pollak (loc.cit.) which is in good agreement regarding the peak at -2.6 eV.

Figure 6.10 shows the optical density of states obtained from the analysis. This can be seen to differ considerably from the free electron picture. Figure 6.11 shows the EDC's obtained from this density of states compared with the experimental results. Although the agreement of the yield at high energy is poor, it may be seen that the agreement of both the structural strength and position are good. The values for the absorption coefficient were taken from Lemonnier et al (1973). The value of l_e obtained from the analysis was 30Å. This is higher than the value of 10Å obtained by Wotherspoon (loc.cit.) but is not inconsistent with the work of Brundle (1974).

6.2.7. Discussion

As in the case of the previous two metals, the liquid specimen shows behaviour characteristic of non-direct transitions, whilst the solid behaviour is characteristic of direct transitions. Again, as previously, the structure observed appears to be invariant over a wide energy range indicating that the effects of matrix elements are small.

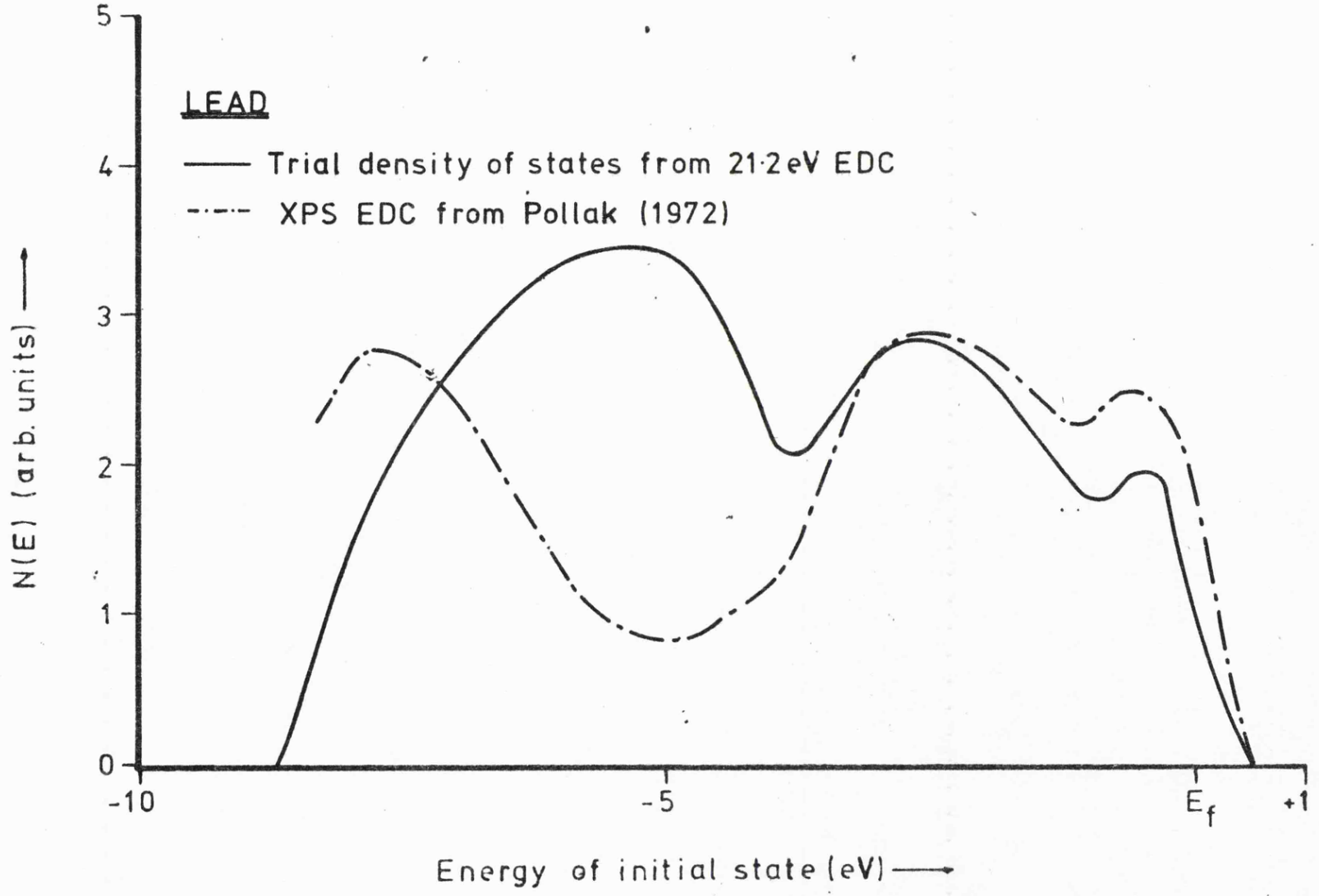

Fig.6.9- Trial optical density of states for liquid Lead

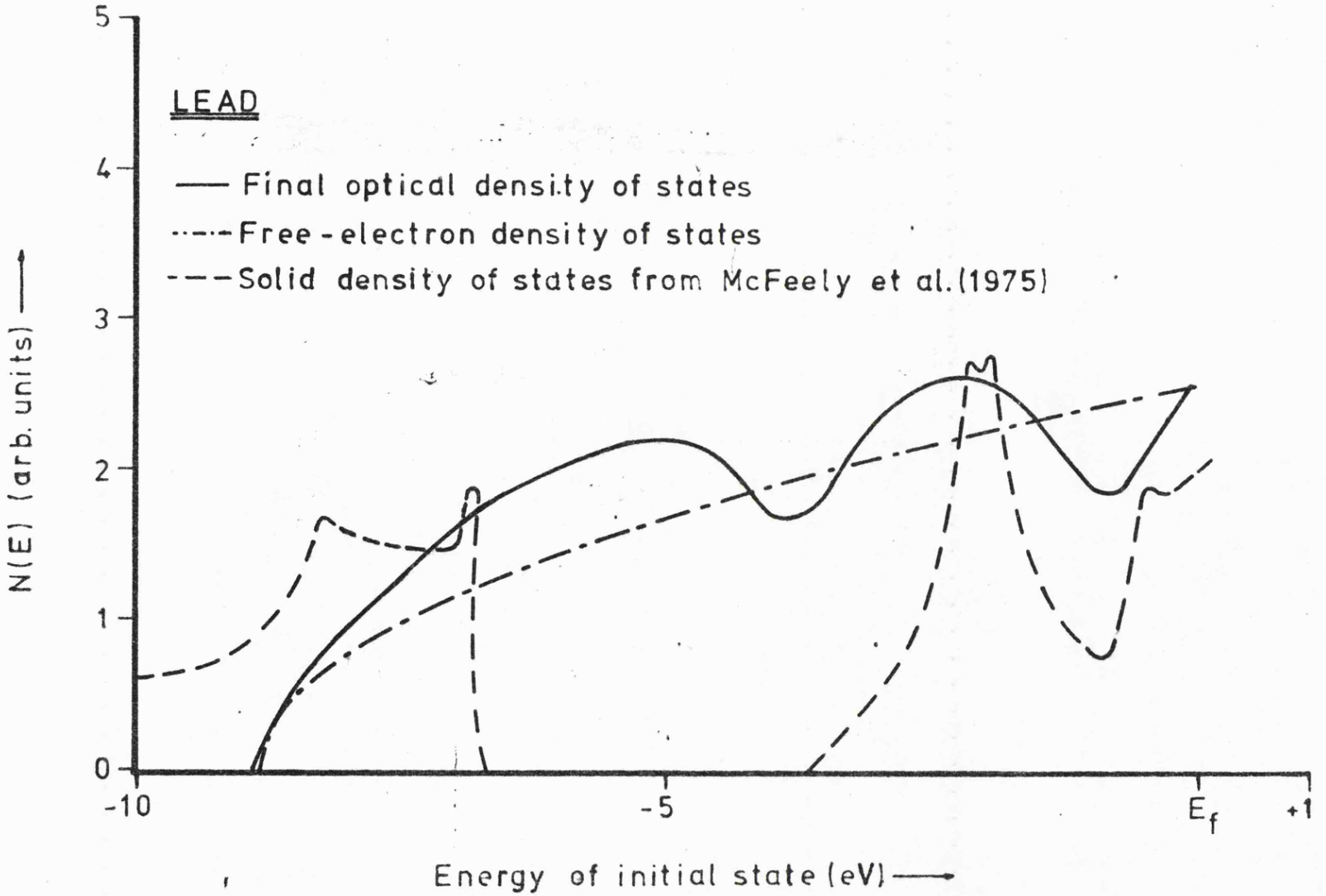

Fig.6.10-Final optical density of states for liquid Lead

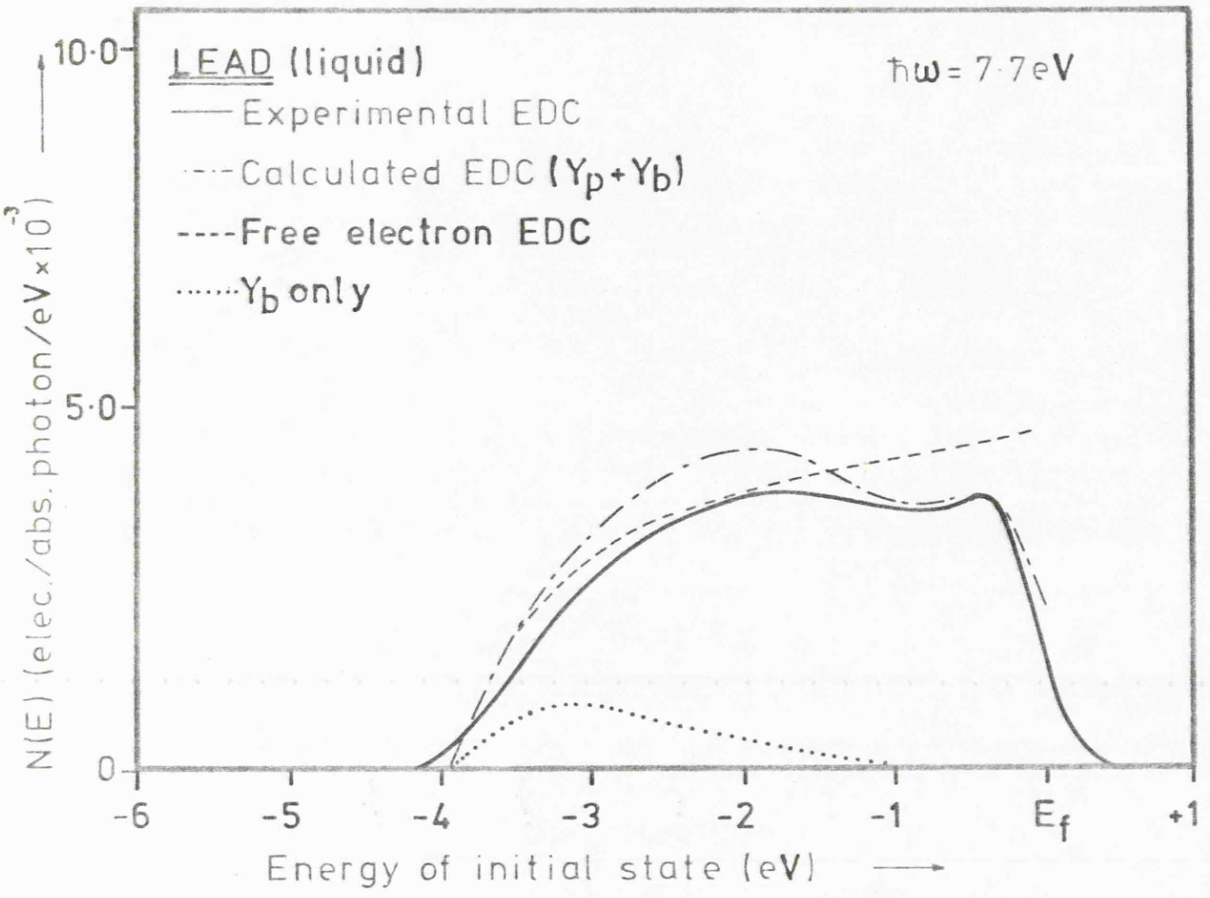

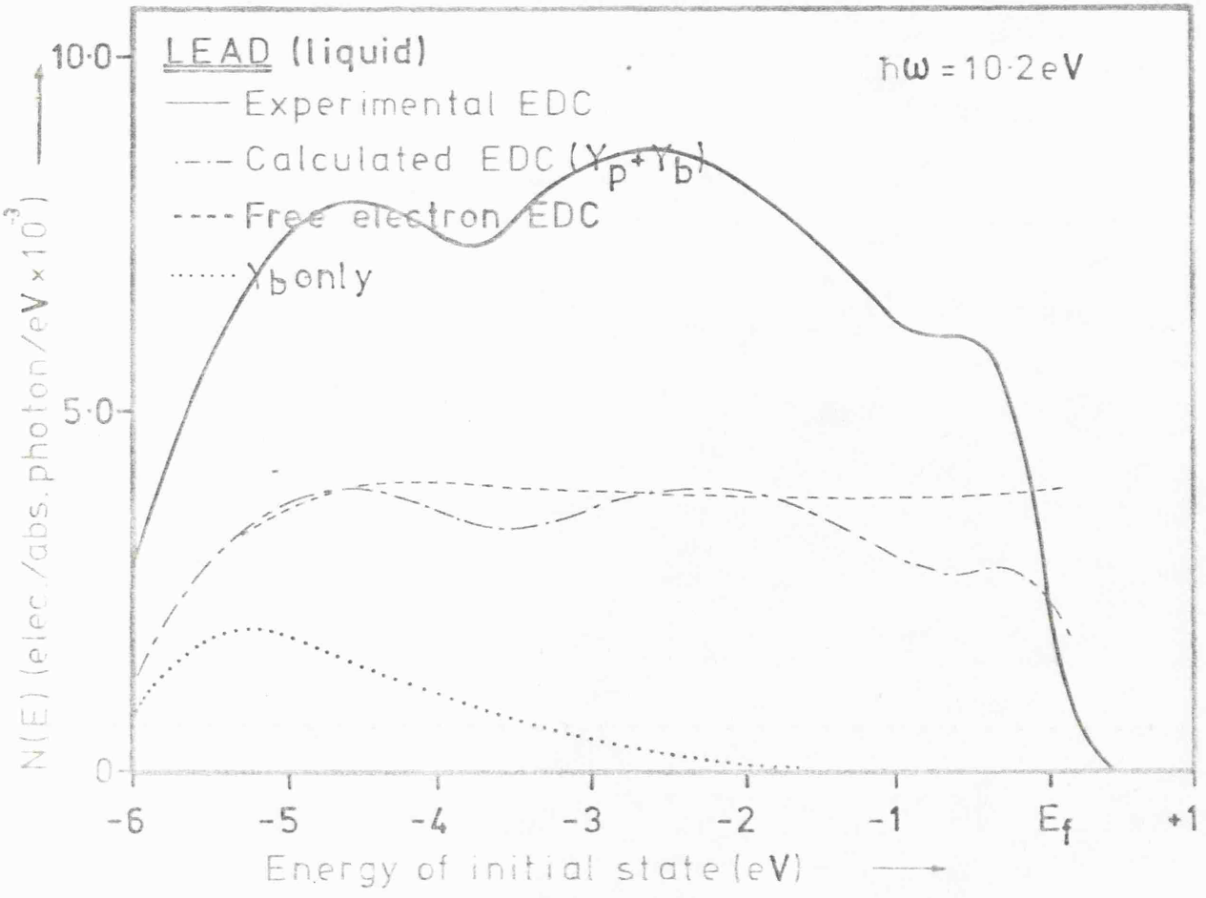

Fig.6.11-Comparison of calculated & experimental EDCs for liquid lead

The band structure for lead shows clearly separated p and s bands and although the photon energies are too low in this experiment for the s band to be clearly defined, due to the large scattered peak on the high energy EDC's, the p band is fully covered and the features seen in the optical density of states may be identified with features in this band. Figure 6.10 shows the final optical density of states compared with the band structure of McFeely et al (loc.cit.) for the spin orbit split situation. The dip in the ODOS at -3.8 eV may be seen to correspond well with the bottom of the p band, whilst the broad peak centered at -2.2 eV corresponds with the major peak in the band. The peak at the Fermi edge may be associated with the minor peak in the p band. The onset of the s band is masked by the effects of scattered electrons. The relative heights of the peaks at -2.2 eV and at the Fermi edge agree with the results of Ley et al (loc.cit.) for XPS, who interpret the well defined dip between them (associated with a dip in the p band at -1 eV) as being indicative of the effects of spin orbit splitting, since theory indicates that this dip would not be well resolved in a non spin orbit split case.

6.3. TIN

6.3.1. Experimental

Tin was also an easy metal to handle experimentally. It has a low melting point ($252^{o}C$) and may be contained in the same way as lead. The results given here are from three separate experiments, some of which have been reported earlier (Norris et al 1972).

6.3.2. Yield of Tin

Figure 6.12 shows the quantum yield of solid and liquid tin. There are several peaks, the major one being at 6.2 eV and notably stronger in the solid than in the liquid. There is a common peak at 7.7 eV. In the solid there is a peak at 9 eV followed by a dip at 9.4 eV and another peak at 11 eV. In the liquid the first peak is broader and occurs at 9.5 eV with the dip at 10.3 eV.

At lower energies, solid and liquid yields are identical. A Fowler plot (Figure 6.13) gives a work function of 4.27 ± .02 eV. This is in reasonable agreement with the value of Goetz (1929) (4.21 eV) but does not agree with the value obtained by Stevenson (1968) of 4.05 eV. In the absence of data on the reflectivity of liquid tin, both solid and liquid yields were arrived at using the data of Lemmonier et al (1967) for an evaporated film (Figure 6.13).

6.3.3. Liquid Tin

Figure 6.14 shows the EDC's for liquid tin at low energy. As previously reported there are two main features. However, later work with improved resolution and signal to noise ratio indicates a slightly different position of these features - peaks occurring at -1.2 eV and -2.6 eV instead of -1.0 and 2.4 as given earlier. There is also a suggestion in an EDC, taken at a higher energy (11.2 eV) than used previously, that the peak at -2.6 may be an unresolved doublet since, at this energy, the peak is very broad and shows signs of splitting. The structure in the EDC's is consistent in position and strength for all photon energies used.

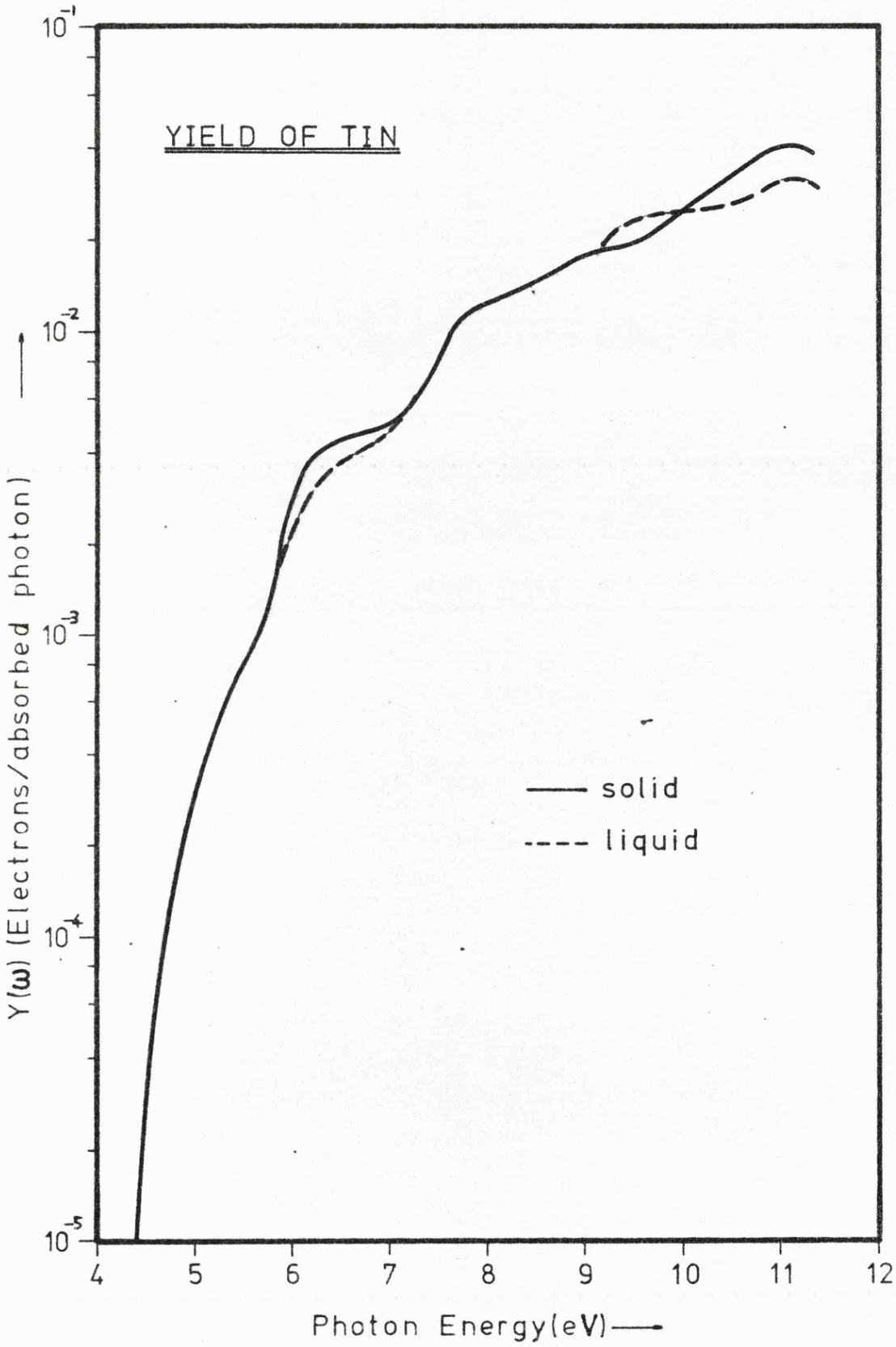

Fig.6.12 -Yield of solid & liquid Tin

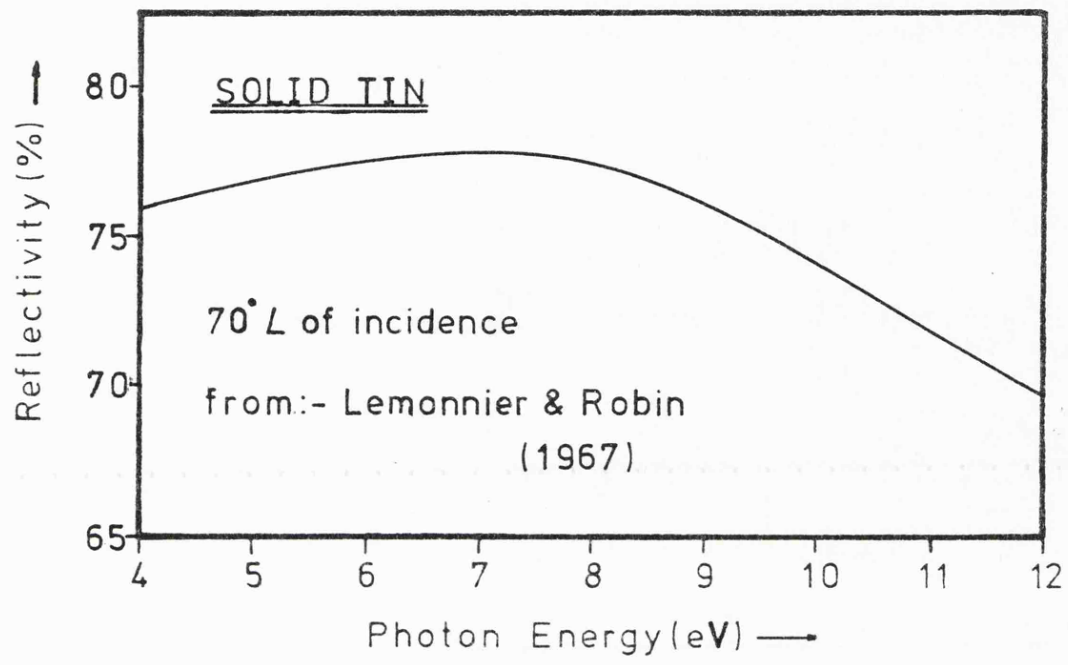

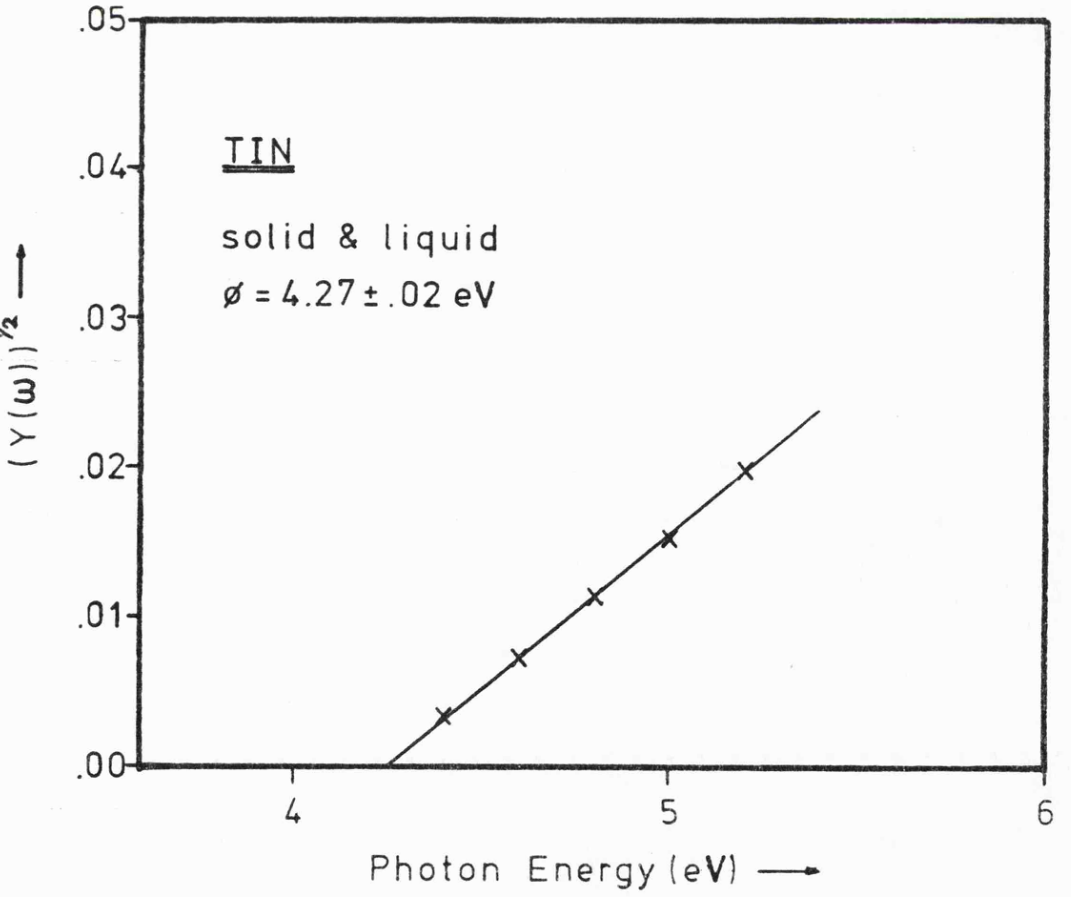

Fig.6.13-Reflectivity & Fowler plot for solid & liquid Tin

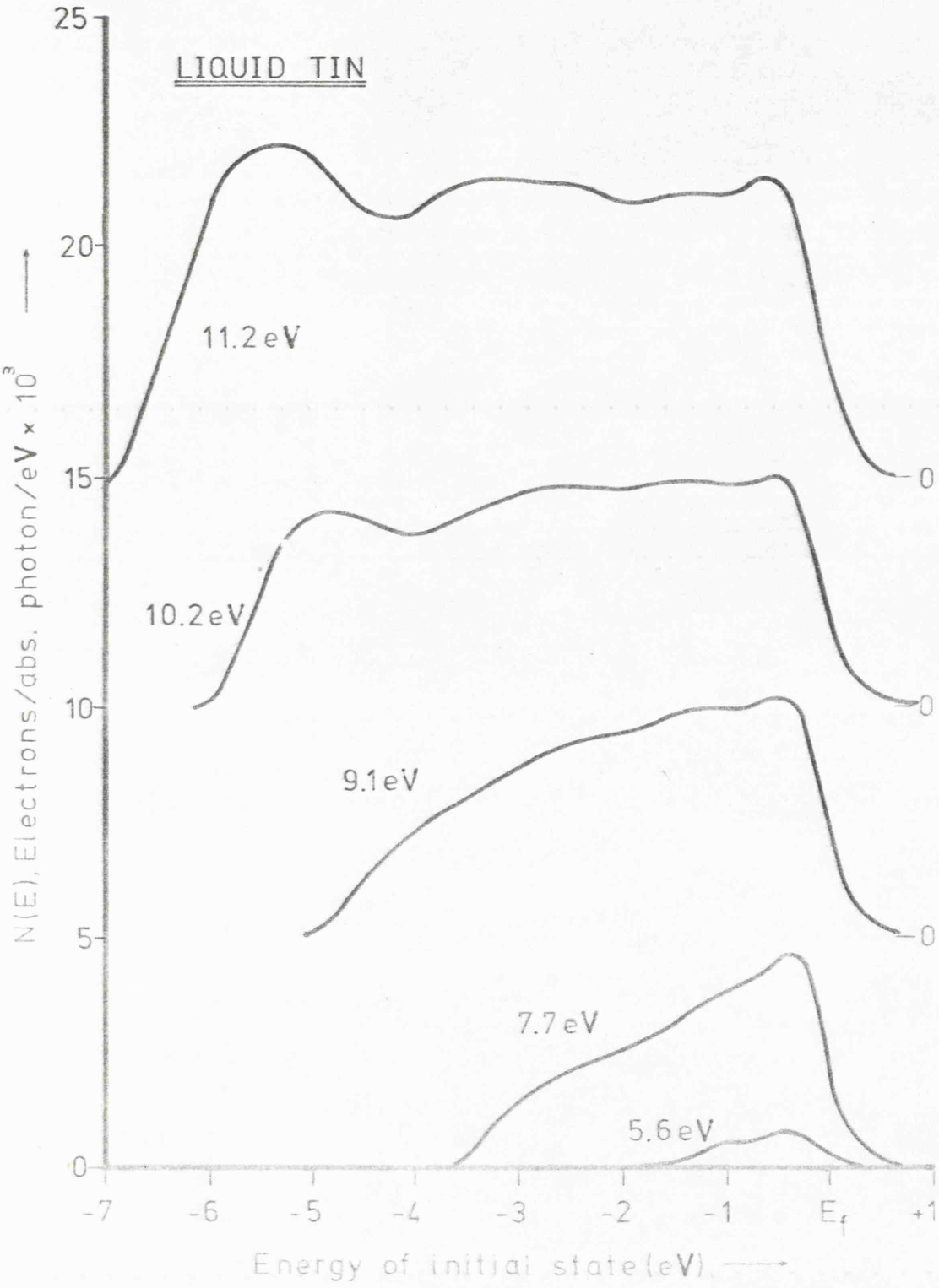

Fig.6.14-Low energy EDCs for liquid Tin

6.3.4. Solid Tin

Figure 6.15 shows a series of EDC's for rapidly frozen tin. With this material, attempts to produce a slowly frozen surface resulted in a very large slow electron peak indicative of contamination of the surface. There did not appear to be much small scale surface structure in the samples as seen in lead (see Figure 6.16), but only large scale deformations. This is borne out by the fact that the feature at -4.1 eV observed by Castelijns et al (1977) on a roughened film, and associated by them with surface states, is not observed.

The EDC's for solid tin appear fairly similar to those for the liquid. There are two major features which are both considerably stronger than in the liquid. One is located at -1.1 eV at low photon energies and moving to -1.5 at higher energies, the strength of the peak also varying. The other feature occurs at -3.2 eV in the 10.2 eV EDC, moving towards the Fermi edge and becoming weaker as the photon energy is reduced. The behaviour of this second peak is in agreement with the observations of Castelijns et al (loc.cit.) - however, they did not observe any movement of the peak closer to the Fermi edge, and this may be associated with the bulk nature of the sample.

6.3.5. High Energy EDC's

As mentioned in 6.3.4., problems were encountered with contamination of the surface on freezing the tin. This problem was encountered even more strongly with the high energy sample, and useful EDC's could not be obtained for the solid. Also, neon was not available at the time of this experiment so that

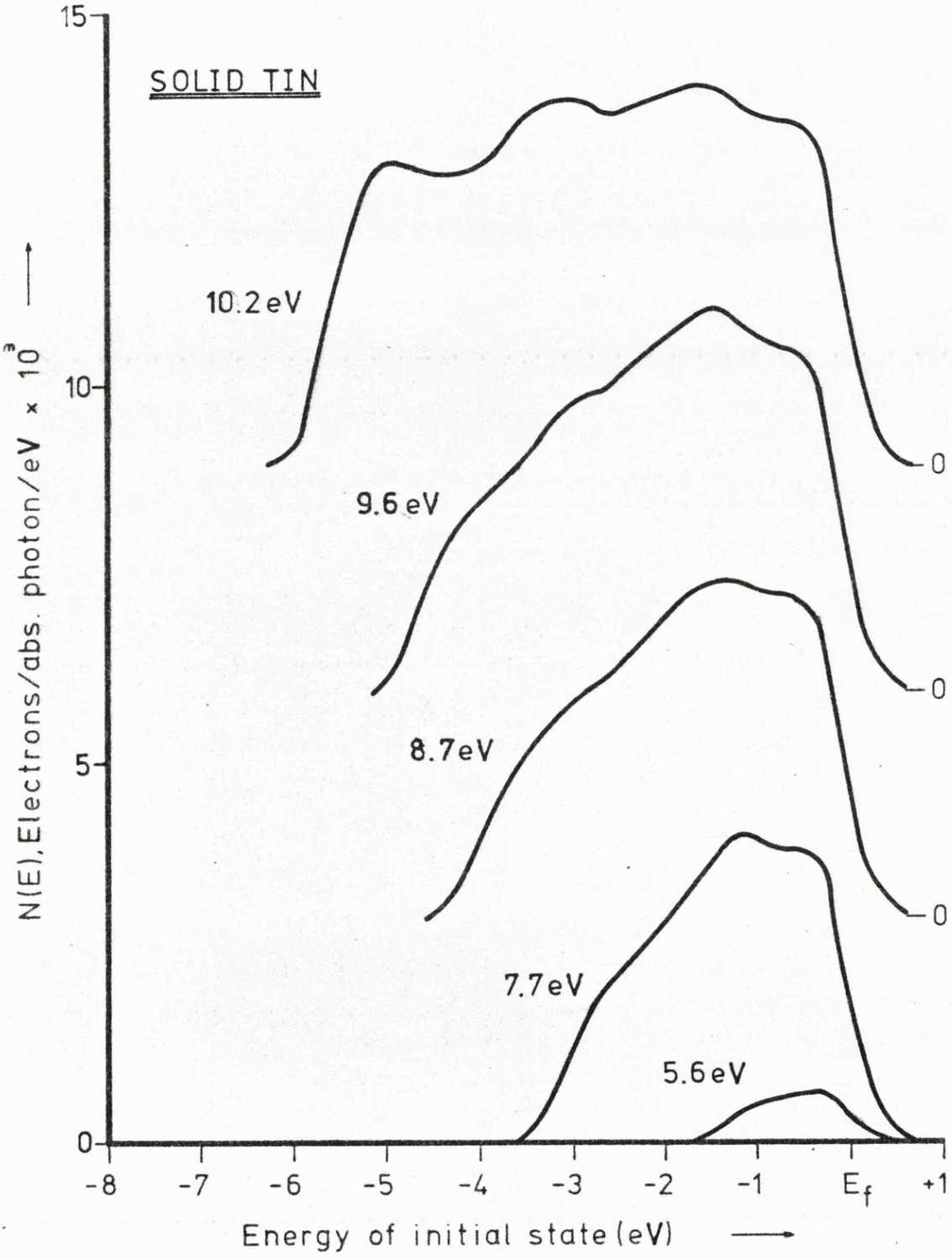

Fig.6.15-Low energy EDC's for solid Tin

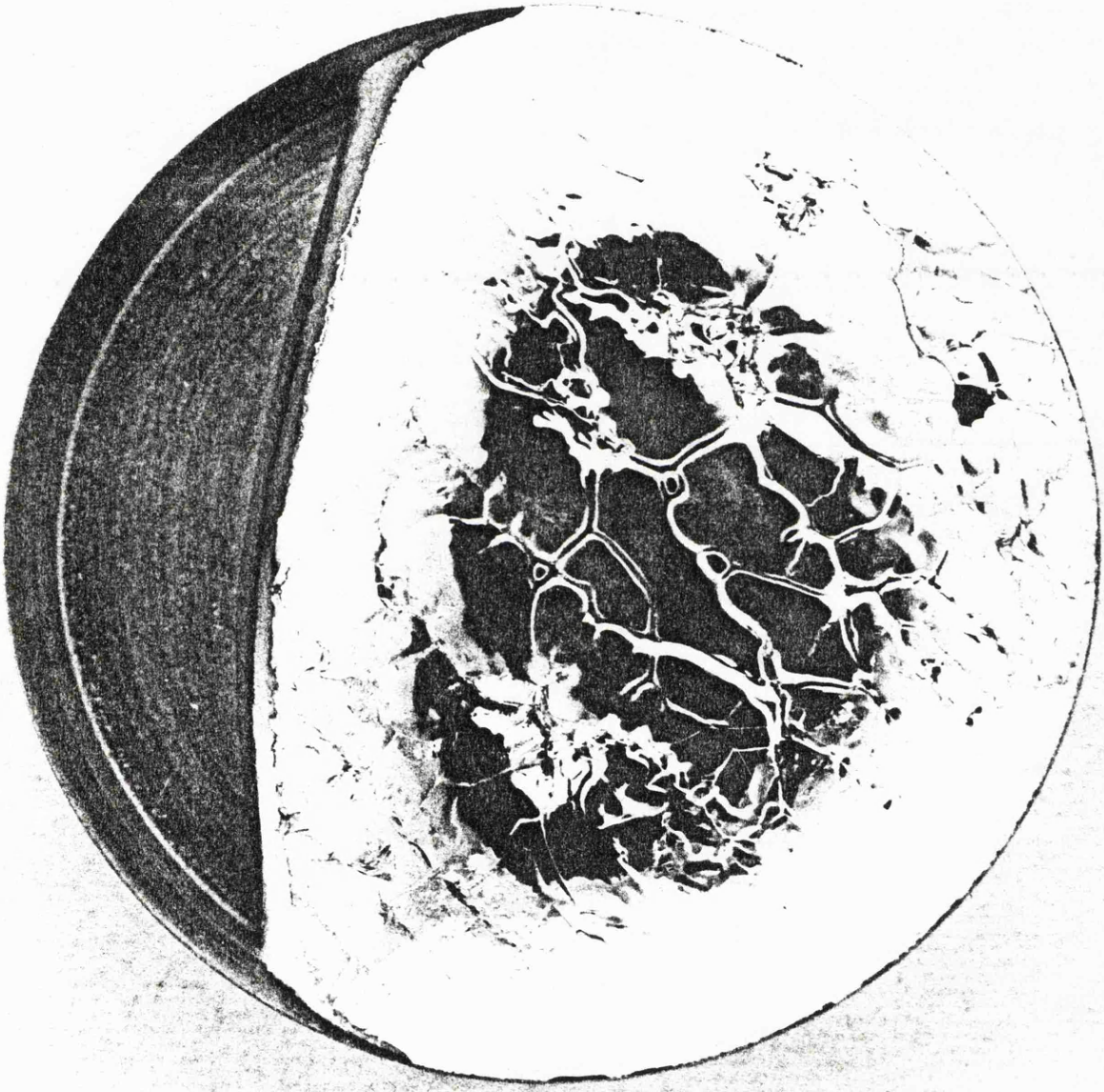

Fig.6.16-Surface of frozen Tin

EDC's could only be taken at 21.2 eV. Figure 6.17 shows an EDC for liquid tin at 21.2 eV. This differs considerably from that originally reported, but the original published results are now believed to have been in error due to problems with the detection system. The EDC shows the feature at -2.6 eV seen in the low energy spectra, and there is also a broad peak centered at -8 eV.

6.3.6. Optical Density of States

The 21.2 eV EDC was used, with the background subtracted, as the starting point for the analysis, and Figure 6.18 shows this compared with Pollak's XPS result. The agreement near the Fermi edge is good, although the structure seen by Pollak at -6 eV is not apparent. Figure 6.19 shows the final optical density of states obtained and, as with previous materials, this differs considerably from the free electron picture. Figure 6.20 shows the predicted EDC's compared with the experimental results. The agreement of the structure is good, although again the yield is not in agreement at the higher energies.

The values used for the absorption coefficient were taken from Lemmonier et al (1967). The value of l_e gained from the analysis was 50Å. This is rather high and suggests that there may be some other factor affecting the yield in this case.

6.3.7. Discussion

As in the previous cases the structure seen in the liquid EDC's is constant in position and strength over a wide range of photon energies, suggesting that the effects of matrix

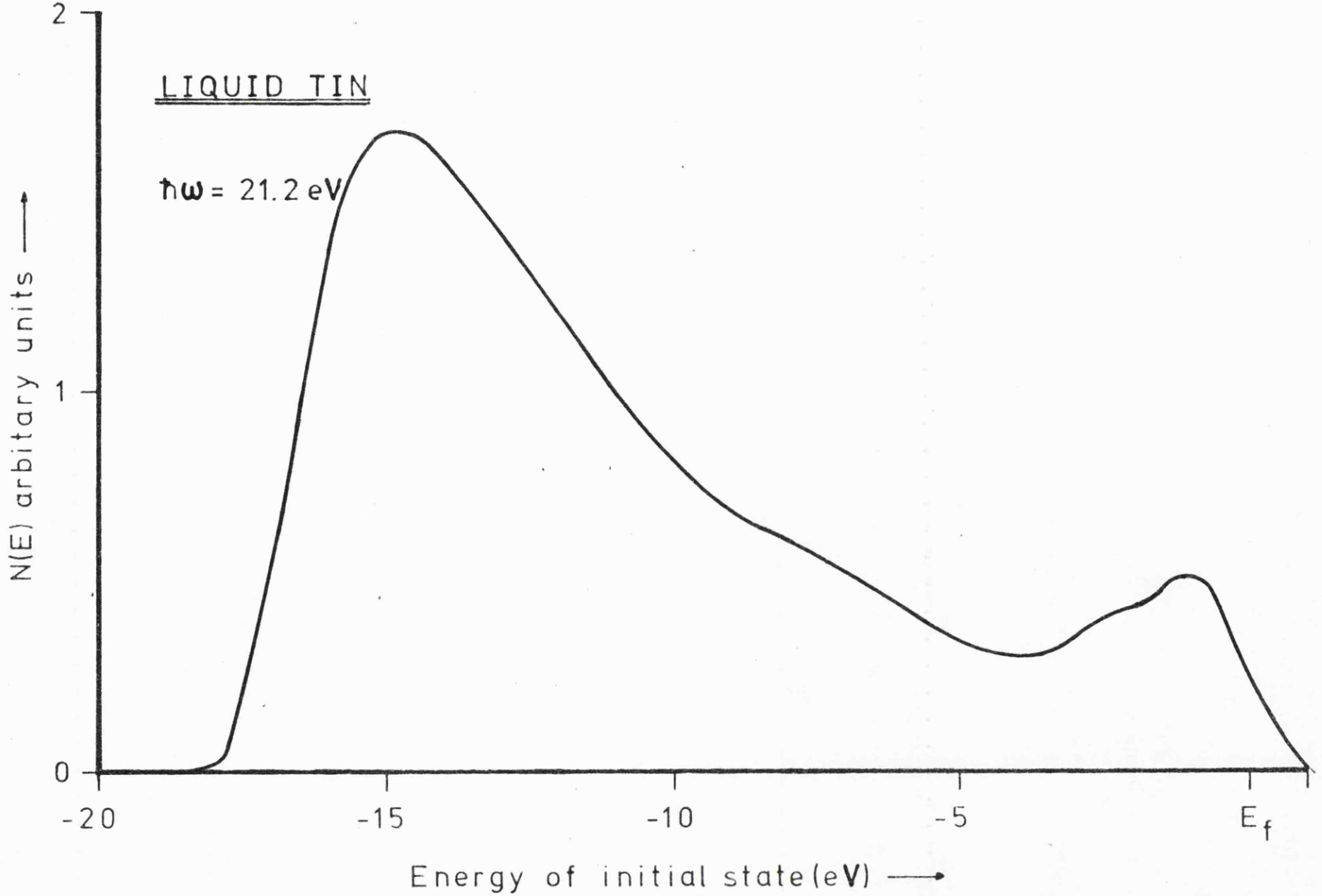

Fig.6.17-High energy EDC for liquid Tin

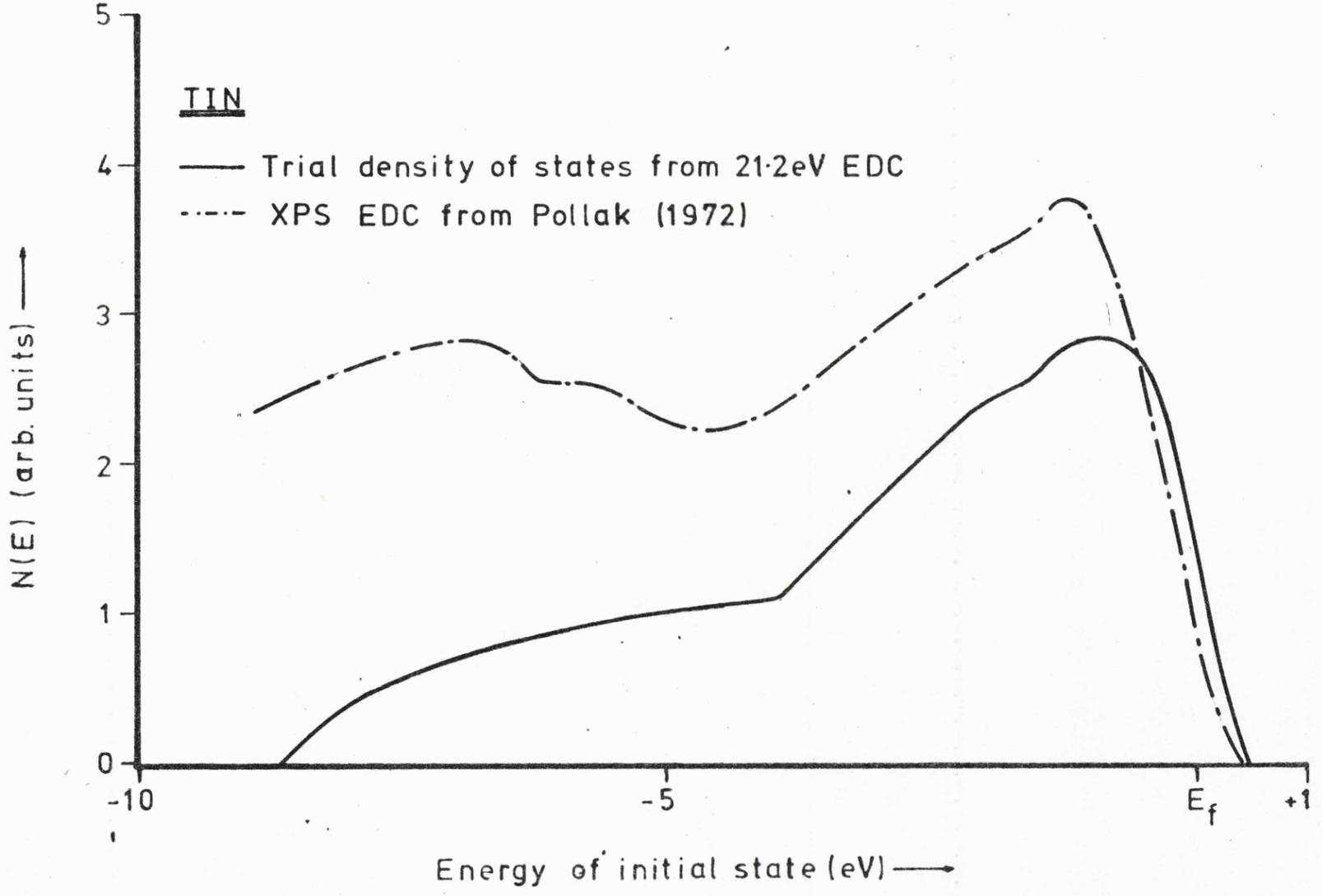

Fig.6.18-Trial optical density of states for liquid Tin

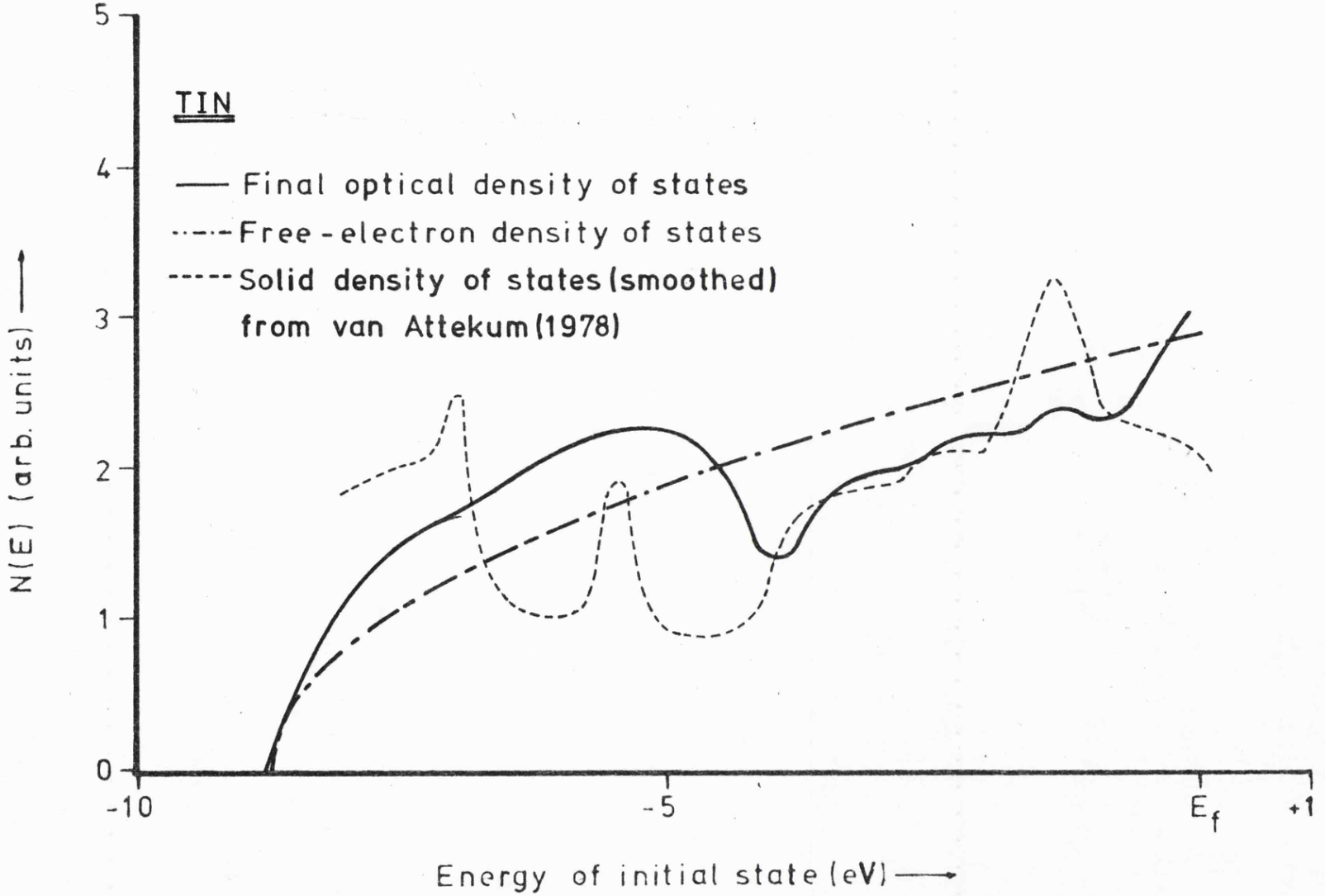

Fig.6.19 -Final optical density of states for liquid tin

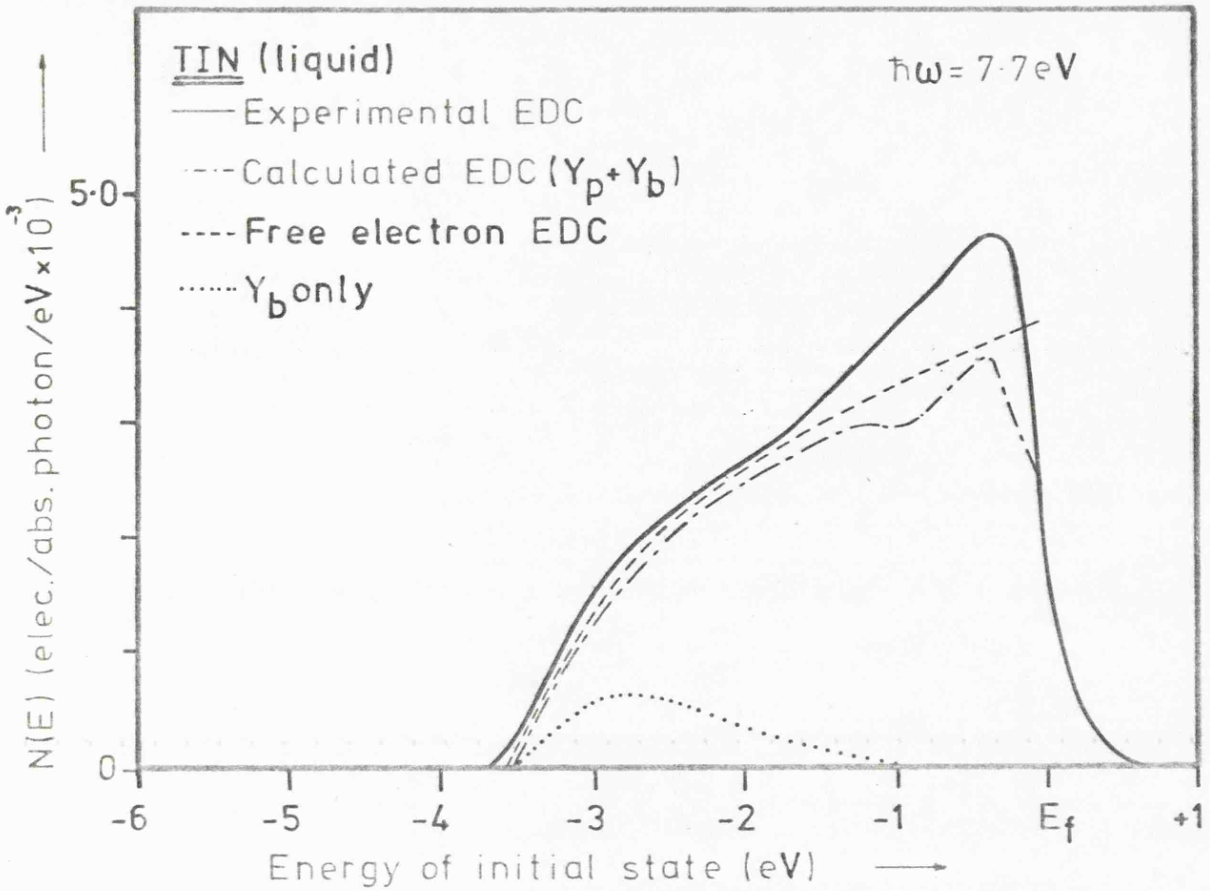

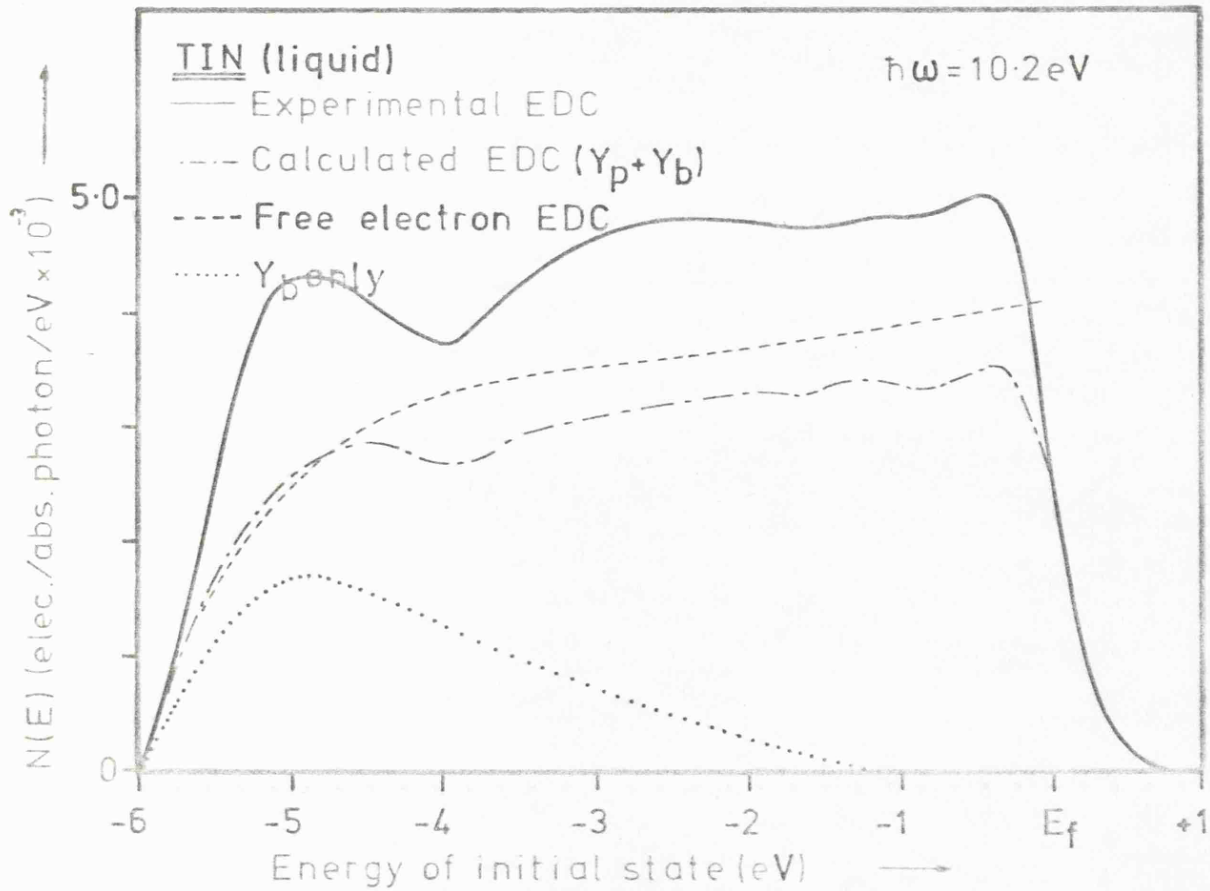

Fig. 6.20 - Comparison of calculated & experimental EDCs for liquid tin

elements are not important. Unfortunately the photon energies used are not great enough for the 5s band of tin to be fully examined, although the peak at -7 eV in the 21.2 eV result corresponds well with the onset of this band. The main dip observed in the optical density of states corresponds well with the bottom of the p band at -4.5 eV.

There is no density of states available for liquid tin. However, Van Attekum (1978) has produced a density of states for the solid. A smoothed version of this is shown in Figure 6.19. There is strong structure in this density of states, particularly in the presence of a peak at -5.3 eV. Although this agrees well with the position of the lower maximum in the ODOS this may be fortuitous as there are effects due to scattered electrons. However, the agreement in the structure in the p band close to the Fermi edge, particularly in the presence of a strong peak at -1.5 eV, is good.

CHAPTER 7:- MERCURY AND MERCURY ALLOYS

7.1. Introduction

Mercury ($6s^2$) is a divalent metal of Group IIA and has a melting point of $-39^{o}C$. It is rhombohedral in the solid phase. The electronic structure of mercury has been of considerable interest for some time, since it was found that its electronic properties, notably the resistivity and thermopower, differ considerably from those of other metals. In order to explain this, Mott (1966) suggested the existence of a strong dip in the density of states near to the Fermi edge (a 'pseudogap'). However later work by Evans et al (1969) and Evans (1970), succeeded in explaining the metal's properties in terms of a new pseudopotential, without recourse to the idea of a pseudogap. Still more recent calculations by Chan and Ballentine (1971) and Ichikawa (1972) have given a density of states with a much weaker dip near the Fermi level than that originally proposed by Mott.

Since photoelectron spectroscopy may provide some evidence as to the nature of the density of states, mercury is a particularly attractive subject for this study. Mercury is an easy metal to alloy so that, besides the possibility of directly perceiving the dip near the Fermi edge, it may also be possible to observe the effects of alloying on this dip. The predictions of Mott indicate that if mercury is alloyed with indium, the dip should be gradually filled in as the concentration of indium is increased. If, however, it is alloyed with an alkali metal such as sodium, it should be possible to observe the opposite effect.

Finally, mercury also has a 5d band close enough to the Fermi edge to be seen at the higher photon energies, and the effect of alloying on this may be examined.

7.2. Mercury

7.2.1. Experimental

Experimentally, mercury presents a problem not encountered with the other materials in this work. Since the vapour pressure at room temperature is $\simeq 2 \times 10^{-4}$ Torr, a mercury diffusion pump must be used. It also means that the sample cannot be baked in the chamber since it would then evaporate totally. The technique adopted for the experiment was as follows. The chamber was assembled with a clean molybdenum table and quartz crucible, but with no mercury in the crucible. The system was baked and pumped down to $< 10^{-10}$ torr and the table outgassed. The system was then brought up to atmospheric pressure by the admission of dry nitrogen, the crucible filled as quickly as possible and the system pumped down again - a pressure of $\simeq 10^{-6}$ torr being attainable due to the small surface area of mercury exposed. After a further outgas of the specimen table, the mercury was then poured. A system for distillation of the mercury into the chamber was tried but this was not satisfactory as it took too long and the sample was usually contaminated by the end of the process. Specimen loss due to evaporation did not prove to be a problem, approximately half of the specimen being lost in 24 hours. The use of a mercury pump had the additional advantage that, by violent movements of the table, the old specimen could be shaken off and a fresh sample poured, allowing more than one sample to be examined on each run without affecting the pumping system.

Obviously, since there is such a high pressure of mercury

in the chamber, it is not possible to deposit a clean gold film during the experiment. It was therefore necessary to conduct a separate experiment, using the sodium salicyclate phosphor mentioned in Chapter 4 as an intermediate standard, to measure the yield. Unfortunately the results given here do not represent a complete picture as the failure of the mercury pump, mentioned in Chapter 4, caused the experimental programme to be curtailed. The ambient vacuum during the experiment as measured by mass spectrometer was $\simeq 2 \times 10^{-5}$ torr of mercury with traces of N_2, H_2O, O_2 and CO_2 totalling 4×10^{-9} torr.

In this chapter UPS results are presented for liquid mercury and three mercury alloys ($Hg_{.50}$-$In_{.50}$, $Hg_{.75}$-$In_{.25}$, $Hg_{.96}$-$Na_{.04}$). These are analysed in terms of the 3-step model, and it is shown that they are consistent with the Mott pseudogap concept.

7.2.2. Yield of Mercury

Figure 7.1. shows the quantum yield of mercury. It may be seen that this is characterised by several strong peaks - at 6.7 eV, 8.8 eV, 9.9 eV and 11 eV. These peaks are constant in position but not in strength, a repeat of the yield measurement one hour after the initial measurement (which was taken just after pouring) showing a considerable change. If this result is compared with the electron impact spectrum of mercury vapour (Skerbele et al 1969) or excitation potential values (Moore 1949) it will be seen that there is extremely good correspondence in the position of the peaks both with peaks in the electron impact spectrum and with known excitation potentials, namely 6 P, 7 P, 9 P and 6p ^{3}P. Since the lowest ionization potential for mercury vapour is 13.4 eV, there obviously cannot be photoemission

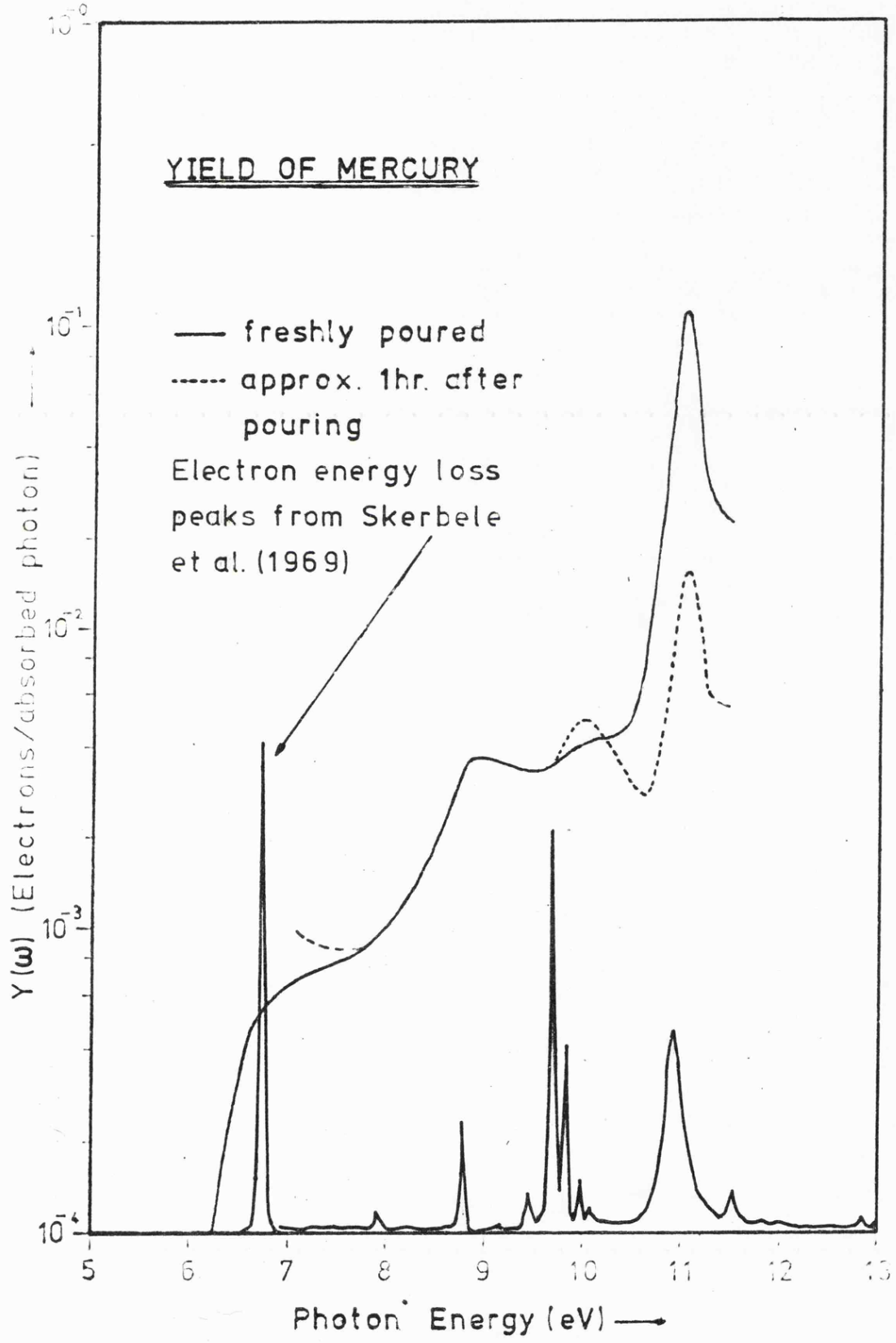

Fig.7.1-Yield of liquid Mercury

taking place from the vapour above the surface. It seems likely, however, that the mercury atoms just above the surface are being excited into a metastable state. These then de-excite, and this results in the formation of photoelectrons in the bulk closer to the surface than would normally accur, with a consequently increased escape possibility (see Figure 7.2.). This is borne out by the following experimental observations. Firstly, the EDC's did not display the time dependence seen in the yield and secondly, contamination of the sample caused the structure to 'wash out' as expected from previous experiments on other metals, whilst emission from the vapour should not be sensitive to this.

The change in strength of the peaks may well be due to a change in the amount of vapour present above the specimen, possibly caused by the rate of evaporation reaching equilibrium with the rate of pumping. Mild contamination did not appear to particularly affect the system pressure - probably the high loss rate of evaporation inhibits the formation of a surface 'skin'.

The reflection data used for calculation of the yield was from Wilson and Rice (1966).

7.2.3. Liquid Mercury

Figure 7.3. shows EDC's for liquid mercury at room temperature. It may be seen that there is a strong feature at -2.3 eV, and a strong negative slope to the Fermi edge. This strong negative slope is in direct contrast to the predictions of Chan and Ballentine (loc.cit.), Ichikawa (loc.cit.) and Evans (loc.cit.) which indicate a density of states sharply rising towards the Fermi edge. The position agrees well with the density of states of Kuroha et al (1977).

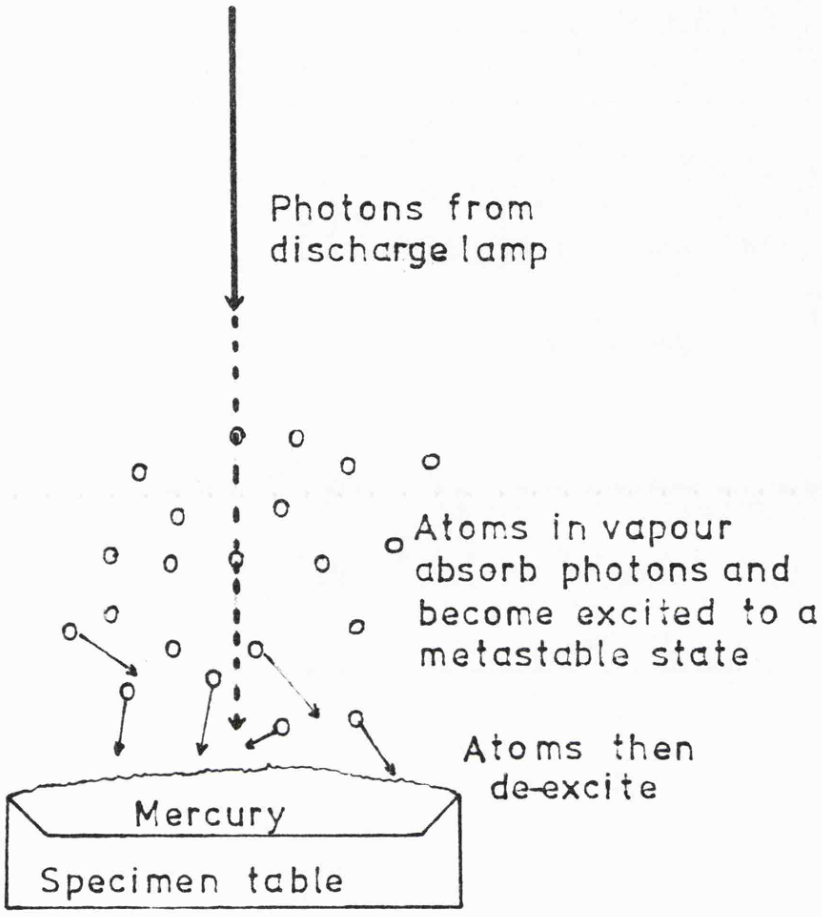

Fig.7.2-Enhancement of mercury yield

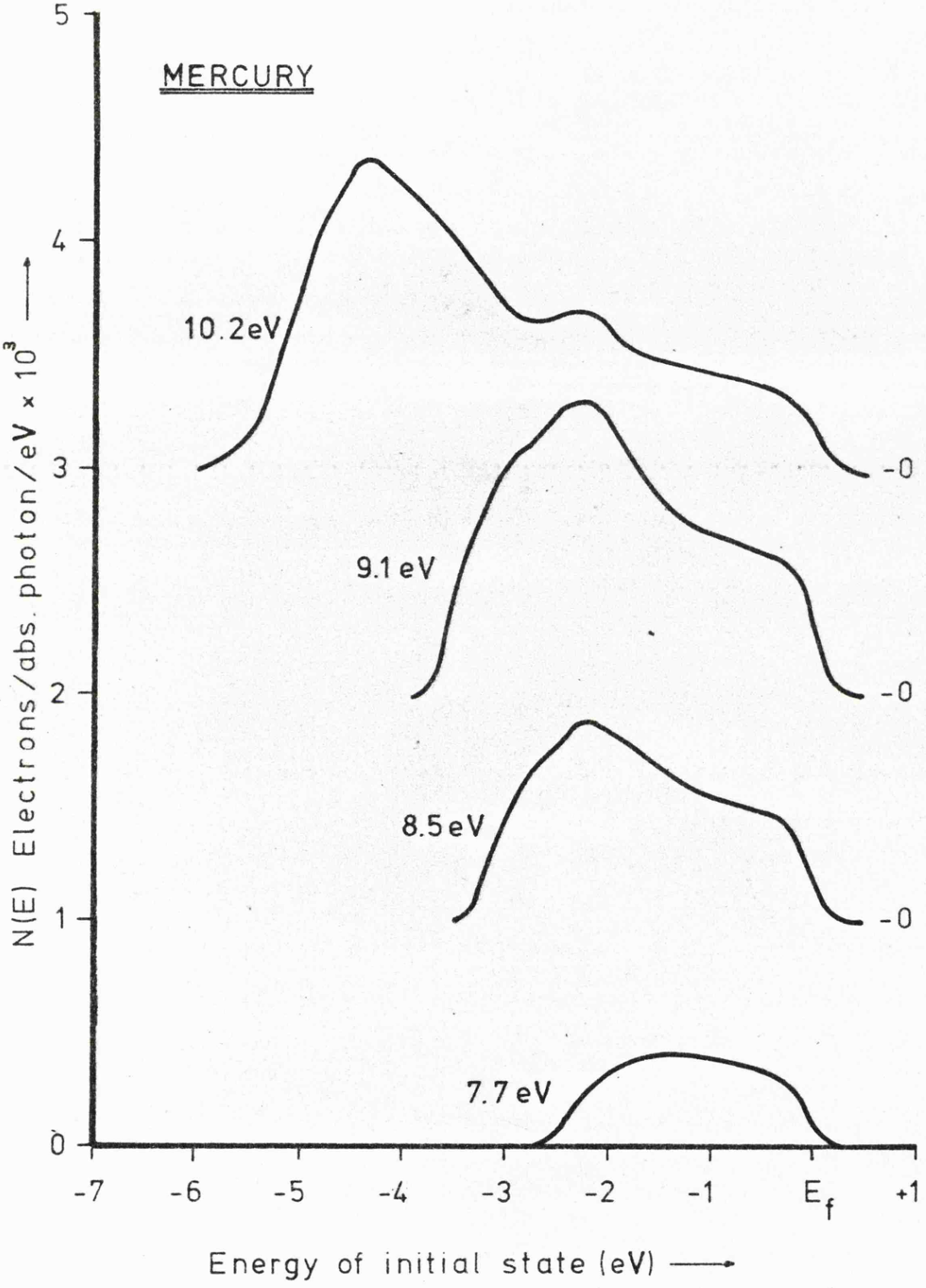

Fig.7.3-Low energy EDCs from liquid Mercury

The feature at -2.3 eV is constant in strength and position. This is close in energy to the point where the first conduction band touches the Brillouin zone face in solid mercury as calculated by Dishman and Rayne (1968) at -2.4 eV and Keeton and Loucks(1966) at -2.7 eV, and may well be due to persistence of some aspects of the solid state band structure on melting. In particular it suggests that the structure in the EDC close to E_F is due to a region of low density of states associated with the overlap of the first and second conduction bands.

Figure 7.4 shows an EDC for mercury at $h\nu = 6$ eV in comparison with one obtained by Cotti et al (1973). It is possible to discern a slight negative slope approaching the Fermi edge, but the feature seen by Cotti et al (loc.cit.) at -1 eV is not resolved.

7.2.4. Solid Mercury

An attempt was made to obtain EDC's from solid mercury using the 'cold table' system of Figure 7.5. However, whilst it proved possible to freeze mercury in this way, it was found that the high vapour pressure of mercury present in the system resulted in the condensation of mercury droplets onto the electrical contacts, shorting them out. This could possibly be avoided by using the distillation system shown in Figure 7.6. instead of the crucible system. By pouring from the capilliary syphon system onto an already cold table, the evaporation of mercury into the system may be kept to a minimum. Additional benefits would be both the ability to bake the system with the mercury present in the still and also to thoroughly outgas the mercury by distillation.

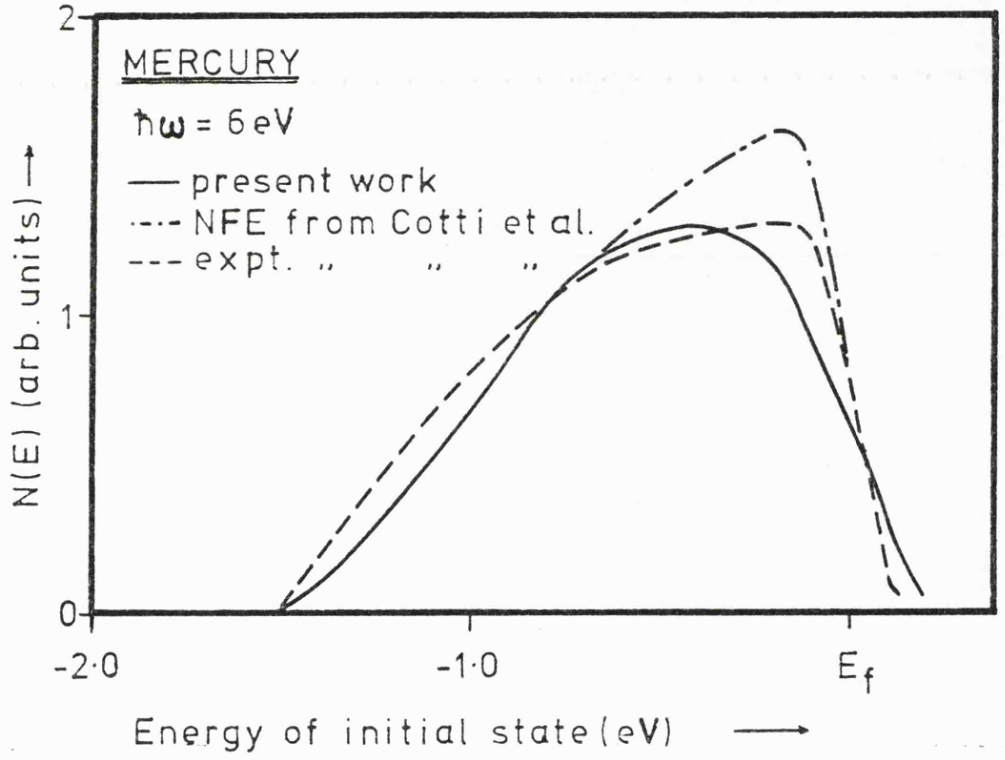

Fig.7.4-EDC near threshold from liquid Mercury.

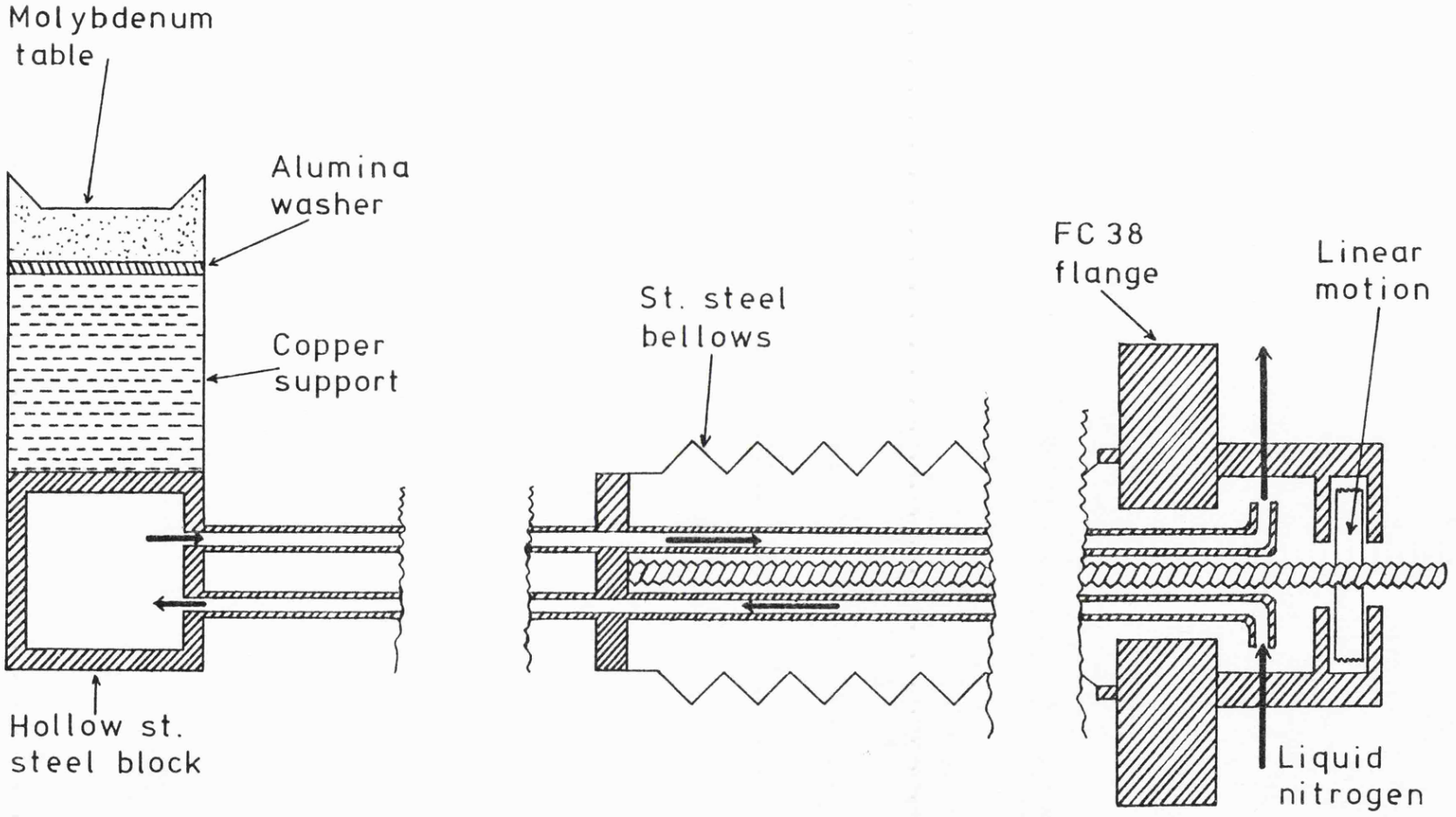

Fig. 7.5 - Cold table system for solid mercury.

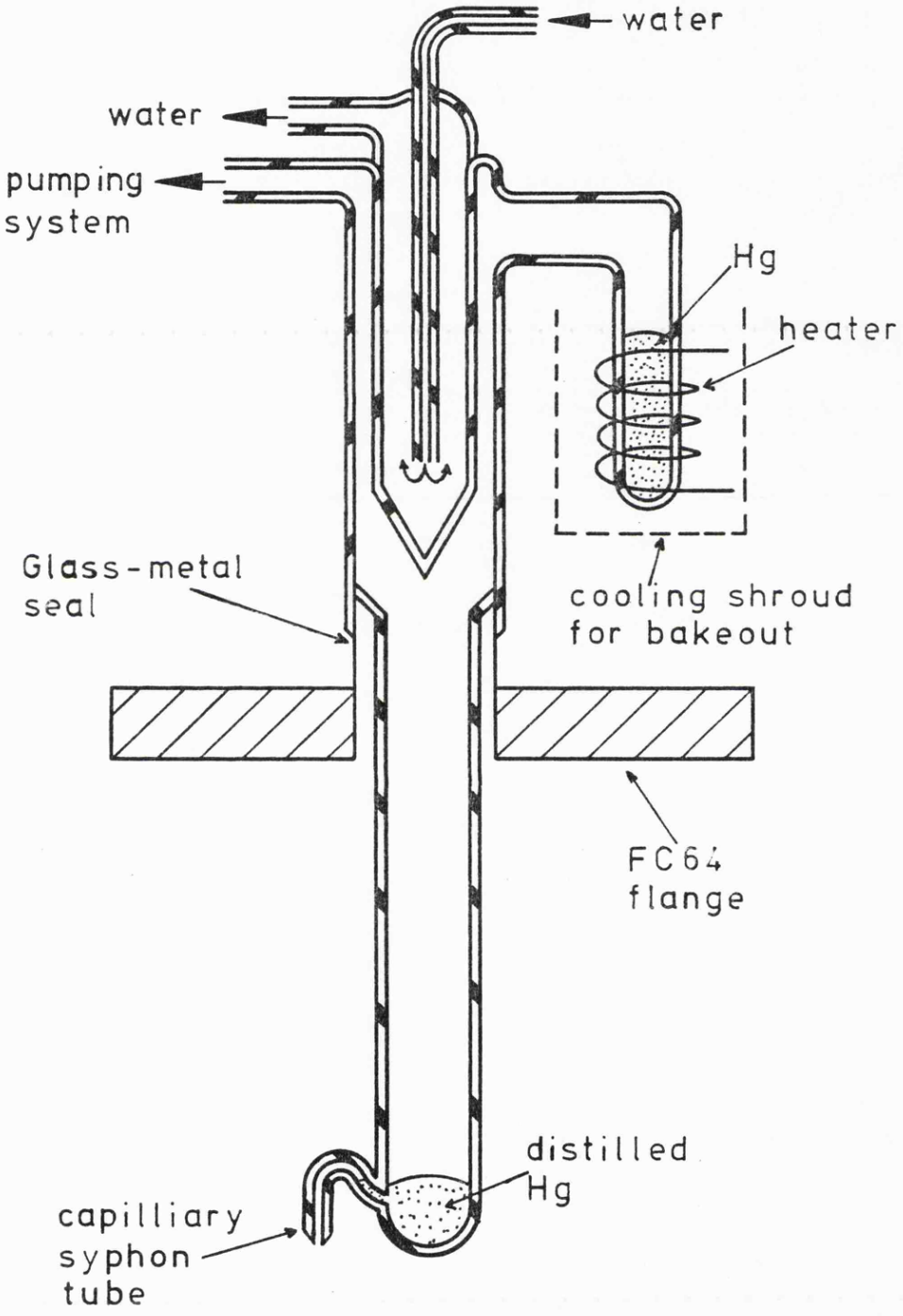

Fig. 7.6 - Proposed mercury distillation system

7.2.5. High Energy EDC's

Figure 7.7 shows EDC's for liquid mercury at 16.8 and 21.2 eV. The two strong d band peaks, due to transitions from the occupied spin orbit split $5d_{5/2}$ and $5d_{3/2}$ core levels, at -7.6 eV and -9.8 eV are clearly defined. This observed spin orbit splitting of 2.2 eV compares with the value of 2.3 eV as deduced from the band structure of Keeton and Loucks (loc.cit.) and with the value of 1.87 eV obtained from atomic term tables (Moore 1958).

The small feature at -2.3 eV is again seen, as is the negative slope to the Fermi edge. There is also a feature at -5.5 eV in the 21.2 eV EDC which is almost certainly due to transitions from the upper d levels incited by the satellite β line in the gas discharge at 23.1 eV. There is a similar feature at -4.5 eV in the 16.8 eV EDC due to the β line in neon at 19.7 eV.

Mott has suggested that the ratio of the density of states at the Fermi level to the free electron value (the g factor) is ≈ 0.7. This agrees well with the ratio of the height of the -2.3 eV feature to the height of the edge in the 21.2 eV EDC (0.66) where the effects of the 'escape profile' and the secondary background are low.

Figure 7.8 shows the effect of air contamination on mercury. This results in the formation of features at -1.9 and -3 eV and, as the contamination becomes very heavy, the d band peaks move away from the Fermi edge (exposure is given in Figure 7.8 in Langmuirs). This shows that the structure observed at -2.3 eV is not due to contamination or to contributions from the vapour.

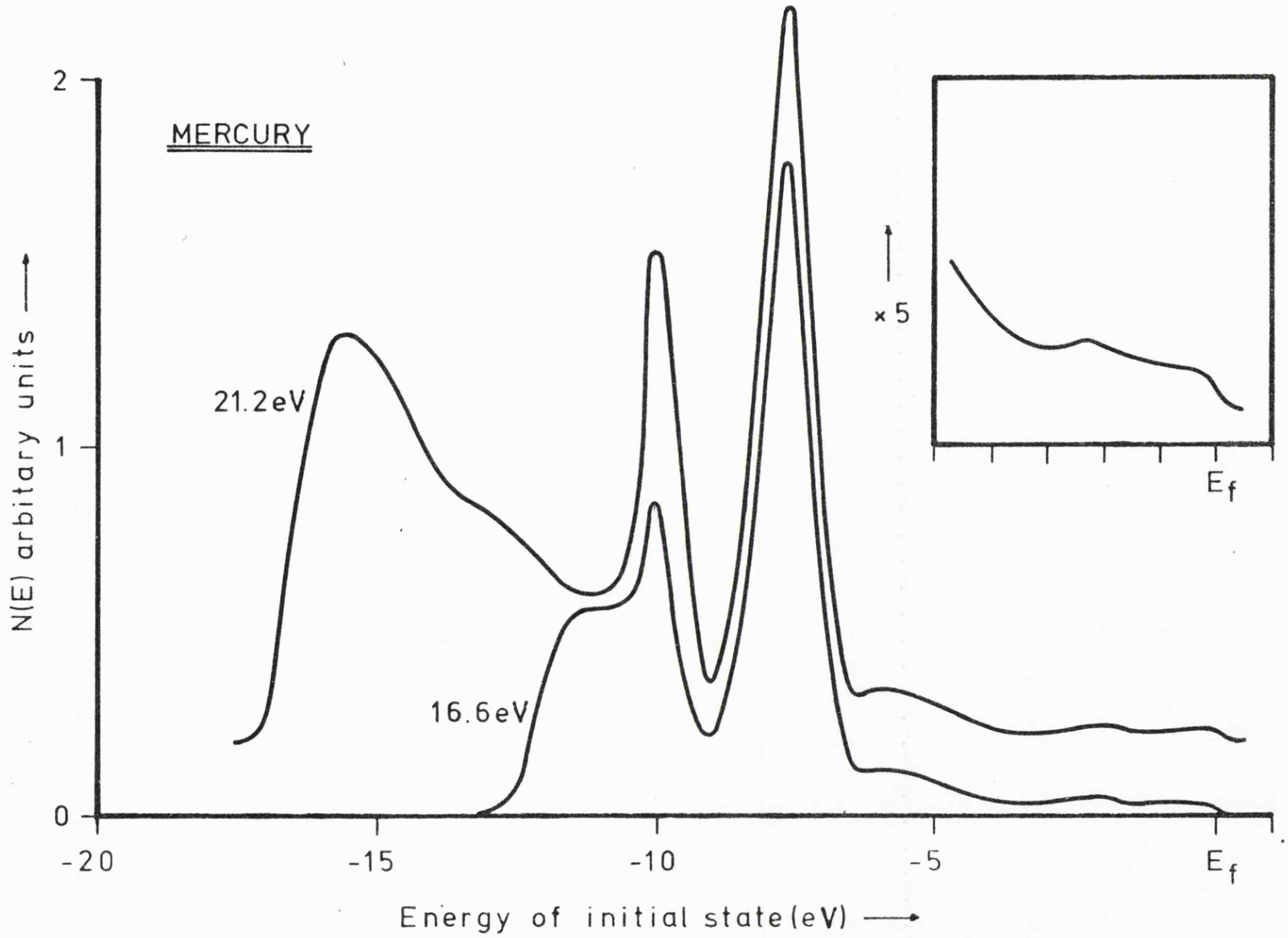

Fig.7.7-High energy EDCs for liquid Mercury

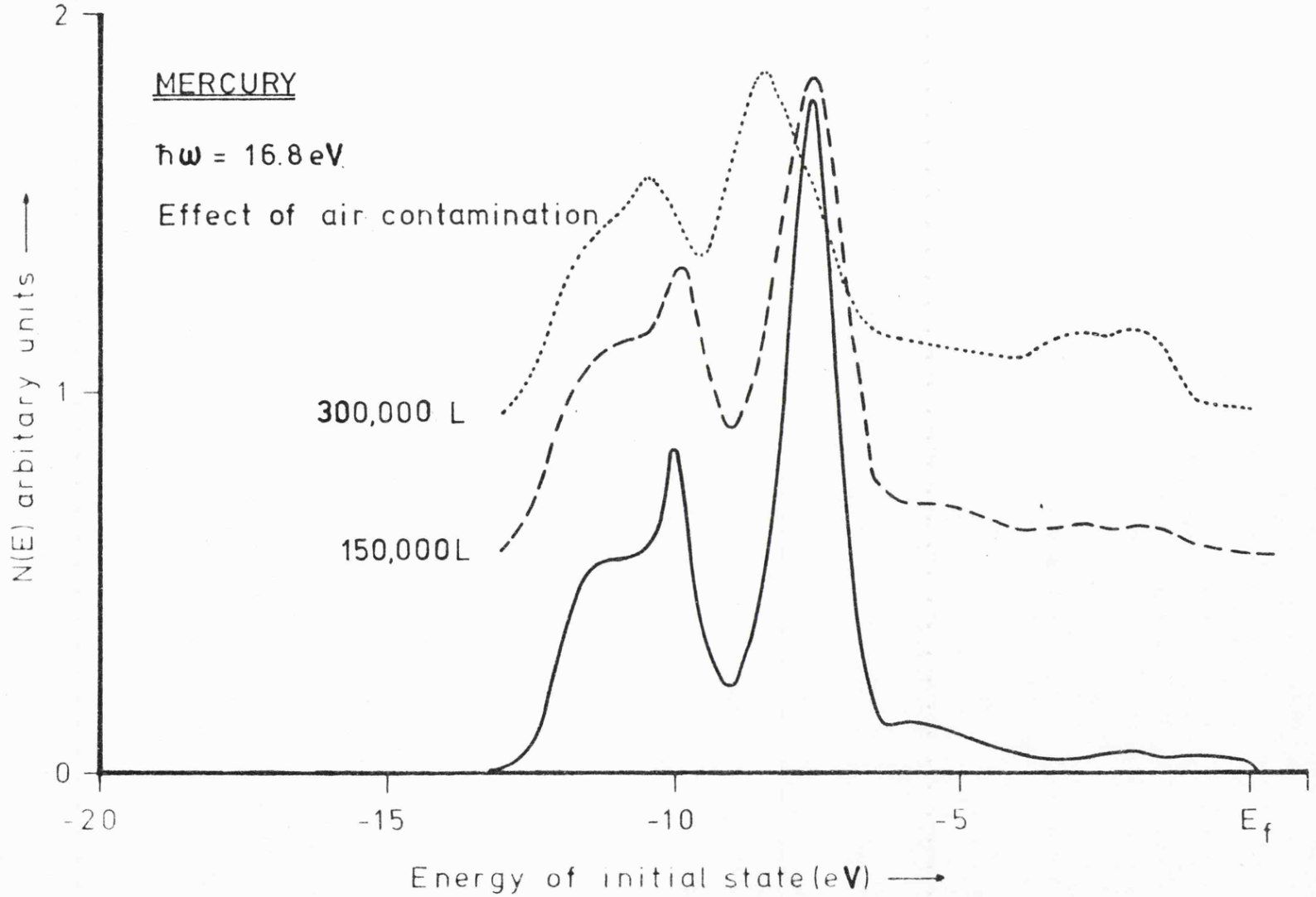

Fig.7.8-Air contamination of liquid Mercury.

7.2.6. Optical Density of States

In view of the effects due to the satellite lines in the high energy EDC's, the 10.2 eV EDC was used as a starting point for the analysis. Using the procedure detailed earlier a final optical density of states was obtained which is shown in Figure 7.9. compared with a free electron density of states. The strong negative slope to the Fermi edge and the strong feature at -2.3 eV are immediately apparent. The values used for the absorption coefficient were taken from the optical data of Wilson and Rice (loc.cit.). The analysis yielded a value of l_e of 10Å. Figure 7.10. shows the calculated EDC's compared with the experimental results. The structural agreement is good, but the agreement of the yields is fairly poor. However, this may be due to the contribution from the large scattered peak.

7.2.7. Discussion

As with the metals previously examined, the structure observed in the density of states is constant both in position and strength relative to the Fermi edge, indicating that the effects due to matrix elements are small. The most noticeable feature in the optical density of states is the strong negative slope below the Fermi edge which Mott (loc.cit.) attributes to the overlap of the first and second conduction bands. Whilst several workers have calculated densities of states for mercury, and that of Kuroha et al (loc.cit.) agrees well in the position of the feature at -2.3 eV, all indicate that the slope below the Fermi edge is positive. Figure 7.10. shows the comparison between the Kuroha density of states and the final optical

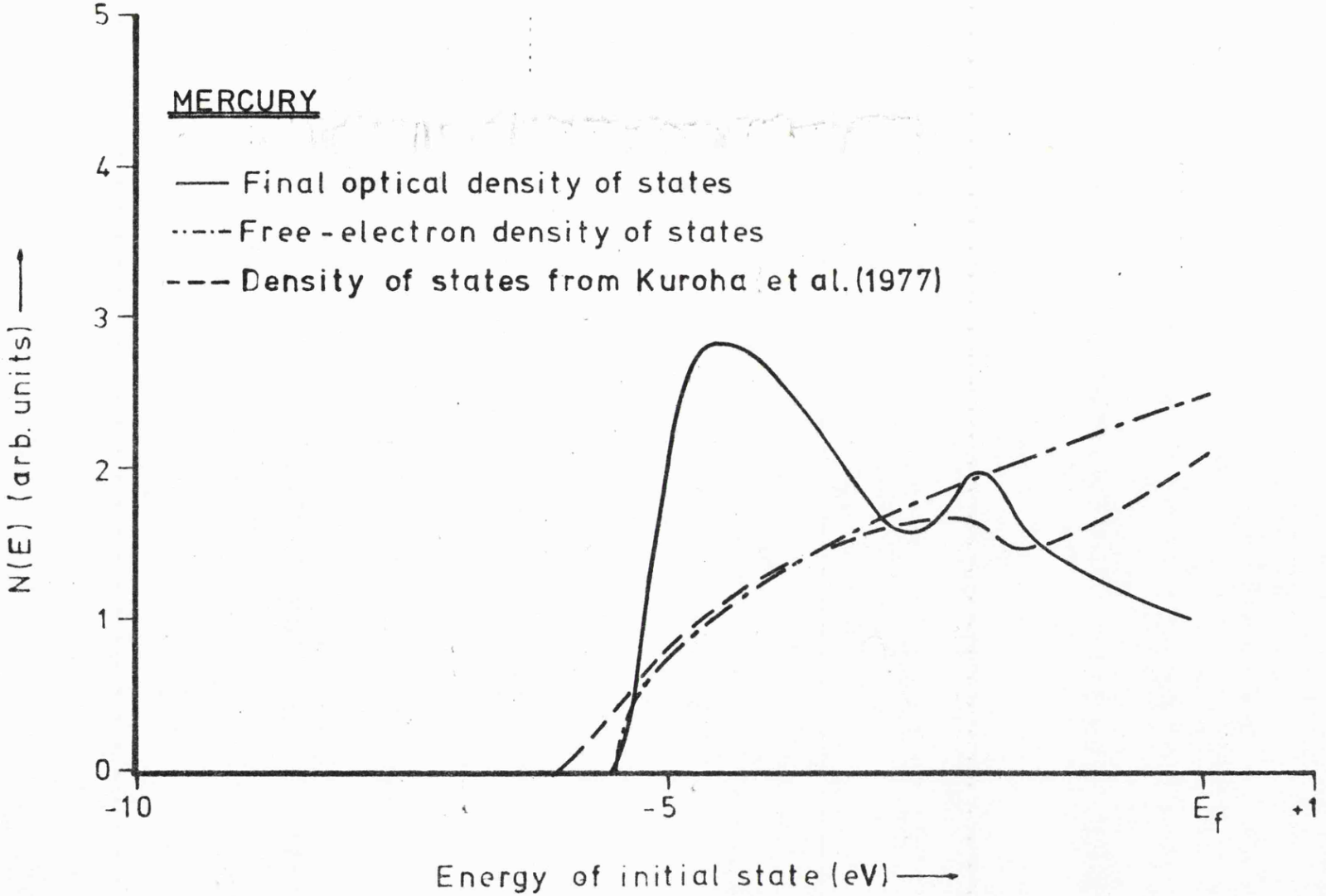

Fig. 7·9 - Final optical density of states for mercury.

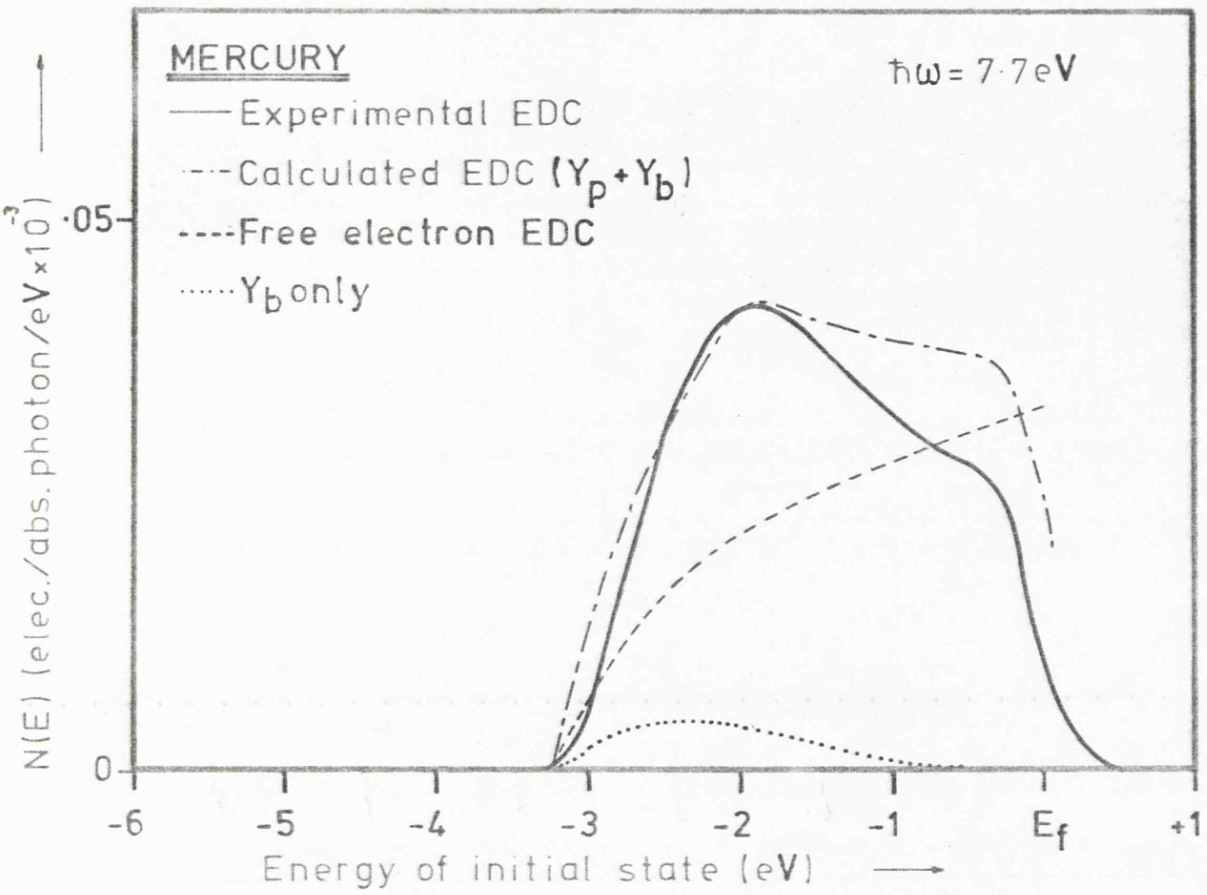

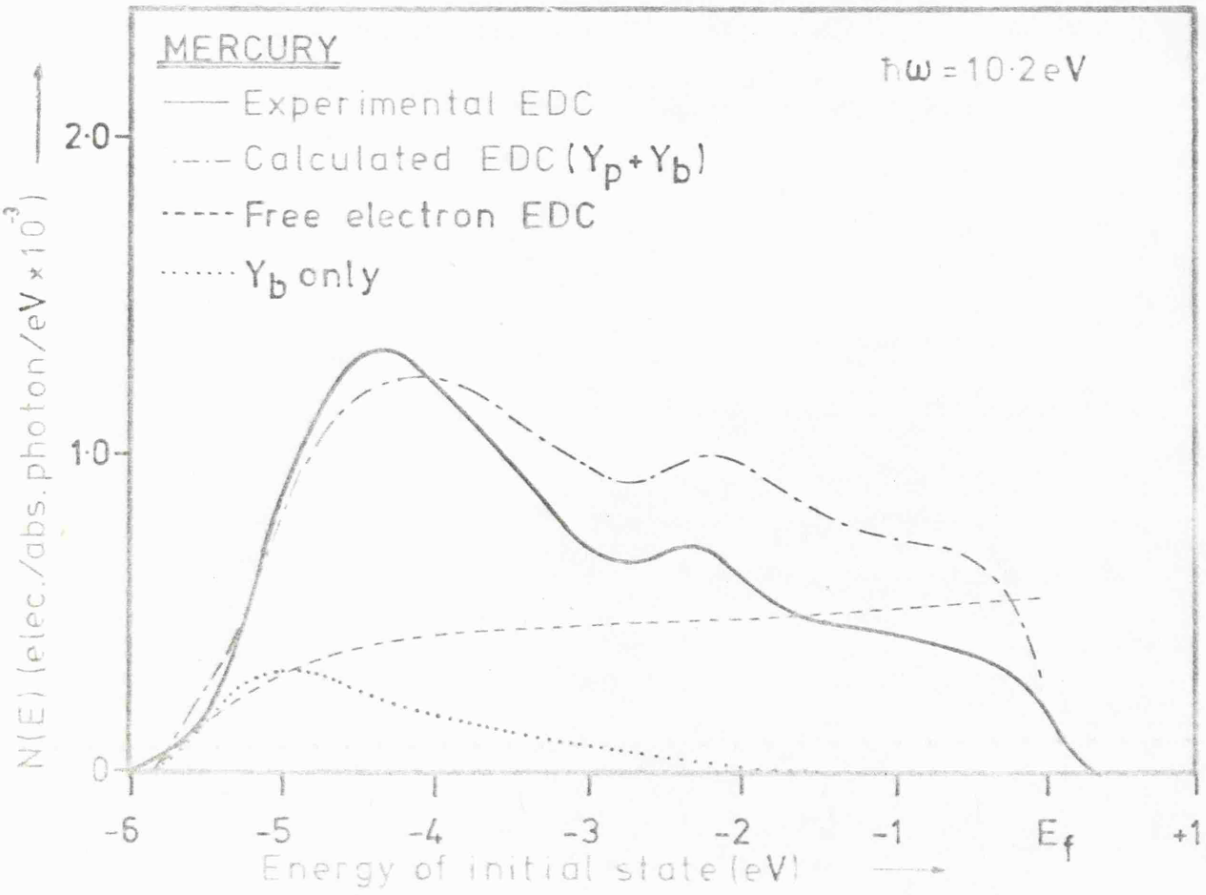

Fig.7.10 - Comparison of calculated & experimental EDCs from liquid mercury.

density of states. The results obtained in this work show better agreement with the original work of Mott than with that of later workers.

7.3. Mercury Alloys

7.3.1. Experimental

Experimentally, mercury alloys presented no more problems than pure mercury. The only alterations to the technique consisted of filtering the alloys through glass wool to remove oxide film and, in the case of mercury-sodium alloy, preparation under argon as the alloying is highly exothermic. Due to the evaporation of mercury during the course of the experiment there is some change in the composition of the alloy, but experiments on the rate of loss of pure mercury indicate this should be less than 5% for $Hg_{.50}-In_{.50}$ and $2\frac{1}{2}$% for $Hg_{.75}-In_{.25}$ over a period of 3–4 hours, which is long enough for the experiment.

7.3.2. Yield of Mercury - Indium Alloys

Figure 7.11 shows the yield of two mercury-indium alloys (taken shortly after pouring) compared with those of pure mercury and pure liquid indium. Reflectivity data is taken here from Siskind et al (1972), the values for 25at.% indium being extrapolated from their results for 20 and 30at.% indium.

As expected, the peaks due to the mercury vapour appear in both yields though it is noticeable that there is a change in the structure between 9 and 10.5 eV, strongest in the 50% indium yield, consistent with the presence of a corresponding peak in the yield of pure indium. No other changes are

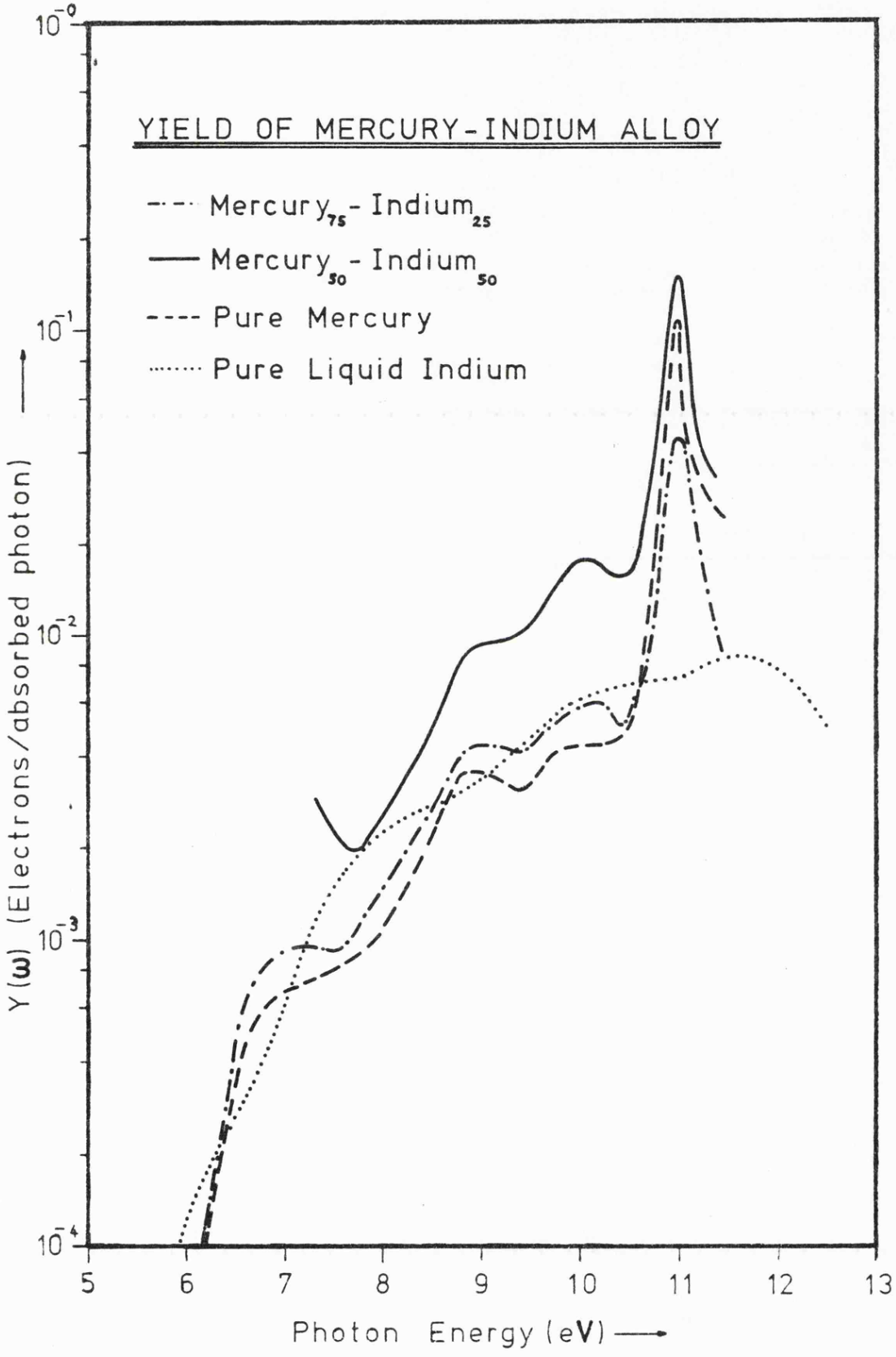

Fig.7.11-Yield of Mercury-Indium alloys

observed, except an overall increase in the yield, which is probably due to the higher reactivity of the indium resulting in a more oxidised surface. Figure 7.12 shows a Fowler plot for $Hg_{.75}$-$In_{.25}$. This gives a value of 4.39 ± 0.03 eV for the work function. Since the value obtained for liquid indium was 3.94 eV and the work function of pure mercury is generally taken as 4.5 eV (Riviere 1969) this result is not unreasonable. Unfortunately similar data for Hg and $Hg_{.50}$-$In_{.50}$ is not available.

7.3.3. Low Energy EDC's - Mercury-Indium

Figures 7.13 and 7.14 show low energy EDC's from two Hg - In alloys. In both alloys the slope approaching the Fermi edge is now positive - slightly so in the 25% alloy, more strongly so in the 50% alloy - and this is consistent with the filling of states near to the edge as predicted by Mott (loc.cit). The feature seen in pure mercury at -2.3 eV is not now observed in either alloy. Although the scattered peak in the 50% alloy is very large and could 'wash out' this feature, the scattered peak in the 25% alloy is not excessive, and this suggests that the peak is either greatly weakened or has been shifted in energy away from the Fermi edge.

Although the bulk composition of the alloy is known, there remains the question of whether there may be surface enrichment. A theory of this effect has been presented by Williams and Nason (1974) based on a pairwise bonding or quasi-chemical approach for solid binary alloys. Results for liquid Ag-Cu alloy (Norris et al 1976) have shown reasonable agreement with this, but it is not clear if in this present case, where

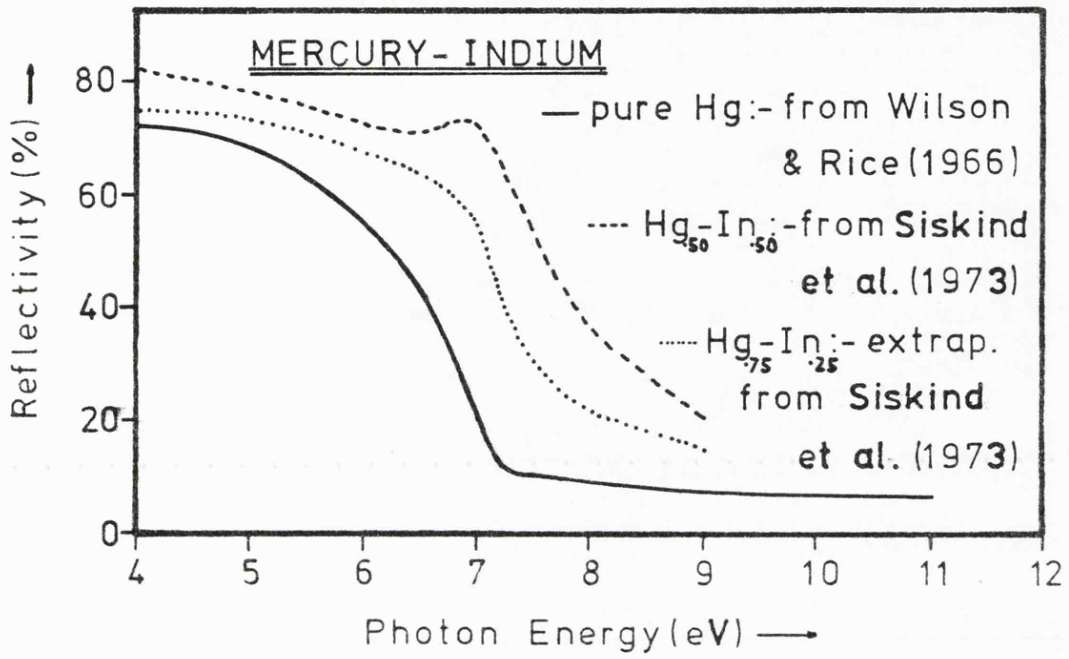

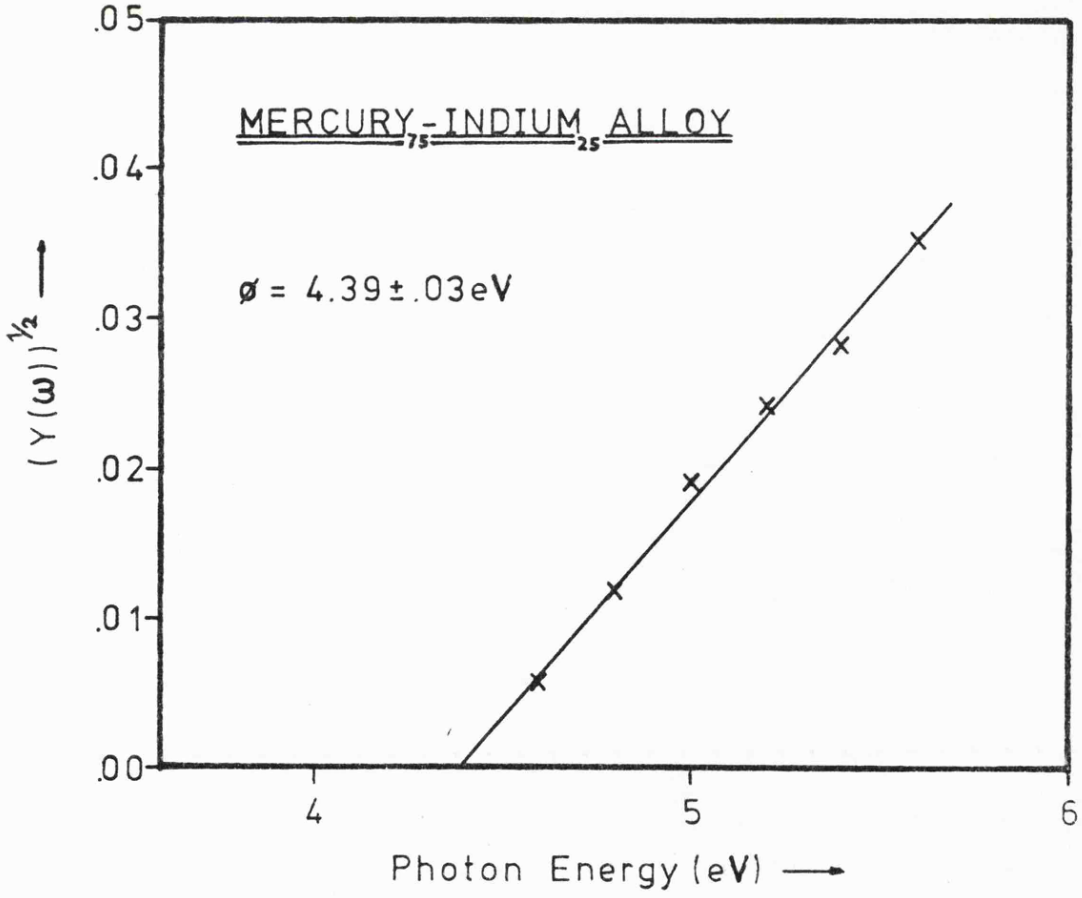

Fig.7.12 - Reflectivity & Fowler plot for Mercury-Indium alloys

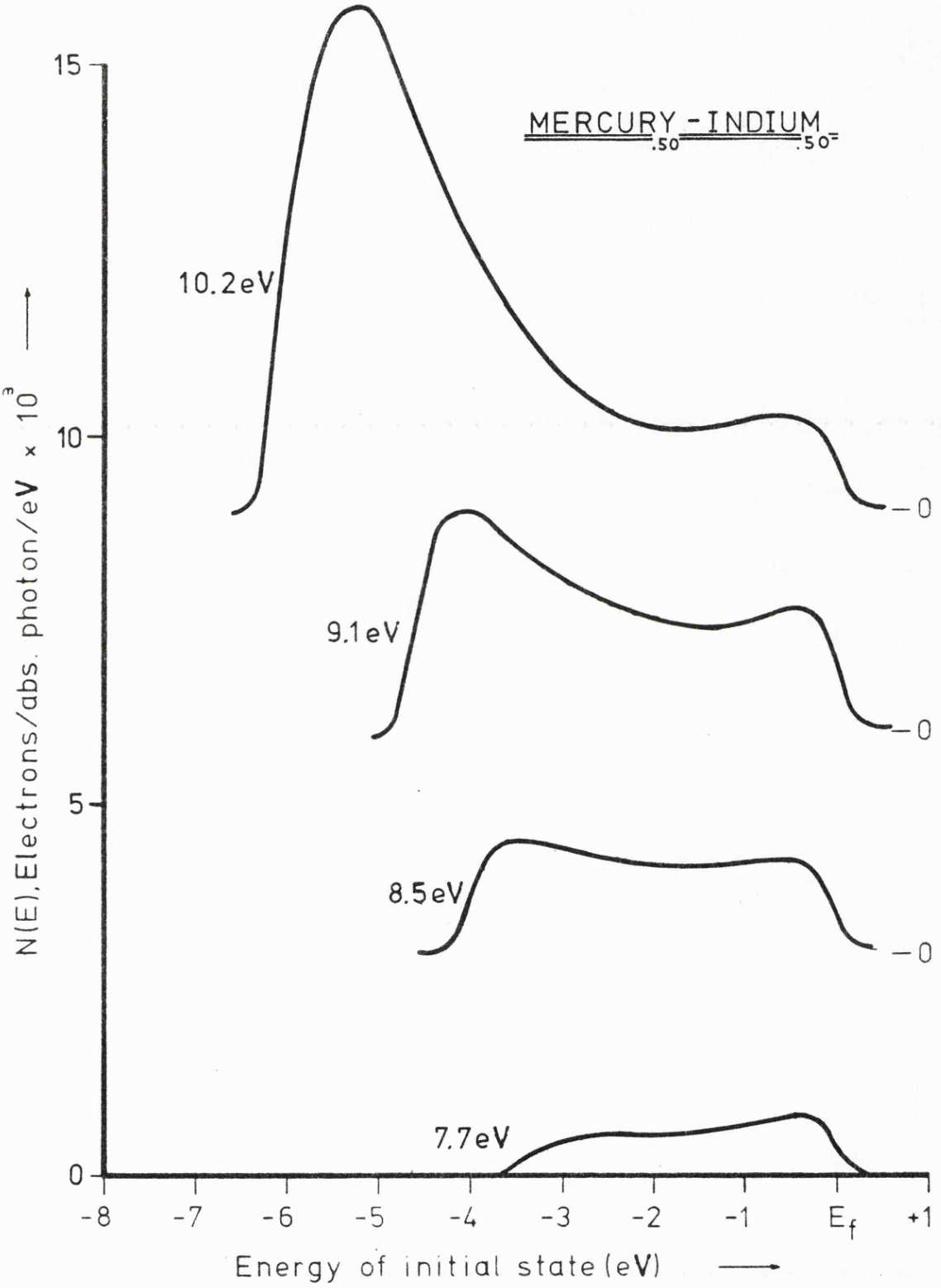

Fig.7.13 Low energy EDCs from Mercury$_{.50}$-Indium$_{.50}$.

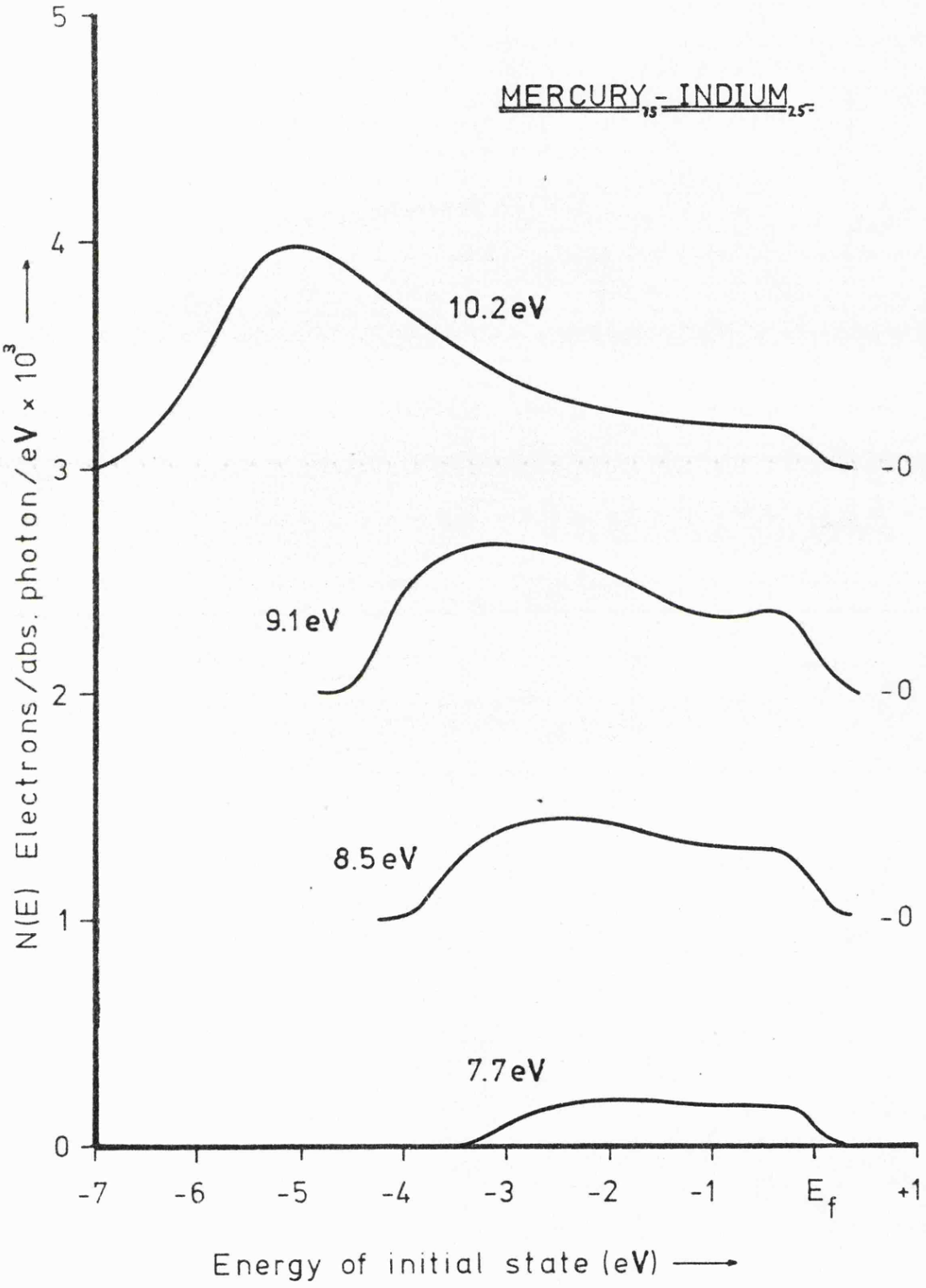

Fig.7.14-Low energy EDCs from Mercury$_{.75}$Indium$_{.25}$

there is a considerable loss of material from the surface and the technique is probing deeper than the surface layer, the theory is applicable. A rough estimate of the alloy concentration, based on the relative slope approaching the Fermi edge for the different alloys and components, gives a result in good agreement with the known bulk concentration.

7.3.4. High Energy EDC's

Figure 7.15 shows EDC's for $Hg_{.50}$-$In_{.50}$ alloy at 21.2 and 16.8 eV. It may be seen that the structure near the Fermi edge is consistent with the low energy EDC's and that a weak feature is now observed at about -2.6 eV (although, as with the weak features in aluminium, precise location is difficult). This again is consistent with the predictions of Mott (loc.cit.).

The d-band peaks are again observed, but shifted both in position and in width. Figure 7.16 summarises the binding energies relative to the Fermi level and the corrected widths for Hg and $Hg_{.50}$-$In_{.50}$.

7.3.5. Mercury-Sodium Alloy

As stated earlier, mercury-sodium alloy is difficult to prepare, due to the very high reactivity of the sodium. Because of this the surface oxidises readily and this results in a large scattered peak in the EDC's. Due to this problem it was possible to obtain a useable EDC at only one photon energy - 7.7 eV where the lamp output is greatest.

Figure 7.17 shows the EDC thus obtained for $Hg_{.96}$-$Na_{.04}$ alloy. It may be seen that there is a strong negative slope to the Fermi edge and that the feature at -2.3 eV has broadened

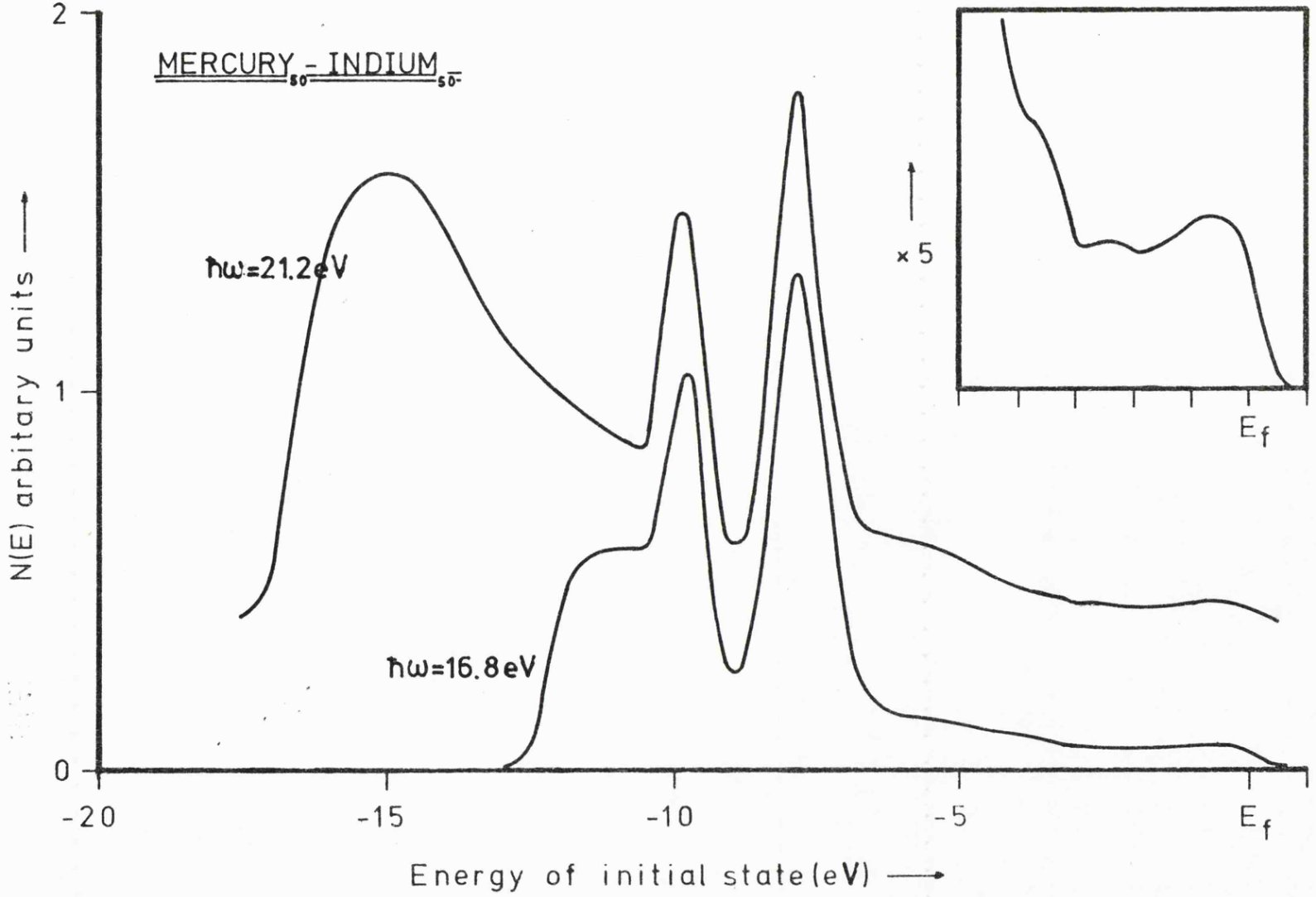

Fig.7.15-High energy EDCs from Mercury$_{80}$ Indium$_{50}$

	Hg		Hg_{50}-In_{50}	
	$5d_{5/2}$	$5d_{3/2}$	$5d_{5/2}$	$5d_{3/2}$
Line Energy (eV)	-7·60	-9·80	-7·85	-9·85
Corrected width* (eV)	1·0	0·50	0·75	0·35

*corrected for broadening using a Gaussian of 0·5eV half width

Fig.7.16-Measured positions of the 5d levels in Mercury and $Mercury_{50}$-$Indium_{50}$ alloy.

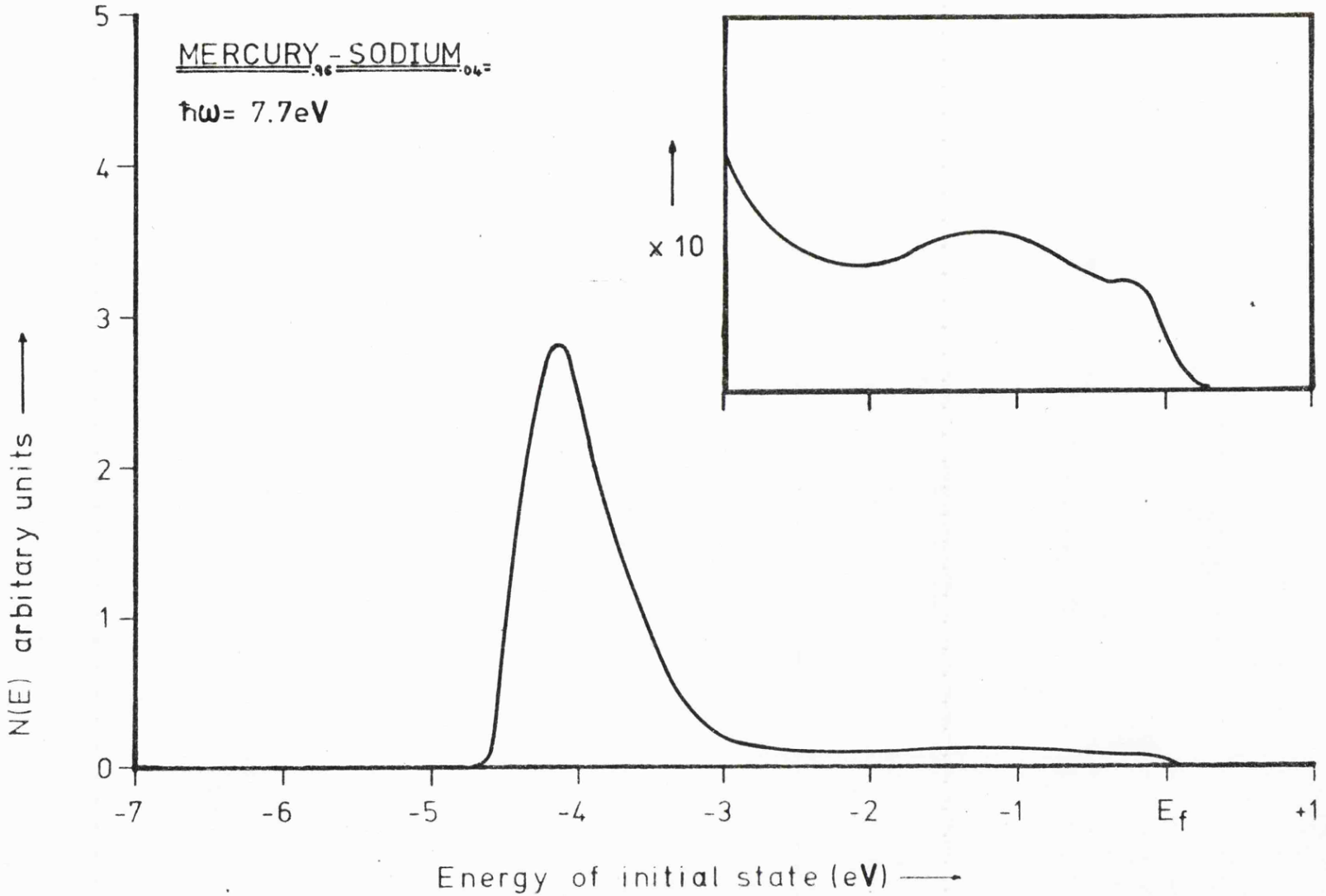

Fig.7.17-Low energy EDC from Mercury - Sodium

and is now centered at $\simeq -1.3$ eV. This again is in accord with the predictions of Mott (loc.cit.), who suggested that on alloying with an alkali metal the minimum in N(E) would be deepened and there would be a shift of the Fermi limit towards higher energies.

7.3.6. Discussion

Figure 7.18 shows the effect of alloying on the slope to the Fermi edge for pure mercury and three mercury alloys at low photon energies. The alteration of this slope and the movement of the feature which occurs at -2.3 eV in pure mercury is consistent with the supposition by Mott of the existence of a pseudogap in mercury, and with his predictions of the effects of alloying.

In the high energy EDC's the d-band peaks observed in pure mercury are observed to alter both in position and in width. This difference in width reflects the greater d-d overlap for the upper state. On alloying, the overlap of the d-wave functions is reduced and the lines narrow. The alteration of the peaks may be explained in fairly simplistic terms. The binding energies reflect changes in the environment of the atoms and there will be local Fermi level differences.
Since mercury is more electronegative than indium, electrons will be attracted to the mercury from the upper part of the indium valence band, causing a shift in the position of the band structure.

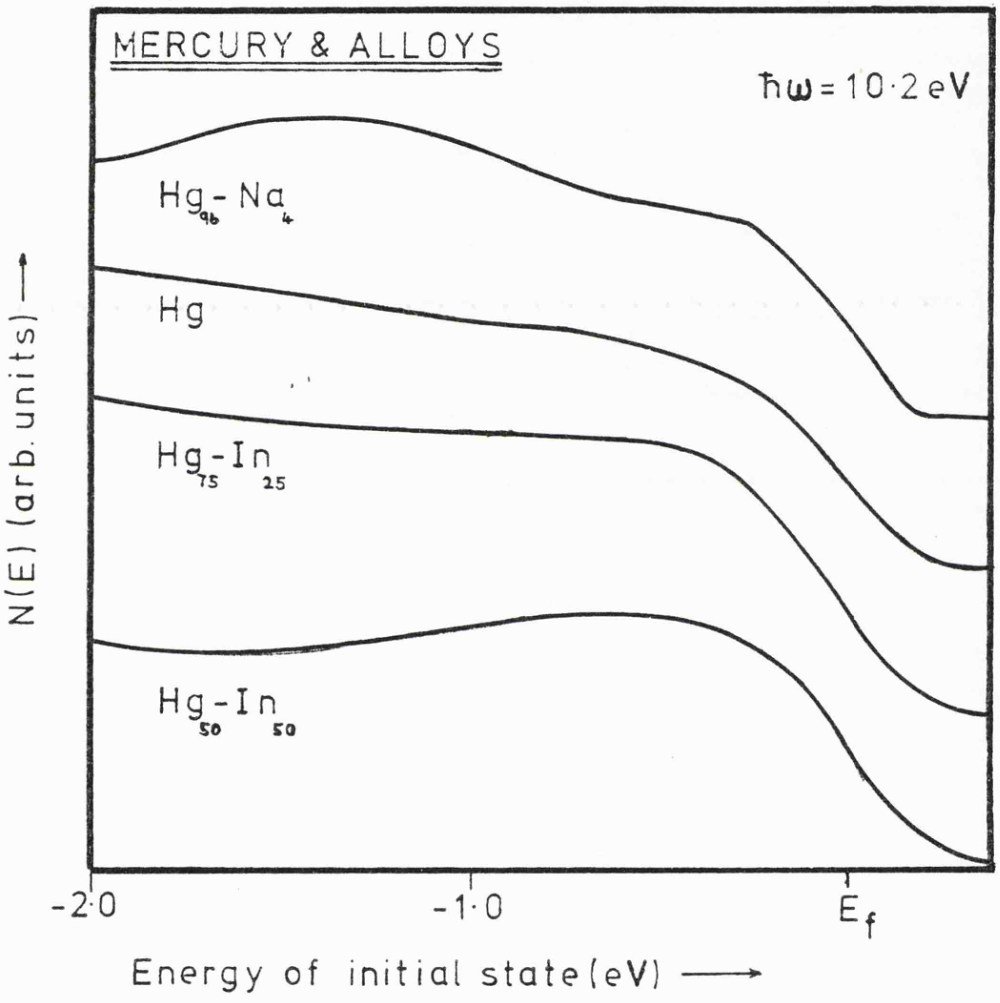

Fig.7.18-Behaviour near the Fermi edge for various Mercury alloys

CHAPTER 8:- SUMMARY AND CONCLUSIONS

8.1. Summary of Yields and Work Function

In Table 8.1 the work function of the elements studied are summarised and compared with the results of other workers. It may be seen that there is very little change observed between the solid and liquid phases, and the change that is observed lies well within the limits of error of the measurement. This is not unexpected considering that very little change is observed in the EDC's on melting. Except in the case of aluminium, the values obtained are in good agreement with those of earlier workers, the differences observed again being well within the limits of experimental error. The value for lead is also in good agreement with the theoretical predictions of Lang and Kohn (1971), which give a value of between 3.80 and 3.95 eV depending on the crystal face. The discrepancy in the case of aluminium is not surprising since the strong oxygen affinity of this metal makes clean surfaces very difficult to prepare and early values of the work function differ considerably. Also, the value quoted here from Riviere (1969) was obtained using a contact potential difference method which frequently gives values that are not in accord with photoelectron measurements.

A systematic movement of the value of the work function with valence is observed, the work function increasing with increasing valence, e.g. the value of 4.02 eV for aluminium lies between that of 3.66 eV for magnesium and 5.4 eV for silicon. In group 5 the progression, ignoring the transition elements, is:-

Element	Work function (eV)		Previous solid results
	liquid	solid	
Aluminium	4·02±·02	4·02±·02	4·19*
Indium	3·94±·07	4·06±·10	4·08×
Tin	4·27±·02	4·27±·02	4·28*
Lead	3·99±·03	3·94±·03	3·94•

*Riviere (1969) ×Van Laar & Scheer (1965) •Norris et al. (1972)

Fig.8.1-Summary of work functions

Rb	Sr	In	Sn	Sb
2.09	2.74	3.94	4.27	4.56

and in group 6:-

Cs	Ba	Tl	Pb	Bi
1.96	2.48	3.84	3.94	4.25

The other values here are taken from Wotherspoon (1978), Riviere (loc.cit.)and the CRC Handbook (1973). This variation of the work function is not inconsistent with the concept that the nucleus is imperfectly screened by the electrons. There is also a general reduction in work function moving from group 4→5→6.

Table 8.2. shows a summary of the quantum yields, at 7.7 and 10.2 eV, of the materials studied. It may be seen that, as in the case of the work function, there is very little difference between the solid and liquid. Again this is not inconsistent with the comparatively small changes seen in the EDC's on melting. It has been shown in Chapter 3 that the effect of the change, on melting, of the electron-phonon mean free path on the yield should be comparatively small and this is borne out by these results. It is worth noting however that there appears to be a correlation between the change in yield on melting and the degree of change in the structure observed in the EDC's, although this is obviously difficult to quantify. The largest change of yield is observed in the melting of rapidly frozen indium, the smallest in the melting of aluminium. This is not inconsistent with the solid showing the most structured EDC's being the most crystalline in nature, and thus having a longer electron-phonon mean free path than solid frozen into a more amorphous state.

Element	Yield (Electrons/absorbed photon)				Calc. l_e at 8·6 eV above E_f (Å)
	$\hbar\omega$ = 7·7eV		$\hbar\omega$ = 10·2eV		
	liquid	solid	liquid	solid	
Mercury	$8{\cdot}0\times10^{-4}$		$6{\cdot}5\times10^{-3}$		10
Aluminium	$7{\cdot}5\times10^{-3}$	$7{\cdot}5\times10^{-3}$	$2{\cdot}8\times10^{-2}$	$2{\cdot}8\times10^{-2}$	18
Indium	$2{\cdot}9\times10^{-3}$	$3{\cdot}2\times10^{-3}$	$8{\cdot}0\times10^{-3}$	$1{\cdot}15\times10^{-2}$	14
Tin	$1{\cdot}08\times10^{-2}$	$1{\cdot}08\times10^{-2}$	$2{\cdot}5\times10^{-2}$	$2{\cdot}8\times10^{-2}$	50
Lead	$8{\cdot}0\times10^{-3}$	$8{\cdot}0\times10^{-3}$	$2{\cdot}9\times10^{-2}$	$3{\cdot}5\times10^{-2}$	30

Fig.8·2 - Summary of yields & l_e values

8.2. Summary of Optical Density of States.

Figures 8.3, 8.4, and 8.5 summarises the optical density of states of the materials in this work and compares them with the results of Wotherspoon (1978) for Ga, Tl and Bi. What is immediately noticeable is that none of the ODOS's are free electron like. In all cases clear, distinct and consistent structure is seen in the ODOS's. If the ODOS's are compared with theoretical densities of states for both the liquid and solid it may be seen that the predicted structure in the liquid is always far weaker than that actually observed, whilst the agreement between the predicted solid densities of states and the ODOS's is good. This is consistent with the idea that some type of band-like structure is retained even after melting has taken place.

Figure 8.3 shows the variation of the optical density of states with valence through the elements Hg, Tl, Pb and Bi. Movement of the main minimum (shown in the diagrams by ↓) away from the Fermi level is apparent as the valence increases. If the ODOS is compared with the solid state band structure, it may be seen that the position of this minimum is consistent with the bottom of the 6p band. This behaviour may be interpreted in terms of the 6s band moving lower in energy with a simultaneous filling of the 6p band. If the ODOS for lead is compared with the theoretical predictions of McFeeley et al (1977) it may be seen that the relative heights of the ODOS at the

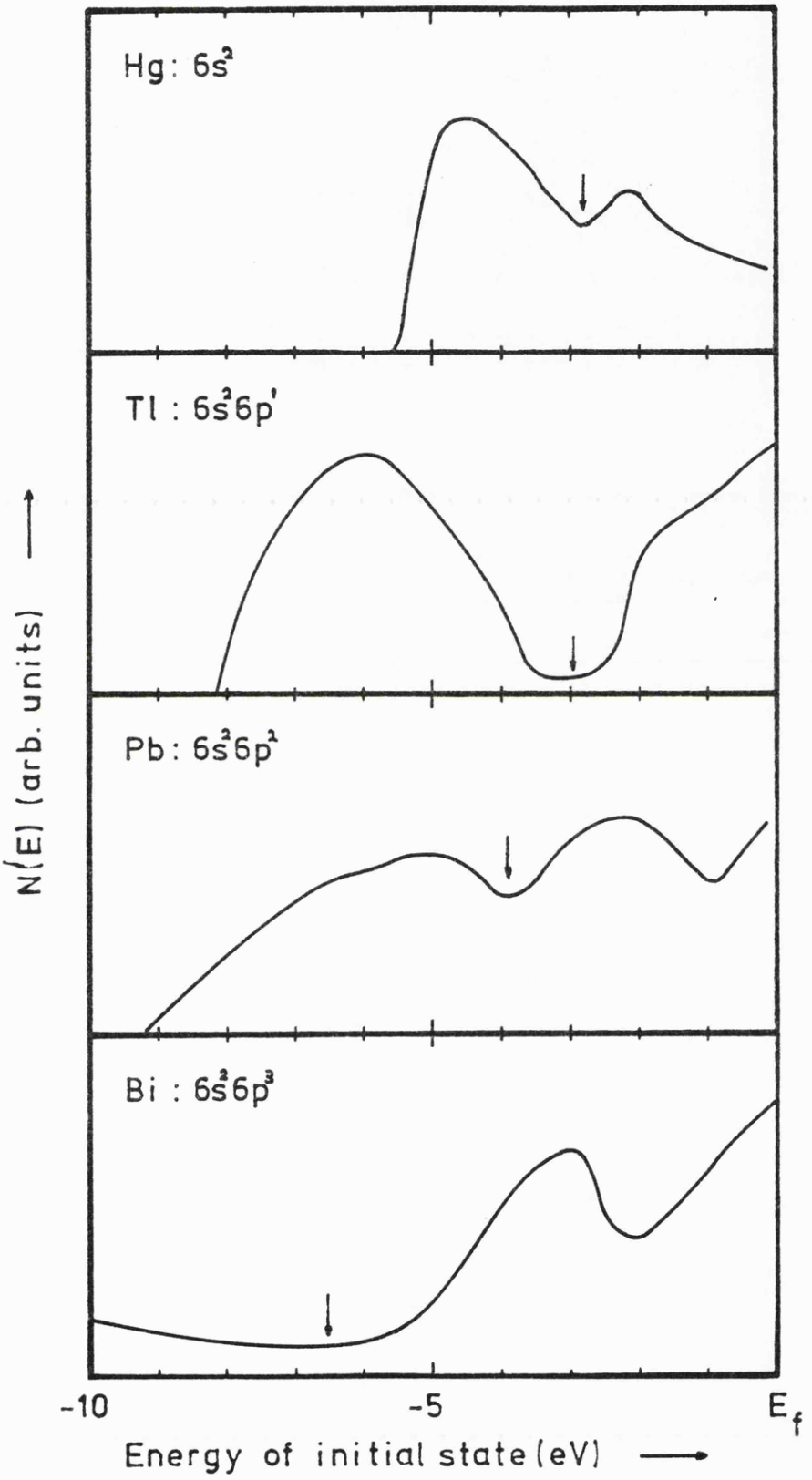

Fig.8.3-Optical densities of states for Hg, Tl, Pb and Bi

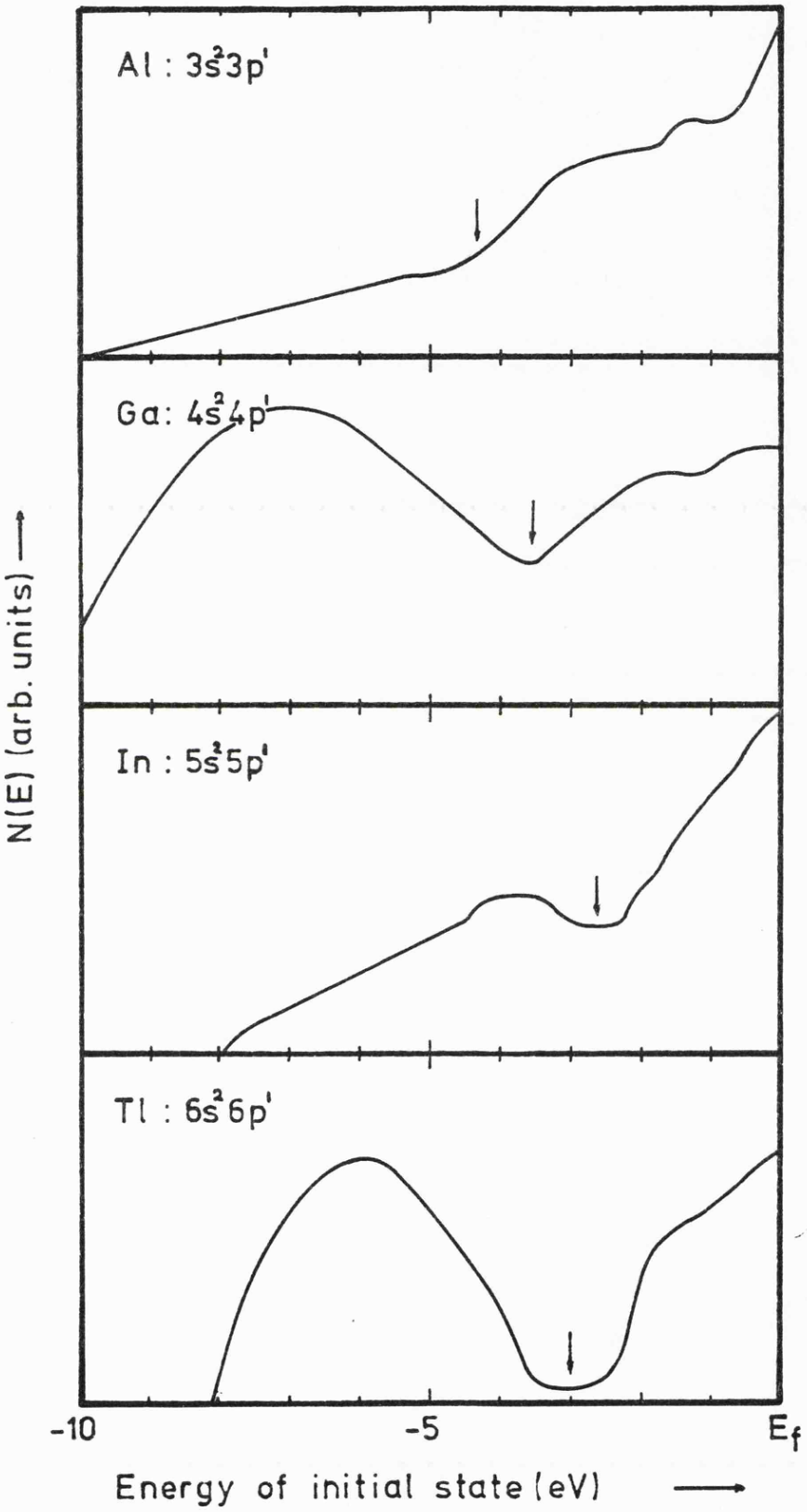

Fig.8.4-Optical density of states for Al, Ga, In and Tl

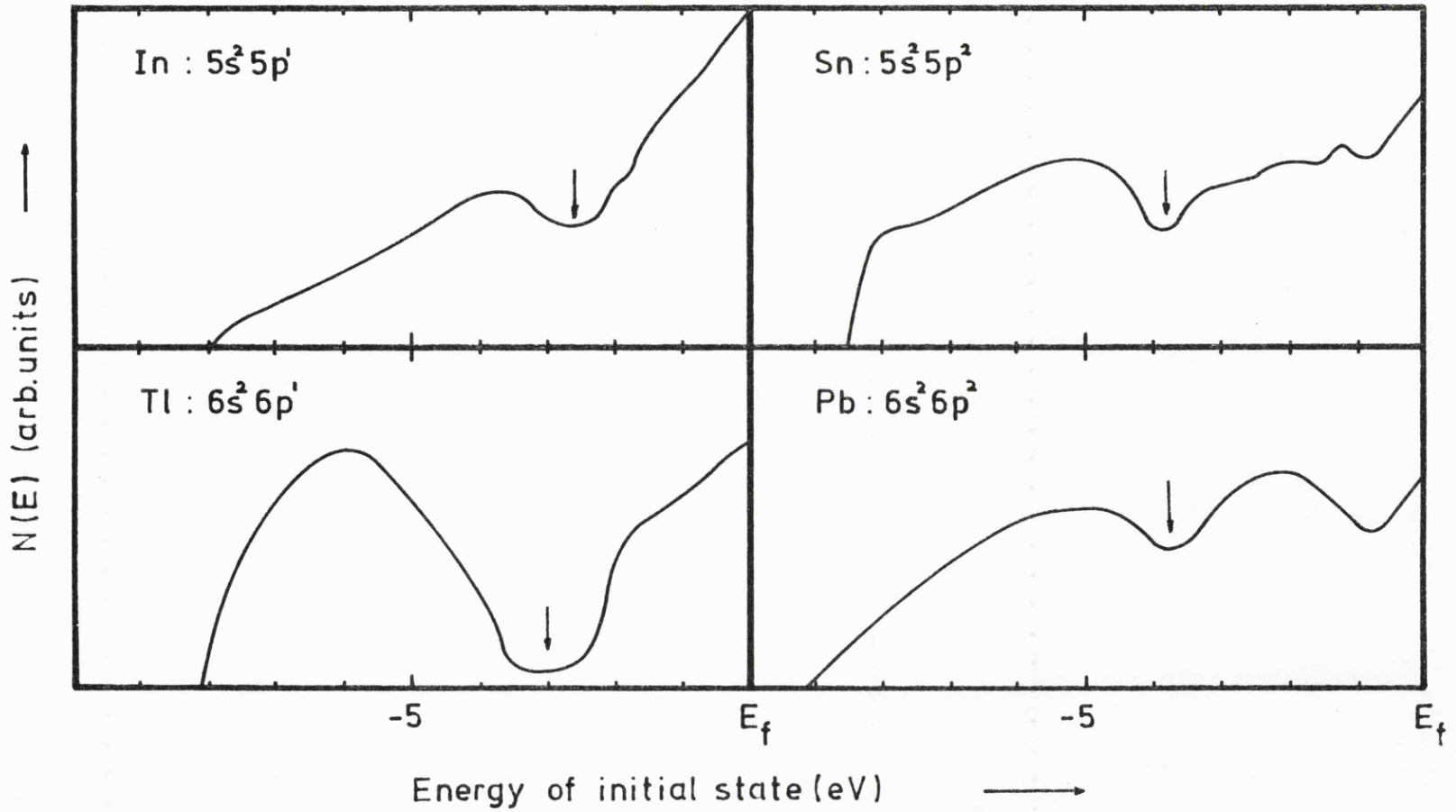

Fig.8.5-Optical densities of states for In, Sn, Tl and Pb

Fermi edge and at the main maximum at -2.6 eV are consistent with McFeely's predictions of the effects of spin orbit splitting.

In the ODOS for In and Sn it may be seen that again there is a movement of the position of the main minimum with increasing valence, consistent with the change in position of the 5p band, although here the 5s and 5p bands overlap to some extent. The fact that the density of states does not go to zero between the bands may indicate either a modification of the structure due to melting or simply be an effect of the convolution of the valence and conduction bands that has not been eliminated by the method of derivation of the ODOS.

Figure 8.4 shows the ODOS for the trivalent elements Al, Ga, In, Tl, i.e. moving from $3s^2\ 3p^1$ to $6s^2\ 6p^1$. As would be expected, there are strong similarities in the ODOS notably in the position of the main minimum at $\simeq -3$ eV, the bottom of the p band. This dip becomes more dominant with increasing z. This is consistent with band structure calculations which indicate a marked overlap of the s and p bands in Al, which lessens with increasing z until, in Tl, the bands are completely separate. This is consistent with the screening of the nucleus being less complete as the atom becomes heavier, resulting in the s electrons being pulled away from the p band. Also as z increases the agreement of the ODOS with the weak scattering calculations becomes poorer.

8.3. Effects of Matrix Elements.

In the preceeding chapters, in order to simplify the interpretation of results using the 3-step process, the assumption has been made that matrix elements are constant in the disordered

liquid system. In an ordered system the conservation of the momentum vector $\underline{k}$ results in the variation of both the position and the strength of the structure observed in the EDC's as a function of photon energy. If however $\underline{k}$ is not conserved and the assumption of constant matrix elements is justified, it would be expected that the structure observed in the EDC's would remain constant over a wide energy range. The results in this study only cover a fairly narrow energy range (i.e. 4 - 21.2 eV) but it may be seen that, for the liquid, the structure does remain constant in both strength and position. Unfortunately this is not really a wide enough energy range to state definitely that the assumption is justified and there is a distinct lack of high energy (XPS) results for liquid metals, (although Baer and Myers (1977) have now published the results of XPS measurements on liquid Bi). However the XPS results that have been used for comparison in this study are for evaporated films and it may be seen, by comparison of the low energy EDC's obtained in this work with low energy EDC's for evaporated films (Norris et al 1974 and Wooten et al 1966) that these films show EDC's more characteristic of the liquid than of the bulk solid. This implies that the films are highly disordered (even if they are not in a reproducible state of disorder).

Comparison of the XPS results for solid with the low energy liquid results (see Figures 5.11, 5.9 and 6.19) show good agreement between the two both in the position and strength of structure within 7 eV of the Fermi edge. This strongly implies that the contribution to the EDC's from the density of states has remained unchanged over this energy range and hence

indicates that any effects from matrix elements are quite small. Thus the assumption of constant matrix elements in this work does appear to be reasonably well justified.

Williams and Norris (1975) have attempted to show whether short range order is of importance to the optical matrix elements by calculating, within the n.f.e. formalism, the photoelectron spectra for a liquid using the quadratic response formalism of Schaich and Ashcroft and avoiding most of the simplifying approximations made in the 3-step process. Their result, using this theory, shows reasonable agreement with experiment in predicting the overall triangular shape of the EDC despite the neglect of electron-electron scattering. However the structure observed experimentally is not reproduced at all. This implies that the weak scattering model is simply not adequate to describe the electronic structure of simple metals.

8.4. The N.F.E. Theory

As may be seen from the results obtained in Chapters 5, 6 and 7, the optical densities of states of the materials examined show considerable variation from the free electron picture although earlier measurements of optical and transport properties (except in the cases of lead, thallium, bismuth and mercury) were in good agreement with this theory.

Wotherspoon (1978) has examined this discrepancy between the optical and UPS measurements for lead and bismuth and offers a possible explanation. Most of the optical measurements made have been at low energy and have involved

determination of ε_2, the imaginary part of the dielectric control. The results for ε_2 are then normally considered in terms of a Drude contribution described by the expression

$$\varepsilon_2^D = \frac{n e^2 \tau}{m \varepsilon_0 (1 + \omega^2 \tau^2)} \qquad (8.1.)$$

and an interband contribution due to the optical excitation of an electron from the filled valence band to a conduction state. In the absence of strong peaks in the ε_2 results, that may be associated with interband transitions, the results are usually fitted to the Drude expression by adjusting the value of n/m to find an effective carrier density. However Smith (1967) has suggested that the fact that this adjustment is necessary is itself indicative of a deviation from a free electron situation.

Wotherspoon has used an optical density of states similar to the one given in this work for lead to calculate ε_2 for liquid lead. From the expression:-

$$\varepsilon_2^B \propto \int_{E_f}^{E_f + \hbar\omega} N_v(E)\, N_c(E - \hbar\omega)\, dE \qquad (8.2.)$$

for the interband contribution to ε_2 based on a non direct transition model, he obtained good agreement with experimental results at low photon energy. This implies strongly that the lack of interband transitions seen in low energy optical work cannot be taken as an indication of a free electron situation and some high energy optical measurements are necessary to settle this point.

Although the results of transport measurements have been taken as evidence for the n.f.e. model, results for heavy polyvalent metals such as lead show considerable discrepancies, particularly in the value of the Hall coefficient,which indicates that the weak scattering formalism simply is not adequate in these cases. With the other metals Al, In and Sn, although the results for these fit the nearly free electron picture reasonably well, it has been shown by Edwards (1962) that the transport properties are not a sensitive indication of variations in the density of states and this agreement cannot be regarded as a necessary indication of a featureless parabolic density of states curve.

8.5. Further Work

Whilst good results were obtained for In, Al, Sn, Pb and Hg, the failure of the mercury diffusion pump meant that a full investigation of the mercury alloys could not be carried out. The results obtained before the failure indicate that there is a need for a complete study of the mercury alloys if the 'pseudogap' controversy is to be resolved.

The apparatus itself has obvious room for improvement both in the analyser and the light source. As stated in Chapter 4, the retarding field type of analyser was chosen because it was anticipated that there would be considerable trouble with evaporation of the sample and consequent condensation in the analyser. However this did not occur and, since a higher resolution would be most desirable, another type of analyser, such as a cylindrical mirror analyser (C.M.A.), could be adopted -

certainly a higher signal/noise ratio could be obtained using counting electronics rather than the system used in this study. The ability to cover a wider photon energy range would also be most desirable. The comparatively narrow range used in this study meant that the effects of matrix elements had to be estimated from solid XPS results. There is a considerable need for high resolution XPS measurements of the liquid phase if a true comparison is to be obtained.

Finally there are further interesting materials that may be examined. Very little work has been done to date on liquid alloys and in particular there is little data on the liquid semiconductors, Ga-Sc, Tl-Te, Mg-Bi and Li-Bi, (see Enderby 1972). These alloys have very high vapour pressures ($\simeq 10^{-3}$ torr) but,with the use of specialised pumping systems using diffusion or high speed turbo-molecular pumps,the work should not be impossible. However because of the problems of surface enrichment, it would be necessary to add an Auger spectrometer to the system to obtain a measure of the surface composition. Again a C.M.A. spectrometer should be used as high sensitivity is necessary for this work.

8.6. Conclusions

This work, taken in conjunction with the later work of Wotherspoon (1978), represents the first systematic photoemission study of liquid metals under ultra clean conditions. Whilst other workers have examined isolated elements, it is only by means of a systematic study, enabling comparison of the elements in a series, that major overall effects can be discerned and generalisations made.

The work function, quantum yield and low energy photoelectron spectra have been measured for Al, In, Sn and Pb in the liquid and solid states and for mercury and some mercury alloys. Comparison of the solid phase data with previous work and examination of the low energy scattered peak in the photoelectron spectra have shown that the liquid surfaces obtained were virtually free of contamination. The results obtained indicate that there is very little change in the yield of Al, In, Sn or Pb on melting and this has been shown to be not inconsistent with the reduction of the electron phonon mean free path on melting. The optical densities of states which have been derived for these four metals are inconsistent with the Ziman weak scattering formalism and agree better with the solid state band structure, indicating that elements of this structure may well persist on melting. No evidence for $\underline{k}$ conservation or for non-constant matrix elements was observed in the liquid state. In the case of mercury and its alloys, it has been shown that their behaviour is consistent with the original Mott prediction of a 'pseudogap' and does not accord well with later theoretical work.

REFERENCES

Ament, M.A.E.A. and De Vroomen, A.R., 1975, J. Phys. F: Metal Phys. 5, 2394

Anderson, J.R. and Gold, A.V., 1965, Phys. Rev. 139, A1459.

Ashcroft, N.W. and Lawrence, W.E., 1968, Phys. Rev. 175, 938.

Ashcroft, N.W. and Leckner, J., 1966, Phys. Rev. 145, 83.

Baer, Y. and Myers, A.P., 1977, Sol. Stat. Comm. 21, 8, 833.

Ballentine, L.E. and Chan, T., 1972, Second Int. Conf. on Liquid Metals, Tokyo.

Berglund, C.N. and Spicer, W.E., 1964, Phys. Rev. 136, A1033 and 1044.

Breeze, A., 1974, Sol. Stat. Comm. 14, 395.

Broden, G., Hagstrom, S.B.M. and Norris, C., 1973, Phys. Kondens Materie, 15, 327.

Brundle, C.R., 1974, J. Vac. Sci. Technol. 11, 212

Callcott, T.A. and Arakawa, E.T., 1975, Phys. Rev. 11, B2750

Catterall, J.A. and Trotter, J., 1963, Phil. Mag. 8, 897

Caroli, C., Lederer-Rozenblatt, D., Roulet, B. and Saint-James, D., 1973, Phys. Rev. 88, 4552.

Castelijns, J.H.P., aan de Brugh, H.W.J.M. and de Vroomen, A.R., 1977, J. Phys. F: Metal Phys. 7, 2457.

Chan, T., and Ballentine, L.E., 1971, Physics Lett. A 35, 385; 1972, Can. J. Phys. 50, 813.

Cotti, P., Guntherodt, H-J., Munz, P., Oelhafen, P. and Wullschleger, J., 1973, Sol. Stat. Comm. 12, 635.

Craven, J.E., 1969, Phys. Rev. 182, 693.

C.R.C. Handbook, 1973, pub. Chemical Rubber Co.

Cusack, N.E., 1963, Rep. Prog. Phys. 26, 361; 1972, Proc. 2nd Int. Conf. on the properties of liquid metals, Tokyo, 1972, Ed. S. Takeuchi.

Dishman, J.M. and Rayne, J.A., 1968, Phys. Rev. 166, 728

DiStefano, T.H. and Pierce, D.T., 1970, Rev. Sci. Instrum. 41, 180.

Eastman, D.E., 1969, J. Appl. Phys. 40, 1387.

Eastman, D.E., 1972, in Techniques of Metals Research, ed. E. Passaglia Vol. 6 pt. 1 p. 412 (New York, N.Y.).

Eden, R.C., 1970, Rev. Sci. Instrum. 41, 252.

Edwards, S.F., 1962, Proc. R. Soc. A 267, 518; 1965, Proc. Phys. Soc., 85, 1.

Ehrenreich, H., Phillipp, H.R., and Segall, B., 1963, Phys. Rev. 132, 5, 1918.

Enderby, J.E., 1972, Proc. 2nd Int. Conf. on the properties of liquid metals, Tokyo, 1972, Ed. S. Takeuchi.

Enderby, J.E., and Hawker, I., J. non-Cryst. Solids, 1972, 8, 687.

Endriz, J.G., and Spicer, W.E., 1971, Phys. Rev. B4, 4144 and 4159.

Einstein, A., 1905, Ann. Physik, 17, 132.

Evans, R., 1970, J. Phys. C, Metal Phys. Suppl., No. 2, S137.

Evans, R., Greenwood, D.A., Lloyd, P. and Ziman, J.M., 1969, Phys. Lett. 30A, 313.

Faber, T.E., 1972, Introduction to the theory of liquid metals, CUP.

Fabian, D.J., 1972, quoted in Cusack (1972).

Fowler, R.H., 1931, Phys. Rev. 38, 45.

Goetz, A., 1929, Phys. Rev. 33, 373.

Hochst, H., Hufner, S., and Goldman, A., 1976, Sol. Stat. Comm. 19, 899.

Hodgson, J.N., 1959, Phil. Mag., 4, 183, 1962 Phil. Mag. 7, 229

Honig, R.G. and Kramer, D.A., 1969, R.C.A. Review, June 1969.

Houston, J.E. and Park, R.L., 1972, Rev. Sci. Instrum. 43, 1437.

Ichikawa, K., 1972, Phil. Mag. 27, 177.

Itami, T. and Shimoji, M., 1972, Phil. Mag. 25, 229.

Keeton, S.C. and Loucks, T.L., 1966, Phys. Rev. 152, 548.

Kittel, C., 1968, in "Solid State Physics" pub. Wiley Press.

Knight, W.D., Berger, A.G. and Heine, V., 1959, Ann. Phys. 8, 173.

Koyama, R.Y., 1968, Ph.D. Thesis, Stanford University.

Koyama, R.Y. and Smith, N.V., 1970, Phys. Rev. B2, 3049.

Koyama, R.Y. and Spicer, W.E., 1971, Phys. Rev. B4, 4318.

Krolikowski, W.F., 1968, Ph.D. Thesis, Stanford University.

Krolikowski, W.F. and Spicer, W.E., 1970, Phys. Rev. B1, 478.

Kuroha, M., Wasada, Y. and Suzuki, K., 1977, J. Phys. Soc. Jap. 42, 107.

Lang, N.D. and Kohn, W., 1971, Phys. Rev. B3, 1215.

Leckey, R.C.E., 1972, Sol. Stat. Comm. 10, 975.

Lemmonier, J.C., Priol, M. and Robin, S., 1973, Phys. Rev. B8, 5452.

Lemmonier, J.C. and Robin, S., 1967, C.R. Acad. Sci. Paris 265, 661.

Lemmonier, J.C., Stephan, G., LeCalvez, Y., and Robin, S., 1969, J. Phys. Chem. Solids, 30, 1147.

Ley, L., Pollak, R., Kowalczyk, S.P. and Shirley, D.A., 1972, Phys. Rev. Lett. 41A, 429.

Lindau, I., Lofgren, H. and Wallden, L., 1971, Phys. Lett 36A, 293.

Liquid Metals Handbook, 1955, Ed. Jackson (Washington: Atomic Energy Commission and U.S. Navy).

Loucks, T.L., 1965, Phys. Rev. Lett. 14, 1072.

Mahan, G.D., 1970, Phys. Rev. B2, 4334.

March, N.H., 1968, "Liquid Metals", pub. Pergamon Press.

McFeeley, F.R., Ley, L., Kowalczyk, S.P. and Shirley, D.A., 1975, Sol. Stat. Comm. 17, 1415.

Moore, C.E., 1949, Natn. Bur. Stand. (U.S.) Circular No. 467.

Mott, N.F., 1966, Phil. Mag. 13, 989.

Nilsson, P.O., Norris, C. and Walden, L., 1970, Phys. Kondens Materie, 11, 220-230.

Norris, C., Rodway, D.C. and Williams, G.P., 1972, Proc. 2nd Int. Conf. on the properties of liquid metals, Tokyo, 1972, Ed. S. Takeuchi.

Norris, C., Rodway, D.C. and Williams, G.P., 1973, Proc. of Structures Metalliques Desordonnees, Strasbourg, 61.

Norris, C. and Wallden, L., 1972, J. Phys. F.: Metal Phys., 2, 002

Ocken, H. and Wagner, C.N.J., 1966, Phys. Rev. 149, 122.

Philipp, H.R., and Ehrenriech, H., 1964, J. App. Phys. 35, 1416.

Pollak, R.A., 1972, Ph.D. Thesis, University of California, Berkeley.

Powell, C.J., 1968, Phys. Rev. 175, 972.

Quinn, J. J., 1962, Phys. Rev. 126, 1453.

Richardson, O. and Compton, K. 1912, Phil. Mag. 24, 575.

Riviere, J.C., 1969, in "Solid State Surface Science", edited by M. Green.

Rousseau, J., Stoddart, J.C. and March, N.H., 1970, Proc. R. Soc. A. 317.

Scaich, W.L., and Ashcroft, N.W., 1970, Sol. Stat. Comm. 8, 1959

Schneider, T. and Stoll, E., 1967, Adv. Phys. 16, 731.

Schultz, L.G., 1957, Adv. Phys. 6, 102.

Seymour, E.F.W., and Styles, G.A., 1964, Physics Lett. 10, 269.

Shaw, R.W. and Smith, N.V., 1969, Phys. Rev. 178, 985.

Siskind, B., Boiani, J. and Rice, S.A., 1973, Can. J. Phys. 51, 894.

Skerbele, A., Ross, K.J. and Lassettre, E.N., 1969, J. Chem. Phys. 50, 4486.

Smith, N.V., 1968, Physics Lett. 26A, 126, 1967, Adv. Phys. 16, 629.

Stevenson, A., 1968, Ph.D. Thesis, University of Sheffield.

Stuart, R., Wooten, F. and Spicer, W.E., 1964, Phys. Rev. 135, 495

Van Attekum, P., 1977, quoted in Castelijns et al, 1977.

Van Laar, J. and Scheer, J.J., 1960, Philips Res. Repts. 15, 1.

Watabe, M., 1976, 3rd. Int. Conf. on liquid metals, Bristol, 1976.

Wasada, Y. and Suzuki, K., 1972, Phys. Stat. Sol. 49, 339.

West, R.N., Borland, R.E., Cooper, J.A. and Cusack, N.E., 1967, Proc. Phys. Soc. 92, 195.

Williams, F.L. and Nason, D., 1974, Surf. Sci. 45, 337.

Williams, G.P. and Norris, C., 1976, Phil. Mag. 34, 851; 1975 Proc. Int. Conf. on Electronic and Magnetic properties of Liquid Metals, Mexico City, ed. J. Keller.

Wilson, E.G. and Rice, S.A., 1966, Phys. Rev. 145, 55.

Wooten, F., Huen, T., and Stuart, R.N., 1966, in "Optical properties and Electronic Structure of Metals and Alloys", ed. F. Abeles (North-Holland Co.) p. 332.

Wotherspoon, J.T.M., 1978, Ph.D. Thesis, University of Leicester.

Ziman, J.M., 1961, Phil. Mag. 6, 1013-34; 1964, Adv. Phys. 13, 89-138

APPENDIX I: The Monte Carlo programme

This version of the programme is in Algol for the Nottingham University 1906 computer. A later version in Fortran will be found in Wotherspoon (1978).

Program symbols

All units of energy are in 0.1eV measured with respect to the bottom of the valence band. The lengths are in Angstrom units.

E1 Valence band width.

E2 Photon energy.

E3 Workfunction.

E4 Energy at any given time.

E5 Energy given up at an electron-ion collision.

E6 Energy of secondary after the scattering event.

E9 Energy at which l_e is defined.

E10 Energy given up filling the valence hole in the Auger process.

E11 Energy of Auger process which is generated.

L1 Length of primary electron walk.

L2 Mean free path of the photoelectron at the particular final state energy.

L3 Electron-ion mean free path.

L4 Length of secondary walk.

L5 l_e corrected for the final state energy.

L6 Absorption coefficient.

L8 Length of Auger walk.

T1 Angle of travel, with respect to the surface normal, for the primary.

T2 Angle of travel, with respect to the surface normal, for the secondary.

T3 Angle of travel, with respect to the surface normal, for the Auger.

X1 Instantaneous distance of electron from the surface.

C3 Sum of generation depths of electrons which have escaped.

U1, U2 Variables used in the Simpson's Rule calculation.

H1 The separation of energy points in the density of states.

Y1, Y2, Y3, Y4 Primary yield in four angular sections.

Y5, Y6, Y7, Y8 Secondary yield in four angular sections.

Y9, Y10, Y11, Y12 Auger yield in four angular sections.

N1 Total number of photons.

N2 Number of slots into which the density of states is split.

D1 Density of states below the Fermi level.

U Density of states above the Fermi level.

```
12/47/30          16/04/75          COMPILED BY XALV 4K.  5A
LINE STATEMENT
  13     0        'TRACE' 2
  14     0        'COMMENT' THIS IS THE FULL PROGRAMME WITH FREE ELECTRON D.O.S.;
  15     0        'UNDIN'
  16     0        'BEGIN''INTEGER''ARRAY'LOCATONLIK[LOCATION:LOCATION];
                BLOCK      1
  17     1        'REAL' 'PROCEDURE' RANDOM(X);
                BLOCK      2
  18     3        'REAL' X;
  19     4        'BEGIN'
  20     4            'REAL' 'PROCEDURE' G05AAA; 'EXTERNAL';
                BLOCK      3
  21     4            RANDOM:=G05AAA;
  22     6        'END' OF RANDOM;
  23     6
  24     6            'REAL' E1,E2,E3,E4,E5,E6,E7,E8,E9,E10,E11,L1,L2,L3,L4,L5,L6,L7,
  25     7                   L8,T1,T2,T3,A1,A2,A3,A4,A5,X,X1,X2,X3,U1,U2,H1,H2;
  26     7              'INTEGER' Y1,Y2,Y3,Y4,Y5,Y6,Y7,Y8,Y9,Y10,Y11,Y12,N,N1,N2,N3,C,Q,
  27     8                        R,V,Z,N4;
  28     8            'REAL' 'ARRAY' D1,D2,B,F,U[0:500];
  29     9              'INTEGER' 'ARRAY' P1,P2,P3,P4,S1,S2,S3,S4,K1,K2,K3,K4,I,W[0:100]
  30    10                               ,G1,G2[0:10000],G3,G4[0:200];
  31    10        'COMMENT' THIS IS THE FATE COUNTER FOR THE PRIMARY PHOTOELECTRONS;
  32    10           'PROCEDURE' COUNTP (Y1,Y2,Y3,Y4,P1,P2,P3,P4,E1,E3,E4,Q,T1);
                BLOCK      4
  33    12            'REAL' E1,E3,L4,T1;
  34    13            'INTEGER' Y1,Y2,Y3,Y4,Q;
  35    14            'INTEGER' 'ARRAY' P1,P2,P3,P4;
  36    15          'BEGIN'
  37    15            Q:=ENTIER(10*(E4-(E3+E1))+.1);
  38    17            T1:=SQRT((E4*(1-(2*T1)+(T1*T1)))/((E4*T1*T1)-(E3+E1)));
  39    18            'IF' Q>100 'THEN' 'GOTO' AAGD;
  40    19            'IF' T1 'GE' 0.41 'THEN' 'GOTO' AABA;
  41    20               Y1:=Y1+1;
```

```
42   21                P1[Q]:=P1[Q]+1;
43   22                'GOTO' AABD;
44   23        AABA: 'IF' T1 'GE' 1.0 'THEN' 'GOTO' AABB;
45   24                Y2:=Y2+1;
46   25                P2[Q]:=P2[Q]+1;
47   26                'GOTO' AABD;
48   27        AABB: 'IF' T1 'GE' 2.4 'THEN' 'GOTO' AABC;
49   28                Y3:=Y3+1;
50   29                P3[Q]:=P3[Q]+1;
51   30                'GOTO' AABD;
52   31        AABC:   Y4:=Y4+1;
53   32                P4[Q]:=P4[Q]+1;
54   33        AABD: 'END';
55   33        'COMMENT' THIS IS THE FATE COUNTER FOR THE SECONDARY PHOTOELECTRONS;
56   33           'PROCEDURE' COUNTS (Y5,Y6,Y7,Y8,S1,S2,S3,S4,E1,E3,E6,Q,T2);
               BLOCK    5
57   35              'INTEGER' Y5,Y6,Y7,Y8,Q;
58   36              'REAL' E1,E3,E6,T2;
59   37              'INTEGER' 'ARRAY' S1,S2,S3,S4;
60   38            'BEGIN'
61   38              Q:=ENTIER(10*(E6-(E3+E1))+.1);
62   40              T2:=SQRT((E6*(1-(2*T2)+(T2*T2)))/((E6*T2*T2)-(E3+E1)));
63   41              'IF' Q>100 'THEN' 'GOTO' AACD;
64   42              'IF' T2 'GE' 0.41 'THEN' 'GOTO' AACA;
65   43                 Y5:=Y5+1;
66   44                 S1[Q]:=S1[Q]+1;
67   45              'GOTO' AACD;
68   46        AACA: 'IF' T2 'GE' 1.0 'THEN' 'GOTO' AACB;
69   47                 Y6:=Y6+1;
70   48                 S2[Q]:=S2[Q]+1;
71   49                 'GOTO' AACD;
72   50        AACB: 'IF' T2 'GE' 2.4 'THEN' 'GOTO' AACC;
73   51                 Y7:=Y7+1;
74   52                 S3[Q]:=S3[Q]+1;
75   53                 'GOTO' AACD;
76   54        AACC:    Y8:=Y8+1;
```

```
 77   55                  S4[Q]:=S4[Q]+1;
 78   56        AACD: 'END';
 79   56        'COMMENT' THIS IS THE FATE COUNTER FOR THE AUGER ELECTRONS;
 80   56           'PROCEDURE' COUNTA (Y9,Y10,Y11,Y12,K1,K2,K3,K4,E1,E3,E11,Q,T3);
              BLOCK      6
 81   58              'REAL' E1,E3,E11,T3;
 82   59              'INTEGER' Y9,Y10,Y11,Y12,Q;
 83   60              'INTEGER' 'ARRAY' K1,K2,K3,K4;
 84   61             'BEGIN'
 85   61                Q:=ENTIER(10*(E11-(E3+E1))+.1);
 86   63                T3:=SQRT((E11*(1-(2*T3)+(T3*T3)))/((E11*T3*T3)-(E3+E1)));
 87   64                'IF' Q>100 'THEN' 'GOTO' AAHD;
 88   65                'IF' T3 'GE' 0.41 'THEN' 'GOTO' AAHA;
 89   66                   Y9:=Y9+1;
 90   67                   K1[Q]:=K1[Q]+1;
 91   68                'GOTO' AAHD;
 92   69        AAHA:   'IF' T3 'GE' 1.0 'THEN' 'GOTO' AAHB;
 93   70                   Y10:=Y10+1;
 94   71                   K2[Q]:=K2[Q]+1;
 95   72                'GOTO' AAHD;
 96   73        AAHB:   'IF' T3 'GE' 2.4 'THEN' 'GOTO' AAHC;
 97   74                   Y11:=Y11+1;
 98   75                   K3[Q]:=K3[Q]+1;
 99   76                'GOTO' AAHD;
100   77        AAHC:      Y12:=Y12+1;
101   78                   K4[Q]:=K4[Q]+1;
102   79        AAHD: 'END';
103   79        'COMMENT' THIS IS THE SIMPSONS RULE PROCEDURE FOR THE D OF S;
104   79           'PROCEDURE' SIMRUL(H1,Q,V,D1,B,F,U1,U2,R);
              BLOCK      7
105   81              'REAL' H1,U1,U2;
106   82              'INTEGER' Q,V,R;
107   83              'REAL' 'ARRAY' D1,B,F;
108   84              'BEGIN'
109   84              'FOR' Q:=4 'STEP' 2 'UNTIL' V 'DO'
110   86                      'BEGIN'
111   86                         U1:=0:U2:=0;
112   89                         'FOR' R:=1 'STEP' 2 'UNTIL' Q-1 'DO'
```

```
113   90                              'BEGIN'
114   90                                 U1:=U1+D1[R];
115   92                              'END';
116   93                           'FOR' R:=2 'STEP' 2 'UNTIL' Q-2 'DO'
117   94                              'BEGIN'
118   94                                 U2:=U2+D1[R];
119   96                              'END';
120   97                           B[Q]:=(H1/3)*(D1[0]+D1[Q]+(2*U2)+(4*U1));
121   98                           'IF' Q=V 'THEN' 'GOTO' AAEA;
122   99                           B[Q+1]:=B[Q]+(H1*D1[Q])+(H1*(D1[Q+1]-D1[Q])/2);

123  100     AAEA:              'END';
124  101                   B[0]:=0; B[1]:=(H1*D1[0])+(H1*(D1[1]-D1[0])/2);
125  103                   B[2]:=(H1/2)*(D1[2]+(2*D1[1])+D1[0]);
126  104                   B[3]:=(H1/2)*((2*(D1[2]+D1[1]))+(D1[3]+D1[0]));
127  105                   'FOR' Q:=0 'STEP' 1 'UNTIL' V 'DO'
128  106                      'BEGIN'
129  106                         F[Q]:=B[Q]/B[V];
130  108                      'END';
131  109             'END';
132  109        'COMMENT' THIS IS THE MONITOR FOR THE INITIAL ENERGY SELECTIOM;
133  109           'PROCEDURE' INTEGD (E1,E2,E4,O,I);
              BLOCK      8
134  111             'INTEGER' Q;
135  112.            'REAL' E1,E2,E4;
136  113             'INTEGER' 'ARRAY' I;
137  114          'BEGIN'
138  114             Q:=ENTIER(((E4-E1)*10)+.1);
139  116             'IF' Q>100 'THEN' 'GOTO' AADA;
140  117             I[Q]:=I[Q]+1;
141  118        AADA: 'END';
142  118        'COMMENT' THIS IS THE PRINTOUT PROCEDURE FOR THE EDC'S;
143  118           'PROCEDURE' PRINTE (V,Z,W);
              BLOCK      9
144  120             'INTEGER' V,Z;
145  121             'INTEGER' 'ARRAY' W;
146  122          'BEGIN'
```

```
147  122
148  122        'BEGIN' STELLWRITE;
149  125                ELLTEXT('('''LI!')');
150  126                ENDELLWRITE;
151  127        'END' ;
152  128
153  128
154  128        'BEGIN' STELLWRITE;  SAMELINE;
155  131                ELLTEXT('(''↑----↑----↑----↑----↑----↑----↑----↑----↑----↑!')');
156  132
157  132                ELLTEXT('(''----↑----↑----↑----↑----↑----↑----↑----↑----↑----↑!'
158  132        )');
159  133                ENDELLWRITE;
160  134        'END' ;
161  135
162  135
163  135        'BEGIN' STELLWRITE;
164  137                ELLTEXT('('''LI!')');
165  138                ENDELLWRITE;
166  139        'END' ;
167  140
168  140              'FOR' V:=0 'STEP' 1 'UNTIL' 100 'DO'
169  141                'BEGIN'
170  141
171  141        'BEGIN' STELLWRITE;
172  144                ELLTEXT('('I!')');
173  145                ENDELLWRITE;
174  146        'END' ;
175  147
176  147                    'FOR' Z:=1 'STEP' 1 'UNTIL' W[V] 'DO'
177  148                      'BEGIN'
178  148
179  148        'BEGIN' STELLWRITE;  SAMELINE;
180  152                ELLTEXT('('''SII')');
181  153                ENDELLWRITE;
182  155        'END' ;
183  155
184  155                          'END';
```

```
185  156
186  156          'BEGIN' STELLWRITE;  SAMELINE;
187  159                  ELLTEXT('(''X!')');
188  160                  ENDELLWRITE;
189  161          'END' ;
190  162
191  162
192  162          'BEGIN' STELLWRITE;
193  164                  ELLTEXT('(''L!!')');
194  165                  ENDELLWRITE;
195  166          'END' ;
196  167
197  167                   'END';
198  168             'END';
199  168          'COMMENT' NOW WE BEGIN THE SETTING-UP BELOW THE FERMI ENERGY;
200  168
201  168          'BEGIN' STELLREAD;
202  171                  H2 :=READ;
203  172                  ENDREADELL;
204  173          'END' ;
205  174
206  174
207  174          H1:=H2;
208  175          'BEGIN' STELLWRITE;
209  177                  ELLTEXT('(''L!!')');
210  178                  ENDELLWRITE;
211  179          'END' ;
212  180
213  180
214  180          'BEGIN' STELLREAD;
215  182                     E1:=READ;
216  183                     E2:=READ;
217  184                     E3:=READ;
218  185                  ENDREADELL;
219  186             'END' ;
220  187
221  187
222  187                  N:=ENTIER((E1/H2)+.1);
```

```
223  188
224  188
225  188        'BEGIN' STELLWRITE;  SAMELINE;
226  191                ELLTEXT('('''NO OF POINTS IN DENSITY OF STATES IS!')');
227  192                PRINTELL(V);
228  193                ENDELLWRITE;
229  194        'END' ;
230  195
231  195
232  195        'BEGIN' STELLWRITE;
233  197                ELLTEXT('('''L!!')');
234  198                ENDELLWRITE;
235  199        'END' ;
236  200
237  200
238  200        'BEGIN' STELLWRITE;  SAMELINE;
239  203                ELLTEXT('('''SPACING OF POINTS IS!')');
240  204                PRINTELL(H1);
241  205                ELLTEXT('('''EV!')');
242  206                ENDELLWRITE;
243  207        'END' ;
244  208
245  208
246  208        'BEGIN' STELLWRITE;
247  210                ELLTEXT('('''L!!')');
248  211                ENDELLWRITE;
249  212        'END' ;
250  213
251  213        'COMMENT' NOW WE READ IN THE D OF S BELOW THE FERMI ENERGY;
252  213                'FOR' R:=0 'STEP' 1 'UNTIL' V 'DO'
253  214                   'BEGIN'
254  214
255  214                D2[R]:=(R*H1)↑0.5;
256  216
257  216                   'END';
258  217        'COMMENT' NOW WE READ IN THE D OF S ABOVE THE FERNI LEVEL;
259  217        'BEGIN' STELLREAD;
260  219                H1:=READ;
```

```
261  220                ENDREADFILE;
262  221        'END';
263  222
264  222                 C:=ENTIER((E2/H1)+30.1);
265  223
266  223        'BEGIN' STELLWRITE; SAMELINE;
267  226                ELLTEXT('('''NO OF POINTS ABOVE FERMI LEVEL IS!')');
268  227                PRINTFILL(C);
269  228                ELLTEXT('('''AT A SPACING OF!')');
270  229                PRINTFILL(H1);
271  230                ELLTEXT('('''L!!')');
272  231                ENDFILLWRITE;
273  232        'END';
274  233              'FOR' R:=0 'STEP' 1 'UNTIL' C 'DO'
275  234        'BEGIN'
276  234                U[R]:=(((F1/H1)+R)*H1)↑0.5;
277  236        'END';
278  237        'COMMENT' NOW WE OFFSET DATA FOR EXCLUSION PRINCIPLE;
279  237                   'FOR' R:=0 'STEP' 1 'UNTIL' ENTIER((E2/H2)+0.5) 'DO'
280  238                       D1[R]:=D2[R+(V-ENTIER((E2/H2)+0.5))]*U[R];
281  239                   V:=ENTIER((E2/H2)+0.5);
282  240                   SIMRUL(H1,Q,V,D1,B,F,U1,U2,R);
283  241
284  241        'BEGIN' STELLREAD;
285  243                 N2 :=READ;
286  244                ENDREADFILL;
287  245        'END' ;
288  246
289  246
290  246        'BEGIN' STELLWRITE;  SAMELINE;
291  249                ELLTEXT('('''NO OF SLOTS IN ENERGY SELECTION IS!')');
292  250                PRINTFILL(N2);
293  251                ENDFILLWRITE;
294  252        'END' ;
295  253
296  253
297  253        'BEGIN' STELLWRITE;
298  255                ELLTEXT('('''L!!')');
```

```
299  256                ENDFILLWRITE;
300  257          'END' ;
301  258
302  258          'COMMENT' NOW WE ASSIGN VALUES TO THE PROBABILITY MATRIX;
303  258                    Q:=0;
304  259                    G3[Q]:=0;G3[V]:=N2;G4[ENTIER((E2+2)*10)]:=N2;
305  262                    'FOR' R:=0 'STEP' 1 'UNTIL' N2 'DO'
306  263                       'BEGIN'
307  263                          G1[R]:=R;
308  265          AAFA:           'IF' E[Q]*N2 'GE' G1[R] 'THEN' 'GOTO' AAFB;
309  266                          G3[Q]:=R;
310  267                          Q:=Q+1;
311  268                          'GOTO' AAFA;
312  269          AAFB:           G1[R]:=Q;
313  270                       'END';
314  271
315  271
316  271          'COMMENT' NOW WE SET UP THE MATRIX FOR ELECTRON-ELECTRON SCATTERING;
317  271                V:=(E2+2)/H1;
318  272                'FOR' R:=0 'STEP' 1 'UNTIL' V 'DO'
319  273                       'BEGIN'
320  273                          D1[R]:=(U[R]*U[V-R]);
321  275                          F[R]:=0;
322  276                       'END';
323  277                    SIMPUL(H1,Q,V,D1,B,F,U1,U2,R);
324  278                    Q:=0;
325  279                    'FOR' R:=0 'STEP' 1 'UNTIL' N2 'DO'
326  280                       'BEGIN'
327  281                          G2[R]:=R;
328  282          AAIA:           'IF' E[Q]*N2 'GE' G2[R] 'THEN' 'GOTO' AAIB;
329  283                          G4[Q]:=R-1;
330  284                          Q:=Q+1;
331  285                          'GOTO' AAIA;
332  286          AAIB:           G2[R]:=Q;
333  287                       'END';
334  288          'COMMENT' THIS IS THE END OF THE SETTING-UP PROCEDURE;
335  288             'BEGIN'
336  288          'COMMENT' NOW SET THE FATE COUNTERS TO ZERO;
```

```
337  288              Y1:=0;Y2:=0;Y3:=0;Y4:=0;Y5:=0;Y6:=0;Y7:=0;Y8:=0;Y9:=0;Y10:=0;
338  299                Y11:=0;Y12:=0;
339  301              X3:=0;
340  302              'FOR' V:=0 'STEP' 1 'UNTIL' 100 'DO'
341  303                 'BEGIN'
342  305                    P1[V]:=0;P2[V]:=0;P3[V]:=0;P4[V]:=0;
343  308                    S1[V]:=0;S2[V]:=0;S3[V]:=0;S4[V]:=0;
344  312                    K1[V]:=0;K2[V]:=0;K3[V]:=0;K4[V]:=0;
345  316                    I[V]:=0;W[V]:=0;
346  318                 'END';
347  319              X:=RANDOM(0);
348  320         'COMMENT' NOW WE READ IN THE REST OF THE DATA;
349  320
350  320         'BEGIN' STELLREAD;
351  322                  N1 :=READ;
352  323                 E5 :=READ;
353  324                 E9 :=READ;
354  325                 L7 :=READ;
355  326                 L3 :=READ;
356  327                 L6 :=READ;
357  328                 ENDREADFILE;
358  329         'END' ;
359  330
360  330
361  330         'BEGIN' STELLWRITE;  SAMELINE;
362  333                 FILLTEXT('('''TOTAL NO OF PHOTONS IS!')');
363  334                 PRINTFILL(N1);
364  335                 ENDFILLWRITE;
365  336         'END' ;
366  337
367  337
368  337         'BEGIN' STELLWRITE;
369  339                 FILLTEXT('('''!!!')');
370  340                 ENDFILLWRITE;
371  341         'END' ;
372  342
373  342
374  342         'BEGIN' STELLWRITE;  SAMELINE;
```

```
375  345                ELLTEXT('(''FERMI ENERGY IS!')');
376  346                PRINTELL(E1);
377  347                ENDELLWRITE;
378  348          'END' ;
379  349
380  349
381  349          'BEGIN' STELLWRITE;
382  351                ELLTEXT('(''L!!')');
383  352                ENDELLWRITE;
384  353          'END' ;
385  354
386  354
387  354          'BEGIN' STELLWRITE;  SAMELINE;
388  357                ELLTEXT('(''PHOTON ENERGY IS!')');
389  358                PRINTELL(E2);
390  359                ENDELLWRITE;
391  360          'END' ;
392  361
393  361
394  361          'BEGIN' STELLWRITE;
395  363                ELLTEXT('(''L!!')');
396  364                ENDELLWRITE;
397  365          'END' ;
398  366
399  366
400  366          'BEGIN' STELLWRITE;  SAMELINE;
401  369                ELLTEXT('(''WORK FUNCTION IS!')');
402  370                PRINTELL(F3);
403  371                ENDELLWRITE;
404  372          'END' ;
405  373
406  373
407  373          'BEGIN' STELLWRITE;
408  375                ELLTEXT('(''L!!')');
409  376                ENDELLWRITE;
410  377          'END' ;
411  378
412  378
```

```
413  378        'BEGIN' STELLWRITE;  SAMELINE;
414  381                ELLTEXT('(''ELECTRON PHONON COLLISION ENERGY IS!')');
415  382                PRINTELL(E5);
416  383                ENDELLWRITE;
417  384        'END' ;
418  385
419  385
420  385        'BEGIN' STELLWRITE;
421  387                ELLTEXT('(''L!!')');
422  388                ENDELLWRITE;
423  389        'END' ;
424  390
425  390
426  390        'BEGIN' STELLWRITE;  SAMELINE;
427  393                ELLTEXT('(''ELECTRON ELECTRON SCATTERING LENGTH AT ENERGY!')');
428  394
429  394                PRINTELL(E9);
430  395                ELLTEXT('(''IS!')');
431  396                PRINTELL(L7);
432  397                ENDELLWRITE;
433  398        'END' ;
434  399
435  399
436  399        'BEGIN' STELLWRITE;
437  401                ELLTEXT('(''L!!')');
438  402                ENDELLWRITE;
439  403        'END' ;
440  404
441  404
442  404        'BEGIN' STELLWRITE;  SAMELINE;
443  407                ELLTEXT('(''ELECTRON PHONON SCATTERING LENGTH IS!')');
444  408                PRINTELL(L3);
445  409                ENDELLWRITE;
446  410        'END' ;
447  411
448  411
449  411        'BEGIN' STELLWRITE;
450  413                ELLTEXT('(''L!!')');
```

```
451  414                ENDELLWRITE;
452  415          'END' ;
453  416
454  416
455  416          'BEGIN' STELLWRITE;  SAMELINE;
456  419                  ELLTEXT('''ATTENUATION DEPTH IS:''');
457  420                  PRINTELL(L6);
458  421                  ENDELLWRITE;
459  422          'END' ;
460  423
461  423
462  423          'BEGIN' STELLWRITE;
463  425                  ELLTEXT('''''!!!''');
464  426                  ENDELLWRITE;
465  427          'END' ;
466  428
467  428          'COMMENT' NOW WE BEGIN THE MAIN PART OF THE PROGRAM;
468  428                'FOR' N:=1 'STEP' 1 'UNTIL' N1 'DO'
469  429                  'BEGIN'
470  429          'COMMENT' NOW WE DECIDE THE INITIAL ENERGY OF THE PHOTOELECTRON;
471  429                     A1:=RANDOM(1);
472  431                     Q:=ENTIER(N2*A1);
473  432                     E4:=E1+(G1[Q]*H2);
474  433                     INTEGD (E1,E2,E4,0,1);
475  434                     N4:=0;
476  435          'COMMENT' NOW WE DECIDE THE DEPTH OF THE PHOTOELECTRON GENERATION;
477  435                     X1:=-LN(RANDOM(2))/L6;
478  436                     X2:=X1;
479  437          'COMMENT' NOW WE CONSIDER THE POSSIBILITY OF AN AUGER ELECTRON;
480  437                     'IF' E1-(E4-E2) 'LE' E3 'THEN' 'GOTO' AAGH;
481  438                       A4:=RANDOM(11);
482  439                       Q:=(E4-E1)*10;
483  440                       R:=ENTIER(A4*(N2-G3[Q]))+G3[Q];
484  441          'COMMENT' NOW CONSIDER AVAILABLE ENERGY FOR AUGER PROCESS;
485  441                       E10:=(E1-E4)+(G1[R]*H2);
486  442                       'IF' E10 'LE' E3 'THEN' 'GOTO' AAGH;
487  443                       A5:=RANDOM(12);
488  444                       Q:=ENTIER(((E2-E10)*10)+0.4);
```

```
489  445                    R:=ENTIER(A5*(N2-G3[Q]))+G3[Q];
490  446  'COMMENT' NOW WE CONSIDER THE ENERGY OF THE AUGER ELECTRON;
491  446                    E11:=(E1-E2)+(G1[R]*H2)+E10;
492  447                    'IF' E11 'LE' E1+E3 'THEN' 'GOTO' AAGH;
493  448  'COMMENT' NOW WE CONSIDER THE WALK OF THE AUGER ELECTRON;
494  448                    L5:=L7*(((E9-E1)/(E11-E1))↑1.5);
495  449                    L2:=(L5*L3)/(L5+L3);
496  450                    L8:=-L2*LN(RANDOM(13));
497  451                    T3:=(2*RANDOM(14))-1;
498  452  'COMMENT' NOW WE EXAMINE THE AUGER ELECTRON FOR BOUNDARY CONDITIONS;
499  452                    'IF' X1-(L8*T3) 'GE' 0 'THEN' 'GOTO' AAGH;
500  453                    'IF' E11*T3*T3 'LE' E1+E3 'THEN' 'GOTO' AAGH;
501  454                    X3:=X3+X2;
502  455                    COUNTA (Y9,Y10,Y11,Y12,K1,K2,K3,K4,E1,E3,E11,Q,T3);
503  456  AAGH:           'IF' E4 'LE' E1+E3 'THEN' 'GOTO' AAGK;
504  457  'COMMENT' NOW WE CONSIDER THE WALK OF THE PRIMARY ELECTRON;
505  457                    L5:=L7*(((E9-E1)/(E4-E1))↑1.5);
506  458                    L2:=(L5*L3)/(L5+L3);
507  459                    L1:=-L2*LN(RANDOM(3));
508  460                    T1:=(2*RANDOM(4))-1;
509  461                    X1:=X1-(L1*T1);
510  462  'COMMENT' NOW WE EXAMINE THE PRIMARY FOR BOUNDARY CONDITIONS;
511  462                    'IF' X1 'GE' 0 'THEN' 'GOTO' AAGA;
512  463                    'IF' E4*T1*T1 'GE' E3+E1 'THEN' 'GOTO' AAGB;
513  464                    X1:=-X1;
514  465                    'GOTO' AAGA;
515  466  AAGB:           X3:=X3+X2;
516  467  'COMMENT' NOW WE DECIDE IF THE ELECTRON IS PRIMARY OR SECONDARY;
517  467                    'IF' N4=1 'THEN' 'GOTO' AAGP;
518  468                    COUNTP (Y1,Y2,Y3,Y4,P1,P2,P3,P4,E1,E3,E4,Q,T1);
519  469                    'GOTO' AAGK;
520  470  AAGP:             E6:=E4;
521  471                    T2:=T1;
522  472                    COUNTS (Y5,Y6,Y7,Y8,S1,S2,S3,S4,E1,E3,E6,Q,T2);
523  473                    'GOTO' AAGK;
524  474  'COMMENT' NOW WE DECIDE THE TYPE OF SCATTERING PROCESS;
525  474  AAGA:           'IF' L2/L5 'GE' RANDOM(5) 'THEN' 'GOTO' AAGD;
526  475  'COMMENT' THIS IS PROCEDURE FOR ELECTRON-PHONON SCATTERING;
```

```
527  475                    'IF' 0.5 'GE' RANDOM(6) 'THEN' 'GOTO' AAGE;
528  476    AAGG:           E4:=E4+E5;
529  477                    'GOTO' AAGC;
530  478    AAGE:           'IF' E4 'LE' E5 'THEN' 'GOTO' AAGG;
531  479                    E4:=E4-E5;
532  480                    'GOTO' AAGC;
533  481    'COMMENT' NOW CONSIDER THE ENERGY LOST IN THE SCATTERING PROCESS;
534  481    AAGD:           N4:=1;
535  482                    E7:=E4-E1;
536  483                    Q:=ENTIER(E7*10);
537  484                    R:=ENTIER(RANDOM(8)*G4[Q]);
538  485                    E8:=E7-(G2[R]*H1);
539  486                    A2:=RANDOM(7);
540  487                    Q:=ENTIER((E2-E8)/H2);
541  488                    'IF' Q 'LE' 0 'THEN' Q:=0;
542  489                    R:=ENTIER(A2*(N2-G3[Q]))+G3[Q];
543  490    'COMMENT' NOW WE DECIDE THE ENERGY OF THE SCATTERER;
544  490                    E6:=(E1-E2)+(G1[R]*H2);
545  491                    E4:=E4-E8;
546  492                    E6:=E6+E8;
547  493                    'IF' E6<E4 'THEN' 'GOTO' AAGD;
548  494                    E7:=E4;
549  495                    E4:=E6;
550  496                    E6:=E7;
551  497    AAGC:           'IF' E6<(E1+E3) 'THEN' 'GOTO' AAGC;
552  498    'COMMENT' NOW CONSIDER THE WALK AND EXAMINE FOR BOUNDARY CONDITIONS;
553  498                    L5:=L7*(((E4-E1)/(E6-E1))↑1.5);
554  499                    L2:=(L5*L3)/(L5+L3);
555  500                    L4:=-L2*LN(RANDOM(9));
556  501                    T2:=(2*RANDOM(10))-1;
557  502                    'IF' X1-(L4*T2) 'GE' 0 'THEN' 'GOTO' AAGC;
558  503                    'IF' E6*T2*T2 'LE' E1+E3 'THEN' 'GOTO' AAGC;
559  504                    COUNTS (Y5,Y6,Y7,Y8,S1,S2,S3,S4,E1,E3,E6,Q,T2);
560  505    AAGC:           'IF' E4 'LE' E1+E3 'THEN' 'GOTO' AAGK;
561  506                    'GOTO' AAGH;
562  507    AAGK:       'END';
563  508
```

```
564   508        'COMMENT' NOW COMMENCE PRINTOUT PROCEDURE;
565   508        'BEGIN' STELLWRITE;
566   510                ELLTEXT('('''L!!')');
567   511                ENDELLWRITE;
568   512        'END' ;
569   513
570   513
571   513        'BEGIN' STELLWRITE;  SAMELINE;
572   516                ELLTEXT('('''YIELD IS!')');
573   517                ELLTEXT('('''S5!!')');
574   518                PRINTELL((Y1+Y2+Y3+Y4)/N1);
575   519                ELLTEXT('('''ELECTRONS/PHOTON!')');
576   520                ENDELLWRITE;
577   521        'END' ;
578   522
579   522
580   522        'BEGIN' STELLWRITE;
581   524                ELLTEXT('('''L!!')');
582   525                ENDELLWRITE;
583   526        'END' ;
584   527
585   527             'IF' X3 'LE' 0 'THEN' 'GOTO' AAGN;
586   528
587   528        'BEGIN' STELLWRITE;  SAMELINE;
588   531                ELLTEXT('('''ESCAPE DEPTH IS :=!')');
589   532                ELLTEXT('('''S5!!')');
590   533                PRINTELL((X3/(Y1+Y2+Y3+Y4+Y5+Y6+Y7+Y8+Y9+Y10+Y11+Y12)));
591   534                ELLTEXT('('''ANGSTROMS!')');
592   535                ENDELLWRITE;
593   536        'END' ;
594   537
595   537
596   537        'BEGIN' STELLWRITE;
597   539                ELLTEXT('('''L!!')');
598   540                ENDELLWRITE;
599   541        'END' ;
600   542
```

```
601   542       AAGN:
602   542       'BEGIN' STELLWRITE;  SAMELINE;
603   545               ELLTEXT('('SECONDARY YIELD IS:=!')');
604   546               ELLTEXT('('''S5!!')');
605   547               PRINTELL((Y5+Y6+Y7+Y8)/N1);
606   548               ELLTEXT('('ELECTRONS/PHOTON!')');
607   549               ENDELLWRITE;
608   550       'END' ;
609   551
610   551
611   551       'BEGIN' STELLWRITE;
612   553               ELLTEXT('('''L!!')');
613   554               ENDELLWRITE;
614   555       'END';
615   556       'BEGIN' STELLWRITE; SAMELINE;
616   559                 ELLTEXT('('AUGER YIELD IS:=!')');
617   560                 ELLTEXT('('''S5!!')');
618   561                 PRINTELL((Y9+Y10+Y11+Y12)/N1);
619   562                 ELLTEXT('('ELECTRONS/PHOTON!')');
620   563                 ENDELLWRITE;
621   564           'END';
622   565       'BEGIN' STELLWRITE;
623   567               ELLTEXT('('''F!!')');
624   568               ENDELLWRITE;
625   569       'END' ;
626   570
627   570             'FOR' Q:=0 'STEP' 1 'UNTIL' 100 'DO'
628   571                   W[Q]:=I[Q]/100:
629   572             PRINTF (V,Z,W);
630   573
631   573       'BEGIN' STELLWRITE;
632   575               ELLTEXT('('''F!!')');
633   576               ENDELLWRITE;
634   577       'END' ;
635   578
636   578             'FOR' Q:=0 'STEP' 1 'UNTIL' 100 'DO'
637   579                   W[Q]:=ENTIER((P1[Q]+P2[Q]+P3[Q]+P4[Q])/10);
638   580             PRINTF (V,Z,W);
```

```
639  581
640  582        'BEGIN' STELLWRITE;
641  583                ELLTEXT('('''F1')');
642  584                ENDELLWRITE;
643  585        'END' ;
644  586
645  586              'FOR' Q:=0 'STEP' 1 'UNTIL' 100 'DO'
646  587                    W[Q]:=S1[Q]+S2[Q]+S3[Q]+S4[Q]+K1[Q]+K2[Q]+K3[Q]+K4[Q];
647  588              PRINTE (V,Z,W);
648  589
649  589        'BEGIN' STELLWRITE;
650  591                ELLTEXT('('NO OF ELECTRONS PER INCIDENT PHOTON-EVI')');
651  592                ENDELLWRITE;
652  593        'END' ;
653  594
654  594              'FOR' Q:=0 'STEP' 1 'UNTIL' 100 'DO'
655  595              'BEGIN'
656  595              E1:=((Q*H1)-E2);
657  597              E3:=(P1[Q]+P2[Q]+P3[Q]+P4[Q])/(N1*H2);
658  598              E4:=(W[Q])/(M1*H2);
659  599              E5:=E4+E3;
660  600
661  600        'BEGIN' STELLWRITE; SAMELINE;
662  603                PRINTELL(E1);
663  604                PRINTELL(E3);
664  605                PRINTELL(E4);
665  606                PRINTELL(E5);
666  607                ENDELLWRITE;
667  608        'END' ;
668  609
669  609        'BEGIN' STELLWRITE;
670  611                ELLTEXT('('''L1')');
671  612                ENDELLWRITE;
672  613        'END' ;
673  614              'END' ;
674  615
675  615        'END';
676  616        'END';
```

APPENDIX II; The modified Krolikowski programme

Program symbols

All units of energy are 0.1eV and the lengths are in Angstroms.

N1	Workfunction.
N2	Photon energy.
A	Absorption coefficient.
IH	Valence band width.
NVAL	Number of valence electrons.
V	Valence density of states.
C	Conduction band density of states.
X	Electron-hole pair inelastic mean free path.
PL	Plasmon loss mean free path.
TL	Total inelastic mean free path.
T	Semi-classical threshold function.
PO1	The internal energy distribution of photoexcited electrons.
TF2	The effective threshold function.
SEE	Distribution function of secondary electrons.
D	External energy distribution of secondary electrons.
HL	Hole scattering length.
SHE	The hole distribution function.
GD	Plasmon loss distribution function.
DPLAS	The external energy distribution of plasmon loss electrons.
PS	The external energy distribution of primary electrons.
TER(I)	The tertiary distribution function.
TER(N)	The external tertiary energy distribution function.

SUM 7	The primary yield.
SUM 8	The secondary yield.
SUM 10	The Auger yield.
SUM 11	The plasmon loss yield.
SUM 12	The tertiary yield.
SUM 9	The total yield.
C2	The total external energy distribution function.
PO2	The total external scattered energy distribution function.

```
0100        PROGRAM AUGER(JTMDAT,INPUT,OUTPUT,TAPE1=INPUT,TAPE2=OUTPUT
0110       1      ,TAPE3=JTMDAT,JTMOUT,TAPE4=JTMOUT)
0120        DIMENSION V(220), C(220),PS(220),SEE(220),HL(220)
0130       1      ,D(220),X(220),T(220),TF2(220),P01(220),C2(220)
0140       2 ,DHOLE(220),DAUG(220),PL(220),TL(220),DPLAS(220)
0150       3 ,TER(220),P02(220)
0160        CALL DARRAY(120)
0170 C
0180 CCCCCCCCCC INPUT DATA ON THE ELECTRONIC STRUCTURE CCCCCCCCCCCCCCC
0190 C
0200        N8=86
0210        WRITE(2,232)
0220        READ(1,*)N1,N3,A,IH
0230        WRITE(2,709)
0240        READ(1,*) NVAL
0250        WRITE(4,723) N3,A
0260        N4=N3
0270        IF(IH.GT.N3) N4=IH
0280        N4=N4+5
0290        IF(N4.LT.N8) N4=N8
0300 C
0310 CCCCCCCCCC NORMALIZE THE DENSITY OF STATES CCCCCCCCCCCCCCCCCCCCC
0320 C
0330        SUM=0.
0340        DO 10 J=1,N3
0350        READ(3,600) V(J)
0360     10 SUM=SUM+V(J)*0.1
0370        DO 11 J=1,N3
0380     11 V(J)=V(J)/SUM*NVAL
0390 C
0400 CCCCCCCCCC FIT FREE ELECTRON DENSITY OF STATES ABOVE FERMI ENERGY
0410 C
0420        N5=N3+1
0430        DO 20 J=N5,N4
0440     20 V(J)=0
0450        DO 30 J=1,N4
0460        PAN3=FLOAT(J+N3)/N3
0470     30 C(J)=V(1)*SQRT(PAN3)
0480 C
0490 CCCCCCCCCC CALCULATE THE INELASTIC E-E SCATTERING LENGTH CCCCCCCCC
0500 C
0510        NM=N4+1
0520        DO 666 J=3,NM
```

```
0530        D2=0
0540        K=J-2
0550        DO 777 I=1,K
0560        DSUM=0
0570        MN=(J-I)/2
0580        DO 555 L2=1,MN
0590   555  DSUM=.01*(C(L2)*C(J-I-L2)*V(I))+DSUM
0600   777  D2=D2+DSUM
0610        PPN3=J+N3
0620        X(J)=(SQRT(PPN3)/D2)
0630   666  CONTINUE
0640 C
0650 CCCCCCCCCC NORMALIZE THE E-E SCATTERING LENGTH AT 8.6 EV. CCCCCCCC
0660 C
0670        WRITE(2,401)
0680        READ(1,*) N9
0690        P5=X(N8)
0700        DO 60 J=3,MM
0710        FNORM=N9/(P5*100000000)
0720    60  X(J)=X(J)*FNORM
0730 C
0740 CCCCCCCCCC CALCULATE THE PLASMON SCATTERING LENGTH
0750 C
0760        WRITE(2,643)
0770        READ(1,*) NP
0780        WP=NP*0.1
0790        NA=NP+1
0800        EF=(N3-1)*0.1
0810        IF(NA.GT.N4) GO TO 645
0820        DO 641 I=NA,N4
0830        E=(N3+I-1)*0.1
0840        DENOM=ALOG((SQRT(WP+EF)-SQRT(EF))/(SQRT(E)-SQRT(E-WP)))
0850        PL(I)=1.0582/WP*E/DENOM*1.E-8
0860        TL(I)=1./(1./PL(I)+1./X(I))
0870   641  CONTINUE
0880   645  NLIM=NP
0890        IF(NP.GT.N4) NLIM=N4
0900        DO 642 I=3,NLIM
0910        TL(I)=X(I)
0920   642  CONTINUE
0930 C
0940 CCCCCCCCCC CALCULATE THE SEMICLASSICAL THRESHHOLD FUNCTION CCCCCCC
```

```
C
      DO 40 J=N1,N4
      TF2(J)=FLOAT(N1+N3)/FLOAT(J+N3)
   40 T(J)=(1-SQRT(TF2(J)))/2
C
CCCCCCCCCC CALCULATE THE  NORMALIZED ENERGY DISTRIBUTION OF
C           EXCITED ELECTRONS                          CCCCCCCCCCCCCCCC
C
      SUM=0.
      DO 800 J=1,IH
      SUM=SUM+C(J)*V(IH-J+1)*0.1
  800 CONTINUE
      DO 900 J=1,IH
      PO1(J)=C(J)*V(IH-J+1)/SUM
  900 CONTINUE
C
CCCCCCCCCC CALCULATE THE EFFECTIVE THRESHHOLD FUNCTION CCCCCCCCCCC
C
      IY=N1+1
      DO 700 J=IY,N4
      AL=A*TL(J)
      PX=(1.+AL)/(1.+AL-2.*AL*T(J))
      TF2(J)=T(J)*(1.-ALOG(PX)/(2.*AL*T(J)))
  700 CONTINUE
C
CCCCCCCCCC CALCULATE THE SECONDARY ELECTRON DISTRIBUTION CCCCCCCCC
C
      IHH=IH-1
      DO 150 I=N1,IH
      P(I)=0.
  150 CONTINUE
      DO 151 IQ=N1,IH
      SUM1=0.
      NIQ=IQ-1
      DO 152 IA=1,NIQ
      NN=IQ-IA
      SUM2=0.
      DO 153 N=1,NN
      SUM2=SUM2+V(NN+1-N)*C(N)*0.1
  153 CONTINUE
      PS(IA)=SUM2*C(IA)
      SUM1=SUM1+PS(IA)*0.1
  152 CONTINUE
```

```
      DO 154 I4=1,NI1
      SEE(IA)=2.*PS(IA)/SUM1
  154 CONTINUE
      DO 155 I4=IQ,IHH
      SEE(IA)=0.
  155 CONTINUE
      IQQ=IQ+1
      DO 156 J=3,IQ
      AL=A*TL(IQ)
      RL=X(J)/TL(IQ)
      B2=RL*(ALOG(1.+1./RL))
      B1=ALOG(1.+AL)/AL
      C2(J)=(B1+B2)/2.
  156 CONTINUE
      DO 157 J=IQQ,IHH
      C2(J)=0.
  157 CONTINUE
      XX=C(IQ)*V(IH-IQ+1)/SUM
      DO 158 I=N1,IHH
      D(I)=D(I)+SEE(I)*XX*C2(I)*0.1
  158 CONTINUE
  151 CONTINUE
C
CCCCCCCCCC CALCULATE THE SCATTERING LENGTH FOR HOLES CCCCCCCCCCC
C
      DO 838 IHOLE=2,N3
      BSUM=0.
      IMOD1=IHOLE-1
      DO 837 IFIN=1,IMOD1
      IMOD2=(IHOLE-IFIN+1)/2
      ASUM=0.
      DO 836 IINT=1,IMOD2
      ASUM=ASUM+0.1*V(IINT)*V(IHOLE-IFIN+1-IINT)
  836 CONTINUE
      BSUM=BSUM+0.1*C(IFIN)*ASUM
  837 CONTINUE
      HL(IHOLE)=SQRT(FLOAT(N3+1-IHOLE))*FNORM/BSUM
      DHOLE(IHOLE)=BSUM
  838 CONTINUE
C
CCCCCCCCCC CALCULATE THE DISTRIBUTION OF AUGER ELCTRONS CCCCCCCC
C
```

```
1800        IMOD3=IH
1810        IF(IH.GT.N3) IMOD3=N3
1820        DO 935 IFIN=IY,IHH
1830        IMOD=IFIN+1
1840        XELEC=TL(IFIN)
1850        SUM=0.
1860        IF(IMOD.GT.IMOD3) GO TO 1001
1670        DO 937 IHOLE=IMOD,IMOD3
1880        SHE=0.0
1890        IMOD2=(IHOLE-IFIN+1)/2
1900        XHOLE=HL(IHOLE)
1910        DO 936 IINT=1,IMOD2
1920        SHE=SHE+0.1*V(IINT)*V(IHOLE-IFIN+1-IINT)
1930    936 CONTINUE
1940        SHE=SHE*C(IFIN)/DHOLE(IHOLE)
1950        C2H=0.5*(ALOG(1.+A*XHOLE)/A/XHOLE+ALOG(1.+XHOLE/XELEC)
1960       1 *XELEC/XHOLE)
1970        SUM=SUM+0.1*SHE*C2H*P01(IH-IHOLE+1)
1980    937 CONTINUE
1990   1001 CONTINUE
2000        SUM=SUM*TF2(IFIN)
2010        DAUG(IFIN)=SUM
2020    935 CONTINUE
2030        DAUG(IH)=0.
2040 C
2050 CCCCCCCCCC CALCULATE PLASMON LOSS TERM CCCCCCCCCCC
2060 C
2070        DO 671 I=IY,IH
2080        SUM=0.0
2090        IF(NA.GT.IH) GO TO 673
2100        DO 672 INP=NA,IH
2110        EXPON=(INP-I-NP)**2*0.01
2120        IF(EXPON.GT.50.) EXPON=50.
2130        GO=EXP(-EXPON)/1.77245
2140        ALP=A*PL(INP)
2150        RAT=PL(INP)/TL(I)
2160        C2P=0.5*(ALOG(1.+ALP)/ALP+ALOG(1.+RAT)/RAT)
2170        SUM=SUM+0.1*C2P*GO*P01(INP)
2180    672 CONTINUE
2190    673 CONTINUE
2200        DPLAS(I)=SUM*TF2(I)
2210    671 CONTINUE
2220 C
```

```
2230 CCCCCCCCCC CALCULATE THE TERTIARY ELECTRON DISTRIBUTION CCCCCCCCC
2240 C
2250       DO 814 I=IY,IH
2260       PO2(I)=O(I)+(OPLAS(I)+OAUG(I))/TF2(I)
2270   814 CONTINUE
2280       IHH=IH-1
2290       DO 450 I=IY,IH
2300       TER(I)=0.
2310   450 CONTINUE
2320       DO 475 IQ=IY,IH
2330       SUM1=0.
2340       NIQ=IQ-1
2350       DO 200 IA=1,NIQ
2360       NN=IQ-IA
2370       SUM2=0.
2380       DO 100 N=1,NN
2390       SUM2=SUM2+V(NN+1-N)*C(N)*0.1
2400   100 CONTINUE
2410       PS(IA)=SUM2*C(IA)
2420       SUM1=SUM1+PS(IA)*0.1
2430   200 CONTINUE
2440       DO 300 IA=1,NIQ
2450       SEE(IA)=2.*PS(IA)/SUM1
2460   300 CONTINUE
2470       DO 303 IA=IQ,IHH
2480       SEE(IA)=0.
2490   303 CONTINUE
2500       IQQ=IQ+1
2510       DO 950 J=3,IQ
2520       AL=A*TL(IQ)
2530       RL=X(J)/TL(IQ)
2540       B2=RL*(ALOG(1.+1./RL))
2550       B1=ALOG(1.+AL)/AL
2560       C2(J)=(B1+B2)/2.
2570   950 CONTINUE
2580       DO 302 J=IQQ,IHH
2590       C2(J)=0.
2600   302 CONTINUE
2610       DO 480 I=IY,IHH
2620       TER(I)=TER(I)+SEE(I)*PO2(IQ)*C2(I)*0.1
2630   480 CONTINUE
2640   475 CONTINUE
```

```
C
C
CCCCCCCCCC CALCULATE THE ELECTRON DISTRIBUTIONS AND WRITE THEM OUT
C
      WRITE(2,2000)
      READ(1,*) IFLAG
      IF(IFLAG.EQ.1) WRITE(2,867)
      WRITE(4,867)
      DO 567 N=IY,IH
      PS(N)=TF2(N)*PO1(N)
      C(N)=TF2(N)*O(N)
      TER(N)=TER(N)*TF2(N)
      C2(N)=PS(N)+C(N)+DAUG(N)+OPLAS(N)+TER(N)
      PO2(N)=C2(N)-PS(N)
      IF(IFLAG.EQ.1)WRITE(2,815)N,PS(N),C(N),DAUG(N),OPLAS(N),
     1                                TER(N),C2(N)
      WRITE(4,815) N,PS(N),C(N),DAUG(N),OPLAS(N),TER(N),C2(N)
  567 CONTINUE
C
CCCCCCCCCC WRITE OUT THE SCATTERING LENGTHS CCCCCC
C
      WRITE(2,2001)
      READ(1,*) JFLAG
      IF(JFLAG.EQ.1) WRITE(2,384)
      WRITE(4,384)
      DO 382 I=3,N4
      J=I-1
      K=-(I-2)
      IF(J.GT.N3) HL(J)=0.
      IF(JFLAG.EQ.1)WRITE(2,383) I,X(I),PL(I),TL(I),TF2(I),K,HL(J)
      WRITE(4,383)I,X(I),PL(I),TL(I),TF2(I),K,HL(J)
  382 CONTINUE
C
C
CCCCCCCCCC CALCULATE THE YIELDS AND WRITE THEM OUT CCCCCCCCCCCCCCC
C
      SUM7=0.
      SUM8=0.
      SUM10=0.
      SUM11=0.
      SUM12=0.
      DO 566 N=IY,IH
      SUM7=SUM7+PS(N)*0.1
```

```
3070        SUM8=SUM8+C(N)*0.1
3080        SUM10=SUM10+0.1*DAUG(N)
3090        SUM11=SUM11+0.1*OPLAS(N)
3100        SUM12=SUM12+0.1*TER(N)
3110   568  CONTINUE
3120        SUM9=SUM7+SUM8+SUM10+SUM11+SUM12
3130        WRITE(4,868) IH,SUM7,SUM8,SUM10,SUM11,SUM12,SUM9
3140        WRITE(2,868) IH,SUM7,SUM8,SUM10,SUM11,SUM12,SUM9
3150 C
3160 CCCCCCCCCC PLOTTING ROUTINES CCCCCCCCCCCCCCCCCCCCCCCCCCCCCCCCCCCC
3170 C
3180        WRITE(2,301)
3190        READ(1,*) NNN
3200        IF(NNN.NE.1) STOP
3210        XPHOT=IH*0.1
3220        XM4X=-N3*0.1
3230        DO 901 I=1,N4
3240        T(I)=-(I-1)*0.1
3250        X(I)= -XPHOT-T(I)
3260   901  CONTINUE
3270        CALL PAPER(1)
3275        CALL PSPACE(0.1,0.95,0.1,0.8)
3280        CALL MAP(XMAX,0.1,1.,1.)
3290        CALL CURVEO(T,V,1,N3)
3300        CALL SCALES
3310        CALL PLACE(10,4)
3320        CALL TYPECS(41HOPTICAL DENSITY OF STATES IN ELECTRONS/EV ,41)
3330        CALL FRAME
3335        CALL PSPACE(0.1,0.95,0.1,0.8)
3336        CALL CTRMAG(5)
3340        CALL MAP(1.,1.,1.,1.)
3350        C2(N1)=0.0
3360        CALL PTPLOT(X,C2,N1,IH,30)
3370        CALL PTPLOT(X,OPLAS,IY,IH,23)
3380        CALL PTPLOT(X,DAUG,IY,IH,11)
3390        CALL PTPLOT(X,TER,IY,IH,03)
3400        CALL PTPLOT(X,PS,IY,IH,26)
3402        CALL REOPEN
3405        CALL PTPLOT(X,P02,IY,IH,12)
3407        CALL BLKPEN
3410        CALL PTPLOT(X,C,IY,IH,29)
3420        CALL PTPLOT(X,C2,IY,IH,30)
```

```
3425        CALL CTRMAG(20)
3430        CALL SCALES
3440        CALL PLACE(10,4)
3450        CALL TYPECS(36HEDCS IN ELECTRONS/ABSORBED PHOTON/EV ,36)
3460        CALL GREND
3470 C
3480 CCCCCCCCCC FORMAT STATEMENTS ONLY BEYOND HERE CCCCCCCCCCCCCCCCCCCC
3490 C
3500   232 FORMAT(1X,/,40H INPUT THE WORKFUNCTION, BANDWIDTH,       /
3510      1             25H ABSORPTION COEFFICIENT  /
3520      2             40H AND PHOTON ENERGY                      /)
3530   868 FORMAT(1X//21H  FOR PHOTON ENERGY = , I6/
3540      1            21H      PRIMARY YIELD = , E12.4/
3550      2            21H    SECONDARY YIELD = , E12.4/
3560      3            21H        AUGER YIELD = , E12.4/
3570      4            21H PLASMON LOSS YIELD = ,E12.4/
3580      5            21H     TERTIARY YIELD = ,E12.4/
3590      6            21H        TOTAL YIELD = , E12.4)
3600   815 FORMAT(I5,6E12.4)
3610   500 FORMAT(I3,5E12.4)
3620   600 FORMAT(F10.5)
3630   867 FORMAT(1X//5H EV*10,2X,9H PRIMRIES,3X,9H SECNDRES,3X,
3640      1  9H  AUGERS ,3X,9HPLAS LOSS,3X,9H TERTIARY,3X,9HTOTAL EDC/)
3650   401 FORMAT(1X//40H INPUT THE SCATTERING LENGTH AT 8.6 EV. /)
3660   301 FORMAT(1X//29H ENTER 1 FOR GRAPHICAL OUTPUT     /)
3670   723 FORMAT(1H1,50HCALCULATED ELECTRON DISTRIBUTIONS FOR BAND OF WIDT
3680      1 ,1HH,I5,7H*0.1 EV/30H AND ABSORPTION COEFFICIENT OF  ,
3690      2 E11.4,4H/CM.  //)
3700   709 FORMAT(1X//47H INPUT THE NUMBER OF VALENCE ELECTRONS PER ATOM /)
3710  2000 FORMAT(1X//44H INPUT 1 FOR TABLE OF ELECTRON DISTRIBUTIONS  /
3720      1            44H       0 FOR YIELDS ONLY                    /)
3730   643 FORMAT(1X//25H INPUT THE PLASMON ENERGY    /)
3740   384 FORMAT(1X//6H EV*10,2X,9HELEC-HOLE,3X,9HELEC-PLAS,
3750      1   3X,9H  TOTAL  ,3X,9HTHRESH EN,5X,6H EV*10,
3760      1   2X,3HHOLE-HOLE/)
3770   383 FORMAT(I5,4E12.4,I0,E12.4)
3780  2001 FORMAT(1X//40H INPUT 1 FOR TABLE OF SCATTERING LENGTHS
3790      1 /          40H       0 FOR YIELDS ONLY                  /)
3800        STOP
3810        END

12.15.41.UCLP, 22,       0.750 KLNS.
```

D.C. RODWAY. Ph.D. Thesis. 1978.

Photoemission Studies of some Liquid Simple Metals and Alloys

Donald Charles Rodway

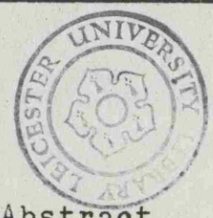

Abstract

Measurements of the work function, quantum yield and low energy ($6.0eV < h\nu < 21.2eV$) photoelectron spectra are presented for the simple metals In, Al, Pb, and Sn in the liquid and frozen solid states, and for Hg and the mercury alloys $Hg_{.5}$-$In_{.5}$, $Hg_{.75}$-$In_{.25}$, $Hg_{.96}$-$Na_{.04}$ in the liquid states only. The results obtained for the solid simple metals are consistent with other published results. The results for the liquid are very similar to those for the solid and are constant over a broad temperature range above the melting point.

A Monte Carlo simulation of the photoemission process, based on the 3-step model of Berglund and Spicer, has been developed and used to examine the effects of variation of the electron-phonon scattering length on the quantum yield and the escape depth of the photoelectrons.

This programme has been used in conjunction with an analytical programme, based on the work of Krolikowski, to derive optical density of valence states functions and electron-electron scattering lengths for the liquids.

In all cases the optical density of states functions show much stronger structure than expected on the basis of a weak scattering description of the liquid system and agree better with theoretical predictions for the solid, indicating that some aspects of the solid state band structure persist on melting. No evidence for conservation of the momentum vector $\underline{k}$ or for non-constant matrix elements is observed.

In the case of mercury and the mercury alloys the results obtained agree well with the 'pseudogap' concept proposed by Mott.